

Structure and Mechanism
of the Flavoenzyme Lipoamide Dehydrogenase
from *Escherichia coli*

Dissertation
for the award of the degree
“Doctor rerum naturalium”
of the Georg-August-Universität Göttingen

within the doctoral program *Biomolecules: Structure-Function-Dynamics*
of the Georg-August-University School of Science (GAUSS)

submitted by

Michael Tietzel

from Holzminden

Göttingen 2015

Members of the Thesis Committee

Prof. Dr. Kai Tittmann (Reviewer)

Department of Molecular Enzymology
Georg-August-Universität Göttingen

Prof. Dr. Ralf Ficner (Reviewer)

Department of Molecular Structural Biology
Georg-August-Universität Göttingen

Prof. Dr. Marina Rodnina

Department of Physical Biochemistry
Max Planck Institute for Biophysical Chemistry Göttingen

Further members of the Examination Board

Dr. Fabian Commichau

Department of General Microbiology
Georg-August-Universität Göttingen

Jun.-Prof. Dr. Ricardo Mata

Institute of Physical Chemistry
Georg-August-Universität Göttingen

Dr. Manfred Konrad

Enzyme Biochemistry
Max Planck Institute for Biophysical Chemistry Göttingen

Date of oral examination: 10.09.2015

Herewith I declare that I prepared this thesis “Structure and Mechanism of the Flavoenzyme Lipoamide Dehydrogenase from *Escherichia coli*” independently and with no other sources and aids than quoted. This thesis (wholly or in part) has not been submitted elsewhere for any academic award or qualification.

Göttingen, 31.07.2015

Michael Tietzel

Table of Contents

Table of Contents	4
List of Figures	8
List of Tables	11
Acknowledgements	12
Abbreviations	14
1 Introduction	17
1.1 Flavin and its biologically Active Derivatives	17
1.2 Reactivity of Flavins.....	18
1.3 Biological Functions of Lipoamide Dehydrogenases.....	19
1.4 Three Dimensional Structure of <i>E. coli</i> Lipoamide Dehydrogenase	21
1.5 Catalytic Mechanism of <i>E. coli</i> Lipoamide Dehydrogenase	23
1.6 The Physiological Importance of <i>E. coli</i> Lipoamide Dehydrogenase	25
1.7 The Relevance of Covalent Flavin-C4a-cysteiny Adducts.....	28
1.8 Motivation	30
2 Material and Methods	31
2.1 Material	31
2.1.1 Fine chemicals	31
2.1.2 Devices	32
2.1.3 Chromatography Columns.....	34
2.1.4 Molecular Weight Marker	34
2.1.5 Kit-Systems	34
2.1.6 Materials for Molecular Biology	34
2.1.7 Restriction Endonucleases.....	35
2.1.8 Bacterial Strains.....	35
2.1.9 Vectors.....	35
2.1.10 Enzymes	35
2.1.11 Crystallization Screens	36
2.1.12 Software.....	36
2.2 Methods.....	37
2.2.1 Molecular Biology	37
2.2.1.1 Concentration Determination of DNA	39
2.2.1.2 Agarose Gelelectrophoresis.....	39
2.2.1.3 Polymerase Chain Reaction (PCR).....	39
2.2.1.4 DNA Sequencing.....	39

2.2.1.5	Plasmid Transformation	39
2.2.2	Protein Chemistry.....	40
2.2.2.1	Sodium Dodecyl Sulfate - Polyacrylamide Gel Electrophoresis (SDS-PAGE)	40
2.2.2.2	Protein Expression and Purification of <i>EcE3</i> and multiple Variants from pGS523..	40
2.2.2.3	Protein Expression and Purification of <i>EcE3</i> and multiple Variants from pET28a ..	41
2.2.2.4	Expression and Purification of <i>EcLip3</i>	42
2.2.2.5	Generation of dihydro- <i>EcLip3</i> (<i>EcLip3H₂</i>).....	43
2.2.2.6	Concentration Determination of Proteins	43
2.2.2.7	Concentration Determination of dihydro- <i>EcLip3</i>	43
2.2.2.8	Determination of Extinction Coefficients of Multiple Variants	44
2.2.2.9	Determination of Redox Potentials of selected <i>EcE3</i> variants	45
2.2.2.10	Photobleaching of <i>EcE3</i> and Variants thereof.....	45
2.2.3	Substrates and Substrate Analogs.....	46
2.2.3.1	Concentration Determination of Substrates and Cofactors	46
2.2.4	Kinetic Methods	48
2.2.4.1	Steady-State Activity Assay	48
2.2.4.2	NAD ⁺ activation Experiments	48
2.2.4.3	pH Dependency Experiments under a constant ionic Strength	48
2.2.4.4	Fast Kinetics-Stopped Flow Absorbance Spectroscopy	48
2.2.5	Biophysical Methods	49
2.2.5.1	UV-Vis Spectroscopy.....	49
2.2.5.2	CD spectroscopy	49
2.2.5.3	Isothermal Titration Calorimetry.....	50
2.2.5.4	EPR.....	50
2.2.6	Mass Spectrometry	51
2.2.6.1	MALDI-TOF Mass Spectrometry	51
2.2.6.2	Determination of the Lipoylation State of <i>EcLip3</i>	51
2.2.6.3	MALDI-TOF Sample Preparation.....	52
2.2.6.4	MALDI-TOF Measurement and Data Evaluation.....	52
2.2.6.5	UPLC-ESI-TOF Sample Preparation	53
2.2.6.6	UPLC-ESI-TOF-MS	54
2.2.6.7	UHPLC-ESI-QTOF-MS.....	54
2.3	X-ray Crystallography	55
2.3.1	Crystallization	55
2.3.2	Data Processing and Molecular Replacement	56
2.3.3	Model Building, Refinement and Validation	56
3	Results and Discussion	57

3.1	Spectroscopic and Crystallographic Characterization of <i>EcE3</i>	57
3.1.1	Kinetic Characterization of <i>EcE3</i> in dependence of Lipoamide, NAD ⁺ and pH.....	57
3.1.2	Detection of Reaction Intermediates using Stopped-flow Absorbance Spectroscopy... 60	
3.1.3	Structure of <i>EcE3</i> – Active Site Dynamics underlie Catalysis.....	63
3.1.4	Spectroscopic and Crystallographic Investigation of the two-electron reduced State – EH ₂	65
3.1.5	Spectral Evidence for the Cysteiny-C4a Adduct in a monothiol variant of <i>EcE3</i>	69
3.1.6	Crystallographic detection of the Cysteiny-C4a Adduct.....	72
3.1.7	Is the geometry of the FAD-C4a-cysteiny adduct the fundament for its transience?... 75	
3.2	Investigation of the reductive half-reaction of <i>EcE3</i> using <i>EcLip3</i> as native Substrate.....	77
3.2.1	Characterization of <i>EcLip3</i> and its Reduction to the dihydro-form (<i>EcLip3H₂</i>).....	78
3.2.2	<i>EcLip3H₂</i> as native Substrate to track the reductive Half-reaction of <i>EcE3</i>	81
3.2.3	Evidence for the Transience of the Cysteiny-C4a Adduct	83
3.3	Mechanistic Investigation of <i>EcE3</i>	85
3.3.1	Characterization of the Reductive Half-Reaction using selected Active Site Variants . 85	
3.3.1.1	Histidine445 and Glutamate450 – The Role of the Catalytic Diad during Catalysis 87	
3.3.1.2	Tyrosine19 acts as structural Element rather than as a catalytic Residue	90
3.3.2	Characterization of the Oxidative Half-reaction using selected Active Site Variants... 91	
3.3.2.1	Lys54 and Glu189 are crucial Mediators of the Flavin Redox Potential.....	97
3.3.2.2	A direct Involvement of Arg386 in a Proton Transfer Reaction is questionable	97
3.4	Converting <i>EcE3</i> into a light-sensitive blue Light Receptor.....	99
3.4.1	<i>EcE3C45A/K54Q</i> and <i>C45S/K54Q</i> – PseudoLOV variants	99
3.4.2	Photobleaching of pseudoLOV Variants leads to irreversible Alterations at the Flavin Site	101
3.4.3	Mass Spectrometric Analysis of the photobleached Flavin Cofactor.....	104
3.4.3.1	C4a-cysteiny Adduct Formation in LOV Domains prevents Photodegradation of the Flavin Cofactor.....	107
3.4.3.2	Photodegradation of enzyme-bound FAD leads to Double Bond formation in the ribityl part.....	109
3.4.4	The H-bonding Network around the Flavin – The next Step on the Way to a light- sensitive Oxidoreductase?	112
3.5	Expanding the Active Site – Glu354 is also a Mediator of the Flavin Redox Potential.....	114
4	Summary	118
5	Appendix	120
5.1	Amino Acid Sequences	120
5.2	UV-VIS Ground-state Spectra.....	122

TABLE OF CONTENTS

5.3	Molar Extinction Coefficients.....	125
5.4	Steady-state Activity of <i>EcE3</i> and Variants thereof.....	126
5.5	Mechanistic Investigation of <i>EcE3</i>	129
5.6	Far-UV CD Spectra.....	134
5.7	Photobleaching of <i>EcE3</i>	135
5.8	EPR.....	136
5.9	Mass Spectrometry - Supplementary.....	137
5.10	Redox Potentials of selected <i>EcE3</i> Variants.....	147
5.11	Isothermal Titration Calorimetry.....	150
5.12	Crystallographic Tables.....	151
5.13	X-ray Figures.....	153
	Bibliography	156
	Curriculum Vitae	169

List of Figures

Figure 1.1 Flavin structure and nomenclature.	18
Figure 1.2 Chemical states of flavin.	19
Figure 1.3 Regeneration of lipoamide cofactors.	20
Figure 1.4 Crystal structure of <i>EcE3</i>	22
Figure 1.5 Typical catalytic cycle of flavoenzymes.	23
Figure 1.6 Simplified, general reaction scheme of lipoamide dehydrogenases.	24
Figure 1.7 Distribution of species at the EH_2 level in <i>EcE3</i>	25
Figure 1.8 Comparison of mixed acid pathway for glucose fermentation.	27
Figure 1.9 LOV domain photocycle and light-driven structural rearrangement.	29
Figure 2.1 Simplified reaction scheme of the <i>EcLip3</i> reduction by TCEP.	43
Figure 2.2 Reaction scheme of the concentration determination of free thiol groups.	43
Figure 2.3 MALDI-TOF mass spectrum of the Peptide Calibration Standard.	53
Figure 3.1 Steady-state characterization of <i>EcE3</i>	59
Figure 3.2 Stopped-flow absorbance traces of <i>EcE3</i> during reduction with NADH.	62
Figure 3.3 Local flexibility of the active site.	64
Figure 3.4 General characterization of <i>EcE3</i> - EH_2	67
Figure 3.5 NAD^+ titration of <i>EcE3C45A</i>	70
Figure 3.6 The flexibility of cysteine50 is determined by its hydrogen bond donor.	73
Figure 3.7 Evidence for cohesive electron density between Cys50 and FAD-C4a.	74
Figure 3.8 Structural model of the covalent C4a-cysteinyl adduct.	75
Figure 3.9 Comparison of the geometries of C4a-cysteinyl adducts in LOV domains and in <i>EcE3</i>	77
Figure 3.10 <i>In vitro</i> and native substrates of lipoamide dehydrogenases.	78
Figure 3.11 Evidence of the structural integrity of <i>EcLip3</i> and <i>EcLip3H₂</i>	80
Figure 3.12 Reduction of <i>EcE3</i> by <i>EcLip3H₂</i> under single turnover conditions.	82
Figure 3.13 Sequential stopped-flow absorbance analysis of the <i>EcE3</i> reduction by <i>EcLip3H₂</i> and subsequent oxidation by NAD^+ at 4 °C.	84
Figure 3.14 Putative position of the lipoamide binding site.	86
Figure 3.15 General characterization of the <i>EcE3</i> catalytic diad.	88
Figure 3.16 Stopped-flow absorbance traces of <i>EcE3Y19F</i>	90
Figure 3.17 Overview of the <i>re</i> face of the FAD.	92
Figure 3.18 Spectral properties of <i>EcE3K54Q</i>	95
Figure 3.19 Stopped-flow absorbance traces of <i>EcE3E189Q</i>	96
Figure 3.20 Converting <i>EcE3</i> into a pseudoLOV protein.	100

Figure 3.21 Comparison of absorbance changes in variants of pseudoLOVs and LOV domains upon blue light illumination.	103
Figure 3.22 UPLC-ESI-TOF-MS analysis of cofactors of bleached and unbleached psLOV.	105
Figure 3.23 UPLC-ESI-TOF-MS analysis of <i>ribityl-ADP-2H</i>	106
Figure 3.24 The double bond in <i>FAD-2H</i> and in <i>ribityl-ADP-2H</i> is located the ribityl part.	107
Figure 3.25 Protective mechanism of LOV proteins.	108
Figure 3.26 Putative FAD derivatives formed upon pseudoLOV photobleaching.	111
Figure 3.27 Comparison of the H-bonding network around the flavin cofactors in YF1 and <i>EcE3</i>	113
Figure 3.28 Kinetic and spectroscopic comparison between <i>EcE3E354K</i> and <i>EcE3wt</i>	115
Figure 3.29 Position of Glu354 in <i>EcE3</i>	117
Figure 5.1 Reduction of <i>EcE3</i> with NADH under single turnover conditions.	129
Figure 5.2 NAD ⁺ titration of <i>EcE3EC45A</i>	130
Figure 5.3 NAD ⁺ titration of <i>EcE3wt</i>	130
Figure 5.4 Primary amino acid sequences of E3 from different organisms.	131
Figure 5.5 Spectral properties of <i>EcE3R386A</i>	132
Figure 5.6 Further spectral properties of <i>EcE3E189Q</i>	133
Figure 5.7 Photobleaching of wild type, monothiol or non-thiol variants of <i>EcE3</i>	135
Figure 5.8 UPLC-ESI-TOF-MS analysis of FAD.	138
Figure 5.9 UPLC-ESI-TOF-MS analysis of FAD released of <i>EcE3C45A/K54Q</i> by heat precipitation.	139
Figure 5.10 UPLC-ESI-TOF-MS analysis of FAD released of <i>EcE3C45A/K54Q</i> by TCA precipitation.	140
Figure 5.11 UPLC-ESI-TOF-MS analysis of FAD released of <i>EcE3C45A/K54Q</i> by acetone precipitation.	141
Figure 5.12 UPLC-ESI-TOF-MS comparison of lumichrom.	142
Figure 5.13 Evidence for lumichrom formation in <i>EcE3C45A/K54Q</i> by UPLC-ESI-TOF-MS.	143
Figure 5.14 Evidence for FAD-2H formation in <i>EcE3C45A/K54Q</i> by UPLC-ESI-TOF-MS.	144
Figure 5.15 Ribityl-ADP-2H formation in <i>EcE3C45A/K54Q</i> by UPLC-ESI-TOF-MS.	145
Figure 5.16 UHPLC-ESI-QTOF-MS/MS analysis of FAD and FAD-2H.	146
Figure 5.17 Determination of the redox potential of <i>EcE3C45A/K54Q</i>	147
Figure 5.18 Determination of the redox potential of <i>EcE3C50A</i>	148
Figure 5.19 Determination of the redox potential of <i>EcE3C45S/C50S</i>	149
Figure 5.20 Titration of <i>EcLip3</i> to <i>EcE3</i>	150
Figure 5.21 ITC titration of <i>EcE3</i> variants with NAD ⁺	150
Figure 5.22 The placeholder ability of sulfate ions serving as precipitant.	153
Figure 5.23 Further bending of the flavin cofactor at the two-electron reduced state.	153
Figure 5.24 B-factor representation of the <i>EcE3</i> active site at 2.69 Å.	154

Figure 5.25 Active site of EcE3 at 2.69 Å.....	155
--	-----

List of Tables

Table 2.1 List of used primer pairs (Synthesized by Sigma-Aldrich, Taufkirchen).....	37
Table 2.2 Overview of buffers used for purification of <i>EcE3</i> from pGS523	41
Table 2.3 Overview of buffers used for purification of <i>EcE3</i> from pET28a.....	41
Table 2.4 Overview of buffers used for purification of Lip3	42
Table 2.5 Molar extinction coefficients of <i>EcE3</i> and respective variants.	44
Table 2.6 Redox pairs for the redox potential titrations.	45
Table 2.7 Spectroscopic characteristics and structures of relevant cofactors.	46
Table 2.8 Acquisition parameters for CD spectroscopy experiments	50
Table 2.9 Possible tryptic fragments of EcLip3 for the lipoylation state analysis	51
Table 2.10 ZipTip preparation for MALDI-TOF samples	52
Table 2.11 Expected and acquired masses of the Peptide Calibration Standard	53
Table 3.1 Steady-state parameters of <i>EcE3</i> variants involved in the reductive half-reaction.	87
Table 3.2 Steady-state parameters of <i>EcE3</i> variants involved in the oxidative half-reaction.	93
Table 5.1 Expected fragmentation pattern of <i>EcLip3</i> after tryptic digestion	137
Table 5.2 Redox potentials of relevant enzymes	147
Table 5.3 Crystallographic data and refinement statistics.	151

Acknowledgements

Many people have been helping me during this thesis and I wish to express my deepest thanks to the following:

I would like to thank Prof. Dr. Kai Tittmann for the supervision of this thesis and for contribution of numerous ideas, discussions and inspirations. Especially during difficult stages of the project he showed great support.

I would like to thank Prof. Dr. Ralf Ficner for external co-supervision of this thesis and for being a member of the thesis committee. I would also like to thank him for the generous ability to use the instruments and facilities of his department.

I would like to thank Prof. Dr. Marina Rodnina for taking part in the thesis committees and for good advices concerning kinetic issues.

Furthermore I am grateful to Dr. Fabian Commichau, Jun. Prof. Ricardo Mata and Dr. Manfred Konrad for being members of the extended thesis committee.

I am deeply thankful to Dr. Piotr Neumann for his continuous support in all theoretical and practical aspects of protein crystallography. Especially, I would like to thank him for carrying out the majority of the x-ray data processing work. I would also like to thank him for suggestions and comments in the field of structural biology in general – and life in general.

Dr. Florian Brodhun and Dr. Piotr Neumann I acknowledge for proofreading of the thesis.

Prof. Dr. Andreas Möglich and Dr. Ralph Diensthuber I would like to thank for a perfect and exciting cooperation in the field of flavoproteins and their photochemistry. In addition, I wish you all the best at your new positions.

I acknowledge Prof. Dr. Ivo Feussner for the generous ability to use the instruments of his department. Moreover, I would like to thank Dr. Kirstin Feussner for the mass spectrometric analysis of several flavin cofactors and many good advices concerning MS sample preparation and MS analysis.

Prof. Dr. Robert Bittl and Christopher Engelhard I acknowledge for several EPR control measurements during the “pseudoLOV”-project.

Prof. Dr. Bruce Palfey and Lena-Sophie Dreher I acknowledge for the determination of redox potentials of selected *EcE3* variants.

Dr. Achim Dickmanns and Michael Franke I would like to thank for the easy access to the pipetting robot and concomitant crystallization trials.

Dr. Kathrin Schröder-Tittmann I would like to thank for a nice collaboration in the structural and functional characterization of the PDH complexes from human and *E. coli*.

I acknowledge Dr. Oliver Valerius for his brilliant assistance in the field of MALDI-TOF mass spectrometry. He made it possible to measure and to evaluate data whenever I needed and thus contributed to the flow of the work.

Prof. Dr. Reinhard Jahn and Dr. Angel Perez Lara I would like to thank for very nice cooperation in the field of Isothermal Titration Calorimetry.

Prof. Dr. Holger Stark, Dr. Ashwin Chari and David Haselbach I acknowledge for our close collaboration embedded in the SFB860 and the ProteoPlex project.

Gerd Mader, Christoph Mader, Daniel Weinrich and Malte Bürsing I would like to thank for their technical support.

I would particularly like to thank Dr. Danilo Meyer for his supervision during the Master Thesis. He always took his time to discuss certain issues about the project which made the work much more comfortable.

I would like to thank all former and present members of the bioanalytics / molecular enzymology department for their help in the lab and the great working atmosphere.

Finally, I am deeply grateful to my parents for their endless support during my studies and life in general.

Abbreviations

Å	Ångström
A ₂₆₀ or A ₂₈₀	absorption at 260 or 280 nm
ACN	acetonitrile
Ala	alanine
app	apparent
Apo	apoenzyme, enzyme without cofactor
Arg	arginine
Asn	asparagine
Asp	asparaginic acid
ATP	adenosine triphosphate
asu	asymmetric unit
bp	base pairs
Carb	carbenicillin
CD	circular dichroism
cm	centimeter
cps	counts per second
CV	column volume
Cys	cysteine
Da	dalton
DHB	2,5-dihydroxybenzoic acid
ϵ	molar extinction coefficient
<i>Ec</i>	<i>Escherichia coli</i>
<i>EcE1</i>	<i>Escherichia coli</i> pyruvate dehydrogenase
<i>EcE2</i>	<i>Escherichia coli</i> dihydrolipoyl transacetylase
<i>EcE3</i>	<i>Escherichia coli</i> dihydrolipoyl dehydrogenase
<i>EcLip3</i>	innermost lipoyl domain of <i>Escherichia coli</i> dihydrolipoyl transacetylase
<i>E. coli</i>	<i>Escherichia coli</i>
EDTA	ethylenediaminetetraacetate
E _{ox}	oxidized form <i>E. coli</i> lipoamide dehydrogenase
EH ₂	two-electron reduced form <i>E. coli</i> lipoamide dehydrogenase
EH ₄	four-electron reduced form <i>E. coli</i> lipoamide dehydrogenase
EIC	extracted ion chromatogram
EPR	electron paramagnetic resonance
ESI	electrospray ionization

ABBREVIATIONS

Θ	ellipticity
FA	formic acid
FAD	flavin adenine dinucleotide
FMN	flavin mononucleotide
Gln	glutamine
Glu	glutamic acid
Gly	glycine
HEPES	4-(2-hydroxyethyl)-1-piperazineethanesulfonic acid
His	histidine
Ile	isoleucine
IPTG	isopropyl- β -D-thiogalactoside
ITC	isothermal titration calorimetry
k	rate constant
K_D	dissociation constant
K	equilibrium constant
KPP	potassium phosphate buffer
λ	wavelength
LB media	Luria-Bertani-Media
Leu	leucine
Lys	lysine
NADH/NAD ⁺	nicotinamide adenine dinucleotide (reduced form/oxidized form)
MS	mass spectrometry
NMR	nuclear magnetic resonance
obs	observed
OD	optical density
PDHc	pyruvate dehydrogenase complex
PDB	protein data bank
pH	negative logarithm of H ⁺ concentration
Phe	phenylalanine
PEG	polyethylene glycol
Pro	proline
PMSF	phenylmethylsulfonylfluorid
rpm	revolutions per minute
Ser	serine
SDS-PAGE	sodium dodecylsulfate polyacrylamide gelelektrophoresis
σ	estimated standard error, standard deviation or standard uncertainty
σ_A	Sigma-A, variance-term accounting for error and incompleteness in structure models

TCA	trichloroacetic acid
TCEP	Tris-(2-carboxyethyl)phosphine hydrochloride
ThDP	thiamin diphosphate
Thr	threonine
TOF	time of flight
Tris	tris (hydroxymethyl)-aminomethan
Trp	tryptophane
TWC	total wavelength chromatogram
Tyr	tyrosine
U	unit
UV/Vis	ultraviolet and visible fraction of electromagnetic radiation
Val	valine

1 Introduction

1.1 Flavin and its biologically Active Derivatives

Enzymes are versatile biocatalysts present in every organism in all domains of life. Understanding their mode of actions at an atomic level is of primary interest since enzymes are both potential drug targets for the pharmaceutical industry and potential catalysts under physiological conditions for the chemical industry. A subclass are flavoenzymes, enzymes that bind derivatives of riboflavin (vitamin B2), and of which a plethora has already been identified and characterized (Palfey and Fagan 2010). Flavoenzymes also harbor the aforementioned versatility with respect to the ability of catalyzing chemical reactions. Hence, they are involved in a multitude of biological processes including energy production, light-induced signal transduction and DNA repair to name only a few (Conrad, Manahan, and Crane 2014; Palfey and Fagan 2010). The probably most fascinating feature of flavoenzymes is their aptitude to act as carriers for reducing equivalents thereby transferring electrons from a donor reactant to an acceptor reactant. Thus, flavoenzymes play a pivotal role in metabolism acting as key players in the respiratory chain.

Flavins consist of a tricyclic isoalloxazine moiety attached to a ribityl chain at the N10 atom (Figure 1.1). The most prominent enzyme bound flavin derivatives are flavin mononucleotide (FMN) and flavin adenine dinucleotide (FAD). FMN results from phosphorylation at the 5'-OH atom of the ribityl chain and FAD is the product from an esterification of AMP and FMN. Generally, flavins and enzymes form noncovalent complexes characterized by small binding constants making a covalent attachment of the cofactor to the enzyme almost unnecessary. The tight binding is achieved by interactions of the protein with the ribityl chain and the 5'-phosphate group, and, in case of FAD, by interactions of a secondary structure element (Rossmann fold) with its ADP portion (Hanukoglu 2015). However, covalent attachment occasionally occurs to form the holoprotein via the 8- α (methyl) or the C6 atom of the dimethylbenzene moiety (Palfey and Fagan 2010) or at both sides at once (Shoyama et al. 2012).

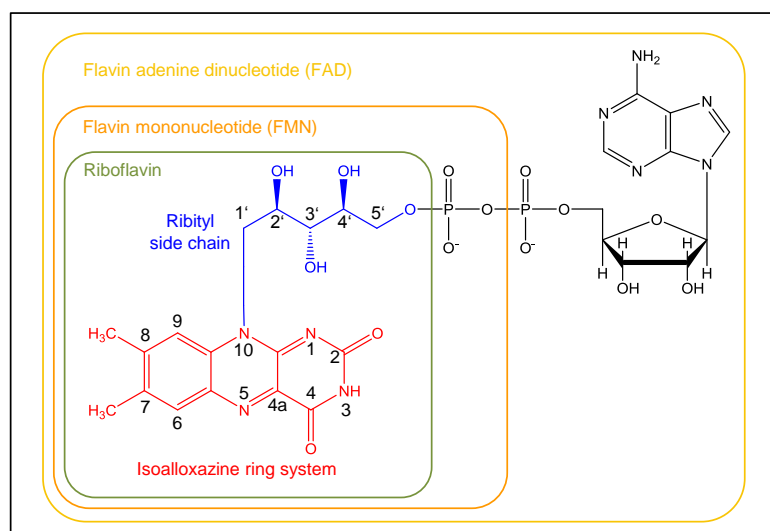


Figure 1.1 Flavin structure and nomenclature.

1.2 Reactivity of Flavins

The reactive part of flavins is the heterocyclic isoalloxazine ring system and three stable oxidation states can be assigned to the cofactor: fully oxidized, semiquinone (1-electron reduced), and hydroquinone (2-electron reduced) (Figure 1.2). The ring system is planar in solution and also in most protein structures, but it was also demonstrated that the flavin redox potential can be tuned by conformational effects leading to deviations from this planarity. Especially bending of the ring system along the N5-N10 axis was demonstrated to influence the ability to accept one or two electrons (Hasford, Kemnitzer, and Rizzo 1997; Lyubimov et al. 2007; Walsh and Miller 2003) making the electron-deficient isoalloxazine a target for nucleophilic attack at N5, C4a, and C6 (Palfey and Fagan 2010). Oxidized flavins harbor a shiny yellow color and are highly polarizable whereas the resulting reactivity is mainly influenced by interactions with the respective enzyme.

The single-electron reduced state is called semiquinone which is thermodynamically unstable in aqueous solutions (Gibson, Massey, and Atherton 1962). However, some proteins provide surroundings drastically increasing the lifetime of the semiquinone whereas others completely prevent its formation (Beel et al. 2012; Massey and Palmer 1966). Flavin semiquinones either exist as neutral (blue) radicals or as anionic (red) radicals in which the free electron is delocalized over the isoalloxazine (Ehrenberg, Müller, and Hemmerich 1967; Müller et al. 1970). EPR spectroscopy demonstrated that the highest spin density can be found at C4a for the neutral radical and at N5 for the anionic radical. During redox reactions they can act as single-electron donors/acceptors or also form radical pairs (Palfey and Fagan 2010).

The flavin hydroquinone is pale yellow. It is the two-electron reduced state which is mostly planar and thus antiaromatic. However, the aforementioned bending along the N5–N10 axis was also observed in

small-molecule structures and some protein structures, but to a much more pronounced extent (>30 °) (Palfey and Fagan 2010). Bending is most likely determined by protonation of N1 since the protonated hydroquinone was shown to adopt a butterfly conformation whereas the anionic hydroquinone is planar (Rizzo 2001; Rodríguez-Otero et al. 2002; Zheng and Ornstein 1996). In contrast to semiquinones, hydroquinones can react as single-electron donors, as hydride donors, or as nucleophiles at N5 or C4a (Palfey and Fagan 2010).

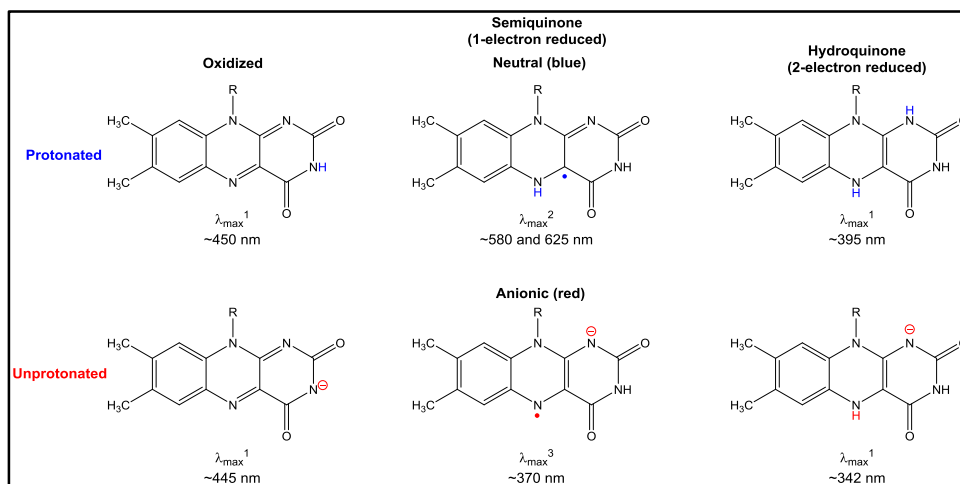


Figure 1.2 Chemical states of flavin.

The absorption maxima are approximate values and may slightly differ due to the respective enzyme surrounding. Wavelengths below 300 nm were not taken into account. ¹(Ghisla et al. 1974) ²(Hitomi et al. 1997; Massey and Palmer 1966) ³(Choong and Massey 1980; Talfournier et al. 2001b).

1.3 Biological Functions of Lipoamide Dehydrogenases

Lipoamide dehydrogenases (EC 1.8.1.4) belong to the flavoenzymes family of pyridine nucleotide-disulfide oxidoreductases which share several structural and mechanistic properties (Palfey and Fagan 2010). This family further includes: glutathione reductase (EC 1.6.4.2), mycothione reductase (EC 1.8.1.15), trypanothione reductase (EC 1.8.1.12), and mercuric reductase (EC 1.16.1.1), all pivotal for maintaining metabolic and cellular functions. Lipoamide dehydrogenases are part of ketoacid dehydrogenase multienzyme complexes and the glycine cleavage system and catalyze the reoxidation of lipoamide cofactors with concomitant transfer of reducing equivalents to NAD^+ thereby generating NADH (Figure 1.3) (Perham 2000; Reed 1974, 2001).

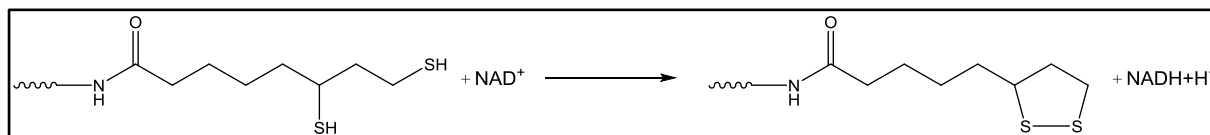


Figure 1.3 Regeneration of lipoyl cofactors.

Lipoamide dehydrogenases catalyze the NAD^+ -dependent oxidation of the dihydrolipoyl cofactors that are covalently linked to the acyltransferase components of multienzyme complexes.

As part of the pyruvate dehydrogenase multienzyme complex (PDHc) lipoamide dehydrogenases are directly involved in energy metabolism by linking glycolysis and citric acid cycle. PDHc is present in a multitude of organisms, namely in respiratory eubacteria and the mitochondria of eukaryotes (Bates et al. 1977; Patel and Roche 1990; Perham 2000). It catalyzes the irreversible conversion of pyruvate, co-enzyme A and NAD^+ into CO_2 , acetyl-CoA and NADH. Acetyl-CoA then serves as a precursor for the citric acid cycle and the biosynthesis of fatty acids and steroids, while NADH eventually feeds reducing equivalents into the respiratory chain for oxidative phosphorylation (ATP synthesis) (Patel and Roche 1990). PDHc consists of multiple copies of three major enzyme components: a thiamine diphosphate-dependent pyruvate dehydrogenase (E1 (EC 1.2.4.1)), a dihydrolipoamide transacetylase (E2 (EC 2.3.1.12)), which carries lipoyl groups covalently linked to the ϵ -amino group of lysine residues (N6-(lipoyl)-lysine, lipoamide cofactor), and the aforementioned lipoamide dehydrogenase (E3) (Korotchkina and Patel 2001; Patel and Korotchkina 2001). An important and outstanding ability of PDHc is the mechanism of covalent substrate channeling between the different components. The N6-(lipoyl)-lysine conjugate is structurally highly flexible. A 14 Å “swinging arm” permits active site coupling between the E1, E2 and E3 components by movement of the lipoyl moiety itself and by additional movement of the whole protein domain. This domain (Lip-domain) carries the lipoamide cofactor thus providing an appendage that is capable to bridge the physical gaps between the active centers on the different components (Perham and Reche 1998; Perham 2000).

In all PDHc, the reaction cycle is catalyzed by those enzymes and can be subdivided into several steps. Initially, E1 binds pyruvate and catalyzes its irreversible decarboxylation yielding 2-hydroxyethyl-thiamine diphosphate. Afterwards, E1 transfers the C2-fragment to the oxidized dithiolane ring of the lipoamide cofactor of E2. This reductive acetylation results in the formation of a high-energy thioester linkage between a sulfur atom of the reduced lipoamide dithiolane moiety and the acetyl fragment derived from pyruvate (Patel and Roche 1990). In the following, E2 itself catalyzes the acyl group transfer from reduced S-acetyldihydrolipoamide to Coenzyme A leading to the formation of acetyl-CoA (Akiyama and Hammes 1981). The reduced lipoamide cofactor must be oxidized in order to permit subsequent cycles of catalysis. This reaction step is catalyzed by lipoamide dehydrogenases under transient reduction of an intrinsic disulfide bond and further transfer of reducing equivalents to

the enzyme-bound flavin (Argyrou, Blanchard, and Palfey 2002). Generation of NADH by E3 finally completes the reaction cycle.

1.4 Three Dimensional Structure of *E. coli* Lipoamide Dehydrogenase

Several crystal structures of lipoamide dehydrogenases from various species have been solved over the years (Brautigam et al. 2005; Mattevi et al. 1993; Mattevi, Schierbeek, and Hol 1991); that of the *E. coli* enzyme recently (Chandrasekhar et al. 2013). The tertiary structures reflect very high similarity and only minor structural differences can be observed in surface exposed loop regions (Chandrasekhar et al. 2013). In addition, lipoamide dehydrogenase is structurally homologous to glutathione reductase, a further member of the flavoenzyme disulfide reductases. All described lipoamide dehydrogenases are homo-dimeric enzymes with two active sites formed at the dimer interface (Figure 1.4A). Each monomer thereby consists of four domains. A large N-terminal FAD-binding domain (residues 1–149; referring to *E. coli* numbering) which contacts the three remaining domains: the NAD-binding domain (150–282), the central domain (283–350), and the interface domain (351–474) (Figure 1.4B). The dimeric form of *E. coli* lipoamide dehydrogenase is based on its active site architectures involving residues of both monomers, respectively. The redox active disulfide bridge Cys45 to Cys50 which directly interacts with lipoamide cofactors is located at the dimer interface on the *si* face of the tightly but non-covalently bound flavin (Figure 1.4C). Above this electron transfer site, at the *re* face of the flavin, the NAD⁺/NADH binding site is housed. The highly conserved catalytic diad (His445 and Glu450) from the adjacent monomer involved in acid/base chemistry completes the active site (Benen, Van Berkel, Dieteren, et al. 1992; Kim and Patel 1992b).

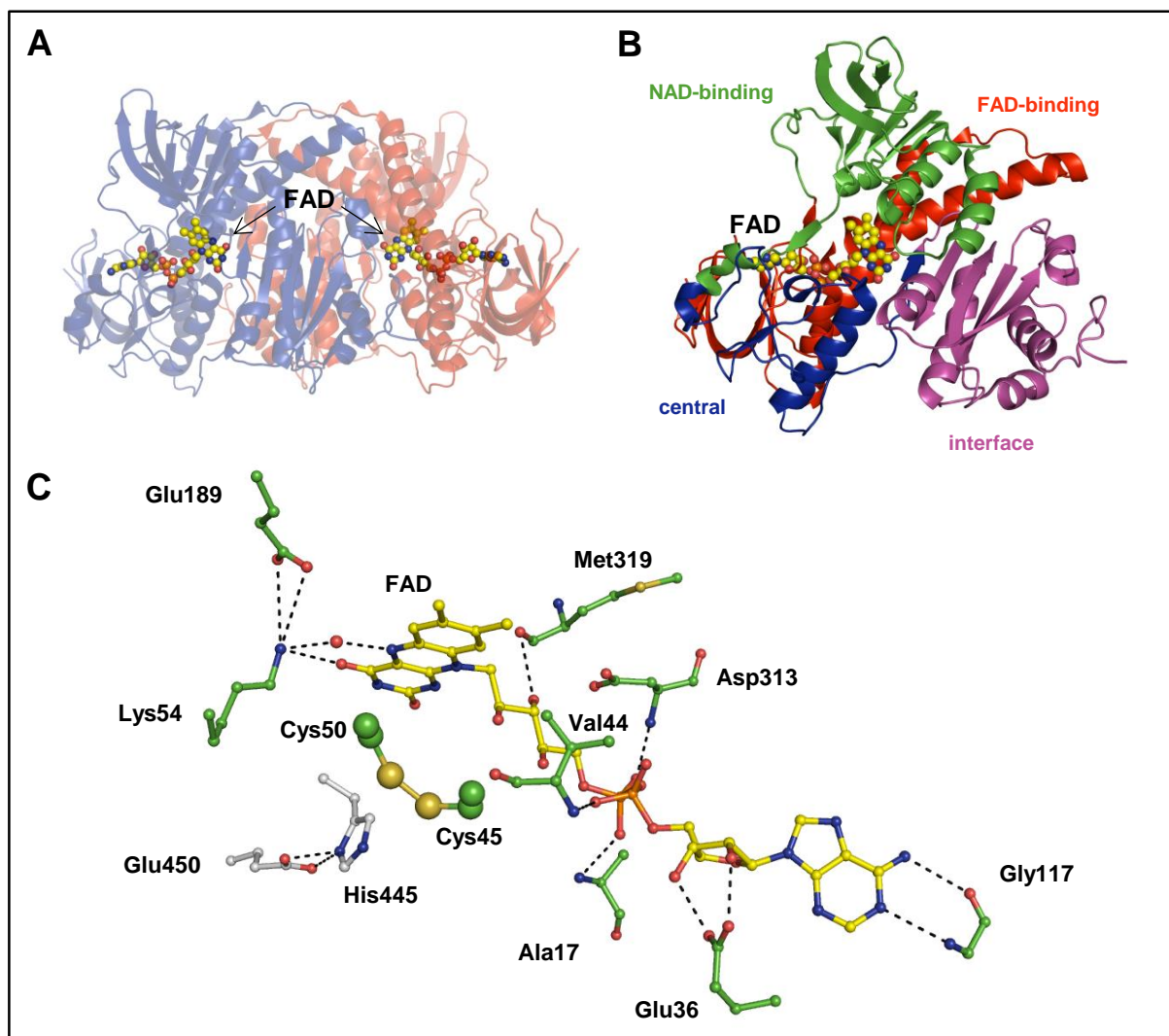


Figure 1.4 Crystal structure of *EcE3*.

(A) Structure of the biologically functional dimer of *EcE3* (Chandrasekhar et al. 2013) in cartoon representation with the bound flavin cofactor (ball representation). Individual monomers are shown in blue and red. (B) Domain structure of *EcE3* in cartoon representation: N-terminal FAD-binding (red), NAD-binding domain (green), central domain (blue) and C-terminal interface domain (purple). (C) Interactions of the FAD molecule with E3. The enzymatic disulfide (ball representation) is located on the *si* face of the flavin. The nearby histidine is involved in acid/base chemistry. Interactions are indicated by dashed lines. Residues from the neighboring subunit are shown in light grey.

1.5 Catalytic Mechanism of *E. coli* Lipoamide Dehydrogenase

Generally, the catalytic cycles of flavoenzymes can be divided into reductive and oxidative half-reactions (Figure 1.5). In the reductive half-reaction, the oxidized flavoenzyme is reduced by the first substrate, yielding in a reduced flavoenzyme. In the oxidative half-reaction, a second substrate oxidizes the reduced enzyme (Palfey and Fagan 2010). This usually results in ping-pong kinetic mechanisms since often the product of the reductive half-reaction dissociates prior to the beginning of the oxidative half-reaction (Palfey and Fagan 2010; Reed 1973).

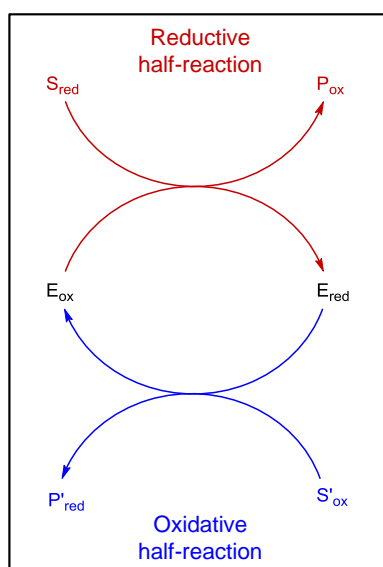


Figure 1.5 Typical catalytic cycle of flavoenzymes.

The ping-pong kinetic mechanism of *EcE3* involves two half-reactions, each completely reversible and has been studied in detail (Argyrou et al. 2003, 2002; Sahlman and Williams 1989; Wilkinson and Williams 1979, 1981). In the reductive half-reaction, the substrate dihydrolipoamide binds to the oxidized state of *EcE3* (E_{ox}), and Cys45 forms a mixed disulfide with the substrate. Transfer of electrons yield to thiolate formation of Cys50 and thus the two-electron reduced state (EH_2). This reaction is general-acid-base catalyzed by an essential and conserved catalytic diad located at the C-terminus of the adjacent monomer of the homo-dimeric enzyme (Benen, Van Berkel, Dieteren, et al. 1992; Kim and Patel 1992b). Release of lipoamide completes the reductive half-reaction (Figure 1.6). In the oxidative half-reaction, NAD^+ binds to the two-electron reduced state of the enzyme (EH_2). This induces an internal electron transfer from the redox active disulfide towards the flavin cofactor yielding in a transiently formed $[NAD^+-FADH_2]$ intermediate. The internal electron transfer is thought to proceed via a covalent adduct between Cys50 and the C4a position of the FAD, which is termed

“FAD-C4a-cysteinyl adduct” (Miller et al. 1990; Thorpe and Williams 1976a, 1976b). The flavin is immediately reoxidized by NAD^+ generating NADH and the oxidized form of the enzyme (E_{ox}). Release of NADH completes the oxidative half-reaction preparing the enzyme for another round of catalysis.

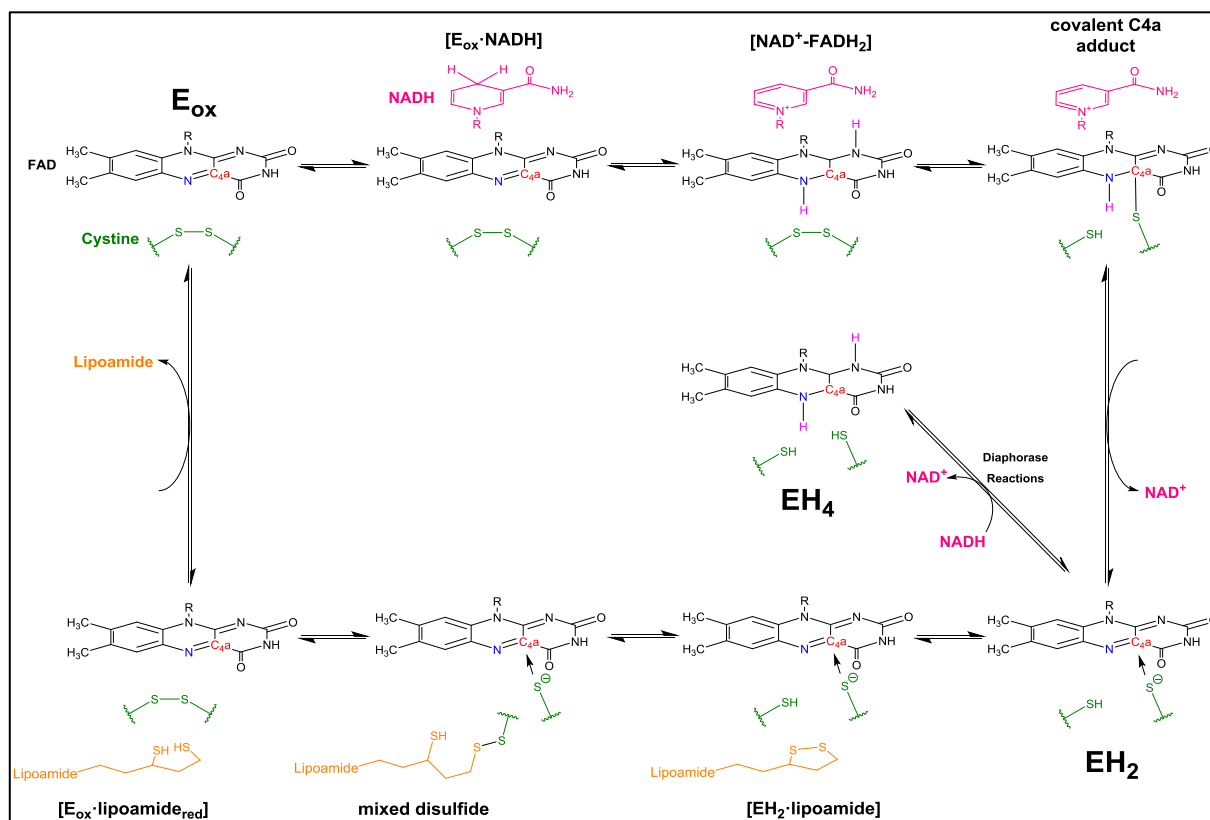


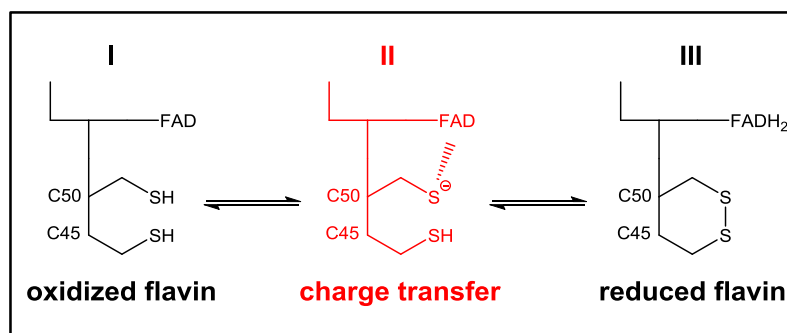
Figure 1.6 Simplified, general reaction scheme of lipoamide dehydrogenases.

E3-catalyzed oxidation of reduced lipoamide cofactors and subsequent generation of NADH: R = ribityl-ADP, E_{ox} oxidized, EH_2 = two-electron reduced and EH_4 = four-electron reduced state of the enzyme. Reaction intermediates are indicated. For explanation see text.

During catalysis, the enzyme cycles between the oxidized and two-electron reduced states. However, the *E. coli* enzyme is easily overreduced by a small molar excess of NADH to the four-electron reduced state (EH_4) (Williams 1965). In this catalytically inactive dead-end complex, the redox-active disulfide and the flavin are reduced (Figure 1.6). NAD^+ has an activating effect because the pyridine nucleotide can oxidize the dead-end complex, increasing the amount of catalytic active EH_2 (Matthews, Ballou, and Williams 1979). The severe susceptibility to overreduction by NADH, and thus NADH inhibition, is based on the redox potentials of the EH_2 and EH_4 states. At first, comparison of the reduction potentials for the two redox couples of lipoamide dehydrogenases from *E. coli* (-264 and -317 mV, respectively) (Wilkinson and Williams 1979), pig heart (-280 and -346 mV) (Matthews and Williams 1976), and *M. tuberculosis* (-309 and -382 mV) (Argyrou et al. 2002)

demonstrate that the *E. coli* enzyme has the most positive E_{ox}/EH_2 and EH_2/EH_4 redox couples. Secondly, the redox potentials of the EH_2 and EH_4 pairs are closer than in the enzymes from the aforementioned organisms. Consequently, due to the closer potentials, the EH_2 state of the *E. coli* enzyme exists as a fast equilibrating mixture of three species: the oxidized flavin–dithiol species (Figure 1.7I), the oxidized flavin–thiolate charge transfer (II), and the reduced flavin-disulfide (III), all harboring different spectroscopic properties (Wilkinson and Williams 1979). The physiological consequences of the NADH inhibition of *EcE3* are highlighted in a following chapter (1.6).

Figure 1.7 Distribution of species at the EH_2 level in *EcE3*. Species II has a characteristic red color derived from the charge transfer interaction between Cys50-thiolate and FAD - adapted from (Wilkinson and Williams 1979).



1.6 The Physiological Importance of *E. coli* Lipoamide Dehydrogenase

As a facultative heterotroph *Escherichia coli* is able to grow under aerobic and anaerobic conditions. While growing aerobically glucose is metabolized using glycolysis, PDH complex and citric acid cycle. The NADH generated during these reactions is oxidized by the final electron acceptor oxygen. In contrast, under anaerobic growth glycolytic intermediates serve as electron acceptors to maintain the redox balance. However, this leads to an increased $NADH/NAD^+$ ratio compared to aerobic growth (Graef et al. 1999; Snoep et al. 1993). In both growth modes, pyruvate is the key intermediate in the catabolism in *E. coli*. Its subsequent conversion by either pyruvate formate lyase (PFL) or the PDH complex can be claimed as the major switch between mixed acid fermentation and the citric acid cycle and subsequent respiration. Though PDH activity is obligate for aerobic growth of the bacterium, its activity was also detected in cell extracts grown under anaerobic conditions albeit at a very low or nearly undetectable amount (Graef et al. 1999; Smith and Neidhardt 1983; Snoep et al. 1993).

The regulation of *E. coli* PDH activity is rather complex, but the E1 and the E3 components have been identified as main targets for regulation several decades ago (Hansen and Henning 1966). Whereas the mammalian E1 is regulated by phosphorylation (Cooper, Randle, and Denton 1974; Hucho et al. 1972;

Seifert et al. 2007), the availability of metabolic intermediates regulate the *E. coli* E1 activity. On the one hand acetyl-CoA inhibits E1 (Hansen and Henning 1966) on the other hand glycolytic intermediates enhance the PDH activity presumably by accelerating the carbon flow towards the citric acid cycle (Shen et al. 1968). As the most efficient activator fructose-1,6-bisphosphate was identified, however PDH activity is also enhanced by fructose-6-P, glyceraldehyde-3-P, phosphoenolpyruvate, dihydroxyacetone-P and glucose-6-P.

EcE3 is regulated by the ratio of reduction equivalents rather than by glycolytic intermediates. As described by WILKINSON & WILLIAMS *EcE3* suffers from severe product inhibition by NADH due to reduction of the catalytically active two-electron reduced enzyme intermediate (EH₂) to the inactive four-electron reduced form (EH₄) while NAD⁺ is able to oxidize this dead-end complex, increasing the amount of EH₂ (Wilkinson and Williams 1981). This inhibitory effect of NADH not only holds true for the isolated *EcE3* but also for the entire *E. coli* PDH (Bisswanger 1981; Hansen and Henning 1966; Wilkinson and Williams 1981). Thus, PDH activity is also modulated by the NAD⁺/NADH pool affecting the redox state of *EcE3*.

As aforementioned, anaerobically growing *E. coli* metabolizes pyruvate with the help of the pyruvate-formate lyase complex (FHL) to acetyl-CoA whereas the reducing equivalents are temporarily stored as formate (Clark 1989). Succinate is only a minor fermentation product (Fraenkel 1996) and lactate is mainly formed under strong acidic growth conditions (Clark 1989). Formate is finally removed by disproportionation to H₂ and CO₂ without influencing the NADH/NAD⁺ ratio (Rosentel et al. 1995). The remaining NADH derived from preceding glycolytic steps is then oxidized using acetyl-CoA as electron acceptor with the penultimate production of ethanol by aldehyde-alcohol dehydrogenase (Clark 1989). However, the reduction of acetyl-CoA to ethanol requires two equivalents of NADH and therefore the degradation of the remaining acetyl-CoA molecule to acetate via acetyl phosphate by phosphotransacetylase and acetate kinase is mandatory. Hence, the fermentation profile of *E. coli* harbors equimolar amounts of ethanol and acetate (Figure 1.8A).

E. coli strain AH242 lacks pyruvate-formate lyase (*pflB*) and fermentative lactate dehydrogenase (*ldhA*) and is therefore defective for anaerobic growth (Clark 1989; Kim, Ingram, and Shanmugam 2007). Kim *et al.* isolated and described an *E. coli* mutant (SE2378) derived of strain AH242 that produced ethanol as the main fermentation product (Kim et al. 2007). The mutation was identified as a single change in the *EcE3* amino acid sequence (Glu354→Lys354). This mutation led to a reduced sensitivity of *EcE3* - and thus the PDH complex - towards NADH inhibition leading to PDH activity under anaerobic growth conditions which concomitantly changed the fermentation profile of mutant SE2378 (Figure 1.8B) (Kim, Ingram, and Shanmugam 2008). With the PDH being active under anaerobic conditions mutant SE2378 produces four NADH molecules during the degradation of one molecule glucose to two acetyl-CoA molecules. In order to maintain the redox balance these four NADH molecules are then reoxidized by reduction of the two acetyl-CoA molecules to two ethanol

molecules by the alcohol/acetaldehyde dehydrogenase (*adhE*). This study further underpinned the physiological importance of *EcE3* and showed that even a single amino acid mutation has the potential to change a bacterium's growth behavior.

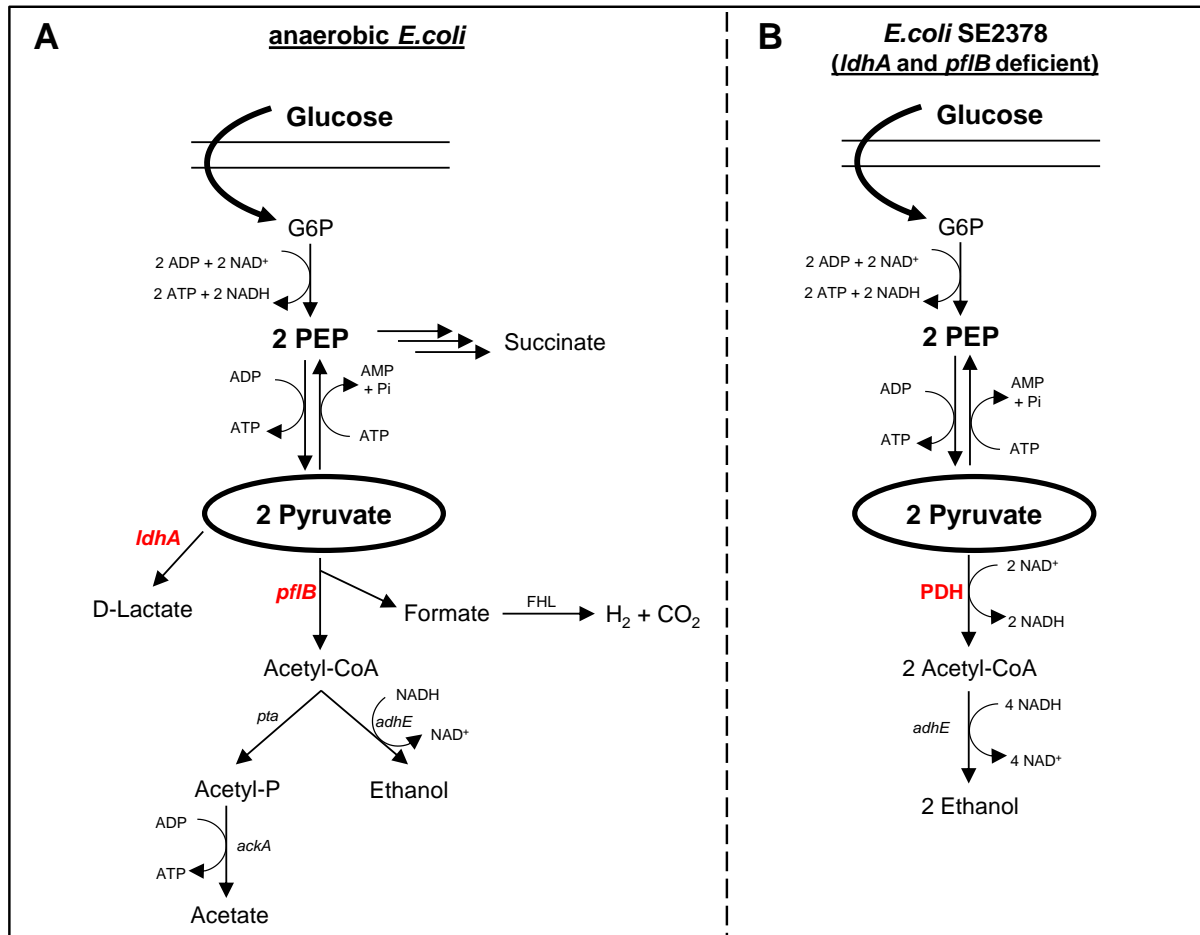


Figure 1.8 Comparison of mixed acid pathway for glucose fermentation.

(A) pathway in native *E. coli* and (B) in the *ldhA* and *pflB* deficient *E. coli* strain SE2378.

G6P, glucose 6-phosphate; PEP, phosphoenolpyruvate; *ldhA*, lactate dehydrogenase; *pflB*, pyruvate formate lyase; FHL, formate hydrogenlyase complex; *pta*, phosphotransacetylase; *adhE*, aldehyde-alcohol dehydrogenase; *ackA*, acetate kinase; PDH, pyruvate dehydrogenase complex.

1.7 The Relevance of Covalent Flavin-C4a-cysteinyl Adducts

As described in the previous chapter (1.5) the FAD-C4a-cysteinyl adduct is a central intermediate during catalysis of *E. coli* lipoamide dehydrogenase. It is also found in other flavoenzymes belonging to the family of pyridine nucleotide-disulfide oxidoreductases, like glutathione reductase and mercuric reductase (Miller et al. 1990; Thorpe and Williams 1981). In these metabolic enzymes, the adduct ensures internal electron transfer from redox active disulfides to the flavin cofactor and vice versa. However, the function of FAD-C4a-cysteinyl adducts is not limited to electron transfer reactions, which involves thiol/disulfide chemistry. The FAD-C4a-cysteinyl adduct is also a central reaction intermediate in a class of flavoprotein light sensors: the light-oxygen-voltage (LOV) domains. These photosensor proteins can be found in plants, fungi, archaea and bacteria and are a subset of the PER-ARNT-SIM domain superfamily containing a noncovalently bound flavin cofactor (FMN or FAD) (Conrad et al. 2014). Using diverse output and effector domains, the photochemistry of LOV domains acts as signal transducer helping to mediate a variety of physiological functions like phototropism, chloroplast and leaf movements, and stomatal opening (Möglich et al. 2010). Blue light exposure induces the formation of a covalent FAD-C4a-cysteinyl adduct between the flavin and a conserved cysteine residue located at the active site (Figure 1.9). However, the structural rearrangements are not limited to the adduct site. Adduct formation requires the flavin N5 becoming protonated which causes a flipping of a conserved glutamine residue interacting with N5 (Figure 1.9B). This flipping was identified as a major event during signal transmission from the LOV domain to the output and effector domains (Raffelberg et al. 2011).

The LOV domain photocycle has been investigated thoroughly, but several key details are controversially discussed (Kennis and Groot 2007; Losi and Gärtner 2011; Zoltowski and Gardner 2011). In the dark state, the flavin is oxidized harboring an absorption maximum at ~447 nm and is not attached to the protein backbone. The blue light induced covalent bond formation between flavin and the conserved cysteine leads to a hypsochromic shift resulting in a new absorption maximum at ~390 nm (Figure 1.9). The intermediate states prior to adduct formation are fast and comprise formation of an excited singlet state (S1) followed by an intersystem crossing yielding an excited triplet state (Alexandre et al. 2009; Pfeifer et al. 2009). The mechanism of the following adduct formation is a matter in controversy. On the one hand, the reaction is thought to proceed via an ionic intermediate, where a proton is transferred to flavin N5 before bond formation (Kennis and Groot 2007; Losi and Gärtner 2011, 2012; Zoltowski and Gardner 2011), on the other hand, further data suggest that the flavin cofactor is unprotonated in the excited triplet state immediately before reacting with the cysteine (Alexandre et al. 2009; Pfeifer et al. 2009). There is also some evidence for a neutral semiquinone intermediate between the triplet and the adduct state (Bauer et al. 2011) so that the identities of the intermediates prior to adduct formation are not quite clear. In addition, the proton source for N5 protonation has not been ultimately identified (Conrad et al. 2014).

The major difference between FAD-C4a-cysteiny adducts in LOV domain photoreceptor proteins and pyridine nucleotide-disulfide oxidoreductases is the lifetime of the adduct. In the oxidoreductases the intermediate is only transiently formed making a direct observation tedious work (Miller et al. 1990; Thorpe and Williams 1976b). On the contrary, LOV domains provide a surrounding which keeps the covalent adduct stable for at least 500 ms, but the lifetime can even be expanded to hours (Conrad et al. 2014). The thermally driven recovery back to the dark state requires flavin N5 deprotonation, covalent bond breakage and protonation of the cysteine sulfur atom (Losi and Gärtner 2012). Generally, the rates of adduct decay depend on solvent access to the active site, the hydrogen bonding network around the flavin and its electronic environment (Conrad et al. 2014). However, it is suggested that the (de)protonation of N5 is the rate limiting step in the LOV photocycle (Kottke et al. 2003; Zoltowski, Vaccaro, and Crane 2009).

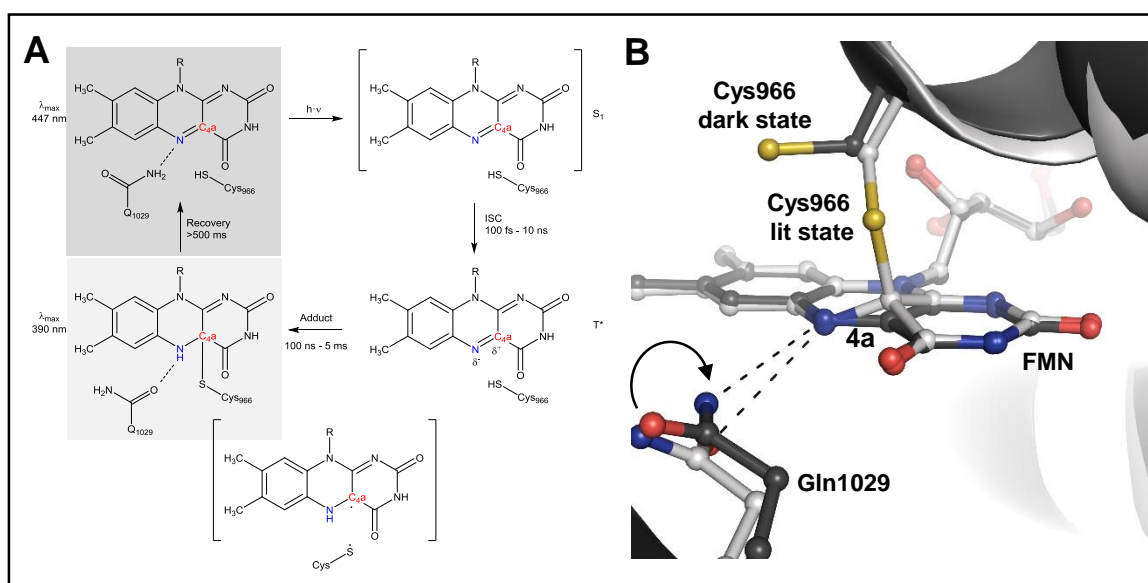


Figure 1.9 LOV domain photocycle and light-driven structural rearrangement.

(A) Light excites the dark-state FMN to a singlet state (S_1) followed by an intersystem crossing (ISC) to an excited triplet state (T^*). T^* stimulates reaction of the C4a position (red) with an active site Cys residue to form a covalent adduct. Protonation of N5 (blue) during adduct formation leads to reorientation of a conserved glutamine residue (adapted from (Conrad et al. 2014)). (B) Crystal structure of *Adiantum* LOV2 in dark (PDB: 1G28) and in lit state (PDB: 1JNU). Light induces covalent bond formation between Cys966 and C4a and the concomitant switch of Gln1029 from a H-bond donor in dark state to an H-bond acceptor towards N5 in lit state.

1.8 Motivation

Lipoamide dehydrogenases have been extensively studied over the last decades and thus a detailed kinetic and structural knowledge about the mode of action of these enzymes could be gained. However, central reactions steps still lack both spectroscopic and structural information. The goal of this project is therefore to provide these information using the enzyme of *E. coli* (*EcE3*). Major emphasis will thereby be devoted to the spectroscopic and structural detection of the covalent FAD-C4a-cysteinyl adduct. The existence of this central intermediate has been predicted, but a direct evidence, especially in wild type enzymes, has not yet been given. Moreover, the reasons for its supposed transience are not fully understood (Argyrou et al. 2002). Structural data might help to explain the basis for the short-lived nature of the intermediate.

Spectroscopic analysis of the wild type enzyme and active-site mutants with conventional and stopped-flow UV-Vis spectroscopy shall be used to detect the FAD-C4a-cysteinyl adduct. Both single wavelength or photodiode array setups may help to identify active site residues which are crucial for adduct formation and/or the reported transience of the intermediate. The Investigations will be carried out from the forward and the reverse direction of the reaction cycle. NADH is a commonly used substrate which allows the investigation of different enzyme species harboring distinct spectroscopic signatures (Argyrou et al. 2002; Matthews and Williams 1976). However, the usage of NADH only allows the tracking of the oxidative half-reaction. Therefore, it is aimed to isolate an entire lipoyl domain from the E2 component of *EcPDHc* which may serve as an *in vivo* substrate for *EcE3* after reduction of its lipoamide cofactor. This would allow the tracking of the reductive half-reaction with the aforementioned methods and further allow investigations in the field of protein-protein interactions.

Besides the characterization of the FAD-C4a-cysteinyl adduct a further intermediate state of the enzyme is of primary interest. The two-electron reduced state (EH_2) of *EcE3* is the catalytically active species prior to generation of NADH. Detailed spectroscopic studies on this species have been carried out, but the ultimate factors stabilizing the anionic form of the cysteine facing the flavin cofactor remain unclear (Hopkins and Williams 1995a; Wilkinson and Williams 1979). An illumination of the thiolate stabilization by means of structural information is therefore obligate to further expand the knowledge about the EH_2 state.

The three-dimensional structure of the lipoamide dehydrogenases enzyme revealed a striking similarity to the active site of LOV (light-oxygen-voltage) blue-light receptors (Chandrasekhar et al. 2013; Conrad et al. 2014; Mattevi et al. 1991). A common feature of the oxidoreductases and the light-sensing proteins is the formation of a covalent FAD-C4a-cysteinyl adduct during the respective reaction cycle (1.7). This study attempts the conversion of the metabolic *EcE3* into a pseudo-LOV blue-light-sensing protein via structure-guided protein engineering which is capable of a light-driven

C4a-cysteinyl adduct formation. If successful, a novel system for the light-driven generation of reducing equivalents could be obtained. An investigation of the photochemical response of re-engineered *EcE3* variants using steady-state and time-resolved absorption spectroscopy.

Further attention will be dedicated to the dimer interface of *EcE3*. It was demonstrated that the dimer interaction modulates the redox properties of the active site flavin cofactor in the *A. vinelandii* enzyme (Benen, Van Berkel, Veeger, et al. 1992). In addition, mutations in the same region reduced the sensitivity towards NADH inhibition of *EcE3* and concomitantly affected the entire fermentation profile of *E. coli* (Kim et al. 2008). Hence, the role of the interface is also of interest and will be investigated with respect to its ability to act as determinate for the flavin redox potential.

2 Material and Methods

2.1 Material

2.1.1 Fine chemicals

Compound	Supplier
Acetic acid	Carl Roth GmbH & Co KG, Karlsruhe
Acrylamide	Carl Roth GmbH & Co KG, Karlsruhe
Agar	AppliChem GmbH, Darmstadt
Agarose	AppliChem GmbH, Darmstadt
Aldrithiol (4,4'-dithiopyridine)	Sigma-Aldrich GmbH, Deisenhofen
Ammonium sulfate	AppliChem GmbH, Darmstadt
Ammonium peroxodisulfate	Carl Roth, Karlsruhe
Calcium chloride	Carl Roth GmbH & Co KG, Karlsruhe
Carbenicillin disodium salt	AppliChem, Darmstadt
Coomassie Brilliant blue G-250	AppliChem GmbH, Darmstadt
Dithiothreitol (DTT)	AppliChem GmbH, Darmstadt
Ethylenediaminetetraacetic acid (EDTA)	AppliChem GmbH, Darmstadt
Ethanol	Carl Roth GmbH & Co KG, Karlsruhe
FAD	AppliChem GmbH, Darmstadt
FMN	AppliChem GmbH, Darmstadt
D-Glucose	AppliChem GmbH, Darmstadt

Glycerol (99 %)	AppliChem GmbH, Darmstadt
Glycine	Carl Roth GmbH & Co KG, Karlsruhe
Hydrochloric acid (37%)	Carl Roth GmbH & Co KG, Karlsruhe
Imidazole	AppliChem GmbH, Darmstadt
Kanamycin sulfate	Carl Roth GmbH & Co KG, Karlsruhe
Lipoamide	Sigma-Aldrich GmbH, Deisenhofen
Lipoic acid	Sigma-Aldrich GmbH, Deisenhofen
Lumichrom	Sigma-Aldrich GmbH, Deisenhofen
Magnesium chloride, hexahydrate	Carl Roth GmbH & Co KG, Karlsruhe
Magnesium sulfate	Carl Roth GmbH & Co KG, Karlsruhe
β -Mercaptoethanol	Carl Roth GmbH & Co KG, Karlsruhe
NAD ⁺ / NADH	AppliChem GmbH, Darmstadt
Phenylmethylsulfonyl fluoride	AppliChem GmbH, Darmstadt
Phosphoric acid (85 %)	Carl Roth GmbH & Co KG, Karlsruhe
Potassium chloride	Carl Roth GmbH & Co KG, Karlsruhe
Potassium dihydrogen phosphate	Carl Roth GmbH & Co KG, Karlsruhe
Potassium hydroxide	AppliChem GmbH, Darmstadt
Polyethylene glycol (PEG) 400	Fluka Chemie AG, Buchs, Switzerland
Polyethylene glycol (PEG) 4000	Carl Roth GmbH & Co KG, Karlsruhe
Riboflavin	Sigma-Aldrich GmbH, Deisenhofen
Sodium chloride	AppliChem GmbH, Darmstadt
N,N,N',N'-Tetramethylethyldiamin	Carl Roth GmbH & Co KG, Karlsruhe
Thiamine hydrochloride	AppliChem GmbH, Darmstadt
Tris(2-carboxyethyl)phosphine hydrochloride	Sigma-Aldrich Chemie, Deisenhofen
Tryptone	AppliChem GmbH, Darmstadt
Yeast extract	AppliChem GmbH, Darmstadt

2.1.2 Devices

ACQUITY UPLC™ System	Waters Corporation, Milford, USA
Äkta Prime Plus	GE Healthcare, Munich
Äkta Purifier	GE Healthcare, Munich
Agilent 6540 UH Accurate-Mass-Q-TOF MS	Agilent Technologies, Böblingen
Agilent 8453 UV-visible spectrophotometer	Agilent Technologies, Santa Clara, USA
Autoclave	Zirbus, Bad Grund
Balance Kern EW	Kern, Balingen-Frommern
Balance Kern ABJ	Kern, Balingen-Frommern

Centrifuge Avanti J-20 XPIJA-20	Beckmann Coulter, Krefeld
Centrifuge Avanti J-30 I	Beckmann Coulter, Krefeld
Centrifuge Hettich Universal 320 R	Hettich, Tuttlingen
Conducting meter FiveEasy	Mettler-Toledo, Giessen
<u>EPR</u>	
Spectrometer: Lab-built X-Band spectrometer with:	
Microwave bridge ER 041 MR	Bruker, Rheinstetten
Microwave controller ER 048 R	Bruker, Rheinstetten
Magnet power supply ER 081 S	Bruker, Rheinstetten
Field controller BH 15	Bruker, Rheinstetten
Cavity resonator ER 4122 SHQ E	Bruker, Rheinstetten
SR 810 lock-In detector	Stanford Research Systems, Sunnyvale, USA
53181A frequency counter	Agilent Technologies, Santa Clara, USA
ESR 910 cryostat	Oxford Instruments, East Grinstead, UK
ITC503 temperature controller	Oxford Instruments, East Grinstead, UK
Sample tubes: 3.0 mm/3.9 mm diameter quartz	Qsil, Ilmenau
<i>Frac-920</i> Fraction Collector	GE Healthcare, Munich
Incubator Unitron	HT Infors, Bottmingen
Incubator CrystalMotion	Rigaku, Kent, England
iTC ₂₀₀ MicroCalorimeter	Microcal, Northampton, USA
LCT Premier™ ESI-TOF-MS	Waters Corporation, Milford, USA
MALDI-TOF Reflex III	Bruker Daltonics, Bremen
Carrier MTP 384 polished steel	Bruker Daltonics, Bremen
Microfluidizer 110 S	Microfluidics, Newton, USA
pH meter FiveEasy	Mettler-Toledo, Giessen
Pipette robot Phoenix RE	Art Robbins Instruments, USA
Rotor JA-30.50 Ti	Beckmann Coulter, Krefeld
Rotor JLA 8.1000	Beckmann Coulter, Krefeld
SDS gel electrophoresis SE250	Hoefler, Holliston, USA
UPLC eLambda 800 nm	Waters Corporation, Milford, USA
X-ray detector mar345	Marresearch, Norderstedt
X-ray diffractometer RU-H3R	Rigaku/MSC, Japan
<u>Spectrometers</u>	
Chirascan (CD)	Applied Photophysics, GB
Stopped-flow system SX.20 MV	Applied Photophysics Ltd., UK
NanoDrop2000	Thermo Scientific, Schwerte
V-650 (UV/Vis)	JASCO, Gross-Umstadt

Stereomicroscope SZ 60	Olympus, Japan
Thermocycler TProfessional	Biometra, Göttingen
Vortex-Genie 2	Scientific Industries, New York, USA
Water bath Isotemp 202	Fisher Scientific, Schwerte
<u>Commodities</u>	
0.2 and 0.45 µm Filter	Sartorius AG, Göttingen
Circular cover slides, 18 mm	Jena Bioscience, Jena
Crystallization plates (24 well)	Costar Corning, Inc., USA
UV- and CD-cuvettes	Hellma, Müllheim
Spin-X® UF concentrator	Corning, Corning, USA
ZipTip _{C18} Pipette Tips	Millipore, Billerica, USA

2.1.3 Chromatography Columns

HiPrep™ 26/10 Desalting	GE Healthcare, Munich
HisTrap™ Ni-NTA-Sepharose (25 ml)	GE Healthcare, Munich
Superdex™ 200 XK 16/600	GE Healthcare, Munich

2.1.4 Molecular Weight Marker

Unstained Protein Molecular Weight Marker	Thermo Scientific, Schwerte
Peptide Calibration Standard	Bruker Daltonics, Bremen

2.1.5 Kit-Systems

NucleoSpin® Extract II	Macherey-Nagel, Düren
NucleoSpin® Plasmid	Macherey-Nagel, Düren
QuikChange site directed mutagenesis kit	Stratagene, USA

2.1.6 Materials for Molecular Biology

6X DNA Loading Dye	Thermo Scientific, Schwerte
dNTPs (Mix 10 mM)	Thermo Scientific, Schwerte
FastAP™ Thermosensitive Alkaline Phosphatase	Thermo Scientific, Schwerte
GeneRuler™ 1 kb DNA Ladder	Thermo Scientific, Schwerte
HF-buffer	Thermo Scientific, Schwerte

Magnesium chloride (25 mM)	Thermo Scientific, Schwerte
Phusion Polymerase	Thermo Scientific, Schwerte
T4 DNA Ligase	Thermo Scientific, Schwerte
T4 DNA Ligase Buffer	Thermo Scientific, Schwerte
<i>Taq</i> Buffer (10-fold)	Thermo Scientific, Schwerte
<i>Taq</i> Polymerase	Thermo Scientific, Schwerte

2.1.7 Restriction Endonucleases

NdeI	Thermo Scientific, Schwerte
XhoI	Thermo Scientific, Schwerte
DpnI	Thermo Scientific, Schwerte

2.1.8 Bacterial Strains

Strain	Genotype	Reference
E. coli BL21 (DE3)	<i>F ompT hsdS_B (r_B⁻ m_B⁻) gal dcm</i> (DE3)	Invitrogen
E. coli BL21 Star™ (DE3)	<i>F ompT hsdS_B (r_B⁻ m_B⁻) gal dcm rne131</i> (DE3)	Invitrogen
E. coli DH5α™	<i>F Φ80lacZΔM15 Δ(lacZYA-argF) U169 recA1 endA1 hsdR17 (r_K⁻, m_K⁺) phoA supE44 λ⁻ thi⁻1 gyr96 relA1</i>	Invitrogen

2.1.9 Vectors

pET15b-EcE2	GENEART, Regensburg
pET28a	Merck KGaA, Darmstadt
pGS523	John R. Guest, University of Sheffield
pET-SUMO	Invitrogen, Darmstadt

2.1.10 Enzymes

DNase I	AppliChem, Darmstadt
Lysozyme	AppliChem, Darmstadt
SUMO-Protease	provided by Dr. Stefan Lüdtko
Thrombin	Sigma-Aldrich GmbH, Deisenhofen
Trypsin	Promega, Mannheim

2.1.11 Crystallization Screens

Ammonium sulfate	Qiagen, Hilden
JCSG	Molecular Dimensions, Suffolk, UK
JBScreen Nuc-Pro HTS	Jena Bioscience, Jena
Morpheus screen	Fabrice Gorrec, Cambridge, UK
Natrix HT	Hampton Research, Aliso Viejo, USA
PGA-LM HT-96	Molecular Dimensions, Suffolk, UK
ProPlex	Molecular Dimensions, Suffolk, UK

2.1.12 Software

CCP4 suite	Winn et al., 2011
Chromas 1.45	McCarthy, C., Griffith University, Australia
Crystallography & NMR System (CNS)	(Brunger 2007)
ESPrpt 3.0	http://esprpt.ibcp.fr/ESPrpt/ESPrpt/index.php
Expasy, ProtParam	http://web.expasy.org/protparam/
FlexAnalysis	Bruker Daltonics, Bremen
Gene runner V.3.05	Hastings Software, Inc.
Origin-7	OriginLab Corporation, USA
PeptideCutter	http://web.expasy.org/peptide_cutter/
Phenix suite	Adams et al., 2010
PYMOL	Schrödinger, LLC
Mass Hunter Qualitative Analysis software (B.06.00)	Agilent Technologies, Böblingen, Germany
MassLynx V4.1 SCN779	Waters Corporation, Milford, USA
METLIN	https://metlin.scripps.edu/index.php
MicroCal ITC-ORIGIN Analysis Software	Microcal, Northampton, USA
MOLPROBITY	http://molprobity.biochem.duke.edu/
Multalin	Corpet 2010
SigmaPlot Version 11.0	Systat Software, Inc.

2.2 Methods

2.2.1 Molecular Biology

The gene of *EcE3* was amplified from pGS523 (Machado, Clark, and Guest 1992), kindly provided from Prof. John Guest (University of Sheffield), and cloned into the pET28a expression vector using the XhoI and NdeI restriction sites. This expression construct encodes for *EcE3* with an N-terminal hexa-histidine tag followed by a thrombin cleavage site. The N-terminal tag extends *EcE3* by 20 amino acids, of which three will remain after thrombin cleavage. The amino acid sequences of all purified proteins are shown in the appendix (5.1).

The *EcLip3* gene encodes for amino acids 201 – 286 of the *E. coli* E2 component and thus represents the isolated innermost lipoyl domain. The *EcLip3* gene was amplified from pET15b-*EcE2* and cloned into the target vector pET-SUMO using the TA cloning[®] strategy according to the Champion™ pET SUMO Protein Expression System manual.

To introduce specific amino acid exchanges within the sequence of *EcE3* site-directed mutagenesis was used. Variants were generated according to the QuikChange-Kit (Stratagene, USA) with oligonucleotides containing the mutated codons. Double variants were generated starting with a single mutated plasmid as template. All used template amplification and mutagenesis primer pairs are listed in Table 2.1.

Table 2.1 List of used primer pairs (Synthesized by Sigma-Aldrich, Taufkirchen).

Restriction sites are underlined, unspecific overhangs are uncapitalized, mutations sites are shown in bold face type.

<u>Template amplification primer pairs</u>	
<i>Primer name</i>	<i>Nucleotide sequence (5'-3')</i>
E3_NdeI_2for	accatg <u>catatg</u> AGTACTGAAATCAA AACTCAGGTCGTGG
E3_Xho_rev	tagcct <u>ctcgag</u> ttaCTTCTTCTTCGCTTTCGGGTTCCGGC
Lip3-201for	GCACCAGCGGCTGGCGTG
Lip3-286for	tcattaCGCAGGCGCTGCGCCTTC
<u>Mutagenesis primer pairs</u>	
<i>Primer name</i>	<i>Nucleotide sequence (5'-3')</i>
E3_Y19F_for	GGCCCCGCAGGTT TTC TCCGCTGCCTTCC
E3_Y19F_rev	GGAAGGCAGCGG GAA ACCTGCGGGGCC

E3_C45A_for	CCTTGGCGGTGTT <u>GCC</u> CTGAACGTCGGC
E3_C45A_rev	GCCGACGTTCAGG <u>GCA</u> ACACCCGCCAAGG
E3_C45S_for	CCTTGGCGGTGTT <u>TCC</u> CTGAACGTCGGC
E3_C45S_rev	GCCGACGTTCAG <u>GGA</u> AACACCCGCCAAGG
E3_C50A_for	GCCTGAACGTCGGC <u>GCT</u> ATCCCTTCTAAAGCACTGC
E3_C50A_rev	GCAGTGCTTTAGAAGGGAT <u>AGC</u> GCCGACGTTCAGGC
E3_C50S_for	GCCTGAACGTCGGC <u>TCT</u> ATCCCTTCTAAAGCACTGC
E3_C50S_rev	GCAGTGCTTTAGAAGGGAT <u>AGA</u> GCCGACGTTCAGGC
E3_C50M_for	GCCTGAACGTCGGC <u>ATG</u> ATCCCTTCTCAAGC
E3_C50M_rev	GCTT <u>GAGA</u> AGGGAT <u>CAT</u> GCCGACGTTCAGGC
E3_K54Q_for	GGCTGTATCCCTTCT <u>CAA</u> GCACTGCTGCACG
E3_K54Q_rev	CGTGCAGCAGTGCT <u>TTG</u> AAGAAGGGATACAGCC
E3_E189Q_for	GGTATCATCGGTCTG <u>CAA</u> ATGGGCACCGTTTACC
E3_E189Q_rev	GGTAAACGGTGCCCAT <u>TTG</u> CAGACCGATGATACC
E3_E354K_for	CCATCGCCTATACC <u>AAA</u> CCAGAAGTTGCATGG
E3_E354K_for	CCATGCAACTTCTGG <u>TTT</u> GGTATAGGCGATGG
E3_R386A_for	GGGCTGCTTCTGGT <u>GCT</u> GCTATCGCTTCCG
E3_R386A_rev	CGGAAGCGATAGC <u>AGC</u> ACCAGAAGCAGCCC
E3_H445A_for	CCATCCACGCG <u>GCCCC</u> GACTCTGCACG
E3_H445A_rev	CGTGCAGAGTCGG <u>GCG</u> CGCGTGGATGG
E3_E450Q_for	CCCGACTCTGCAC <u>CAG</u> TCTGTGGGCCTGG
E3_E450Q_rev	CCAGGCCACAG <u>ACTG</u> GTGCAGAGTCGGG

2.2.1.1 Concentration Determination of DNA

DNA concentrations were determined spectroscopically using a NanoDrop2000 by measuring the absorption at 260 nm. The following correlation was used to determine the concentrations: $1 A_{260} = 50 \mu\text{g/ml}$ doubled stranded DNA.

2.2.1.2 Agarose Gelelectrophoresis

Agarose gelelectrophoresis was used for analysis of DNA fragments after PCR reactions. Samples were supplemented with DNA loading dye (6 x DNA loading dye: 30 % (v/v) glycerol, 0.25 % (w/v) bromophenol blue) and were separated using a horizontal electrophoresis. Gels typically contained 1 % agarose and 1 x TAE buffer (40 mM Tris, 1 mM EDTA, 20 mM acetate, pH 8.5). For visualization the gel was transferred into a solution containing 2 $\mu\text{g/ml}$ ethidium bromide and incubated for 5-10 min prior to detection under UV light in a gel documentation system.

2.2.1.3 Polymerase Chain Reaction (PCR)

PCR was used for both amplification of gene fragments and for site directed mutagenesis. A standard reaction of a total volume of 50 μl contained 10 μl 5x HF buffer, 1 μl dNTP mix (10 mM), 5-50 ng template DNA, 25 pmol sense and antisense primer, and 0.5 μl Phusion DNA Polymerase (2 U/ μl). The PCR protocol included an initial denaturation step (step 1; 95 °C, 1 min), another denaturation step (step 2; 95°C, 30 s), a primer annealing step (step 3; 50-60 °C, 30 s), an elongation step (step 4; 72 °C, 20 s per kb product), and an end elongation (step 5; 72 °C, 7 min). Steps 2-4 were repeated 25 times. If site-directed mutagenesis PCR was carried out the mixture was supplemented with DpnI after the PCR to digest template DNA (see QuikChange site-directed mutagenesis kit).

2.2.1.4 DNA Sequencing

Correctness of was confirmed using two commercially available sequencing services from Seqlab-Microsynth GmbH, Göttingen and GATC Biotech AG, Cologne.

2.2.1.5 Plasmid Transformation

Transfer of plasmid DNA into different *E. coli* strains was performed using the following standard protocols chemical-competent cells were prepared according to Inoue et al. (Inoue, Nojima, and Okayama 1990). Competent cells were stored at -80 °C. In a standard transformation, 1 μl of plasmid DNA was mixed with 50 μl of chemo-competent *E. coli* cells followed by an incubation step for 20 min on ice. For DNA transformation the cells were heat-shocked for 45 s at 42 °C and subsequently cooled on ice for 2 min. Afterwards, 500 μl of SOC medium (2 % (w/v) tryptone, 0.5 % (w/v) yeast

extract, 0.05 % (w/v) NaCl, 2.5 mM KCl, 10 mM MgCl₂, 2 % (w/v) glucose) was added and the cells were incubated for 45 min at 37 °C under shaking. Transformed cells were selected on LB-agar plates supplemented with the appropriate antibiotic. Final antibiotic concentrations in media were 50 µg/ml kanamycin, or 50 µg/ml carbenicillin.

2.2.2 Protein Chemistry

2.2.2.1 Sodium Dodecyl Sulfate - Polyacrylamide Gel Electrophoresis (SDS-PAGE)

All proteins were analyzed by SDS-PAGE based on a protocol of Laemmli and Weber (Laemmli 1970). The stacking gel consisted of 5 % acrylamide, 125 mM Tris (pH 6.8) polymerized with 0.3 % w/v APS and 0.03 % TEMED, whereas the separating gel contained 12-15 % acrylamide, 375 mM Tris (pH 8.8) polymerized with 0.3 % APS and 0.3 % TEMED. Prior to loading protein samples were mixed with SDS loading buffer (4 % (w/v) glycerol, 80 mM SDS, 150 mM Tris, pH 6.8) and heated to 95 °C for 5 min. Gels were usually run at 1 mA/cm² in SDS running buffer (25 mM Tris, 200 mM glycine und 3.5 mM SDS). After protein separation was completed the gels were stained with 0.25 % (w/v) Coomassie Brilliant Blue in 30 % ethanol and 6 % acetic acid for 30 min and destained in 30 % ethanol and 10 % acetic acid. For short-term storage gels were covered with ddH₂O and kept at room temperature.

2.2.2.2 Protein Expression and Purification of *EcE3* and multiple Variants from pGS523

Expression and purification of *EcE3* was basically described by LINDSEY (Lindsay et al. 2000). The expression plasmid pGS523 (encoding the entire *EcPDHc*) was transformed into chemical competent *E. coli* BL21™ cells. An overnight preculture grown at 37 °C in Luria-Bertani medium containing 50 µg/mL carbenicillin was used to inoculate a main culture of the same medium to an OD₆₀₀ of 0.1. Cells were grown at 37 °C to an OD₆₀₀ of 0.8 and expression was started by addition of 50 µM IPTG and 100 µM FMN. After four hours of expression the cells were harvested by centrifugation at 5000 x g, resuspended in lysis buffer supplemented with lysozyme (tip of a spatula) and DNase I (tip of a spatula). Cell disruption was performed using a Microfluidizer 110 S followed by removal of the cell debris by centrifugation (74,000 x g for 30 min at 4 °C). The supernatant was subjected to a heat precipitation at 65 °C for 10 minutes using a water bath. Precipitated proteins were removed by centrifugation (74,000 x g for 30 min at 4 °C). Subsequently the clarified supernatant was loaded onto a HiLoad™ 26/10 Q Sepharose™ HP anion exchange column equilibrated in buffer A. *EcE3* was eluted using a linear gradient of high salt buffer (buffer B) over two CV. Fractions containing *EcE3* were combined and desalted using a HiPrep™ 26/10 Desalting column equilibrated in buffer C.

Table 2.2 Overview of buffers used for purification of *EcE3* from pGS523

Lysis buffer		Buffer A		Buffer B		Buffer C	
Imidazole	20 mM			Imidazole	20 mM	KH ₂ PO ₄	20 mM
MgCl ₂	1 mM	Imidazole	20 mM	NaCl	1 M	NaCl	100 mM
PSMSF	1 mM		pH 6.5				
	pH 6.5				pH 6.5		pH 7.6

2.2.2.3 Protein Expression and Purification of *EcE3* and multiple Variants from pET28a

For expression, pET28a*EcE3* was transformed into chemical competent *E.coli* BL21 StarTM cells. An overnight preculture grown at 37 °C in Luria-Bertani medium containing 50 µg/mL kanamycin was used to inoculate a main culture of the same medium to an OD₆₀₀ of 0.1. Cells were grown at 37 °C to an OD₆₀₀ of 0.8 and expression was started by addition of 500 µM IPTG. After four hours of expression the cells were harvested by centrifugation at 5000 x g, resuspended in lysis buffer supplemented with lysozyme (tip of a spatula), DNase I (tip of a spatula). Cell disruption was performed using a Microfluidizer 110 S followed by removal of the cell debris by centrifugation (74,000 x g for 30 min at 4 °C). The supernatant was loaded onto a Ni-NTA FF Sepharose FF equilibrated in buffer A and N-terminal His₆tagged-*EcE3* was eluted using high imidazole buffer B in a single step. Appropriate fractions were pooled, desalted with low imidazole buffer and the His-tag was removed by thrombin cleavage in the presence of 5 mM CaCl₂ in the cold room for 12 hours. Cleaved His-tags were trapped by a second cycle of IMAC. Subsequently, the flow through was concentrated and loaded onto a HiLoad 16/600 S200 gel filtration column equilibrated in buffer C. If the His₆-tag remained on *EcE3* the protein was directly desalted against buffer C after the Ni-NTA column. All pET28a*EcE3* variants were expressed and purified to homogeneity according to the method for the wild type.

Table 2.3 Overview of buffers used for purification of *EcE3* from pET28a

Lysis buffer		Buffer A		Buffer B		Buffer C	
Hepes	50 mM						
NaCl	300 mM	Hepes	50 mM	Hepes	50 mM	KH ₂ PO ₄	50 mM
Imidazole	20 mM	NaCl	300 mM	NaCl	300 mM	NaCl	100 mM
MgCl ₂	2 mM	Imidazole	20 mM	Imidazole	250 mM		
PSMSF	1 mM		pH 7.6		pH 7.6		pH 7.6
FAD	100 µM						
	pH 7.6						

2.2.2.4 Expression and Purification of *EcLip3*

For expression pET-SUMO-*EcLip3* was transformed into chemical competent *E.coli* BL21 Star™ cells. An overnight preculture grown at 37 °C in Luria-Bertani medium containing 50 µg/mL kanamycin was used to inoculate a main culture of the same medium to an OD₆₀₀ of 0.1. In addition, the main culture contained 1 % (w/v) glucose to prevent basal expression. Cells were grown at 37 °C to an OD₆₀₀ of 0.8 and expression was started by addition of 500 µM IPTG. To ensure a sufficient degree of lipoylation expression was carried out in chicane flasks and in the presence of 0.2 mM lipoic acid. After four hours of expression the cells were harvested by centrifugation at 5000 x g, resuspended in lysis buffer supplemented with lysozyme (tip of a spatula), DNase I (tip of a spatula). Cell disruption was performed using a Microfluidizer 110 S followed by removal of the cell debris by centrifugation (74,000 x g for 30 min at 4 °C). The supernatant was loaded onto a Ni-NTA FF Sepharose FF equilibrated in buffer A and N-terminal His₆tagged-SUMO-*EcLip3* was eluted using high imidazole buffer B in a single step. Appropriate fractions were pooled, desalted with low imidazole buffer and the SUMO part was removed by cleavage with SUMO protease (16.1 µM in 50 % (v/v) glycerol, 25 mM Tris-HCl pH 8.0, 250 mM NaCl, 0.5 mM dithiothreitol, 0.1 % (v/v) IGEPAL) in a 1:2000 molar ratio at 4 °C for 12 hours. Cleaved SUMO protein, protease and residual uncleaved fusion protein were trapped by a second cycle of IMAC. Subsequently, the flow through was desalted using a HiPrep™ 26/10 Desalting column equilibrated in buffer C.

Table 2.4 Overview of buffers used for purification of *EcLip3*

Lysis buffer		Buffer A		Buffer B		Buffer C	
KH ₂ PO ₄	50 mM						
Imidazole	20 mM	KH ₂ PO ₄	50 mM	KH ₂ PO ₄	50 mM	KH ₂ PO ₄	50 mM
NaCl	300 mM	Imidazole	20 mM	Imidazole	250 mM	NaCl	100 mM
MgCl ₂	1 mM	NaCl	300 mM	NaCl	300 mM		
PSMSF	1 mM		pH 7.6		pH 7.6		pH 7.6
	pH 7.6						

2.2.2.5 Generation of dihydro-*EcLip3* (*EcLip3H₂*)

Purified *EcLip3* was transferred in its dihydro form by reduction of the lipoamide cofactor with a 5-fold molar excess of TCEP for 5 minutes at room temperature. The reducing agent was removed from the protein by applying the reaction mixture to a HiPrep™ 26/10 Desalting column equilibrated in buffer C.

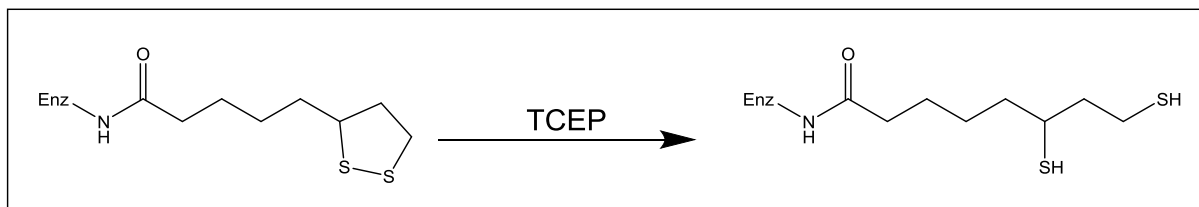


Figure 2.1 Simplified reaction scheme of the *EcLip3* reduction by TCEP. Reduction of the dithiolane moiety by TCEP leads to a ring opening and a concomitant loss of the chromophoric nature of the cystine at 333 nm (Levitch 1958; Seifert 2010).

2.2.2.6 Concentration Determination of Proteins

The concentration of proteins harboring a chromophoric cofactor was determined spectroscopically at the appropriate wavelength. *EcE3* enzyme bound FAD was determined at 455 nm with an $\epsilon = 11,300 \text{ M}^{-1}\text{cm}^{-1}$ (Wilkinson and Williams 1981). The concentration of *EcLip3* was determined at 333 nm with an $\epsilon = 150 \text{ M}^{-1}\text{cm}^{-1}$ due to the absorption of the dithiolane moiety of the lipoamide cofactor (Levitch 1958).

2.2.2.7 Concentration Determination of dihydro-*EcLip3*

The concentration of *EcLip3H₂* was determined from the reduction of excess 4,4'-dithiopyridine to generate 4-thiopyridone (324 nm, $\epsilon = 21,400 \text{ M}^{-1}\text{cm}^{-1}$) (Argyrou et al. 2003). Note that one molecule *EcLip3* harbors two thiol groups.

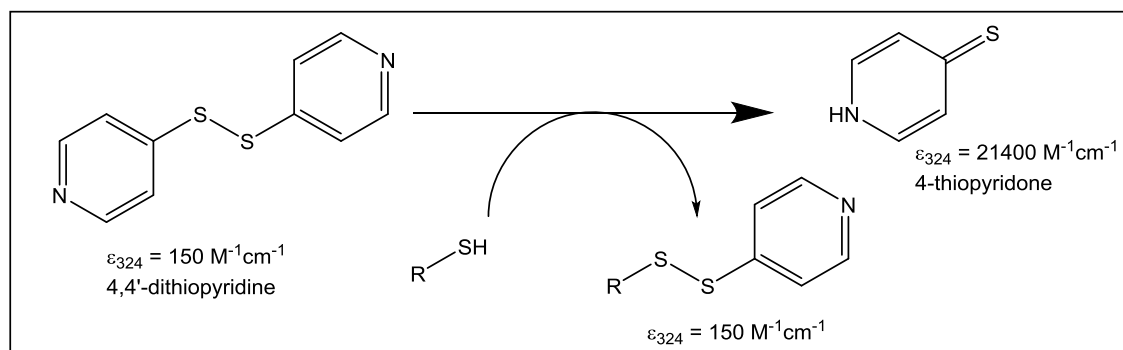


Figure 2.2 Reaction scheme of the concentration determination of free thiol groups.

2.2.2.8 Determination of Extinction Coefficients of Multiple Variants

The extinction coefficient of protein-bound FAD was determined by releasing the FAD from the protein followed by quantitating the free FAD (Hopkins and Williams 1995b). The absorbance at the flavin peak was measured at concentrations between 8-180 μM in 50 mM KPP, pH 7.6 and 100 mM NaCl. Guanidinium chloride (8 M, in 10 mM KPP pH 7.6) was added to a final concentration of 4.5 M at room temperature. Samples supplemented with guanidinium chloride were centrifuged for 30 min at 21000 x g. The extinction coefficient of free FAD is enhanced in the presence of 4.5 M guanidinium chloride to a value of $11800 \text{ M}^{-1}\text{cm}^{-1}$ and thus was used in the calculations to determine the extinction coefficients of enzyme-bound FAD.

Table 2.5 Molar extinction coefficients of *EcE3* and respective variants.

Enzyme variant	Spectroscopic characteristic	Reference
wild type	$E_{455 \text{ nm}} = 11300 \text{ M}^{-1}\text{cm}^{-1}$	Wilkinson & Williams 1981
Y19F	$E_{455 \text{ nm}} = 11300 \text{ M}^{-1}\text{cm}^{-1}$	This work
C45A	$E_{448 \text{ nm}} = 11940 \text{ M}^{-1}\text{cm}^{-1}$	This work
C45A/K54Q	$E_{452 \text{ nm}} = 9530 \text{ M}^{-1}\text{cm}^{-1}$	This work
C45S/K54Q	$E_{455 \text{ nm}} = 9950 \text{ M}^{-1}\text{cm}^{-1}$	Hopkins & Williams 1995
C45S	$E_{444 \text{ nm}} = 9950 \text{ M}^{-1}\text{cm}^{-1}$	Hopkins & Williams 1995
C50S	$E_{444 \text{ nm}} = 12140 \text{ M}^{-1}\text{cm}^{-1}$	Hopkins & Williams 1995
C45S/C50S	$E_{444 \text{ nm}} = 12140 \text{ M}^{-1}\text{cm}^{-1}$	Hopkins & Williams 1995
C50M/K54Q	$E_{451 \text{ nm}} = 10232 \text{ M}^{-1}\text{cm}^{-1}$	This work
C50A	$E_{455 \text{ nm}} = 11300 \text{ M}^{-1}\text{cm}^{-1}$	This work
K54Q	$E_{455 \text{ nm}} = 11300 \text{ M}^{-1}\text{cm}^{-1}$	Maeda-Yorita et al. 1991
E189Q	$E_{455 \text{ nm}} = 11300 \text{ M}^{-1}\text{cm}^{-1}$	This work
E354K	$E_{455 \text{ nm}} = 11300 \text{ M}^{-1}\text{cm}^{-1}$	This work
R386A	$E_{455 \text{ nm}} = 11300 \text{ M}^{-1}\text{cm}^{-1}$	This work
H445A	$E_{455 \text{ nm}} = 11300 \text{ M}^{-1}\text{cm}^{-1}$	This work
E450Q	$E_{455 \text{ nm}} = 11300 \text{ M}^{-1}\text{cm}^{-1}$	This work

2.2.2.9 Determination of Redox Potentials of selected *EcE3* Variants

Measurements were performed by Lena-Sophie Dreher in the laboratory of Prof. Bruce Palfey at the University of Michigan, Ann Arbor, USA. The redox potential of FAD bound to *EcE3* variants was determined by reductive titration of ~20 μ M enzyme under anaerobic conditions in presence or absence of ~20 μ M dye (Table 2.6) (McDonald, Liu, and Palfey 2013). All solutions were made anaerobic by multiple rounds of vacuum and oxygen-free argon flushing. 3 mM sodium dithionite was used to titrate the enzyme, the enzyme-dye mixture and the dye to complete reduction. The titration of the dye in absence of the enzyme served as control. All measurements were carried out at 25 °C in a 1 mL reaction volume monitored by a UV-2550 spectrophotometer (Shimadzu Corp.) recording spectra from 300-700 nm. Data were fitted by Nernst analysis of the absorbance changes of enzyme and dye using eq. 2.1.

$$\log \left[\frac{A_i - A_{red}}{A_{ox} - A_i} \right]_{Enz} = (E_{m;dye} - E_{m;Enz}) \frac{n_{Enz} F}{2.303 RT} + \frac{n_{Enz}}{n_{dye}} \log \left[\frac{A_i - A_{red}}{A_{ox} - A_i} \right]_{Dye} \quad \text{eq. 2.1}$$

Where n is the number of electrons in the reduction; F = Faraday's constant; R = gas constant; T = absolute temperature; $E_{m;dye}$ and $E_{m;Enz}$ are the midpoint potentials of the dye and enzyme, respectively; A_i is an absorbance during the experiment; A_{ox} is the absorbance at the start of the experiment when enzyme and dye are oxidized and A_{red} is the absorbance at the end of the experiment when enzyme and dye are reduced. Enz and Dye refer to absorbance values sensitive to these components. Corresponding wavelengths of the used enzyme/dye-pairs are listed in Table 2.6. Redox potentials were taken from BIRD and MANSFIELD (Bird and Kuhn 1981; Mansfield 1960). The recorded UV-Vis spectra are listed in the appendix (5.10).

Table 2.6 Redox pairs for the redox potential titrations.

Enzyme-dye pair	wavelengths	Redox potential (Dye)
		$E_{m7.6}$
<i>EcE3C45A/K54Q</i> / phenosafranin	403 nm / 530 nm	-275 mV
<i>EcE3C45S/C50S</i> / methylviologen	450 nm / 600 nm	-440 mV
<i>EcE3C50A</i> / neutral red	380 nm / 550 nm	-358 mV

2.2.2.10 Photobleaching of *EcE3* and Variants thereof

EcE3 and variants thereof (in 50 mM KPP pH 7.6, 100 mM NaCl) were exposed to 455 nm light (50 mW/cm²) at room temperature and concomitant spectral read-out on a photo diode array attached to an Agilent 8453 UV-visible spectrophotometer. Solution recovery experiments were measured with

the same experimental setup. EPR samples (2.2.5.4) were taken at time points indicated in the results part and subsequently frozen in liquid nitrogen. Photobleached cofactors were released from the enzyme and analyzed by ESI-TOF-MS (2.2.6.5).

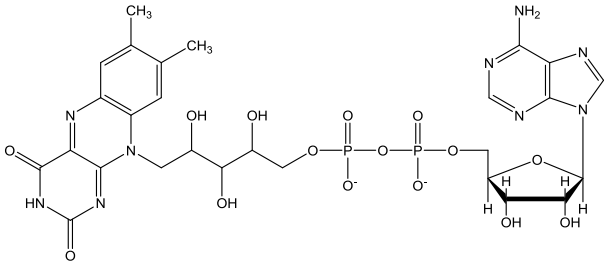
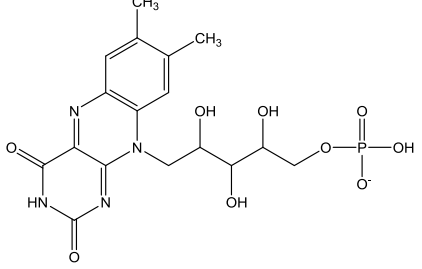
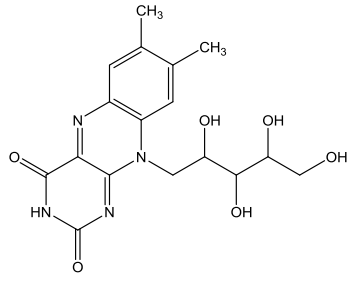
2.2.3 Substrates and Substrate Analogs

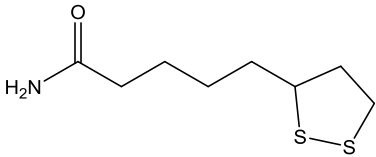
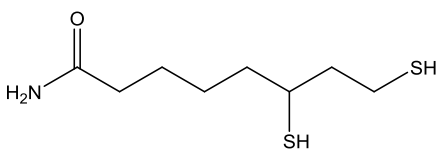
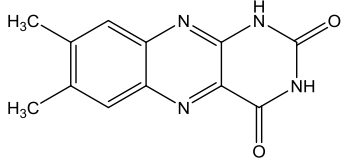
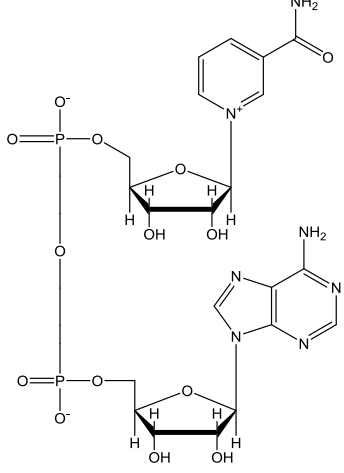
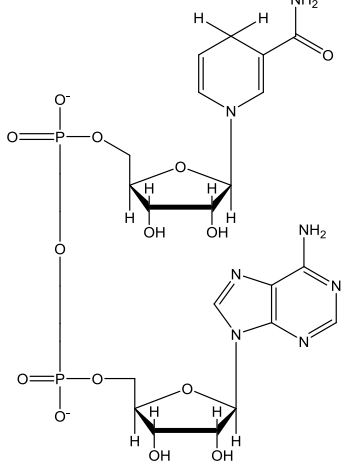
Substrates used for functional assays and for crystallization were purchased from Sigma-Aldrich or AppliChem.

2.2.3.1 Concentration Determination of Substrates and Cofactors

The concentration of substrates and the cofactor analogues was determined spectroscopically using molecular absorbance coefficients listed in Table 2.7.

Table 2.7 Spectroscopic characteristics and structures of relevant cofactors.

Cofactor	Spectroscopic characteristics	structure
FAD	$\epsilon_{450 \text{ nm}} = 11300 \text{ M}^{-1}\text{cm}^{-1}$ (Koziol 1971)	
FMN	$\epsilon_{446 \text{ nm}} = 12200 \text{ M}^{-1}\text{cm}^{-1}$ (Aliverti 2010)	
Riboflavin	$E_{450 \text{ nm}} = 12200 \text{ M}^{-1}\text{cm}^{-1}$ (Whitby 1953)	

Lipoamide	$\epsilon_{333 \text{ nm}} = 150 \text{ M}^{-1}\text{cm}^{-1}$ (Levitch 1958)	
Dihydrolipoamide	-	
Lumichrom	$\epsilon_{350 \text{ nm}} = 9830 \text{ M}^{-1}\text{cm}^{-1}$ (Ahmad and Armstrong 1984)	
NAD ⁺	$\epsilon_{260 \text{ nm}} 17400 \text{ M}^{-1}\text{cm}^{-1}$ (Hald, Lehmann, and Ziegenhorn 1975)	
NADH	$\epsilon_{340 \text{ nm}} 6220 \text{ M}^{-1}\text{cm}^{-1}$ (Hald et al. 1975)	

2.2.4 Kinetic Methods

2.2.4.1 Steady-State Activity Assay

The activity of *EcE3* and all variants was determined under pseudo steady state conditions in the presence of 100 μM NADH, 500 μM NAD⁺, 0.125 – 3 mM lipoamide and 5.25 % ethanol in 50 mM KPP pH 7.6 and 100 mM NaCl. Measurements were carried out at 20 °C and the reaction was started by addition of the enzyme while the consumption of NADH was tracked at 340 nm. If applicable, the dependency of the initial rates on the substrate concentration was analyzed according to eq. 2.2. It should be noted that the solubility of lipoamide is limited at 3 mM in the used buffer condition resulting in an underdetermined . Therefore, the determined specific activities represent the maximum substrate turnover in the presence of 3 mM lipoamide and 500 μM NAD⁺ at pH 7.6.

$$v = \frac{V_{\max} \cdot [S]}{K_M + [S]} \quad \text{eq. 2.2}$$

2.2.4.2 NAD⁺ activation Experiments

NAD⁺ activation experiments were carried out under the same conditions as described for the steady-state activity assay. The lipoamide was kept constant at a concentration of 3 mM while the NAD⁺ concentration was varied between 0 and 3 mM. The dependency of the initial rates on the NAD⁺ concentration was used to determine the specific activity.

2.2.4.3 pH Dependency Experiments under a constant ionic Strength

The pH dependency of the *EcE3* activity was determined under steady state conditions (2.2.4.1) in the presence of 100 μM NADH, 0 - 500 μM NAD⁺, 3 mM lipoamide and 5.25 % ethanol. A mixture comprised of 50 mM Acetic Acid, 50 mM MES and 100 mM Tris served as buffer system ensuring a constant ionic strength in a pH range from 4.5 to 9.5 (Ellis and Morrison 1982). Measurements were carried out at 20 °C and the reaction was started by addition of the enzyme while the consumption of NADH was tracked at 340 nm. The dependency of the initial rates on the pH was used to determine the pH optimum.

2.2.4.4 Fast Kinetics-Stopped Flow Absorbance Spectroscopy

Rapid reaction measurements experiments were carried out on an Applied Photophysics SX20 MV stopped-flow spectrophotometer at 4 °C. Spectra were recorded in equidistant time intervals on a photo diode array detector whereas single wavelength measurements were recorded with a logarithmic

time scale. Final concentrations of enzymes, cofactors and substrates after mixing are shown individually in the results part.

Single mixing experiments

Single wavelength measurements were performed at wavelengths of 380, 487, 523 and 650 nm. Enzyme and substrates were mixed in all cases in a 1 to 1 volume ratio. The final concentrations of enzymes, cofactors and substrates after mixing are shown in the figures in the results part.

Sequential mixing experiments

Sequential mixing experiments were used to study the reoxidation of the two-electron reduced state (EH₂) of *EcE3* by NAD⁺. First, *EcE3*-EH₂ was formed by pre-mixing *EcE3* and *EcLip3*H₂ (both at the same concentrations) followed by mixing with the final electron acceptor NAD⁺. The optimal time point for the second mixing step was obtained from the single mixing experiments. The final concentrations of enzymes, cofactors and substrates after the second mixing step are shown in the figures in the results part.

2.2.5 Biophysical Methods

2.2.5.1 UV-Vis Spectroscopy

UV-Vis spectra were collected between 300 – 700 nm in a Jasco V-650 spectrophotometer using Quartz cuvettes with a path length of 1 cm and a band width of 1 nm. The acquisition speed was 100 nm/min with a data pitch of 1 nm. As buffer system for all UV-Vis experiments served 50 mM potassium phosphate pH 7.6 and 100 mM NaCl.

2.2.5.2 CD spectroscopy

Circular dichroism spectra were recorded for *EcE3* and *EcLip3* including active site variants with a Chirascan CD-spectropolarimeter. Secondary structure elements were detected by collection of far UV spectra between 180 – 260 nm with a path length of 1 mm at in 50 mM potassium phosphate buffer pH 7.6. Near UV/Vis spectra were collected between 300 – 500 nm with a path length of 1 cm. Used buffers and added substrates are indicated in the figure legend.

Table 2.8 Acquisition parameters for CD spectroscopy experiments

	Far UV spectra	Near UV spectra
enzyme concentration	0.1 – 0.2 mg/mL	2.5 mg/mL
data interval	1 nm	1 nm
band width	1 nm	1 nm
response	2 s	3 s
path length	1 mm	1 cm
wavelength	180 – 260 nm	300 – 500 nm

2.2.5.3 Isothermal Titration Calorimetry

Isothermal titration calorimetry (ITC) allows the direct and quantitative determination of the binding thermodynamics of a biological process. Under optimal conditions the association constant, the binding enthalpy, the binding entropy and the stoichiometry of a binding event can be calculated from a single ITC experiment. An ITC200 MicroCalorimeter system was used to investigate both the interaction between *EcE3* and *EcLip3* and the cofactor binding of NAD^+ to *EcE3* and variants thereof.

The enzymes were buffer exchanged into the same buffer (50 mM KPP pH 7.6, 100 mM NaCl). The ITC cell was filled with 100 μM (active sites) *EcE3*. The injection syringe was filled with 1 mM of *EcLip3*. Measurements were performed at 20 °C with a stirring speed of 500 min^{-1} . A titration of 1 mM *EcLip3* into buffer served as control to check for heat effects due to dilution. The interaction of NAD^+ with the enzymes was assayed under the same conditions while dissolving NAD^+ directly in the buffer system.

2.2.5.4 EPR

Measurements on *EcE3C45A/K54Q* (pseudoLOV) were performed by Christopher Engelhard in the laboratory of Prof. Robert Bittl at the Freie Universität Berlin. Acquisition parameters were as follows:

- Modulation amplitude: 3G
- Time constant: 30ms
- Lock-in frequency 100 kHz
- Sensitivity: 1 mV
- Microwave frequency: ~9.38 GHz, all spectra frequency-corrected to 9.60 GHz
- Microwave power: 63.2 nW (-35 dB on a standard 200 mW microwave source)

2.2.6 Mass Spectrometry

2.2.6.1 MALDI-TOF Mass Spectrometry

It could be shown that MALDI-TOF Mass Spectrometry is suitable method to detect the state of a lipoylation of an isolated hybrid lipoyl domain of *E. coli* PDHc (Wei et al. 2003). This method was also applied to the lipoyl domain II of the human PDHc by members of this group (Güttler 2008; Seifert 2010). In both cases, the entire domain was subjected to MALDI-TOF MS. In this work a MALDI-TOF mass spectrometric approach of an isolated lipoyl domain of the *E. coli* PDH after tryptic digestion of the latter will be presented.

2.2.6.2 Determination of the Lipoylation State of *EcLip3*

Digestion of a protein with trypsin leads to fragments showing specific cleavages after arginine or lysine residues, respectively. These tryptic peptides are then used for exact mass determination, also allowing the detection of putative post-translational modifications of amino acid side chains. On the one hand, the lipoamide cofactor bound to *EcLip3* directly leads to an increase in mass of the distinct peptide on the other hand it also leads to an altered digestion pattern since the covalent bond between lipoic acid and the ϵ -amino group of lysine45 prevents a tryptic digestion at this site. Tryptic peptides of *EcLip3* including their corresponding masses were predicted with the PeptideCutter interface (Table 5.1). The peptides required for analysis of the lipoylation state of *EcLip3* are listed in Table 2.9.

Table 2.9 Possible tryptic fragments of *EcLip3* for the lipoylation state analysis

Peptide sequence	Peptide mass [Da]	property
VAAEQLITVEGD K *	1459.6	<i>unlipoylated I</i>
ASMEVPAPFAGVVK*	1402.6	<i>unlipoylated II</i>
VAAEQLITVEGD K (lip)ASMEVPAPFAGVVK	3032.5	<i>lipoylated</i>

In the case of fully lipoylated *EcLip3*, the peptides *unlipoylated I* and *II* are not expected occur since trypsin will not cleave due to the covalent attachment of lipoic acid to lysine45 (highlighted in yellow). In contrast, only one bigger fragment should appear after tryptic digestion (*lipoylated*). This fragment has a total mass of 3032.5 Da comprising the masses of the two individual fragments (*unlipoylated I* and *II*) including the bound lipoamide cofactor.

2.2.6.3 MALDI-TOF Sample Preparation

Samples of *EcLip3* for tryptic digestion were taken after purification. 15 μL sample were added to 25 μL 25 mM ammonium hydrogen carbonate and 10 μL trypsin (100 $\mu\text{g}/\text{mL}$). After an overnight digestion at 37 $^{\circ}\text{C}$ the reaction was stopped by the addition of 85 % FA in a 1:1 volume ratio. MALDI-TOF samples were desalted using ZipTips pipette tips containing C_{18} -silica beads with a binding capacity of 5 μg protein. ZipTips were washed three times with a solution made of 10 μL 70 % ACN / 0.3 % FA followed by an equilibration with 10 μL 1 % FA. After the loading of the sample the column was washed again with 10 μL 1 % FA as described above. Tryptic peptides were eluted with 10 μL of 70 % ACN / 0.3 % FA Table 2.10.

Table 2.10 ZipTip preparation for MALDI-TOF samples

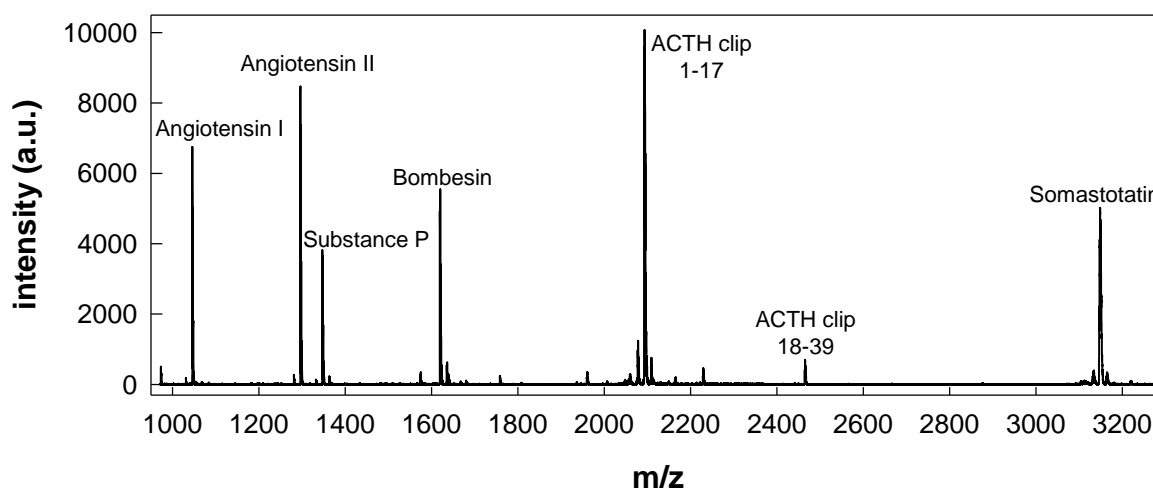
Desalting step	Cycles	Solution
Washing	3x	70 % ACN / 0.3 % FA
Equilibration	5x	1 %FA
Loading	5x	Sample
Washing	5x	1 %FA
Elution	1x	70 % ACN / 0.3 % FA

2.2.6.4 MALDI-TOF Measurement and Data Evaluation

The MALDI-TOF device was calibrated using the Peptide Calibration Standard (Table 2.11 and Figure 2.3). 2 μL of desalted sample were mixed with 2 μL of saturated DHB matrix solution. 2 μL thereof were then pipetted on a MTP 384 polished steel sample carrier. The mixture was dried on air. Data were acquired in a mass range from m/z 650 to 3500 using an acceleration voltage of 20 kV. 40 shots were collected with a laser intensity of 40 % per measurement. In total, ten measurements were carried out resulting in the accumulation of 400 shots. Data acquisition and analysis were done using the Flex analysis software package and corresponding graphs were compiled with SigmaPlot.

Table 2.11 Expected and acquired masses of the Peptide Calibration Standard

Peptide Calibration Standard	[M+H] ⁺ Mono isotopic expected	[M+H] ⁺ Mono isotopic acquired
Angiotensin II	1046.51	1046.18
Angiotensin I	1296.68	1296.25
Substance P	1347.73	1347.27
Bombesin	1619.82	1619.25
ACTH clip 1-17	2093.08	2093.96
ACTH clip 18-39	2465.19	2465.33

**Figure 2.3** MALDI-TOF mass spectrum of the Peptide Calibration Standard

2.2.6.5 UPLC-ESI-TOF Sample Preparation

The enzyme-bound flavin cofactor was released before and after photoexcitation (2.2.2.10), respectively, by different protein precipitation methods. First, *EcE3* and variants thereof were heated to 95 °C for ten minutes with occasional vortexing. Secondly, *EcE3* was precipitated by addition of ice cold 50 % (w/v) TCA to a final concentration of 5 % (w/v) followed by an incubation on ice for ten minutes. Thirdly, one volume of protein solution was mixed with four volumes of ice cold acetone followed by an incubation step at -70 °C for ten minutes. In all cases precipitated protein was removed by three rounds of centrifugation at 21,000 x g for 30 minutes at 4 °C. Prior to MS and MS/MS analyses, the resulting supernatant containing the released cofactor was diluted with ddH₂O as indicated in the results part.

2.2.6.6 UPLC-ESI-TOF-MS

Analysis of the released *EcE3* cofactor was performed on an ultra-performance liquid chromatography (UPLC) ACQUITY system coupled to an UPLC eLambda 800 nm photo diode array detector (Waters Corporation, Milford, USA), followed by an LCT Premier orthogonal electrospray ionization time-of-flight mass spectrometer (ESI-TOF-MS, Waters Corporation, Milford, USA). For analysis, the UPLC was equipped with an ACQUITY UPLC HSS T3 column (1.0 x 100 mm, 1.8 μ m particle size, Waters Corporation, Milford, USA) held at 40 °C and a flow rate of 0.2 mL/min. The following gradient program was run: 0 – 0.5 min 1 % B, 0.5 – 3 min 1 % B to 20 % B, 3 – 8 min 20 % B to 100 % B, 8 – 10 min 100 % B, 10 – 10.1 min 100 % B to 1 % B, 10.1 – 14 min 1 % B (solvent system A: water:formic acid (100:0.1, v/v); B: acetonitrile:formic acid (100:0.1, v/v)). UV-VIS data were collected between 190 – 800 nm in 1.2 nm steps.

The ESI-TOF-MS was run at negative ionization mode for all samples. Data were collected over a mass range from m/z 50.00 – 1200.00 and a runtime from 0 - 13 min using a capillary voltage of 2500 V. The cone voltage was maintained at 30 V, the desolvation temperature at 350 °C and the source temperature at 80 °C. Data acquisition was carried out by using the MassLynx software in centroid data format. Nitrogen was used as cone and desolvation gas at a flow of 30 and 800 l/h, respectively. The dynamic range enhancement mode was used for data recording. All analyses were calibrated by applying the lock spray reference compound leucine-enkephaline ($[M-H]^-$ 554.262 as well as its ^{13}C isotopologue ($[M-H]^-$ 555.2653; Sigma-Aldrich, Deisenheim, Germany) at a concentration of 0.5 μ g/mL in acetonitrile:water (50:50, v/v) and a flow rate of 20 μ L/min. The measurements for the lumichrom reference were run at positive ionization mode using the same parameters except a capillary voltage of 2700 V and a calibration by applying the aforementioned lock spray reference ($[M+H]^+$ 556.2766 as well as its $2x^{13}C$ isotopologue $[M+H]^+$ 558.2833). UPLC-ESI-TOF-MS measurements and subsequent data analysis were carried out by Dr. Kirstin Feussner.

2.2.6.7 UHPLC-ESI-QTOF-MS

MS/MS fragmentation experiments were performed via UHPLC-ESI-QTOF-MS. For UHPLC, an Agilent 1290 Infinity series UHPLC system (Agilent Technologies, Böblingen, Germany) with an ACQUITY UPLC BEH C18 column (2.1 x 100 mm, 1.7 μ m particle size, Waters Corporation, Milford, USA) kept at 40 °C was used with a flow rate of 0.5 mL/min. The solvent system and the applied gradient were comparable to that of method 2.2.6.6. Mass detection was performed with an Agilent 6540 UH Accurate-Mass-Q-TOF MS (Agilent Technologies, Böblingen, Germany). The MS was operated using an ESI source with Agilent Dual jet Stream Technology (Agilent Technologies, Böblingen, Germany) in negative and positive ionization mode. Ionization parameters were as follows: gas temperature 300 °C, gas flow 8 L/min, nebulizer pressure 35 psi, sheath gas temperature 350 °C,

sheath gas flow 11 L/min, VCap 3 kV, nozzle voltage 100 V. As a collision cell, a linear hexapole collision cell with nitrogen as collision gas was used with collision energies of 40 eV – 45 eV. For data acquisition, the Mass Hunter Workstation Acquisition Software was used (B.05.01.), with Mass Hunter Qualitative Analysis software (B.06.00) as analysis tool. For structure elucidation the MS/MS spectra of FAD derivatives were interpreted in comparison to FAD spectra (METLIN ID2302) deposited in the METLIN database. UHPLC-ESI-QTOF-MS measurements and subsequent data analysis were carried out by Dr. Kirstin Feussner

2.2.7 X-ray Crystallography

X-ray diffraction datasets, collected in-house or at different synchrotron radiation facilities (BESSYII, Berlin; DESY, Hamburg), were processed with XDS (Kabsch 2010). Protein models were iteratively refined and improved with PHENIX (Adams et al. 2010) and validated with MOLPROBITY (Davis et al. 2007).

2.2.7.1 Crystallization

Crystallization of *EcE3*

Crystals were obtained using the hanging drop vapor-diffusion method. *EcE3* (derived from pGS523) was concentrated to 14-16 mg/mL in 50 mM imidazole pH 6.5, 150 mM NaCl. All further steps were performed at 6-8 °C. *EcE3* was mixed with equal amounts of reservoir solution, comprising 1.8 – 2.4 M ammonium sulfate and 0.1 M potassium phosphate buffer pH 7.0. Drop size was 4 µL. Crystals were cryoprotected using reservoir solution supplemented with 25 % glycerol (v/v) before flash freezing and storage in liquid nitrogen. For substrate soaking experiments the cryo solution was supplemented with 5 mM NAD⁺.

Crystallization of *EcE3C45S*

EcE3C45S was desalted against 50 mM imidazole pH 6.5, 150 mM NaCl and concentrated to 13.5 mg/mL. The protein solution was mixed with equal amounts of reservoir solution, comprising 2.4 M ammonium sulfate and 0.1 M MES buffer pH 6.5. Directly after preparation drops were microseeded with wild type crystals pre-grown in 8 – 13 % (w/v) PEG 4000, 200 mM NaCl, 1-4 % (v/v) PEG400 and 0.1 M MES pH 6.5. Crystals were cryoprotected the same way as the crystals of the wild type enzyme.

2.2.7.2 Data Processing and Molecular Replacement

Datasets were processed and scaled with XDS (Kabsch 2010). Data processing was mainly done by Dr. Piotr Neumann (Department for Molecular Structural Biology, University of Göttingen). Data collection- and structure refinement statistics can be found in the appendix (Table 5.3). The structure of *EcE3* was determined by molecular replacement using dihydrolipoamide dehydrogenase of *Neisseria meningitidis* (PDB: 1OJT) as initial search model with PHASER (McCoy 2006).

2.2.7.3 Model Building, Refinement and Validation

Structure refinement was carried out using PHENIX (Adams et al. 2010) employing the maximum likelihood method, with 1.5 to 5% of randomly chosen data for validation by the R_{free} factor (Brünger 1992). After a rigid body refinement models were inspected manually with COOT (Emsley et al. 2010) checking the conformation of side chains and the position of water molecules or other ligands. Validation of the refined models was carried out using COOT and MOLPROBITY. Sigma A-weighted electron density maps ($2m\text{Fo}-\text{DFc}$, $m\text{Fo}-\text{DFc}$) were generated with PHENIX. Simulated-annealing (SA) omits maps were calculated as implemented in CNS (Brunger 2007) by Dr. Piotr Neumann (Department for Molecular Structural Biology, University of Göttingen). Figures were compiled with PYMOL (DeLano 2003).

3 Results and Discussion

3.1 Spectroscopic and Crystallographic Characterization of *EcE3*

Major emphasis was devoted to the spectroscopic and crystallographic detection of reaction intermediates of the *EcE3* reaction cycle. Therefore a convenient and robust expression system has been established which allowed the subsequent study of the wild type enzyme and selected active site variants thereof. These enzymes were first characterized by conventional UV-Vis spectroscopy and steady-state kinetics and then further investigated by stopped-flow absorbance spectroscopy and transient kinetic analyses. Based on these results crystallization trials with active site mutants capable of stabilizing a distinct reaction step were conducted to expand the gained spectroscopic knowledge by crystallographic data.

3.1.1 Kinetic Characterization of *EcE3* in dependence of Lipoamide, NAD^+ and pH

Steady-state parameters of lipoamide dehydrogenase from *Escherichia coli* have been investigated in detail over the last decades (Wilkinson and Williams 1981; Williams 1965; Williams et al. 1967). In addition, the mechanism of the severe product inhibition by NADH could be determined in significant detail (Wilkinson and Williams 1981). The following results briefly summarize the effects of lipoamide, NAD^+ and pH on the steady-state catalysis of *EcE3* purified from modern expression systems and demonstrate the consistency with already published data (Figure 3.1). In the absence of NAD^+ the initial velocity of *EcE3* is very low when tracking the reverse reaction with NADH as reductant and lipoamide as electron acceptor. With increasing NAD^+ concentrations the inhibitory effect of NADH is overcome leading to enhanced initial rates (Figure 3.1A). The activation by NAD^+ is complete at about 2.0 mM added NAD^+ under the conditions tested (Figure 3.1B). The apparent binding constant was determined to be 400 μM (Wilkinson and Williams 1981). Although the activating effect of NAD^+ is unquestionable the absolute influence of the pyridine nucleotide is also pH dependent (Figure 3.1C) (Reed, Koike, and Shah 1960; Wilkinson and Williams 1981). At all tested pH values the reverse reaction is very slow without externally added NAD^+ . In the presence of 50 μM NAD^+ the enzyme shows a clear catalytic optimum at pH 8.5 harboring a ~5-fold increased reaction rate compared to the reactions lacking externally added NAD^+ . When adding 500 μM NAD^+ the pH profile is bell shaped peaking at pH 8.0. It is obvious that the chosen pH acts as a determinate whether NAD^+ functions only as an activator or, at higher concentrations, both as activator and an inhibitor. This phenomenon has already been discussed elsewhere (Wilkinson and Williams 1981).

A standard steady-state assay was therefore used to compare the relative activities of active site mutants during the course of the study. This assay comprised 500 μM NAD^+ , 3 mM lipoamide and 100 μM NADH at pH 7.6. The chosen pH was a consequence of high catalytic activity with respect to *EcE3* but was further determined by the usage of an isolated lipoyl domain of the *EcE2* component (*EcLip3*) as reductant to track the reductive half-reaction (3.2). This isolated domain showed to be most stable at pH 7.6 and thus a pH below 8.0 was obligate for further investigations. Hence, the used standard steady-state assay reflected a compromise with respect to activity of *EcE3* and stability of *EcLip3* at pH 7.6. The resulting steady-state kinetic under the assay conditions chosen for *EcE3* is shown in Figure 3.1D. Due to the limited solubility of lipoamide in aqueous solutions (Argyrou and Blanchard 2001) the resulting plot lacks a hyperbolic shape. Catalytic activities will therefore be referred to units/mg. Catalytic activities for all investigated (double) variants of *EcE3* under the conditions described can be found in the appendix (5.4).

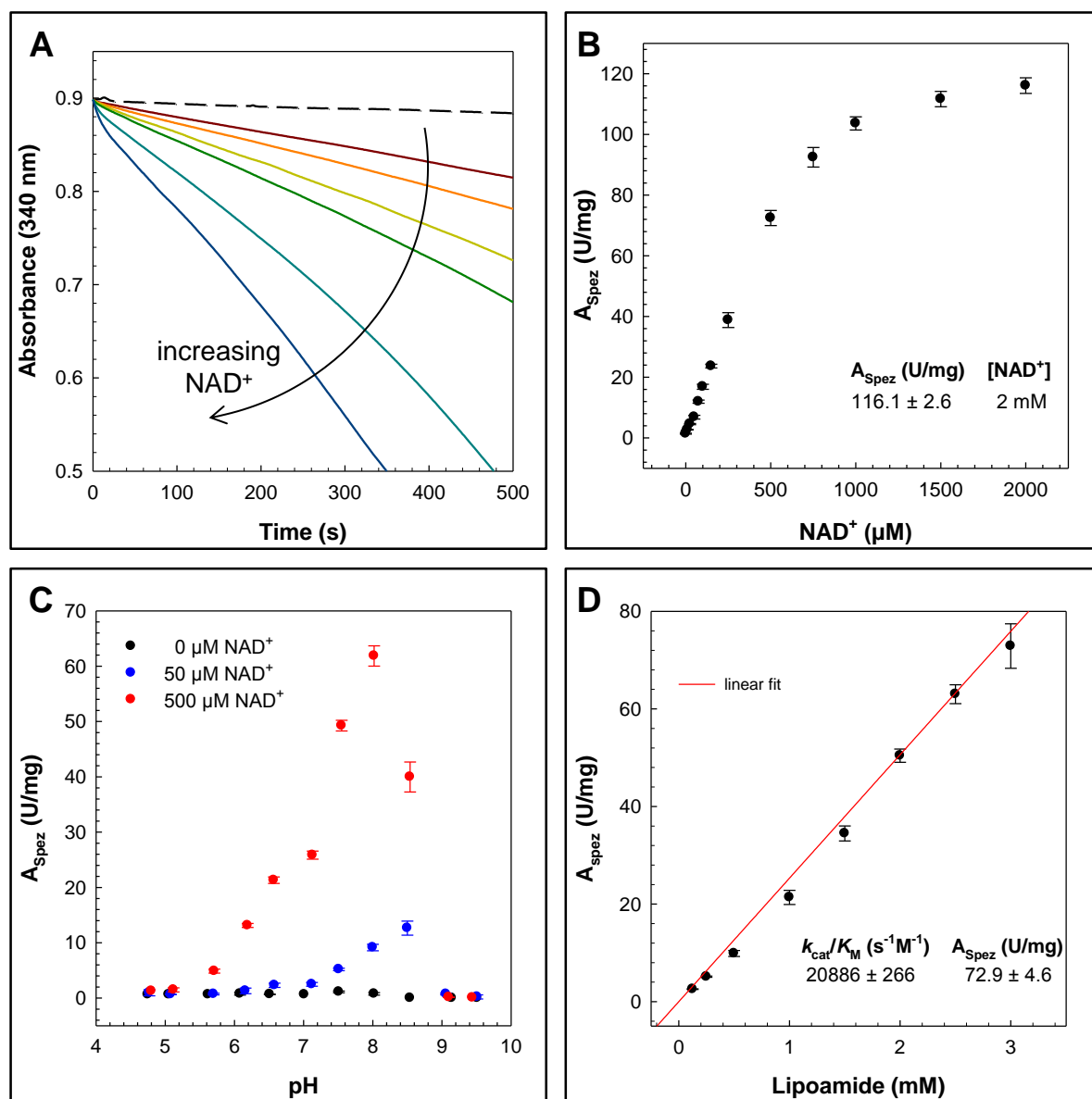


Figure 3.1 Steady-state characterization of *EcE3*.

(A) Time course of the NADH-lipoamide reaction, effect of added NAD^+ . The assay comprised 100 μM NADH and 3 mM lipoamide. (B) Effect of NAD^+ on the observed initial rates in the NADH-lipoamide reaction. Conditions of the assay are as in A, except that NAD^+ was added at the indicated concentrations before the addition of enzyme. (C) pH activity profile for the NADH-lipoamide reaction, effect of added NAD. (D) Lipoamide dependence standard assay of *EcE3* comprising 500 μM NAD^+ 3 mM lipoamide and 100 μM NADH. The reaction was started by addition of the enzyme. All experiments were carried out at pH 7.6.

3.1.2 Detection of Reaction Intermediates using Stopped-flow Absorbance Spectroscopy

Besides the establishment of a standard steady-state assay also transient kinetic analyses should be performed at appropriate conditions using stopped-flow absorbance spectroscopy. It was demonstrated that this technique is suitable to study both the spectroscopic and kinetic properties of lipoamide dehydrogenase from *Mycobacterium tuberculosis* (Argyrou et al. 2002). Hence, the kinetic rate constants for single reaction steps could be determined in significant detail. It was therefore the aim to transfer the method established by ARGYROU and co-workers to the *E. coli* system which consequently allowed the spectroscopic characterization of the *EcE3*wt and active site mutants. Major emphasis was thereby devoted to the detection of the covalent FAD-C4a-cysteinyl adduct.

As described for all lipoamide dehydrogenases the reaction cycle consist of multiple reaction steps, which are completely reversible (Massey, Gibson, and Veeger 1960). This allows to follow the reaction cycle from both half-reactions, from the reductive half-reaction (dihydrolipoamide as reductant; forward direction) or from the oxidative half-reaction (NADH as reductant; reverse direction). Due to the absence of commercially available dihydrolipoamide the reduced pyridine nucleotide was chosen as reductant, which harbors further advantages compared to dihydrolipoamide besides its unlimited availability. In contrast to lipoamide, NADH does not show limited solubility in aqueous solution as (dihydro)lipoamide does (Argyrou and Blanchard 2001) and secondly, it was demonstrated that NADH has the ability to overreduce lipoamide dehydrogenases to the EH_4 state, which allows the observation of further reaction intermediates (Argyrou et al. 2003, 2002). In addition, it was evident that stopped-flow experiments had to be conducted at low temperature (4 °C) due to the high turnover rates of the enzyme (Wilkinson and Williams 1981).

Oxidized *EcE3* (E_{ox}) has absorbance maxima at 369 and 455 nm, a shoulder at 482 nm, and minima at 312 and 395 nm (Figure 3.2A). Upon reduction with an equimolar amount of NADH the enzyme is transformed into its two-electron reduced form (EH_2) by intramolecular transfer of electrons from the reduced flavin to the disulfide. At the EH_2 state the flavin remains oxidized while the redox active cysteine is reduced. The flavin absorbance is attenuated and the entire spectrum is blue-shifted relative to the spectrum of E_{ox} . In addition, the absorbance rises in the longer wavelengths region yielding in a shoulder at 523 nm which was attributed to the Cys50-thiolate FAD charge transfer complex (Thorpe and Williams 1976a, 1976b, 1981). This specific absorption change is based on an electron donor-acceptor relation rather than on formation of a flavin radical species as demonstrated by independent experiments: At first, the complex shows clear pH-dependent absorption changes yielding in a loss of the charge transfer signal at lower pH values which is indicative for protonation of the anionic electron donor (Matthews and Williams 1976). Secondly, the EH_2 state was shown to be devoid of any detectable EPR signal (Massey and Gibson 1964; Searls, Peters, and Sanadi 1969) further

underpinning the presence of a thiolate rather than a flavin radical giving rise to the absorption in the 523 nm region.

Flavin reduction and thiolate formation occur at the same apparent rate constant with $\sim 55 \text{ s}^{-1}$ (Figure 3.2C and Figure 5.1). Though the flavin peak resides in its blue-shifted form during the recorded time the thiolate starts to decay. This is most likely due to the property of the EH_2 state of the *E. coli* enzyme which is indeed a mixture of different spectrally distinct species (Wilkinson and Williams 1979). At the pH used for the experiments (pH 7.6) it is possible that Cys50 becomes protonated and concomitantly the interchange thiol (Cys45) becomes deprotonated leading to a prototropic tautomer which explains the loss in absorbance at 523 nm. Further reduction to the four-electron reduced state (EH_4) requires the flavin also being reduced. This is accompanied by reduction with a 5-fold molar excess of NADH (Figure 3.2B). In the EH_4 state the absorbance maxima are further reduced and the 523 nm charge transfer decayed entirely. Moreover, the excess of NADH enables the detection of the $\text{FADH}_2\text{-NAD}^+$ intermediate giving rise in absorption between 600 and 700 nm (Argyrou et al. 2002). The latter complex can only be observed to minute amounts under equimolar conditions (Figure 3.2A). However, its formation is completed within the dead-time of mixing at both used substrate concentrations indicating the transience of the complex. The transience can be related to the redox potential of the flavin cofactor which is significantly more positive compared to the ones of pig heart and *Mycobacterium tuberculosis* lipoamide dehydrogenase, respectively (Argyrou et al. 2002; Matthews and Williams 1976; Wilkinson and Williams 1979). Noteworthy, no significant increase in absorbance at 380 nm was observed in the reaction of E_{ox} with NADH under single turnover conditions (Figure 3.2D). The absence of an increase in absorbance at this wavelength, that is typical for flavin-C4a adducts, suggests that the C4a-cysteinyll adducts does not accumulate to detectable amounts in the forward direction in *EcE3* using NADH as reductant. The finding of this high instability of the intermediate is consistent with previously reported observations (Argyrou et al. 2002). It was suggested that this instability could arise if formation of the covalent adduct in both directions is considerably slower than its decay in both directions (Argyrou et al. 2002). Apparently, this also holds true for this central intermediate in *EcE3*.

In summary, the spectral properties of the three enzyme species detected are very similar to the spectra of the corresponding species of the pig heart and the aforementioned *Mycobacterium tuberculosis* lipoamide dehydrogenase (Argyrou et al. 2002; Matthews and Williams 1976). A transfer to the *E. coli* system was therefore successful and was thus used to study active site mutants to further investigate the reaction mechanism of *EcE3* (3.3). A trustworthy approach to track the reductive half-reaction of *EcE3*, and thus the ability to test for the accumulation of the covalent C4a-flavin adduct in the forward direction, is presented in 3.2.

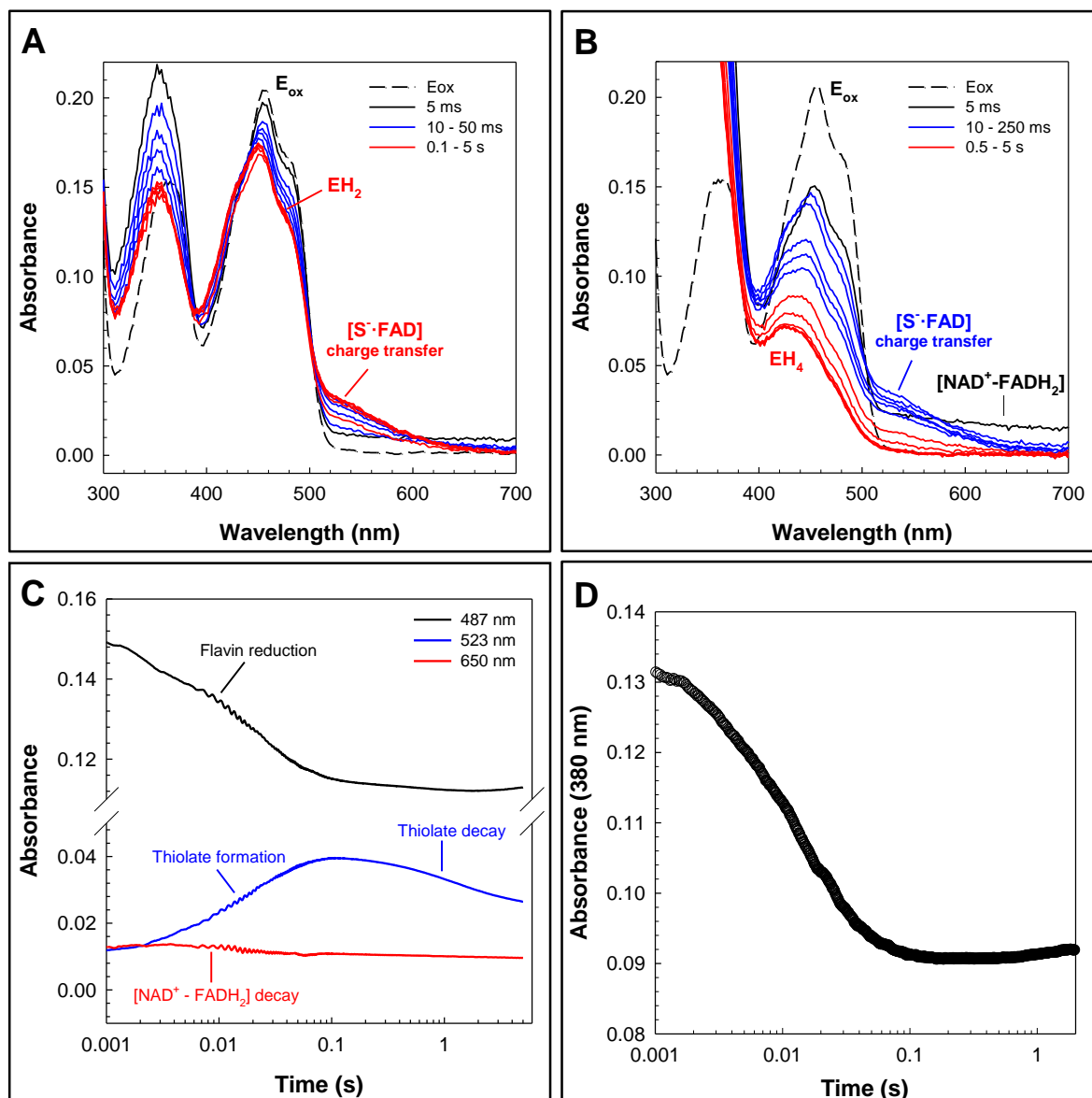


Figure 3.2 Stopped-flow absorbance traces of *EcE3* during reduction with NADH. 20 μ M *EcE3* were mixed with 20 μ M (A) or with 100 μ M NADH (B) at 4 $^{\circ}$ C and pH 7.6. The dashed line represents the oxidized form of *EcE3* (E_{ox}) derived from a single mixing event with buffer. The solid spectra were recorded using a diode-array detector after mixing with NADH at the concentrations indicated. Panel C indicates selected absorbance traces for the reduction under equimolar conditions. D Absorbance trace at 380 nm under single turnover conditions. No increase in absorbance can be detected indicating that the covalent C4a-cysteinylyl adduct does not accumulate during the reduction process. Note the logarithmic time-scales.

3.1.3 Structure of EcE3 – Active Site Dynamics underlie Catalysis

The crystal structure of EcE3 was recently solved at medium resolution (2.5 Å, PDB: 4JDR) (Chandrasekhar et al. 2013) and thus expanded the plethora of already determined structures of lipoamide dehydrogenases. The crystals belonged to space group I422 with two monomers assembled as functional dimer occupying the asymmetric unit. However, it was the aim this study to improve the existing structural data by means of resolution and model quality. An improved structural knowledge may help to gather insights in the transient nature of the enzyme's reaction cycle (3.1.2). Thus, a correlation of the structural findings with spectroscopic results in solution was applied whenever possible.

EcE3wt could be crystallized in a new polymorphic form and the crystal structure was determined successfully with improved resolution and atomic model reliability as judged by refinement statistics (5.12). As described previously ammonium sulfate was used as precipitant but the crystallization condition harbored an increased pH (7.0). Crystals exhibited a shiny yellow color clearly indicating the presence of the flavin cofactor (Figure 3.4) and belonged to space group P2₁2₁2₁. Six monomers were present in the asymmetric unit corresponding to a solvent content of 59.99 %, labeled A – F, assembled into three functional dimers. The altered space group and the increased number of monomers occupying the asymmetric unit is likely due to the increased pH in the crystallization buffer which most likely influenced crystal packing. The structure of EcE3 was solved by molecular replacement with PHASER (McCoy et al. 2007) using a monomer of lipoamide dehydrogenase from *Neisseria meningitidis* as search model (PDB: 1OJT) and could be refined at 2.1 Å resolution to $R_{\text{work}}/R_{\text{free}}$ of 17.7 / 20.8 % (Table 5.3). After model completion and refinement, several difference map peaks (mFo-DFc at 3 sigma level) could be observed. Owing to the presence of sulfate in the crystallization condition and glycerol served as cryoprotectant, these peaks were modelled as sulfates and glycerols taking into account the character of interactions with surrounding residues. Interestingly, a sulfate acts as a placeholder molecule residing very close to the binding site for the diphosphate anchor of NAD⁺ (Figure 5.22). At least 469 out of the 474 residues were visible in each of the six molecules occupying the asymmetric unit whereas the missing residues are housed in the C-terminal part are most likely disordered. The structure EcE3 is similar to the already published one, for instance, dimerAB can be superimposed with an r.m.s.d. of 0.49 Å calculated on Ca positions, indicates the high similarity.

Despite the high similarity with respect to the overall fold essential differences around the active site, particularly at the redox active cystine, could be observed. It was stated that the geometry of the redox active disulfide bridge in the *E. coli* enzyme deviates from the geometry observed in other organisms (Chandrasekhar et al. 2013). The dihedral angles (Cβ-Sγ-Sγ-Cβ) were reported to be 29 and 46 ° in one functional dimer. However, based on improved structural data presented here these results seem to be questionable. The dihedral angle in chain A was -131 ° and is thus consistent with earlier published

geometries (Brautigam et al. 2005; Mande et al. 1996; Mattevi et al. 1991). Moreover, it was possible to model both an open and a closed conformation for the disulfide bridge contributing to the redox center (Figure 3.3A). Multiple refinements with different occupancies as starting point all converged into a defined model with a distribution of 50 % open and 50 % closed conformation for the cystine. Partial opening of the disulfide bridge is induced by the synchrotron radiation and leads to formation of two different redox states of *EcE3* simultaneously. The closed conformation of the cystine resembles the oxidized state (E_{ox}) and the open conformation resembles the two-electron reduced form (EH_2) of the enzyme. This radiation-induced reduction enabled the observation of structural rearrangements required for catalysis and gave first insights into the local plasticity of the active site. Further structural changes which are pivotal to stabilize the two-electron state of *EcE3* and the formation of the covalent FAD-C4a-cysteinyl adduct are described below (3.1.4 and 3.1.5).

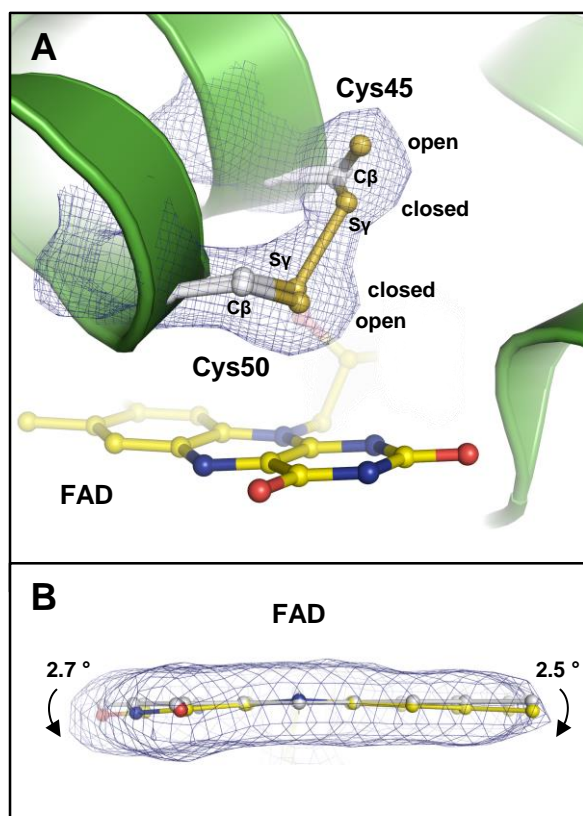


Figure 3.3 Local flexibility of the active site.

(A) The redox active disulfide bridge of *EcE3* is formed between Cys45 and Cys50. Its open and closed conformation could be refined with 50 % occupancy, respectively. The 2mFo-DFc electron density map is countered at 2σ . The closed conformation reflects the oxidized, the open conformation the two-electron reduced state of *EcE3*.

(B) Deviation from planarity of the flavin cofactor. Superposition of the flavin cofactor from PDB: 4JDR (light grey) and *EcE3* at 2.1 Å (yellow). The pteridine part deviates $\sim 2.7^\circ$, the dimethylbenzene part $\sim 2.5^\circ$ from planarity (2mFo-DFc map countered at 2σ).

The flexibility of the active site is not restricted to the redox active cystine. The aromatic isoalloxazine moiety of the flavin cofactor also deviates from planarity. The pteridine part is bent $\sim 2.7^\circ$, the dimethylbenzene part $\sim 2.5^\circ$ with respect to the N5-N10 axis of the cofactor (Figure 3.3B). It was demonstrated that the flavin redox potential can be tuned by conformational effects, especially by bending (Hasford et al. 1997; Lyubimov et al. 2007; Walsh and Miller 2003). Apparently, *EcE3* also

uses this tool maintaining the optimal redox potential. However, deviation from planarity is not as pronounced as observed in other studied flavoenzymes (Müller et al. 1994; Neumann et al. 2008).

3.1.4 Spectroscopic and Crystallographic Investigation of the two-electron reduced State – EH₂

The two-electron reduced state (EH₂) of *EcE3* is the catalytically active species that is formed prior to generation of NADH (3.1.2). During studies on the redox active disulfide it could be demonstrated that replacement of Cys45 to a serine residue (*EcE3C45S*) leads to a stable formation of an artificial EH₂ state in which the remaining cysteine (Cys50) is present to ~95 % in its anionic form (Hopkins and Williams 1995a, 1995b). The residual ~5 % were estimated to be a fluorescent species in which Cys50 resides in its thiol form. *EcE3C45S* harbored an orange-red color and its UV-Vis spectrum resembled that of the two-electron reduced wild type enzyme. It is characterized by an ~10 nm blue shifted flavin peak and the presence of an broad thiolate-FAD charge transfer absorbance between 500 to 600 nm (Figure 3.4A). The absence of an absorbance in the 380 nm range excluded the accumulation of a cysteinyl-C4a adduct in the resting state (Figure 3.4A, inset). It has been suggested that binding of oxidized pyridine nucleotides may facilitate flavin-disulfide interaction (Matthews et al. 1979). Therefore, *EcE3C45S* was subjected to NAD⁺-titrations, which were carried out at 10 °C in order to slow down a putative FAD-C4a-cysteinyl adduct formation. However, even in the presence of the pyridine nucleotide a significant absorption increase in the characteristic wavelength region at 380 nm was not detectable (Figure 3.4B) and hence an NAD⁺-induced collapse between Cys50 and FAD-C4a is unlikely. The mechanism of cysteinyl-C4a adduct formation will be discussed below in detail (3.1.5 and 3.1.6).

To extend the understanding of how the two-electron reduced state of the *E. coli* lipoamide dehydrogenase is stabilized, *EcE3C45S* was crystallized and the crystal structure was determined successfully. As for the wild type, the presence of ammonium sulfate as precipitant *EcE3C45S* was necessary. However, a lower pH value was required (pH 6.5 compared to pH 7.0). The obtained crystals also showed a pale orange-red color indicating that the charge transfer interaction is still active *in crystallo* (Figure 3.4C). *EcE3C45S* crystals belonged to space group I422 and contained two monomers per asymmetric unit assembled into a functional homodimer. The structure was solved by molecular replacement using the ground state *EcE3* structure as search model (3.1.3) was refined to $R_{\text{work}}/R_{\text{free}}$ of 23.3 %/27.4 % against data to 2.50 Å resolution (Table 5.3). Difference map peaks (mFo-DFc at 3 sigma level) of tetrahedral shape were modeled as sulfate ions as described for the ground state structure. 472 out of the 477 residues were traceable in both molecules whereas the residues resulting from cloning artefacts and the last C-terminal residues could not be traced and are most likely disordered. The overall fold of *EcE3C45S* is similar to the ground state structure. Two catalytic

functional dimers can be superimposed with an r.m.s.d. of 0.67 Å calculated on Ca positions indicating the high similarity. However, slight differences can be observed which, are mainly located in the surface exposed regions of the NAD⁺- and FAD-binding domain whereas the enzyme's core regions are almost identical. Since the structural data of *EcE3C45S* was of reasonable quality the resulting model resembles a snapshot of the two-electron reduced state of the enzyme and thus provides structural information about a central intermediate during catalysis. In this intermediate step the disulfide bridge is entirely broken and the cysteine residue facing the flavin cofactor is present as a thiolate (3.1.2). Major emphasis was therefore devoted to the hydrogen bond network at the active site which stabilizes the anionic form of Cys50.

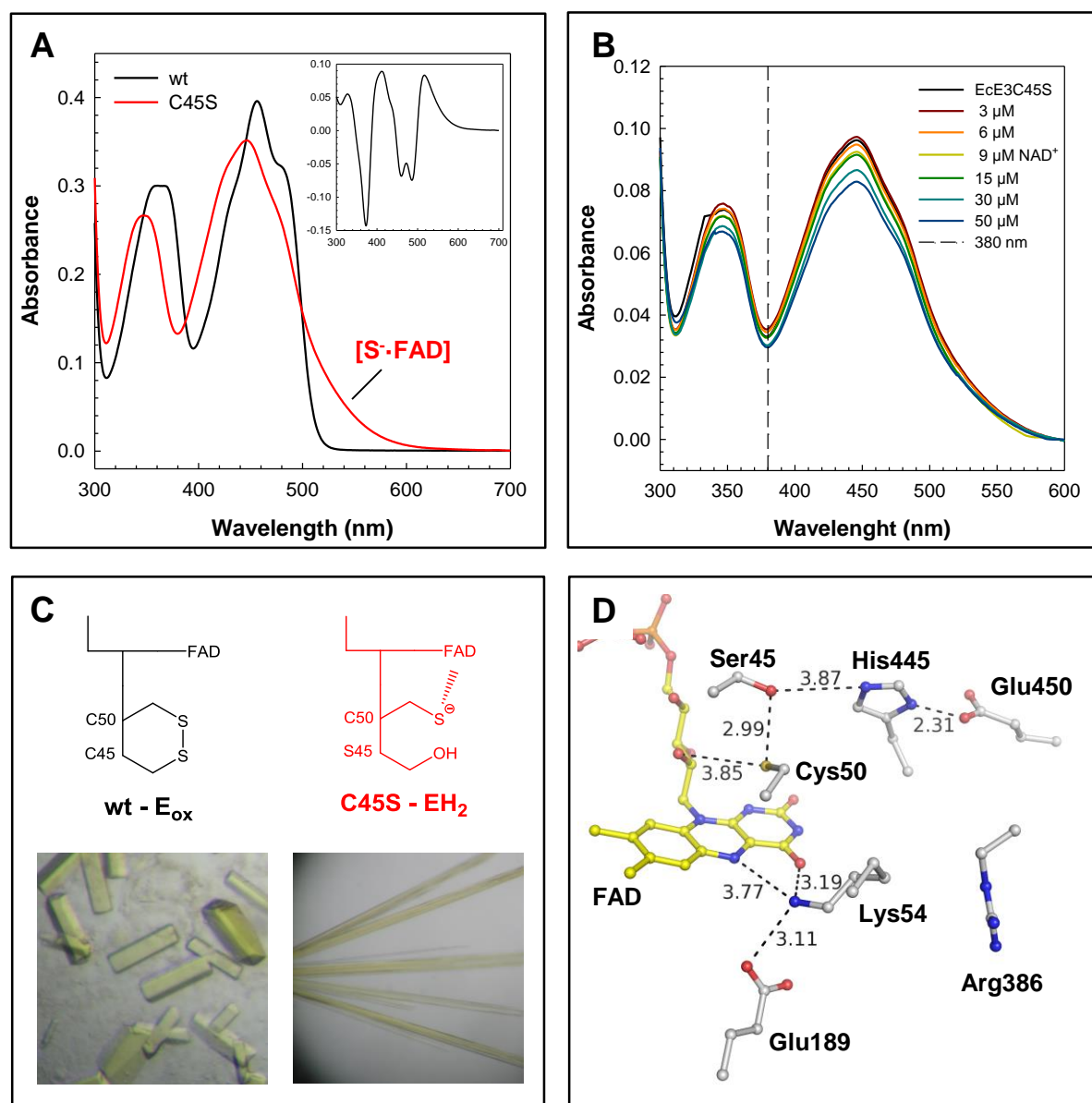


Figure 3.4 General characterization of *EcE3-EH₂*.

(A) Resting state absorbance spectra of *EcE3*wt and C45S. The broad absorbance band between 500 and 600 nm indicates the charge transfer complex between the anionic Cys50 and FAD. (B) NAD⁺-titration of *EcE3C45S* at pH 7.6. Addition of NAD⁺ does not lead to increase in absorbance at 380 nm. An accumulation of the cysteinyl-C4a adduct is therefore unlikely. (C) Schematic of the active sites in *EcE3*wt and C45S (top) and corresponding protein crystals. *EcE3C45S* retained its orange-red color *in crystallo* indicating that the charge transfer complex between Cys50 and FAD is still active. (D) Hydrogen bond network in *EcE3-EH₂*. The thiolate of Cys50 is stabilized by a hydrogen bond to the OH-group of Ser45 and the 2'-hydroxyl group of the ribityl chain (distances in Å).

A direct interaction of the Cys50-thiolate between the hydroxyl group of Ser45 and the 2'-hydroxyl of the ribityl side chain could be observed (Figure 3.4D). In addition, Ser45 might be stabilized by a polar interaction with His445. However, the mentioned polar interactions span distances in the range of $>3 \text{ \AA}$ and are thus of a weak nature. Therefore, it is likely that additional elements contribute to thiolate stabilization (see discussion below). The ϵ -amino group of Lys54 is coordinated by the flavin cofactor as well as by Glu189. The N5 and O=4 atom of the isoalloxazine form polar interactions to Lys54 as well as to the carboxylic function of the adjacent residue. Arg386, an active site nearby residue, is not involved in the hydrogen bond network. The role of the catalytic diad (His445 and Glu450) and of Lys54 and Arg386 during catalysis will be discussed later (3.3.1 and 3.3.2).

The stabilization of the thiolate in lipoamide dehydrogenases has been discussed controversially over the last decades. It was assumed that the imidazole of the conserved histidine directly functions as stabilizer of the thiolate (Kim and Patel 1992b; Matthews et al. 1979). The structural investigation of the ground state structure and of *EcE3C45S* revealed that the N3 atom of His445 cannot donate a hydrogen bond to Cys50 (3.3.1.1). However, weak interaction is observed to Ser45 the major hydrogen bond donor to the thiolate attributing a more indirect role for His445 during thiolate stabilization. The pKa for Cys50 was determined to be 2.7 and is thus relatively low compared to other cystine containing oxidoreductases (Hopkins and Williams 1995a). This denotes that the particular milieu of the redox active cystine is pivotal for the acidity of the respective thiol. Besides the hydrogen bond network described above further factors may contribute to thiolate stabilization and the lowering of the pKa value. At first, the redox active cystine is part of a long alpha helix belonging to the FAD-binding domain located in the core of the catalytic unit (3.1.3). It was suggested that the positive end originating from such helix dipole might contribute to stabilization of the thiolate (Benen et al. 1991). Secondly, π -stacking interactions between the electron-rich sulfur and the electron-deficient FAD cofactor also may contribute to stabilization implying that cofactor and cysteine residue truly act as an electron-donor-acceptor complex. The concomitant alteration in the electronic property of the FAD is underpinned by a further bending of the cofactor compared to the ground state structure (Figure 5.23).

In summary, the crystal structure analysis of the two-electron reduced state of *EcE3* revealed that the catalytic role of the interchange thiol (Cys45) has to be expanded. So far, this residue was stated to be solely important with regard to bond formation with the substrate dihydrolipoamide forming a mixed disulfide and the subsequent electron transfer to Cys50 yielding the charge transfer complex. However, Cys45 also stabilizes the latter complex by a hydrogen bond contributing directly to a further central catalytic state. Moreover, the results obtained allow the prediction that Cys45 is protonated during this state of catalysis in the wild type enzyme.

3.1.5 Spectral Evidence for the Cysteiny-C4a Adduct in a monothiol Variant of *EcE3*

Rapid reaction experiments showed that the covalent C4a-flavin adduct is highly instable leading to a limited accumulation which make this central intermediate undetectable during the transfer of electrons from the reduced flavin to the redox active cystine (3.1.2). These results are consistent with previously published data for the lipoamide dehydrogenase from *Mycobacterium tuberculosis* (Argyrou et al. 2002). Further, a direct kinetic observation of the intermediate during catalysis has never been possible. The putative accumulation from the opposite direction, transfer from the reduced disulfide to the oxidized flavin is discussed in 3.2.3. Thus far, the C4a-cysteiny adduct has only been observed under non-physiological conditions using several enzymes belonging to the class of flavin-dependent oxidoreductases. At first, in monoalkylated pig heart lipoamide dehydrogenase upon addition of NAD^+ (Thorpe and Williams 1976b, 1981), secondly, in the two electron reduced thioredoxin reductase substituted with 1-deaza-FAD at low pH (O'Donnell and Williams 1984), and thirdly, also at low pH in mercuric reductase upon rapid mixing with NADPH (Sahlman, Lambeir, and Lindskog 1986). In the latter three cases, the spectrum of the adduct was estimated by extrapolation. However, there was also direct spectral evidence for the C4a adduct, when an oxidized active site triple variant (three out of the four catalytic cysteines were replaced by an alanine, ACAA mutant) of mercuric ion reductase was titrated with NADP^+ also at low pH (Miller et al. 1990).

Therefore, a monothiol variant (*EcE3C45A*) was generated in which the interchange thiol forming the mixed disulfide during catalysis was replaced by an alanine. This catalytically almost inactive variant (5.4) was then subjected to NAD^+ titrations at lower pH values since it is apparent that both lower pH values and the presence of the pyridine nucleotide facilitate adduct formation. The UV-Vis ground state spectrum of *EcE3C45A* is clearly different from that of the wild type enzyme (5.2B). The spectrum shows a hypsochromic shift yielding in a $\lambda_{\text{max}} = 448 \text{ nm}$, a way less pronounced shoulder in the 470 nm region and a very small absorbance between 500 and 700 nm. Interestingly, the spectral property is congruent with the spectrum of the aforementioned lipoamide dehydrogenase from pig heart in which the interchange thiol had been alkylated (Thorpe and Williams 1976b). No indicative band in the range of 380 nm is present in the difference spectrum suggesting that the remaining cysteine residue is not bound to the cofactor *per se*. (5.2B, inset). A comparison with the EH_2 mimic *EcE3C45S* leads to the assumption that Cys50 is mostly present in its thiol form since the typical charge transfer band in the 530 nm region indicating the thiolate-FAD interaction is missing. The fact that the main hydrogen bond donor - Cys45 during the EH_2 state - stabilizing the anionic form of Cys50 was removed further underpins this assumption (3.1.4). Moreover, it was demonstrated that replacement of active sites cysteine residues with alanines in mercuric ion reductase increased the hydrophobicity and thus consequently raised the pK_a leading to formation of the thiol form. (Miller et al. 1990).

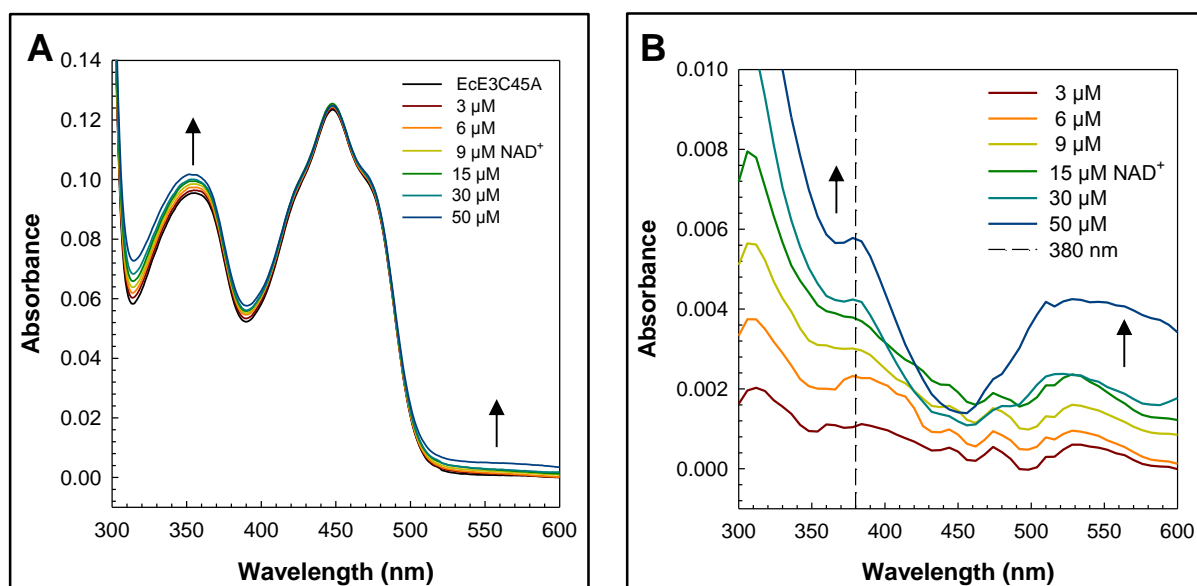


Figure 3.5 NAD^+ titration of *EcE3C45A*.

(A) Lower temperature NAD^+ titration at 10 °C and in 100 mM MES pH 6.0. Binding of NAD^+ leads to increase in absorbance between 300 – 400 nm and between 500 – 600 nm, respectively. (B) Difference spectra of the same titration. NAD^+ induces a band formation peaking at 380 nm with a concomitant broad increase in absorbance from 500 to 600 nm. Difference spectra were smoothed according to a bisquare weighting technique and a polynomial regression. The experiments were performed in duplicates.

Addition of NAD^+ led to small changes in the spectrum of *EcE3C45A* (Figure 3.5A). An increase in absorbance occurs from 300 to 400 nm with a concomitant smaller increase from 500 to 600 nm. However, the changes in absorption are not as pronounced as compared to the changes observed in the mercuric reductase ACAA mutant where a loss of the typical oxidized flavin absorption was observed (Miller et al. 1990). However, the generated difference spectra clearly indicated the presence of a band peaking at 380 nm with increasing NAD^+ concentrations albeit with a small amplitude (Figure 3.5B). This increase is accompanied with a quenching of the flavin peak around 450 nm and a more pronounced increase in the red part of the spectrum. Strikingly, comparable spectral changes could be observed at pH 8.3 (Figure 5.2) indicating that the spectral changes also occur in a more basic environment. NAD^+ titrations under the same conditions for the wild type enzyme did not lead to any increase throughout the entire spectrum, solely the quenching in the 450 nm region was visible (Figure 5.3).

The obtained spectra suggest that a covalent adduct populated in minor fractions since the rise in absorption at 380 nm is completely consistent with the formation of FAD-C4a-adducts (Ghisla et al. 1974, 1977). Further, the necessity for NAD^+ binding to induce adduct formation is consistent with previous studies (Matthews et al. 1979; Miller et al. 1990; Thorpe and Williams 1976b, 1981). It was

suggested that binding of the positively charged nucleotide at the *re* face of the flavin increases the electrophilicity of the oxidized flavin, thereby promoting C4a-cysteinylation (Miller et al. 1990). However, recent results generally demonstrated that structural perturbations at the active site seem to be essential to close internuclear distances (Klinman 2009, 2010). The role of NAD⁺ during catalysis might therefore be expanded. Given the inevitable presence of NAD⁺ to drive adduct formation combined with the structural geometry of the FAD-C4a-cysteinylation bond (3.1.6), it is not unlikely that the pyridine nucleotide permits an active site compression which is pivotal for the enzyme's transient catalysis.

Formation of the C4a-adduct in the *EcE3* monothiol variant was possible at both low and high pH. It is therefore likely that the remaining thiol delivers the proton required for N5 protonation during FAD-C4a-cysteinylation adduct formation. For mercuric reductase ACAA mutant it was suggested that this process might be assisted by polarization of the thiol by general-base catalysis (Miller et al. 1990), however the residue qualified for this polarization (Tyr441) turned out to be not correctly positioned (Ledwidge et al. 2005). Further, the distance of the *EcE3* active site His445 is too long for a direct interaction with the adduct forming thiol based on the information provided by the ground state structure (Figure 3.15). It is therefore likely that a general base catalysis is not required to drive a thiol-based adduct formation so that the increased electrophilicity of the oxidized flavin upon NAD⁺ binding is sufficient to promote the collapse.

3.1.6 Crystallographic detection of the Cysteinyl-C4a Adduct

During the course of this study it was possible to gather structural information of two distinct catalytic states of the *EcE3* reaction cycle. Thereby, the ground state structure represents the oxidized state of the enzyme (3.1.3) and the structure of *EcE3C45S* mimics the two-electron reduced state (3.1.4). Moreover, the ground state structure also demonstrated the local flexibility of the active site due to opening of the redox active disulfide bridge by radiation damage during data collection. Given the information that the synchrotron X-ray radiation can partially alter the enzyme's redox state this radiation was used to trigger the formation of the covalent FAD-C4a-cysteinyl adduct *in crystallo*. Two prerequisites were therefore necessary, at first, a further accumulation of the *open* state of the reactive cysteines and, secondly, the presence of NAD^+ in the crystal at the time-point of the data collection since the nucleotide is thought to facilitate adduct formation. The necessity of the presence of NAD^+ to induce adduct formation was further discussed in 3.1.5.

A single wild type crystal was therefore soaked with 5 mM NAD^+ during the cryo protection step and the structure was determined using the wild type structure as the starting model (3.1.3). The six monomers present in the asymmetric unit were accordingly labeled A – F. The structure was refined to $R_{\text{work}}/R_{\text{free}}$ of 17.6 / 22.1 % against data to 2.6 Å resolution using NCS restraints (Table 5.3). Difference map peaks (mFo-DFc at 3 sigma level) which was not related to the protein or water molecules after structure refinement were modelled as described above. At least 469 out of the 474 residues were visible in each of the six molecules occupying the asymmetric unit whereas the missing residues are housed in the C-terminal part, a fact which was also observed in the structure resolved at higher resolution. Despite the reasonable quality of the structure no clear evidence for presence of an NAD^+ molecule at the *re* face of the flavin cofactor was found. It was demonstrated that NAD^+ bound to human lipoamide dehydrogenase can adopt different conformations at the binding site (Brautigam et al. 2005) explaining a certain flexibility of this ligand-enzyme interaction. Moreover, the usage of a highly concentrated sulfate solution as precipitant (2.4 M compared to 5 mM NAD^+) intrinsically leads to a higher occupancy of the precipitant at the diphosphate anchor binding site prohibiting a higher population for NAD^+ (Figure 5.22). However, the usage of higher concentrations of the pyridine nucleotide during the phase of cryo protection led to deterioration of the diffraction properties of the crystals and was therefore not taken into consideration for further experiments.

Occupancy refinements as conducted for the ground state structure revealed that the catalytic disulfide resided to ~90 % in the open conformation. The first requirement, a further radiation-induced reduction of the catalytic cystine, was therefore fulfilled. Moreover, during the phase of model improvement cohesive electron density between Cys50 and the C4a atom of the flavin cofactor could be observed in subunits A and F in the 2mFo-DFc density map. To further elucidate the nature of this density 2mFo-DFc and mFo-DFc difference maps were calculated using CNS program (Brunger 2007). This analysis revealed the presence of positive difference peaks near Cys50 pointing towards

FAD-C4a (Figure 3.6A) in all *EcE3* molecules present in the asymmetric unit. Since the default settings of the refinement program did not allow a further converging of Cys50 towards the flavin due to repulsive interactions the flavins were flagged as alternate conformations corresponding to Cys50 in open and closed state, which resulted in overcoming the restriction. Subsequent refinement led to a further convergence of Cys50 towards the positive difference peaks and thus the cofactor (Figure 3.6A).

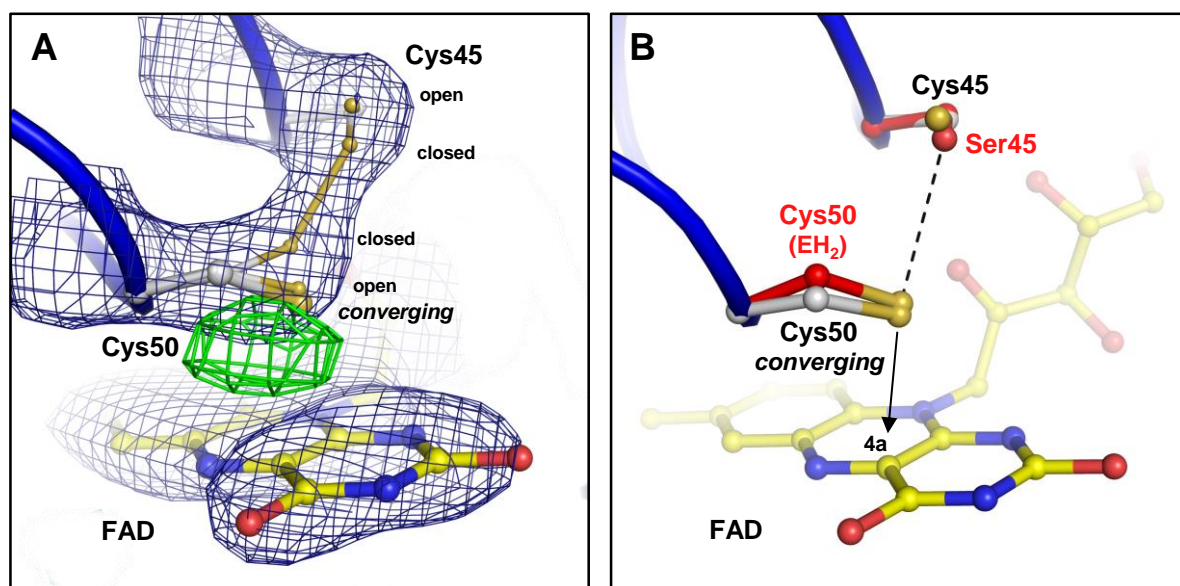


Figure 3.6 The flexibility of cysteine50 is determined by its hydrogen bond donor.

(A) Convergence of Cys50 towards FAD-C4a. CNS calculated 2mFo-DFc map countered at 2 σ (blue mesh) and mFo-DFc difference map countered at 3 σ (green mesh) in molecule A. Applying an alternate conformation of FAD allowed a further convergence of Cys50 towards FAD since repulsive interactions restraints were overcome. The converging conformer of Cys50 is displayed by an enlarged ball and stick representation. Residual five molecules in the asu showed comparable difference peaks.

(B) Superposition of the catalytic cystine of the *EcE3*-NAD structure (light grey) with the EH₂ state of *EcE3C45S* (red). In *EcE3C45S* a further migration towards FAD-C4a is prevented. The hydrogen bond between Ser45 and Cys50 is indicated by a dashed line. For convenience the *closed* conformation of the *EcE3*-NAD structure is not shown.

A comparison with the structure of the two-electron reduced enzyme (*EcE3C45S*) revealed that the converged Cys50 residue is in lower distance to the C4a atom of the cofactor (Figure 3.6B). Multiple rounds of PHENIX refinements with the same parameters, which led to convergence of Cys50 in the E3-NAD⁺ structure, confirmed that the anionic Cys50 of the EH₂ structure resided at its position. This result is consistent with in solution experiments which showed that C4a-cysteinyll adduct formation

EcE3C45S is impeded (Figure 3.4). In addition, this impairment is further confirmed by a significantly reduced enzyme activity compared to the wild type enzyme (5.4). The structural and electronic properties leading to this inertance of the thiolate in the variant have been discussed in 3.1.4. Though the convergence of Cys50 could be proven an appropriate model building was not possible since the difference map peak were at a position within the B-factor spread of the *open* conformation.

To rule out that the additional density was only based on elevated atomic displacement parameters and was thus model biased the possible presence of a covalent conjugate between Cys50 and FAD-C4a was investigated by the generation of simulated-annealing OMIT maps in which both the flavin cofactor and the cystine were omitted. The calculated model-bias free mFo-DFc electron density map revealed the presence of prominent cohesive density between cysteine50 and the C4a atom of the flavin in molecule A and molecule F of the asymmetric unit and thus the likely presence of a populated covalent FAD-C4a-cysteinyll adduct (Figure 3.7).

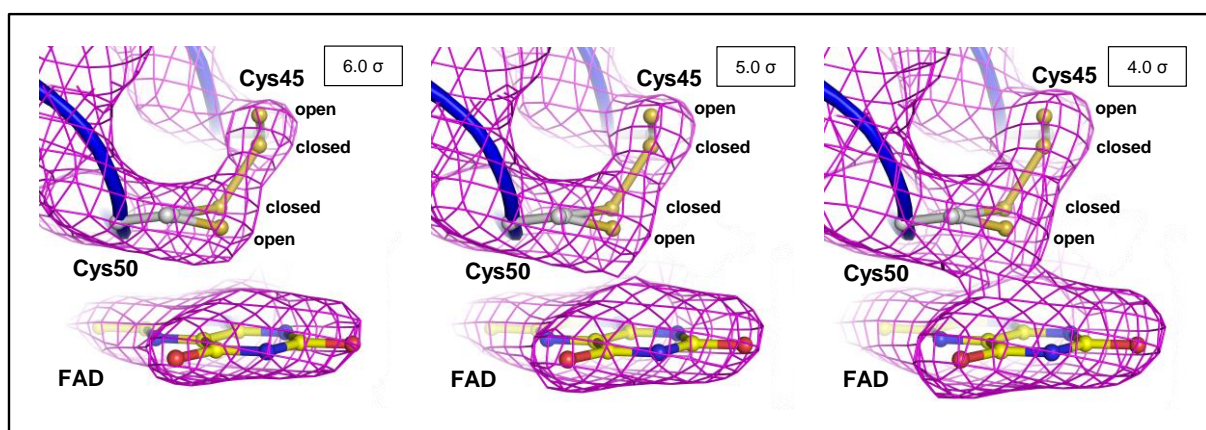


Figure 3.7 Evidence for cohesive electron density between Cys50 and FAD-C4a.

The presence of cohesive density implicating a covalent linkage between Cys50 and FAD-C4a is supported by an mFo-DFc simulated-annealing OMIT map displayed at different sigma levels (magenta mesh) for one of the active sites (monomer F). Note that with decreasing sigma level the electron density converges from both omitted parts, the cystine and the FAD. An overview of SA OMIT maps for all molecules in the asymmetric unit countered at equal sigma level is shown in the appendix (Figure 5.25).

Two aspects have to be considered underpinning the likely presence of a covalent linkage between Cys50 and FAD-C4a. At first, the density approaches from both interacting partners towards each other, from the cysteine as well as the FAD. Thus, the congruent density is not only based on a highly mobile cysteine further migrating towards the cofactor but also on structural rearrangements at the flavin site presumably the formation of a tetrahedral C4a atom pointing towards Cys50. Secondly, the

atomic displacement parameters of the cofactor and the redox active cystine are not significantly elevated compared to the residues around the active site (Figure 5.24). Taking these considerations into account an appropriate model building of the covalent adduct was possible.

The electron density allowed the modelling of additional conformations of both the flavin and Cys50. An additional side chain rotamer for Cys50 (50 % probability) taken from the *Coot* side chain library (Emsley et al. 2010) suitable fitted into the SA OMIT maps without the need of further adjustments (Figure 3.8). A covalent adduct at the C4a position of the flavin requires a tetrahedral geometry of this part of the isoalloxazine moiety. Therefore, a tetrahedral FAD with the C4a atom pointing towards Cys50 was modeled in the OMIT density using a rigid body fit. This fit implicated a restraint concerning the bond length between the C4a and sulfur atom of Cys50 which was set to 1.81 Å, a typical length for a C-S bond (Figure 3.8). The resulting overall model adequately fitted into calculated OMIT maps and thus likely reflects the crystallographic detection of the FAD-C4a-cysteinylyl adduct which has been predicted to exist but an experimental proof was thus far missing. This study supports the existence of this long-sought-after intermediate not only by UV-Vis spectroscopic studies (3.1.5) but further underpins its existence by means of X-ray crystallography.

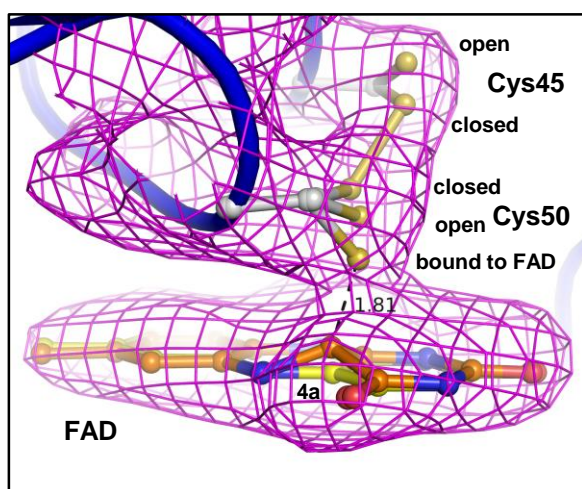


Figure 3.8 Structural model of the covalent C4a-cysteinylyl adduct.

The model represents an additional redox state of *EcE3*. Besides the previously described *open* and *closed* conformation of the redox active cystine the modelling of the conformer which is bound to the FAD is possible. The tetrahedral FAD was modelled into the mFo-DFc SA-OMIT map (countered at 4σ ; magenta mesh) using a rigid body fit implying a bond length of 1.81 Å between C4a and S γ of Cys50.

3.1.7 Is the geometry of the FAD-C4a-cysteinylyl adduct the fundament for its transience?

Given the spectroscopic and structural information about the transient nature of the FAD-C4a-cysteinylyl adduct in *EcE3* a comparison with this type of adduct present in LOV domains is possible. In

solution data suggested that the C4a-cysteinyl adduct only accumulates to a minor extent (3.1.5). In addition, a direct spectroscopic observation during the reaction cycle was also not possible, neither with the oxidative half-reaction (NADH as reductant) nor with the reductive half-reaction (Lip3H₂ as reductant) as starting point (3.1.2 and 3.2.3). The half-life was estimated to be <2 ms and the decay is thus at least 250-fold faster compared to C4a-cysteinyl adducts in LOV domains. Here, the thermally driven dark state recovery is generally larger than 500 ms but can also last hours (Conrad et al. 2014). The decay in LOV domains is modulated by numerous of effects like the accessibility of solvent towards the active site, the electronic environment of the flavin and the hydrogen bonding network to the cofactor (Losi and Gärtner 2011, 2012; Zoltowski et al. 2009). Moreover, the presence of a base also has the ability to modulate adduct decay (Alexandre et al. 2007). The differences in the hydrogen bonding network of *EcE3* compared to LOV domains around the flavin cofactor will be discussed later (3.4.4).

Besides this plethora of key modulators, a geometrical aspect was also taken into account acting as driving force responsible for adduct decay. The energy content of the adduct state in LOV domains was estimated to be 110 – 140 kJ mol⁻¹ indicating a strained protein conformation (Losi, Kottke, and Hegemann 2004; Losi, Quest, and Gärtner 2003). These results are in slight disagreement with X-ray crystallographic data (Crosson and Moffat 2001, 2002). Dark and lit state structures revealed that only minor rearrangements in the protein are required to induce both adduct formation and decay. Indeed, the structural changes seem to be limited to the FMN on the one, and the bond forming cysteine on the other hand yielding a tetrahedral C4a-cysteinyl adduct (Crosson and Moffat 2002) (Figure 3.9A). The small α -helix of which the bond-forming cysteine is part of is positioned in a way that a simple rotamer movement of the latter cysteine is sufficient to fulfill adduct formation. On the contrary, the redox active cystine of *EcE3* is part of a long α -helix protruding through the entire *EcE3* monomer which does not allow the formation of relaxed tetrahedral flavin-cysteinyl adducts. A more detailed comparison of these structural data revealed that the adduct in *EcE3* deviates from tetrahedral geometry harboring a C β -S γ -C4a angle of >117 ° (Figure 3.9B). Since geometrical aspects have been shown to be crucial to enhance enzyme catalysis (Lüdtke et al. 2013; Tittmann 2014) it is possible that this aspect also have to be taken into account for lipoamide dehydrogenases. It is therefore most likely that the high transience of the adduct is, at first, based on its distorted geometry of the C4a-cyteinyl adduct and secondly based on the necessity of the presence of NAD⁺ which is required *per se* to facilitate adduct formation (3.1.5).

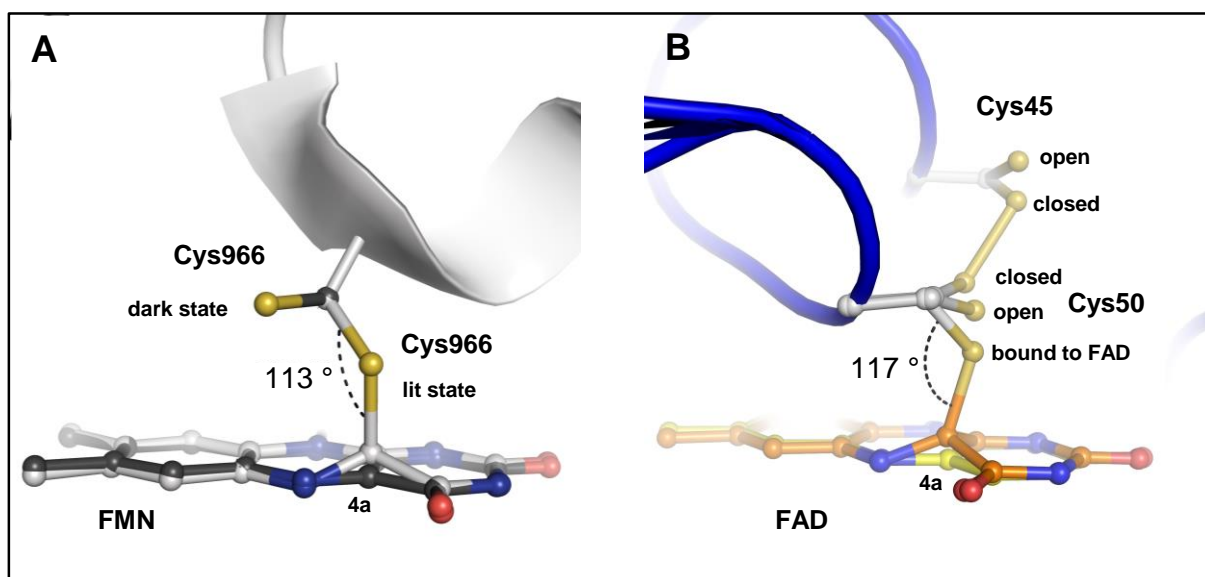


Figure 3.9 Comparison of the geometries of C4a-cysteinylyl adducts in LOV domains and in *EceE3*. (A) Superposition of the dark (dark grey) and lit state (light grey) of *Adiantum* LOV2 (PDB: 1G28 and 1JNU). The angle of 113° between Cβ-Sγ-C4a allowed a tetrahedral modelling. (B) Structural model of the covalent adduct in *EceE3*. The Cβ-Sγ-C4a angle of >117° reveals an extended deviation from tetrahedral geometry.

3.2 Investigation of the reductive half-reaction of *EceE3* using *EcLip3* as native Substrate

The assignment of different reaction intermediates starting from the oxidative half-reaction with NADH as reductant was successfully established (3.1.2). To further investigate the reaction mechanism of *EceE3* the isolated reductive half-reaction was also subjected to stopped-flow absorbance spectroscopy. The native substrate of lipoamide dehydrogenases are the reduced lipoamide arms of the E2 component of several multienzyme complexes. Thus, the most elementary *in vitro* substrates would be D,L-dihydrolipoamide or D,L-dihydrolipoate. However, these substrates show high K_M values, and in addition, D,L-lipoamide has limited solubility in aqueous solutions (2.2.4.1) (Argyrou and Blanchard 2001). There has been effort to mimic the physiological substrate more closely thereby improving substrate affinity and water solubility by the synthesis of D,L-lipoylbutanoate and D,L-lipoylpentanoate (Argyrou et al. 2003). Both artificial substrates, containing an extended lipoyl acid arm, with three and four additional methylene groups, respectively, were used successfully as substrates after reduction with borohydride yielding the respective dihydro-form. Significant higher k_{cat}/K_M values for both synthesized substrates relative to that of D,L-lipoamide reflected the increased specificity (Argyrou et al. 2003). However, transient kinetic and spectroscopic data with the

physiological substrate as reductant are missing. Therefore, the entire third lipoyl domain of the *E. coli* dihydrolipoyl transacetylase (*EcE2*) was isolated, transferred in its dihydro-form under physiological conditions and used as substrate during both stopped-flow and sequential stopped-flow absorbance spectroscopy. The isolated lipoyl domain was termed *EcLip3*.

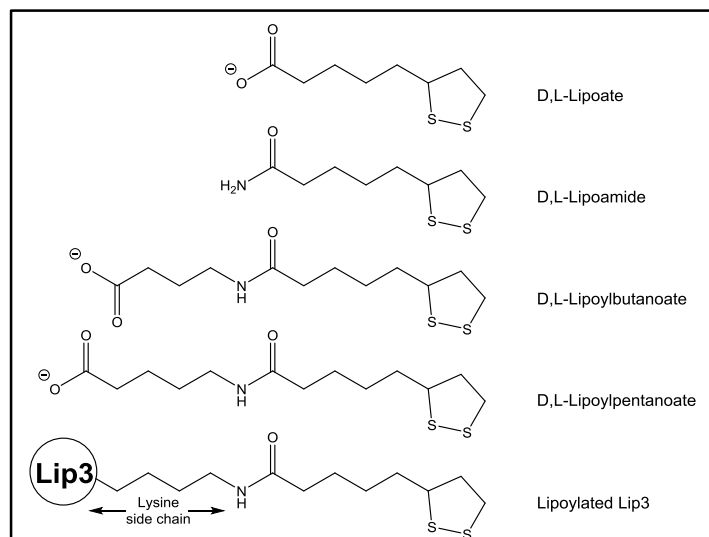


Figure 3.10 *In vitro* and native substrates of lipoamide dehydrogenases. D,L-lipoate and D,L-lipoamide reflect the most elementary artificial substrates and suffer from high K_M values and limited water solubility. D,L-lipoylbutanoate and D,L-lipoylpentanoate were synthesized and successfully used as substrates to overcome the mentioned problems showing increased catalytic proficiencies (Argyrou et al. 2003). *EcLip3* is composed of the innermost lipoyl domain of *EcE2* including lipoic acid

3.2.1 Characterization of *EcLip3* and its Reduction to the dihydro-form (*EcLip3H₂*)

Isolation and characterization of a single lipoyl domain has already been achieved, however, this isolated domain represented a hybrid between the first and third lipoyl domains of the *E. coli* E2 component (Ali and Guest 1990). In contrast, *EcLip3* harbors the native *EcE2* amino acid sequence (5.1). His₆-SUMO-*EcLip3* could be purified in high amounts and removal of the fusion protein lead to the desired isolated domain. Since *EcLip3* should serve as substrate for *EcE3* the lipoylation status of the isolated domain after purification was essential since unlipoylated domains would compete with the active sites of the oxidoreductase and thus influence kinetic and spectroscopic parameters. The lipoylation status was checked by MALDI-TOF MS of tryptic fragments of *EcLip3* (2.2.6.2). An MS approach without prior tryptic digestion to check the presence of the post-translational modification was described earlier (Seifert 2010; Wei et al. 2003). However, the application of the latter method is limited to the use of single isolated domains since a discrimination of two individual lipoylation sites is not possible. On the contrary, the generation and further analysis of tryptic fragments offers the potential for an future application on multidomain constructs, e.g. *EcLip2-Lip3*, or even the full-length *EcE2* component. MALDI-TOF MS revealed that *EcLip3* was fully lipoylated after purification

ensuring homogeneity of the future substrate (Figure 3.11A). Therefore, an *in vitro* post-translational modification using lipoyl-protein ligase A was not necessary.

Interaction of *EcLip3* with *EcE3* was investigated by ITC using the same buffer conditions as used for the kinetic experiments (3.2.2). Binding between the two individual components was evident, however detected changes in enthalpy were rather small (Figure 5.20). Thus, a reliable determination of binding parameters was not possible. A comparable binding behavior was described for the interaction of the human lipoyl domain 2 (*hLip2*) and the human pyruvate dehydrogenase (*hE1*) (Seifert 2010). It might be concluded that binding of lipoyl domains to other PDH components is always of a weak nature, however, this contrasts with earlier published results which showed binding constants in the lower micromolar range (Kato et al. 2008). The interaction of the motile parts of the PDH complexes are thus still a matter of controversial and were not further studied during this project. The affinity of reduced *EcLip3* (*EcLip3H₂*) to *EcE3* was not investigated since *EcLip3H₂* is able to serve as substrate (see below) and thus detected heat changes would reflect reduction of the flavin cofactor rather than binding events.

Reduction of a dithiolane moiety usually requires borohydride and low pH values (Argyrou et al. 2003), conditions which are not suitable for isolated proteins. Therefore, the transfer into dihydrolipoamide under physiological conditions is required and can be realized by the usage of TCEP (Wang et al. 2014). Reduction of *EcLip3* to *EcLip3H₂* by TCEP leads to opening of the dithiolane moiety and an concomitant loss in absorbance at 333 nm (Figure 3.11B). According to far-UV CD spectra the secondary structure of *EcLip3* is not affected by the reduction retaining its signature typical for β -turns (Perczel and Fasman 1992). The spectroscopic results are moreover in line with previously published NMR data of the aforementioned hybrid lipoyl domain (Green et al. 1995).

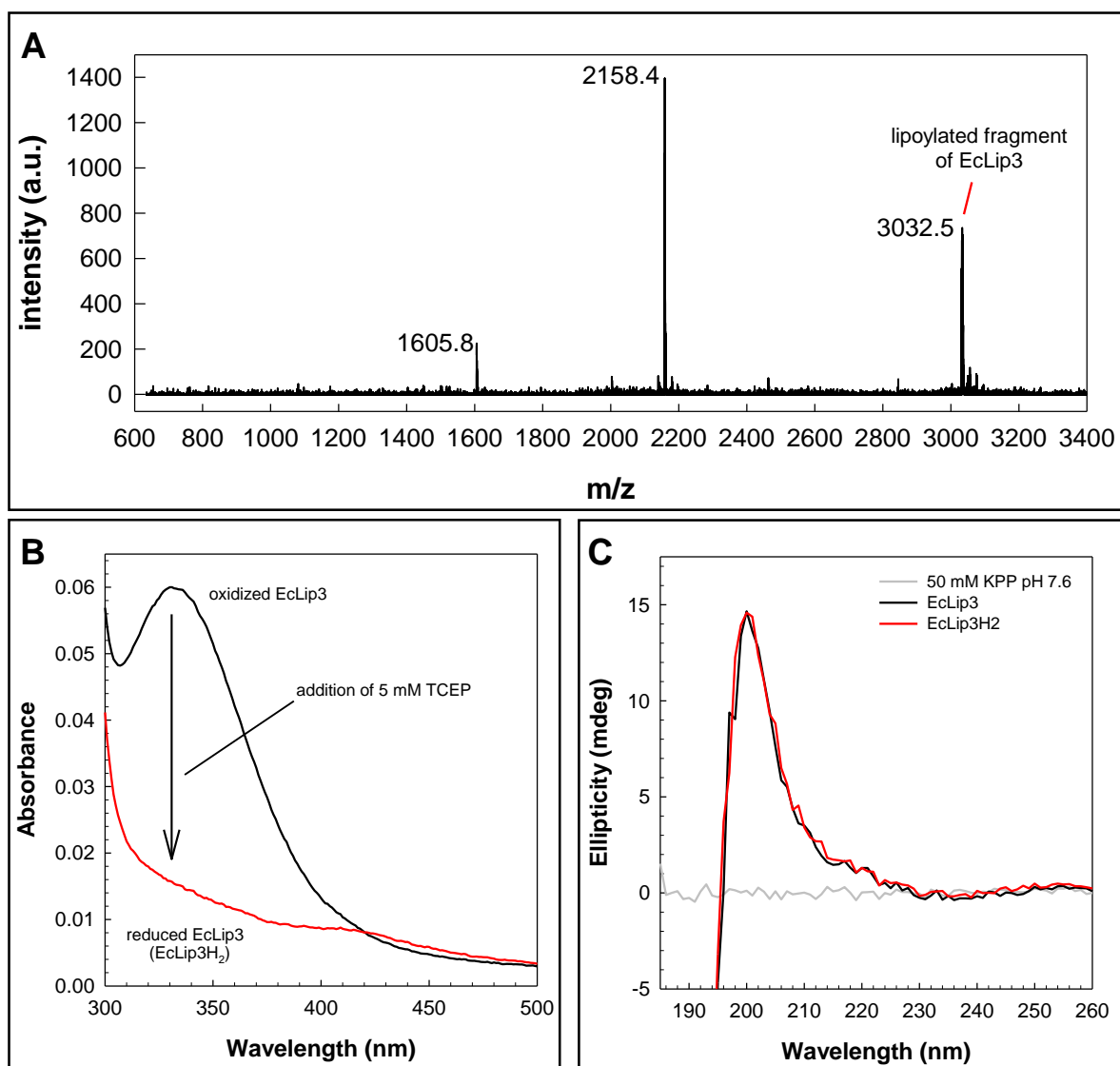


Figure 3.11 Evidence of the structural integrity of *EcLip3* and *EcLip3H₂*.

(A) MALDI-TOF MS analysis of tryptic *EcLip3*. Presence of the fragment with an m/z 3032.0 shows that *EcLip3* is fully lipoylated after purification (2.2.6.2). (B) Reduction of *EcLip3* by TCEP to *EcLip3H₂* leads to decrease in absorbance at 333 nm. (C) Far-UV-Vis CD spectra of *EcLip3* and its dihydro-form (0.1 mg/mL each). Reduction of the dithiolane moiety has no influence on the secondary structure.

3.2.2 *EcLip3H₂* as native Substrate to track the reductive Half-reaction of *EcE3*

Since reduction of *EcLip3* to *EcLip3H₂* was successful, the reduced form should serve as native reducing agent for *EcE3* to track the reductive half-reaction using stopped-flow absorbance spectroscopy. Major emphasis was thereby devoted to the detection of the covalent FAD-C4a-cysteinyl adduct. Rapid reduction of E_{ox} by *EcLip3H₂* under single turnover conditions transferred the oxidized form of the enzyme into its two-electron reduced state (EH_2). The absorbance increased at 390-440 and 500-620 nm, and decreased at 340-380 and 440-500 nm. The presence of the broad absorption band between 500-620 nm and the concomitant blue shift of the flavin peak reflects the charge-transfer situation between the anionic form of Cys50 and the flavin cofactor (Figure 3.12A). Titration of *EcE3* with >10-fold molar excess of *Lip3H₂* did not lead to EH_4 formation indicating that the enzyme resided in the catalytically active EH_2 state. This result is in disagreement with a previous study which demonstrated that dihydrolipoic acid is indeed able to overreduce the *E. coli* enzyme to the EH_4 state under anaerobic conditions (Reed et al. 1960). The comparable reversible midpoint potential for dihydrolipoic acid was determined to be - 325 mV at pH 7 and 25 °C and is thus on par with that of NADH (Ke 1957; Uden and Bongaerts 1997). A comparable reduction behavior should be the consequence; however, reduction of *EcE3* by the native domain seems to be more complex than with the low molecular weight substrates.

Formation of the charge-transfer band at 530 nm occurs monoexponentially with $\sim 180\text{ s}^{-1}$ (Figure 3.12C), which is approximately 3.5-fold faster compared to single turnover conditions during the oxidative half-reaction using NADH as reductant (3.1.2). The following decay proceeds with at least two exponentials and probably results in the multiple equilibria of the EH_2 state as described in detail in 3.1.2 and 3.1.4. According to the absorbance trace at 380 nm there is no evidence for a significant accumulation of the covalent FAD-C4a-cysteinyl adduct, neither during Cys50-thiolate-formation nor during development of the different equilibrium species (Figure 3.12D). The decrease in this absorbance range absorbance is in fact based on the blue shift of the entire EH_2 flavin signature.

Though a direct evidence for the cysteinyl-C4a adduct was not found, *EcLip3H₂* was successfully used as a native reductant for *EcE3* allowing the spectroscopic and kinetic investigation of the reductive half-reaction. Besides the usage during rapid reaction measurements, an application of *EcLip3H₂* during classic steady-state kinetics is also imaginable. Purification yields and the fact that *EcLip3* could be highly concentrated (>3 mM) would thus allow the determination of its catalytic proficiency.

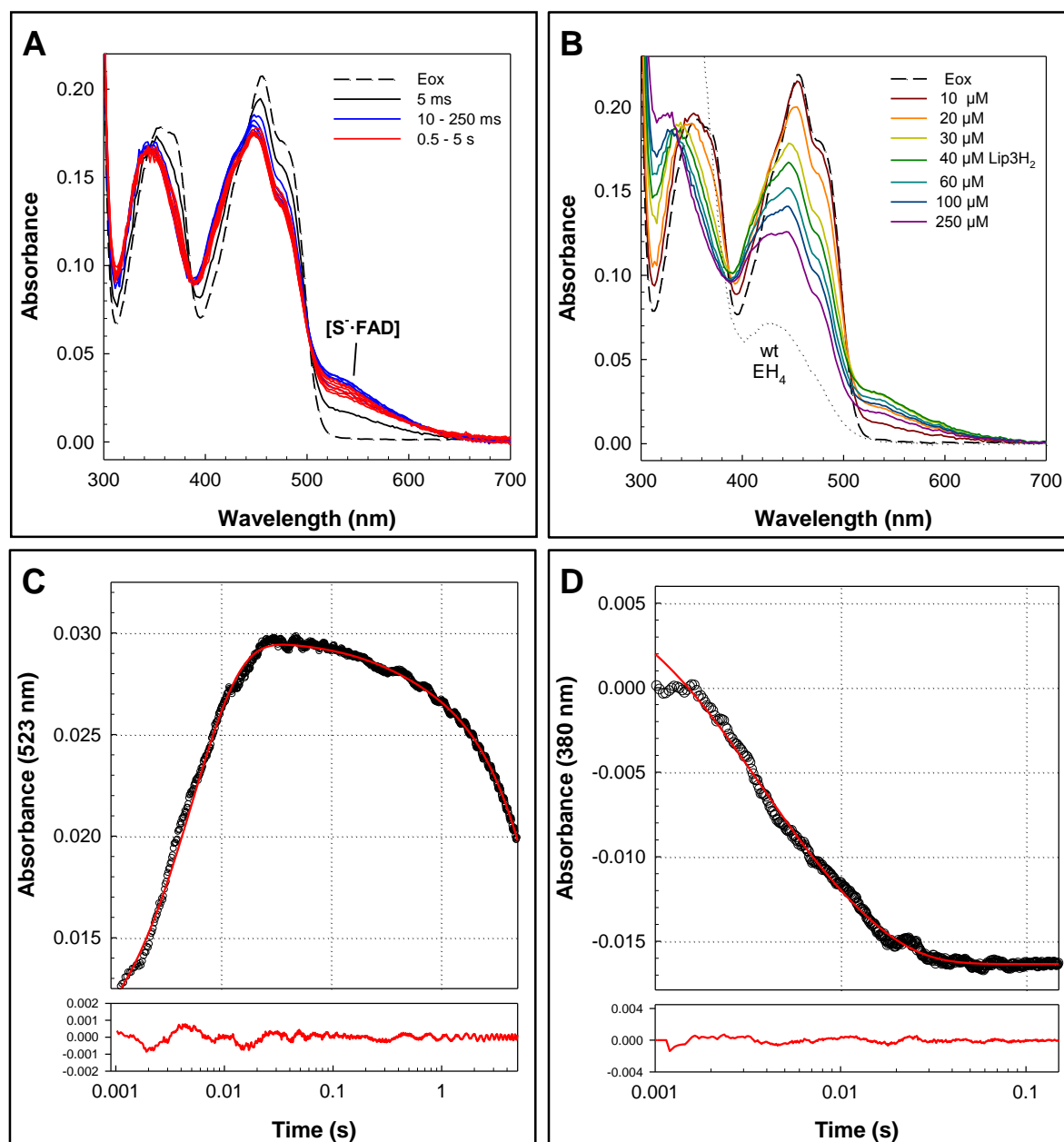


Figure 3.12 Reduction of *EcE3* by *EcLip3H₂* under single turnover conditions.

(A) Stopped-flow absorbance traces after mixing 20 μM *EcE3* with 20 μM *EcLip3H₂* at 4 $^{\circ}\text{C}$ and pH 7.6. The broad absorption band at 530 nm shows the presence of charge transfer between the Cys50 thiolate and the FAD. (B) Titration of *EcE3* with *EcLip3H₂*. The dotted line reflects a typical wt- EH_4 spectrum after reduction with excess of NADH. >10-fold molar excess of *EcLipH₂* did not lead to formation of EH_4 . (C and D) Absorbance traces at 523 and 523 nm and corresponding fits. The fits to a double exponential equation ($A = A_1 \cdot e^{-k_1 \cdot t} + A_2 \cdot e^{-k_2 \cdot t}$), respectively. The points are the experimental data, and the solid lines are the fits to a triple and a double exponential equation ($A = A_1 \cdot e^{-k_1 \cdot t} + A_2 \cdot e^{-k_2 \cdot t}$), respectively. Note the logarithmic time-scales.

3.2.3 Evidence for the Transience of the Cysteinyl-C4a Adduct

As described above, the covalent C4a-flavin adduct did not accumulate significantly neither in the whole reverse direction (3.1.2) nor during the isolated oxidative half-reaction (3.2.2). However, a spectroscopic evidence for an NAD⁺-induced adduct formation was achieved using a monothiol variant of *EcE3* using conventional absorbance spectroscopy (3.1.5). According to the latter, the accumulation of the adduct in solution under equilibrium conditions is rather minute. The successful establishment of *EcLip3H₂* as native reductant of *EcE3* allows the spectroscopic characterization of the entire reaction cycle with the oxidative half-reaction as starting point. Therefore, *EcE3* was transferred into the EH₂ state by rapid reduction with *EcLip3H₂* followed by a second rapid mixing event with NAD⁺ to complete the cycle using low-temperature sequential stopped-flow absorbance spectroscopy (Figure 3.13A). A comparable method was described earlier for the *Mycobacterium tuberculosis* lipoamide dehydrogenase, however, the EH₂ pre-equilibrium was generated by titration with dithionite and not with a native substrate as described here (Argyrou et al. 2003).

The first mixing event generated the EH₂ state of *EcE3* indicated by its characteristic charge-transfer band at 530 nm (Figure 3.13B and C). After generation of the pre-equilibrium (50 ms) NAD⁺ (equimolar and 5-fold molar excess) was added in a second step leading to a loss in absorbance in the 530 nm range and concomitant increase at 340 nm within the dead-time of mixing. Though the first spectrum was recorded after 5 ms the generation of NADH (340 nm) and loss of the charge-transfer band indicate that a spectroscopic detection of the C4a-flavin adduct was not possible since the reaction already came to an end (Figure 3.4B and C). Hence, a spectroscopic detection of the EH₂·NAD⁺-complex was also not possible. The latter complex is characterized by a red-shifted (to ~ 600 nm) charge-transfer band which could be detected for the *Mycobacterium tuberculosis* and the pig heart enzymes (Argyrou et al. 2003; Wilkinson and Williams 1979). The increased overall reaction velocity of the *E. coli* enzyme compared to mentioned isoforms further complicates not only the detection of the C4a-flavin adduct. Moreover, the determination of absolute k_{cat} values in dependence of NAD⁺ is not possible with the setup described above.

In conclusion, there is evidence that the covalent C4a-flavin adduct does not accumulate to a significant extent during catalysis. Its high instability and its transience were confirmed by monitoring the *EcE3* reaction cycle from the forward (EH₂ + NAD⁺) and the reverse direction (E_{ox} + NADH). It was proposed that the instability of the intermediate is based on a faster decay compared to its relatively slow formation in both directions for the *Mycobacterium tuberculosis* enzyme (Argyrou et al. 2003). Thus, the transient nature of the covalent C4a-flavin adduct in lipoamide dehydrogenases seems to be a hallmark in this enzyme class.

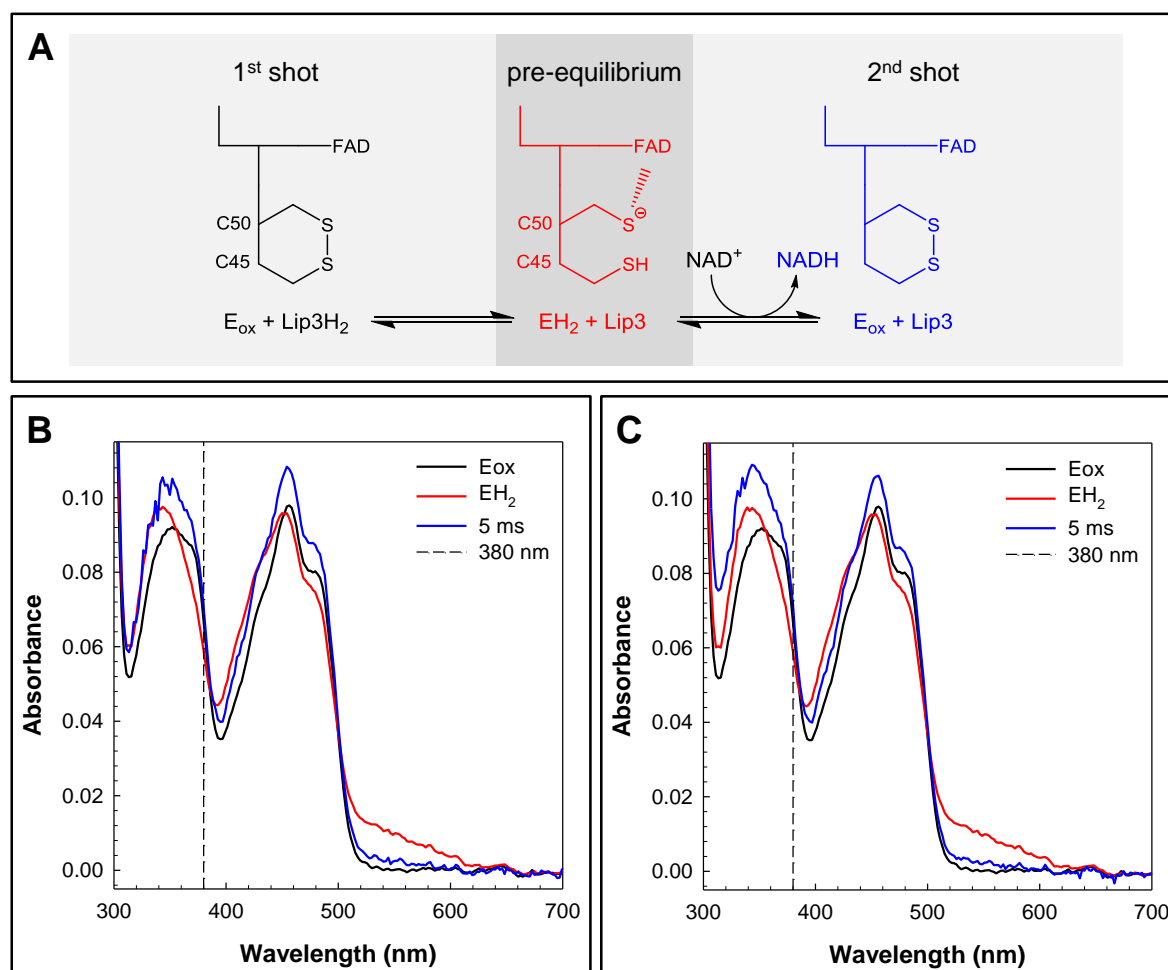


Figure 3.13 Sequential stopped-flow absorbance analysis of the *EcE3* reduction by *EcLip3H₂* and subsequent oxidation by NAD^+ at 4 °C.

(A) Schematic of the sequential mixing experiment. First, *EcE3* (40 μ M) is mixed with *Lip3H₂* (40 μ M), forming the pre-equilibrium EH_2 status of *EcE3*. Oxidation of EH_2 is accomplished by the second mixing step (50 ms after the first step) with NAD^+ . (B) Oxidation of the pre-equilibrium with an equimolar amount (20 μ M) and (C) with an 5-fold molar excess (100 μ M) NAD^+ . E_{ox} reflects the oxidized spectrum – obtained by mixing solely with buffer, EH_2 is the two-electron reduced state – obtained as described above – with subsequent mixing with buffer. 5 ms reflects the first possible spectrum recorded after mixing with NAD^+ .

3.3 Mechanistic Investigation of *EcE3*

The study thus far provided new insights in the catalytic function of lipoamide dehydrogenases. The findings were thereby mainly based on mutations targeting the redox active cystine moiety of the oxidoreductase. However, it was demonstrated that several other residues located around the active site harbor crucial functions during the catalytic cycle (Benen et al. 1991; Benen, Van Berkel, Dieteren, et al. 1992; Benen, Van Berkel, Veeger, et al. 1992; Maeda-Yorita et al. 1994). These and further residues were therefore investigated with the aforementioned methods to broaden the understanding of the reaction mechanism of *EcE3*.

It is described that the level to which lipoamide dehydrogenases are reduced beyond the EH_2 state allows qualitative statements about the flavin redox potential (Maeda-Yorita et al. 1994). The latter fact will be used to expand the knowledge about the sensitivity of the flavin surrounding against structural alterations. Since the reaction cycle can be subdivided into a reductive and an oxidative half-reaction the results will be presented following the order of this subdivision starting with the reductive half-reaction (3.3.1). The oxidative half-reaction will be investigated in 3.3.2. An overview of all studied residues and their occurrence in lipoamide dehydrogenases from several organisms is given in the appendix (Figure 5.4).

3.3.1 Characterization of the Reductive Half-Reaction using selected Active Site Variants

In the reductive half-reaction, the substrate dihydrolipoamide binds to the E_{ox} form of *EcE3*, and Cys45 forms a mixed disulfide with the substrate. Transfer of electrons leads to formation of the Cys50- thiolate and thus the two-electron reduced state (EH_2) (1.5). This reaction is general-acid-base catalyzed by the essential and conserved catalytic diad located at the C-terminus of the adjacent monomer, namely His455 and Glu450 (Figure 3.14). Release of lipoamide completes the oxidative half-reaction. A further investigation of the Glu-His pair with respect to their individual roles during catalysis is therefore interesting. In addition, a highly conserved tyrosine residue is also located at the putative lipoamide entry site (Figure 3.14). In order to elucidate whether Tyr19 also harbors an essential catalytic function as it has been described for the diad (Benen et al. 1991; Benen, Van Berkel, Dieteren, et al. 1992; Kim and Patel 1992a) it was also targeted for the mechanistic investigation.

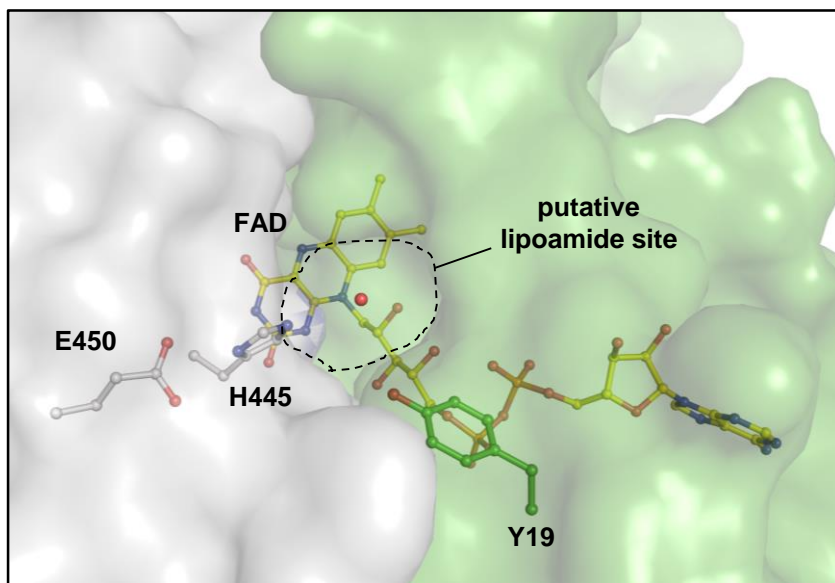


Figure 3.14 Putative position of the lipoamide binding site.

The residues studied involved in the reductive half-reaction are located at the *si* face of the FAD and comprise the highly conserved catalytic diad; His445 and Glu450; and Tyr19. The putative entry site for the lipoamide cofactor is located at the dimer interface. The displayed water molecule

The visible absorption spectra of *EcE3Y19F*, *H445A* and *E450Q* are very similar to that of the wild type enzyme (5.2). This indicates that the mutations did not influence the surrounding of the flavin to a significant amount. Mutations at the site of the catalytic diad, however, had severe impact on the catalytic activity (Table 3.1). *EcE3H445A* showed below 0.1 % residual activity under standardized assay conditions (5.4), but it should be noted that the actual activity might even be lower. When NADH served as reductant it cannot be excluded that reducing equivalents are transferred to other electron acceptors than lipoamide during diaphorase reactions. Hence, it is most likely that molecular oxygen oxidizes the reduced flavin intermediate leading to NADH consumption (5.4). The impact of mutation of Glu450 was not that drastic compared to its bonding partner showing ~4 % residual activity. According to far-UV CD spectroscopy mutation of Tyr19 to phenylalanine did not affect the secondary structure of the enzyme though it is located directly at the dimer interface (5.6). In addition the mutation only slightly altered the rate of substrate turnover (Table 3.1).

Table 3.1 Steady-state parameters of *EcE3* variants involved in the reductive half-reaction. Parameters were calculated from data of the reverse steady-state assay (2.2.4.1). Plots of lipoamide dependence for individual variants are shown in the appendix (5.4).

Variant	A_{Spec} (U/mg)	K_D (NAD ⁺) (μM)
wt	72.9 ± 4.6	400*
Y19F	70.7 ± 3.3	n.d.
H445A	0.06 ± 0.01	n.d.
E450Q	2.9 ± 0.1	n.d.

*(Wilkinson and Williams 1981)

3.3.1.1 Histidine445 and Glutamate450 – The Role of the Catalytic Diad during Catalysis

As the steady-state assays demonstrated mutation of the catalytic diad severely slowed down the reaction rates of the respective enzyme. Therefore, they were likely candidates that are potentially able to stabilize the covalent C4a-cysteinyl adduct. An investigation using rapid reactions measurements was hence obligate. Reduction of *EcE3*H445A with NADH leads to spectroscopic properties which differ from that of the wild type enzyme (Figure 3.15A and B). Though a decrease in absorbance of the flavin is observable under single turnover conditions the typical blue-shift of the latter is way less pronounced. Moreover, there is no significant rise in absorbance in the 523 nm range indicating the Cys50-thiolate charge transfer complex with the FAD. However, the highly transient NAD⁺-FADH₂ complex is significantly stabilized in this variant indicated by the broad charge transfer band in the longer wavelength region. Reduction with 5-fold excess of NADH lead to a complete flavin reduction (Figure 3.15B), but also in this case there is no spectroscopic evidence for reduction of the disulfide. On the contrary, the NAD⁺-FADH₂ complex accumulates to a way higher extent according to the broad absorption band between 600 and 700 nm. Reduction of *EcE3*E450Q with NADH leads to comparable results with respect to accumulation of the nucleotide-flavin complex. However, the presence of the charge transfer bands at 523 nm suggests that the intramolecular electron transfer to the disulfide is still possible albeit retarded when compared with the wild type enzyme (Figure 3.15C). During all experiments using NADH as reductant no increase in the 380-nm absorbance range was detected that would indicate a stabilization of the flavin adduct.

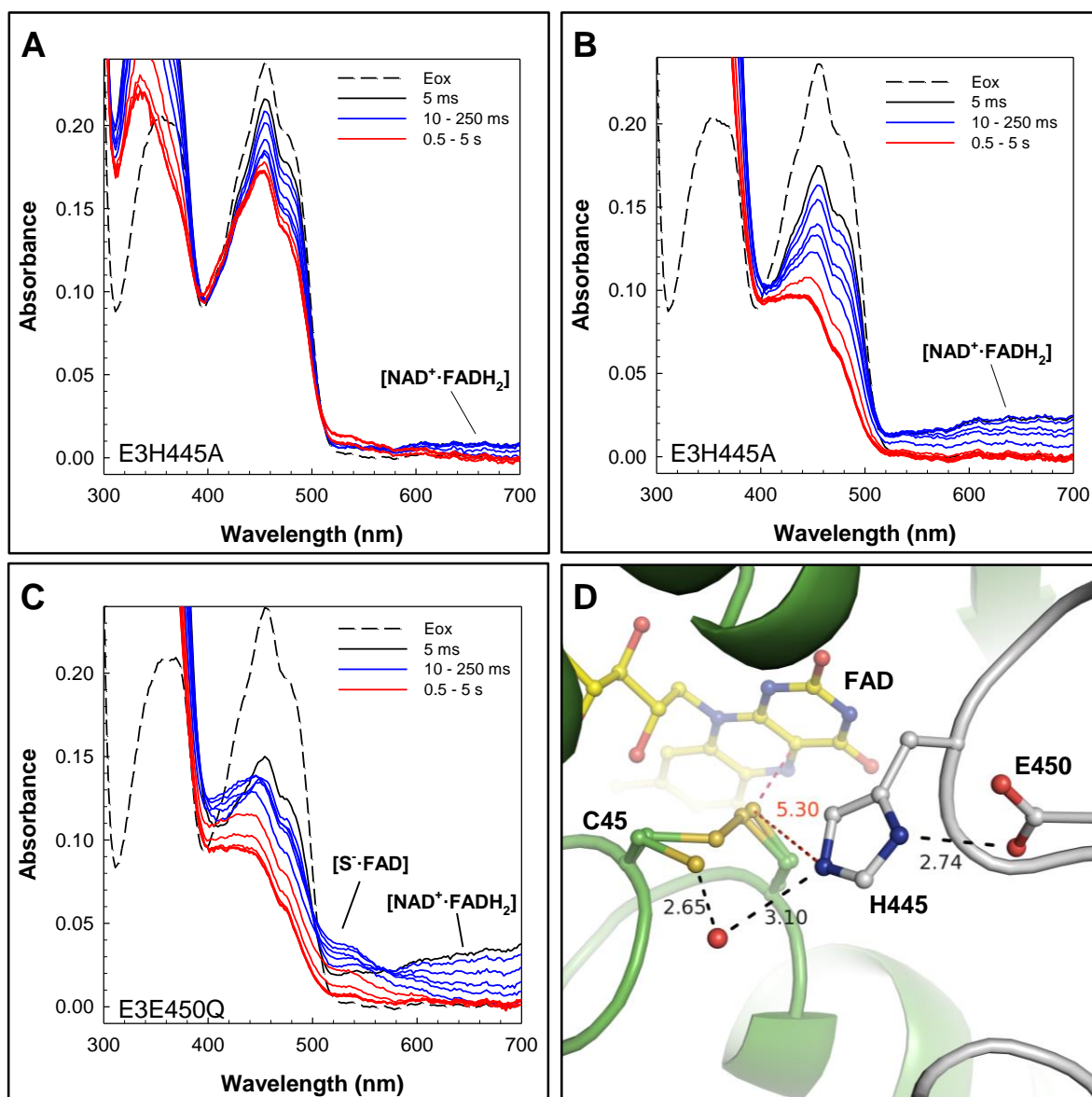


Figure 3.15 General characterization of the *EcE3* catalytic diad – His445 and Glu450.

Stopped-flow absorbance traces of *EcE3* variants upon reduction with NADH (A - C). 20 μM *EcE3*H445A were mixed with 20 μM (panel A) or with 100 μM NADH (B) at 4 °C and pH 7.6. (C) Reduction of *EcE3*E450Q with 100 μM NADH. The dashed line represents the oxidized form of the respective enzyme (E_{ox}) derived from a single mixing event with buffer. The solid spectra were recorded using a diode-array detector after mixing at the concentrations indicated. (D) Hydrogen bond network between the catalytic diad and the redox active cysteine. N3 of His445 is too far away for a direct stabilization of the Cys50-thiolate (see 3.1.4). A putative interaction with a Cys45-thiolate is likely mediated via a water molecule (red sphere). Glu450 ensures the correct orientation of the imidazole moiety of His445 (distances in Å).

The reduction of the mutated enzymes with NADH allowed the distinction of separate reactions steps and a subsequent comparison to the wild type. In both cases, the hydride transfer from NADH to FAD is fast and leads to a pronounced accumulation of the NAD⁺-FADH₂ complex in comparison to the wild type. This indicates, that the transfer of reducing equivalents from the reduced flavin to the redox active disulfide is significantly slowed down (E450Q) or even impaired (H445A). The H445A mutant

was not capable to stabilize the Cys50-thiolate charge transfer neither under single turnover conditions, nor in the presence of a five-fold molar excess of NADH. The small increase in the 523 nm region which can be observed in Figure 3.15A is most likely due to the offset correction of the spectra rather than the formation of a true thiolate species. The absence of a hypsochromic shift of the flavin peak underpins the assumption that no reduction of the disulfide occurs. Further, the almost complete loss of catalytic activity of *EcE3H445A* enhances the latter assumption. These results are in agreement with previous studies on the E3 from *A. vinelandii* which showed that the conserved histidine acts as catalyst being involved in (de)protonation of the interchange thiol (Cys45) and the substrate dihydrolipoamide, a step which is essential for an opening of the disulfide (Benen et al. 1991; Benen, Van Berkel, Dieteren, et al. 1992). Structural data suggest that a direct interaction of His445 with the Cys50-thiolate is not very likely (Figure 3.15D). Stabilization of the latter thiolate was discussed in a previous chapter (3.1.4). However, it was suggested that the interchange thiol can also be present in its anionic form since the EH_2 state of *EcE3* is actually a mixture of distinct spectroscopic species (Benen, Van Berkel, Dieteren, et al. 1992; Wilkinson and Williams 1979). It was suggested that the interchange thiolate can be stabilized by an interaction with an hydronium ion (Benen et al. 1991) due to the easy accessibility of the latter residue to the solvent. In fact, the *EcE3* ground state structure revealed the presence of such water molecule which is coordinated by both His445 and the open conformer of Cys45 (Figure 3.15D).

When combining the spectroscopic and structural data the catalytic role of Glu450 during catalysis can be proposed. Glu450 ensures the correct orientation of the imidazole moiety of His445 towards Cys45 and the putative entry site for dihydrolipoamide (Figure 3.15D). A substitution of this residue with glutamine consequently leads to a weakening or a loss of the hydrogen bond with the imidazole of His445 which most likely alters the orientation of the histidine relative to the interchange thiol. Further, this might also influence the pK_a of the histidine, an aspect which has been discussed elsewhere (Benen et al. 1991). In contrast to His445, Glu450 is not essential for catalysis, but it is indicative that the carboxylic group of Glu450 functions as both as mediator for the pK_a (Benen et al. 1991) and as structural element positioning the imidazole N3 towards the redox active disulfide.

Though the transfer of the reducing equivalents is slowed down (~5-fold with respect to thiolate formation) in *EcE3E450Q* there has not been evidence for the accumulation of the covalent flavin-cysteinyll intermediate. It was suggested that the decay of the C4a adduct might be faster than its formation in either direction making an spectroscopic detection tedious work (Argyrou et al. 2002; Benen, Van Berkel, Dieteren, et al. 1992). Apparently, this also holds true for the *E. coli* enzyme. In the case of the His445 mutant the absence might be even more coherent assuming that an opening of the disulfide is entirely impaired in this variant.

3.3.1.2 Tyrosine19 acts as structural Element rather than as a catalytic Residue

Mutation of Tyr19 to a phenylalanine did not influence the specific activity of the enzyme to high extent in the standard assay (5.4). In addition, rapid reaction experiments confirmed that the latter mutation also did not have an effect on the spectral properties during both reduction with NADH and *EcLip3H₂* (Figure 3.16). Formation of the Cys50-thiolate flavin complex can be observed during both reduction processes with similar rates, respectively, when comparing to the wild type enzyme. In addition, the highly transient NAD⁺-FADH₂ complex does not accumulate during reduction with NADH indicating that the transfer of reducing equivalents to the redox active cystine is not influenced.

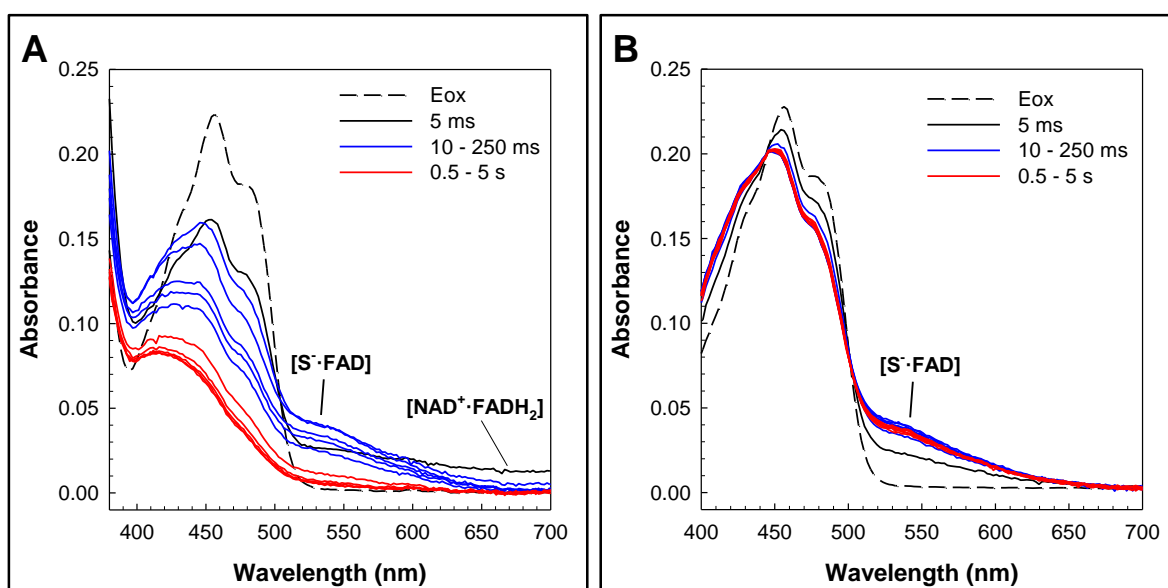


Figure 3.16 Stopped-flow absorbance traces of *EcE3Y19F*.

20 μM *EcE3Y19F* were mixed with 100 μM NADH (A) or with 20 μM *EcLip3H₂* (B) at 4 °C and pH 7.6. The dashed lines represent the oxidized form of *EcE3Y19F* (E_{ox}) derived from a single mixing event with buffer. The solid spectra were recorded using a diode-array detector after mixing at the concentrations indicated.

According to the results obtained it is most likely that Tyr19 does not contribute to catalysis in *EcE3* since removal of the hydroxyl function did not alter the catalytic abilities of the enzyme to a significant extent. However, these results are contradicting with studies on the corresponding residue in the *A. vinelandii* E3 (Tyr16 according to *A. vinelandii* numbering). For this enzyme variant no activity was observed during steady-state assays using NADH as reductant (Benen, Van Berkel, Veeger, et al. 1992). Moreover, the mutated enzyme was easily overreduced by NADH while lacking the thiolate-flavin complex upon reduction demonstrating that the reducing equivalents mainly resided on the flavin rather than being transferred to the disulfide (Benen, Van Berkel, Veeger, et al. 1992).

These spectral properties are similar to that of the *EcE3* variants which were used to study the oxidative half-reaction (3.3.2). Hence, the tyrosine raised the redox potential of the flavin in the *A. vinelandii* enzyme. This elevation was not observed in the *E. coli* mutant where a 5-fold molar excess of NADH was required to overreduce the enzyme to the dead-end EH_4 state – the same amount which was also required for *EcE3*wt.

In the *A. vinelandii* enzyme Tyr16 hydrogen bonds with His470 of the C-terminal part of the other subunit (Mattevi et al. 1991). It was speculated that this interaction stabilizes the homodimer thus contributing to optimal catalysis and protection against inhibition/overreduction by NADH (Benen, Van Berkel, Veeger, et al. 1992). However, it remained unclear how this interaction could influence the flavin redox potential since this interaction is far away from the active site. It was therefore speculated that the dimer interaction itself modulates the redox properties, but a clear proof was not given (Benen, Van Berkel, Veeger, et al. 1992). In *EcE3*, Tyr19 does not contribute to the subunit interaction *via* hydrogen bonding to a residue of the other subunit. Thus, a cross-talk between the two monomers assisted by Tyr19 is not likely. Moreover, the aforementioned histidine of the *A. vinelandii* enzyme is not present in the *EcE3* (Figure 5.4). Hence, the results obtained for *EcE3Y19F*, which reflects a wild type behavior, are not unexpected in the light of catalysis potentially regulated by monomer-monomer interaction. That the flavin redox potential indeed can be regulated by mutation of a another residue present at the dimer interface (Glu354) will be shown and discussed in a following chapter (3.5).

3.3.2 Characterization of the Oxidative Half-reaction using selected Active Site Variants

In the oxidative half-reaction, NAD^+ binds to the two-electron reduced state of the enzyme (EH_2). This induces an internal electron transfer from the redox active disulfide towards the flavin cofactor yielding a transiently formed FADH_2 intermediate. The flavin is immediately reoxidized by NAD^+ generating NADH and the oxidized form of the enzyme (E_{ox}). Release of NADH completes the reductive half-reaction.

Replacements of residues at the site of the catalytic diad significantly decreased or even depleted the rate of substrate turnover, but an accumulation of the flavin-C4a-cysteinyl adduct did not occur (3.3.1.1). Therefore, the investigation was expanded to residues at the *re* face of the flavin which are thought to assist (de)protonation of the N5 atom of the flavin cofactor during the oxidative half-reaction (Maeda-Yorita et al. 1994) and therefore site directed mutagenesis of the residues involved might lead to *EcE3* variants that accumulate the covalent intermediate.

The ammonium function of Lys54 is located close to the isoalloxazine ring and makes a weak polar interaction with N5 (Figure 3.17). The previously solved structure of *EcE3* (PDB: 4JDR) demonstrated that the interaction of Lys54 with N5 is further mediated by a water molecule (Figure 1.4) (Chandrasekhar et al. 2013). Difference map peaks (mFo-DFc at 3 sigma level) were visible in the same region for the structure presented here, but the peaks were too weak to allow an appropriate model building. However, the presence of a water molecule at the mentioned position is not unlikely. Besides the interaction with the cofactor, the lysine residue forms an ion pair with Glu189 positioning the positive end of this salt bridge towards the flavin (Figure 3.17). These two residues are not only conserved in E3s from different organisms (Figure 5.4), but also in all homologous enzymes of the pyridine nucleotide-disulfide oxidoreductase family. It has been suggested and later on demonstrated that the positive charge of the lysine plays a crucial role in mediating the redox potential of the flavin in both glutathione reductase as well in *EcE3* thus contributing to optimal catalysis (Maeda-Yorita et al. 1994; Schulz and Pai 1983). Both residues were therefore mutated to glutamines, respectively, which lead to a disruption of the ion pair interaction but still allowed hydrogen bonding interactions.

Arg386 of the adjacent monomer is located at the dimer interface and the distance of its guanidinium group is $\sim 7 \text{ \AA}$ to the ϵ -amino group of Lys54 (Figure 3.17). The corresponding residue (Arg382) in *E. coli* mercuric ion reductase is thought to participate in a proton transfer reaction during catalysis by a direct interaction with the catalytic lysine (Susan Miller, University of California, personal communication). Hence, this residue was also targeted for the mechanistic investigation aiming to elucidate whether a perturbation of its proposed function yields in stabilization of the covalent flavin adduct.

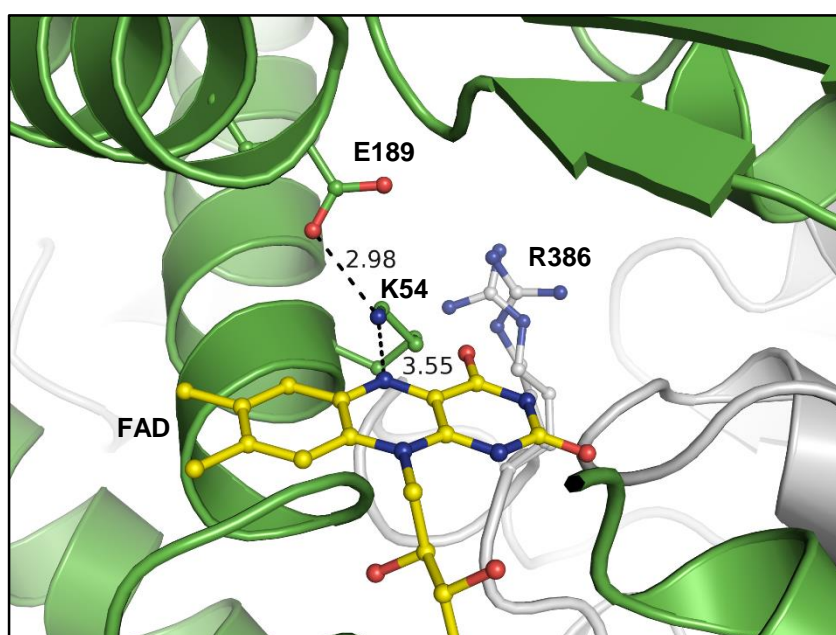


Figure 3.17 Overview of the *re* face of the FAD.

Lys54 makes a polar interaction with N5 (distances in \AA). The residue is thereby positioned by Glu189. In the previously solved structure of *EcE3* (PDB: 4JDR) the interaction of Lys54 with N5 is further mediated by a water molecule (Chandrasekhar et al. 2013). Arg386 of the adjacent monomer (grey) is located at the dimer interface. For the putative role of this residue see text.

The visible absorption spectra of *EcE3K54Q* and *E189Q* harbor minor changes when compared to the wild type (5.2). In both cases the main flavin band is slightly blue-shifted and the shoulder at 487 nm is less pronounced. This might be indicative for a more hydrophilic environment around the flavin (Harbury et al. 1959). In contrast, the UV-Vis spectrum of *EcE3R386A* was almost identical to that of the wild type enzyme. Mutations near the flavin N5 site had severe impact on the catalytic activity (Table 3.2). *EcE3K54Q* only showed ~0.5 % residual activity under standardized assay conditions. Moreover, replacement of the negatively charged Glu189 lead to a further reduction of the enzymatic activity (<0.2 %). However, the latter activity also tends to be defective according to aforementioned limitations of the reverse assay (3.3.1). Mutation of Arg386 to alanine did not abolish the catalytic function of the enzyme. The variant showed ~22 % residual activity indicating that an involvement of the latter residue into a proton transfer reaction is questionable, at least with respect to its steady state activity.

Table 3.2 Steady-state parameters of *EcE3*variants involved in the oxidative half-reaction. Parameters were calculated from data of the reverse steady-state assay (2.2.4.1). Plots of lipoamide dependence for individual variants are shown in the appendix (5.4).

Variant	A_{Spec} (U/mg)	K_D (NAD ⁺) (μM)
wt	72.9 ± 4.6	400*
K54Q	0.33 ± 0.01	42.0 ± 1.8
E189Q	0.14 ± 0.01	n.d.
R386A	16.3 ± 0.4	155 ± 16

* (Wilkinson and Williams 1981)

Reduction of *EcE3K54Q* with NADH under single turnover conditions in a stopped-flow apparatus demonstrated a strong accumulation of the NAD⁺-FADH₂ charge transfer band between 600 – 700 nm. Moreover, almost a complete reduction of the flavin could be observed thereby lacking the characteristic blue shift and the Cys50-thiolate FAD charge transfer (Figure 3.18A). NAD⁺-FADH₂ complex formation occurs monoexponentially with $\sim 103 \text{ s}^{-1}$ and results in stabilization of the latter complex for $\sim 300 \text{ ms}$ (Figure 3.18B) prior to its decay. NADH titration revealed that in fact one equivalent NADH is sufficient to reduce one equivalent of *EcE3K54Q* (Figure 3.18C). Hence, internal transfer of reducing equivalents from the flavin site towards the redox active disulfide seems to be impaired. The pronounced nucleotide–flavin charge transfer indicates a strong binding of NAD⁺ to the enzyme. This tightened binding was confirmed by NAD⁺-titrations giving an apparent K_D of 42 μM.

The binding constant for NAD^+ is thus almost 10-fold lower to that observed for the wild type enzyme (Wilkinson and Williams 1981).

Interestingly, the same qualitative results were observed for *EcE3R386A*; for this variant the apparent K_D was ~3-fold higher than for *EcE3K54Q* (Figure 5.5). In addition, *EcE3R386A* was able to form the Cys50-thiolate FAD charge transfer when *EcLip3H2* served as reductant (Figure 5.5D).

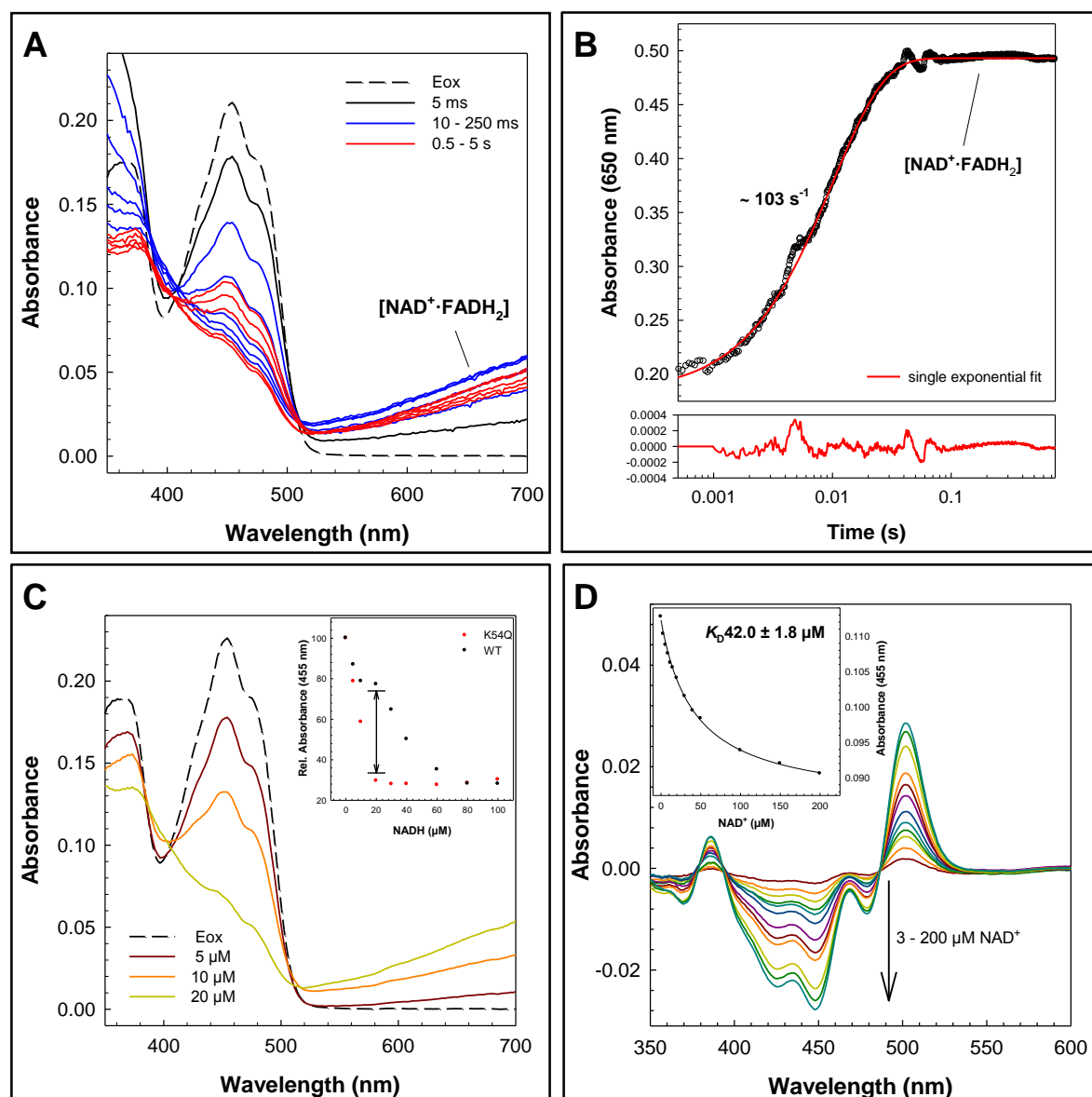


Figure 3.18 Spectral properties of *EcE3K54Q*.

(A) Stopped-flow absorbance traces after mixing of 20 μM *EcE3K54Q* with 20 μM NADH at 4 $^{\circ}\text{C}$ and pH 7.6. The dashed line represents the oxidized form of the respective enzyme (E_{ox}) derived from a single mixing event with buffer. The solid spectra were recorded using a diode-array detector after mixing. (B) Stopped-flow absorbance trace at 650 nm under same conditions. The points are the experimental data, and the solid line is the fit to a single exponential equation ($A = A_1 \cdot e^{-k_1 \cdot t}$). Note the logarithmic time-scale. NAD^+ -FADH₂ complex formation occurs with $\sim 103 \text{ s}^{-1}$ and runs into an transient equilibrium prior to its decay. (C) Absorbance traces derived from a stopped-flow NADH titration at 4 $^{\circ}\text{C}$ and pH 7.6. Complete reduction of the flavin can be achieved using an equimolar amount of NADH. The inset shows the relative absorbances at 455 nm plotted against the respective NADH concentration. Internal transfer of reducing equivalents to the disulfide is therefore most unlikely. (D) Lower temperature NAD⁺ titration (difference spectra) at 10 $^{\circ}\text{C}$ and pH 7.6. The inset shows a hyperbolic fit for the decrease in absorbance at 455 nm giving an apparent binding constant of $\sim 42 \mu\text{M}$ for the nucleotide.

A 5-fold molar excess of NADH was not sufficient to induce EH4 formation thus, *EcE3E189Q* did not suffer from severe overreduction by NADH (Figure 3.19A and Figure 5.6A). However, the more pronounced accumulation of the NAD^+ -FADH₂ complex and the absence of the Cys50-thiolate FAD charge transfer were also present in this variant. NAD^+ titrations did not indicate a lowered binding constant for the nucleotide since no significant quenching of the flavin was observed (Figure 5.6B). Further, E189Q is also not capable to stabilize the Cys50-thiolate FAD charge transfer to a significant amount when using *EcLip3H₂* as reductant (Figure 3.19B) and reoxidation of the cofactor occurs remarkably faster than in the wild type enzyme.

In summary, the alterations at residues near the flavin N5 influenced the spectroscopic and catalytic behavior of all three mutated enzymes studied. However, during all experiments using NADH or *EcLip3H₂* as reductant no increase in the 380-nm absorbance range was detected that would indicate a stabilization of the covalent flavin adduct.

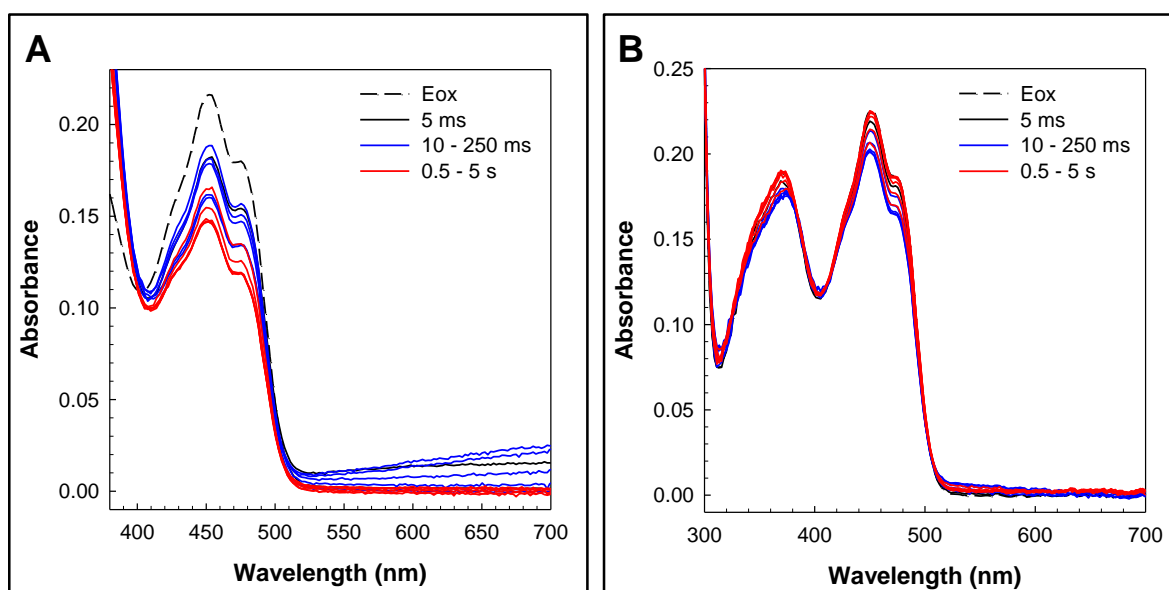


Figure 3.19 Stopped-flow absorbance traces of *EcE3E189Q*.

20 μM *EcE3E189Q* were mixed with 100 μM NADH (**A**) or with 20 μM *EcLip3H₂* (**B**) at 4 °C and pH 7.6. The dashed line represents the oxidized form of the enzyme (E_{ox}) derived from a single mixing event with buffer. The solid spectra were recorded using a diode-array detector after mixing at the concentrations indicated.

3.3.2.1 Lys54 and Glu189 are crucial Mediators of the Flavin Redox Potential

EcE3K54Q showed severe overreduction by NADH and a remarkably increased affinity for NAD⁺. The absence of thiolate-FAD charge transfer complex and the fact that one equivalent of NADH were sufficient for complete flavin reduction indicate that its flavin redox potential is way less negative than that of the wild type enzyme. Mutation of the same residue to arginine raised the FAD potential by approximately 60 mV (Maeda-Yorita et al. 1994), whereas the redox active disulfide potential was unaffected. The results presented here suggest that the redox potential of the FAD has been raised even further and underlie the already proposed sensitivity of the isoalloxazine ring to its electrostatic environment, especially the surrounding of the N5 atom. The positive charge donated by the ammonium group of the lysine residue to the latter atom is thus pivotal for the enzyme. An absolute determination of the flavin redox potential could be achieved using the method which was described in 2.2.2.9 (McDonald et al. 2013).

The role of Lys54 is presumably not limited to its redox-mediating function. It has been suggested that the ammonium group of the lysine repels the positively charged NAD⁺ from the active site in the related human glutathione reductase (Schulz and Pai 1983). The relatively high binding constant for the pyridine nucleotide in *EcE3* might support this function. Further, ITC data suggest that binding of NAD⁺ to K54Q is characterized by an increased change in enthalpy (Figure 5.21). The increased affinity towards NAD⁺ in the variant is therefore most likely based on two aspects: At first, the repulsion of the nucleotide became abolished due to removal of the positive charge at the enzyme and secondly, hydrogen bonding between Glu54 and the nicotine amide part of NAD⁺ might have tightened the interaction.

The mutation of Glu189 to glutamine had the opposite effect with respect to the flavin redox potential. NADH titrations revealed that the potential has been lowered compared to the wild type enzyme. The absence of thiolate-FAD charge transfer complex during both reduction with NADH and *EcLip3H₂* suggest that the internal transfer of reducing equivalents from the flavin site towards the disulfide and vice versa is almost completely impaired. As observed for Glu450 in the studies on the reductive half-reaction (3.3.1.1), Glu189 presumably acts as structural element that is responsible for positioning the ϵ -amino group of Lys54 towards the flavin N5 atom. Removal of the carboxylic group of Glu189 might lead to a relaxation of Lys54 from its strained conformation (Figure 3.17) and hence a perturbation of the interaction with N5.

3.3.2.2 A direct Involvement of Arg386 in a Proton Transfer Reaction is questionable

In *E. coli* mercuric ion reductase the Arg386 homolog (Arg382) is thought to participate in a proton transfer reaction during catalysis by a direct interaction with the catalytic lysine. Most likely this transfer reaction is required to protonate FAD-N5 during the reductive half-reaction to induce covalent

adduct formation (Susan Miller, University of California, personal communication). Indeed, the fact that Arg386 could be modeled using two alternate conformations implies that this residue harbors certain motility (Figure 3.17) which may indicate that an interaction with Lys54 cannot be totally excluded. However, this would require Lys54 to undergo huge structural rearrangements as well, a scenario which is due to its interactions with Glu189 and FAD-N5 unlikely. In addition, kinetic and spectroscopic data further underpin that replacement of Arg386 reduces the enzyme activity but not to that amount which one would expect if a proton transfer reaction was completely disturbed. Assuming ~1 % residual activity in a case of a fully abolished proton transfer reaction the detected 22 % residual activity are significantly higher. Though it cannot be excluded that a water molecule now occupies the space which became available due to the mutation it remains doubtful that a latter molecule can compensate the complex proposed role of Arg386.

The data presented demonstrate that the mutation raised the redox potential of the flavin already leading to overreduction to the catalytically inactive EH_4 state at equimolar concentrations of NADH. However, the steady-state activity shows that NAD^+ can oxidize the enzyme to the active EH_2 state that results in substrate turnover. Further, though the detection of the Cys50-thiolate FAD charge transfer was not possible when NADH served as reducing titrant, *EcE3R386A* was able to form this complex when *EcLip3H2* served, albeit with a smaller amplitude than the wild type. It can be speculated, the less pronounced thiolate FAD charge transfer was masked by the enhanced NAD^+ - FADH_2 complex during reduction with NADH. These data suggest that *EcE3R386A* is still capable to form all the intermediates required for catalysis and hence the role of Arg386 has to be seen from a more structural point of view: Mutations at the dimer interface of E3s have the ability to drastically alter the catalytic properties of the enzyme (3.3.1.2 and 3.5). Though the exact reasons for this alteration have not been identified yet, it was speculated that residues at the interface stabilizing the homodimer contribute to optimal catalysis and provide protection against inhibition/overreduction by NADH (Benen, Van Berkel, Veeger, et al. 1992). Since Arg386 is also located at the interface it is likely that the altered observed behavior is due to destabilization of the homodimer rather than a direct involvement in a proton transfer reaction. That the enzyme behavior can indeed be regulated by mutation of a residue present at the dimer interface (Glu354) will be shown and discussed in a following chapter (3.5).

3.4 Converting *EcE3* into a light-sensitive blue Light Receptor

A common feature of lipoamide dehydrogenases and LOV proteins is the formation of a covalent FAD-C4a-cysteinyl adduct during the respective reaction cycle. However, according to spectroscopic and structural data (3.1 and 3.2) and previous reports (Argyrou et al. 2002) the covalent adduct only accumulates to a minor fraction in lipoamide dehydrogenases. On the contrary, the lifetime of the same class of adducts can also last up to hours in LOV blue light photoreceptors (Conrad et al. 2014). To therefore extend the lifetime of the adduct in *EcE3* a conversion of this oxidoreductase into a light-sensitive LOV protein using a minimal system was attempted. The aim was to stabilize the adduct upon light activation and by this to overcome its transient nature which prohibited a more detailed spectroscopic and structural study. On the one hand, an accumulation of the C4a-cysteinyl adduct would allow the usage of different spectroscopic analyses and on the other hand further crystallographic studies, which may expand the gained knowledge about this reaction central intermediate during the course of this study. Further, this structure-guided protein engineering approach should combine the catalytic properties of a LOV protein and the *EcE3* enzyme leading to a blue-light absorbing oxidoreductase capable of reducing NADH with light as the main driving force. The envisaged reaction cycle would include a photochemical induced C4a-cysteinyl adduct followed by binding of NAD⁺ to generate NADH. The required reduction of the thiol would be achieved by an externally added sulfhydryl-free reducing agent (TCEP).

3.4.1 *EcE3C45A/K54Q* and *C45S/K54Q* – PseudoLOV variants

Based on the structural and functional similarities of both protein classes minimal systems were created in which the active site of *EcE3* was modified to mimic that of a LOV protein. Whereas LOV domains harbor a conserved cysteine residue close to the FMN cofactor lipoamide dehydrogenases exhibit a redox active cysteine (Figure 3.20). Thus, mono-thiol variants of *EcE3* were generated for the required active site modification. As aforementioned, UV-Vis spectroscopic data suggested that Cys50 in *EcE3C45A* is present in its thiol form (3.1.5) and, moreover, is capable of NAD⁺-induced adduct formation (Figure 3.5 and Figure 5.2). Hence, *EcE3C45A* seemed to be a suitable starting point for the establishment of a pseudoLOV minimal system. In another mono-thiol variant, *EcE3C45S*, the remaining cysteine (Cys50) is present in its anionic form leading to a permanent charge transfer complex between the Cys50-thiolate and the flavin cofactor (3.1.4). Since the charge transfer complex is on-pathway in the reaction cycle of the native enzyme this variant was chosen as second mono-thiol variant. Besides targeting the cysteine moiety as a site for mutations, another residue crucial for H-bonding with FAD-N5 during the respective reaction cycle is different in both enzymes and was therefore the second target for site-directed mutagenesis. A highly conserved glutamine residue hydrogen bonds to flavin N5 in LOV proteins and has a key role in transducing the light signal

(Conrad et al. 2014) whereas a conserved lysine residue is thought to facilitate N5 protonation during the reaction cycle and to mediate the FAD redox potential (Maeda-Yorita et al. 1994). Thus, Lys54 was mutated to Gln54 leading to the pseudo LOV proteins *EcE3C45A/K54Q* (pseudoLOV) and *EcE3C45S/K54Q* (thiolateLOV) (Figure 3.20).

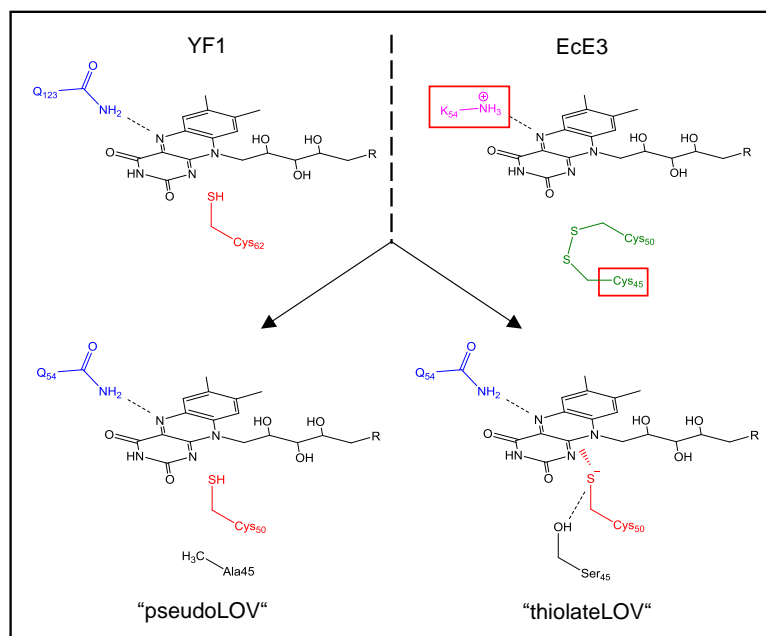


Figure 3.20 Converting *EcE3* into a pseudoLOV protein.

(top) Schematics of the active sites of YF1 and *EcE3*. YF1 numbering is taken from PDB 4GCZ. Targeted residues during mutagenesis are marked with a red box. (bottom) Schematics of the “pseudoLOV” variants *EcE3C45A/K54Q* and *EcE3C45S/K54Q*. For detailed description of the chosen mutations see text.

Both double-variants could be purified to homogeneity and their structural integrity was verified by far-UV CD spectra (5.6). In addition, both pseudoLOV proteins retained their typical color (yellow and orange-red, respectively) which was also observed for the respective single variant. UV-Vis ground-state spectra proved that substitution of Lys54 did not change the respective protonation state in each mono-thiol variant (5.2D and E). Thus, the pseudo- and the thiolateLOV variant fulfill the requirements to reflect a minimal LOV protein system.

3.4.2 Photobleaching of pseudoLOV Variants leads to irreversible Alterations at the Flavin Site

In order to investigate the photochemical response of re-engineered E3 variants the proteins were subjected to blue-light exposure with concomitant read out on a photodiode array. Exposure of *EcE3C45A/K54Q* to blue light (455 nm, 50 mW/cm⁻²) changed the absorption properties, indicating that the protein is photochemically reactive. The typical flavin band at 450 nm decreased during the time course with concomitant increase in the lower wavelength region at 340 to 350 nm showing an isosbestic point at 380 nm (Figure 3.21A). The final spectrum is different to that of a fully reduced flavin (Ghisla et al. 1974). Recovery kinetics showed that the absorbance change is irreversible. Photoreduction *EcE3C45S/K54Q* under the same conditions lead to comparable absorbance changes but with less drastic effects. However, the tendency of a decrease in absorbance in the longer wavelength range and increase in lower range is evident. As for the thiol variant these processes were irreversible. Noteworthy, the thiolate charge transfer between Cys50 and chromophore was only slightly affected (Figure 3.21B). In both variants, a significant increase in absorbance between 380 – 390 nm was missing leading to the assumption that formation of a cysteinyl-C4a adduct is unlikely.

Control experiments were performed to determine, at first, the photoreactivity of *EcE3wt* towards blue light and secondly to verify whether the observed absorbance changes were due to adduct formation involving the flavin N5 atom. It was demonstrated that light induced N5-adducts harbor a comparable spectroscopic signature as described above (Ghisla and Massey 1975) and therefore the investigation of a putative interaction of Cys50 with N5 was of special interest. The results obtained for the controls can be found in the appendix (5.7). *EcE3* wild type also showed a certain photochemical reactivity but with a much lower extent than the pseudoLOV variant. Further, the formation of covalent N5-adducts is unlikely since the mono- or non-thiol variants showed comparable spectroscopic changes upon light illumination: mutation of Cys50 facing the flavin cofactor to either alanine (*EcE3C50A*) or serine (*EcE3C50S*) made adduct formation unlikely due to steric or chemical reasons. To further exclude a covalent bond formation between protein and cofactor during photobleaching the proteins denatured with 6 M guanidinium chloride which lead to a release of the chromophore in all cases. The formation of a flavin radical species during photobleaching is also unlikely since the UV-Vis signatures did not show specific bands for neither the neutral nor the anionic semiquinone radical (Choong and Massey 1980; Massey and Palmer 1966). Time-resolved EPR measurements confirmed that radical species do not accumulate to an significant amount (5.8).

Low intensity (5 mW/cm⁻²) blue light illumination of LOV domain YF1 (Diensthuber et al. 2013) drastically leads to changes in the UV-VIS signature of the protein. In the dark state, the flavin is fully oxidized having an absorption maximum at 447 nm. Formation of the flavin-(C4a)-cysteinyl covalent bond blue-shifts the absorbance to a new maximum at 390 nm (Figure 3.21C). Ten-fold higher light intensities (50 mW/cm⁻²) lead to the same spectroscopic changes and, more importantly, the lit state

spectrum was stable for at least one hour during photobleaching under the harsher conditions (personal communication by Prof. Andreas Möglich). In contrast, YF1C62A, a variant in which the bond-forming cysteine residue is replaced by an alanine, was not resistant against long-term photobleaching (Figure 3.21D). The spectroscopic changes for this enzyme were similar to those observed for the pseudoLOV protein: a decrease of the main flavin peak with a simultaneous increase in the lower wavelength region, with an isosbestic point at 380 nm. However, in contrast to the pseudoLOV protein a broad absorption band with maxima at 570 and 610 nm developed during photobleaching. This spectral property is similar to those of other flavoprotein neutral radicals (Massey and Palmer 1966; Talfournier et al. 2001a). Radical formation came along with loss in absorbance at 447 nm but then also diminished during the further bleaching process leading to a single peak formation at ~330 nm. The entire bleaching process was also irreversible.

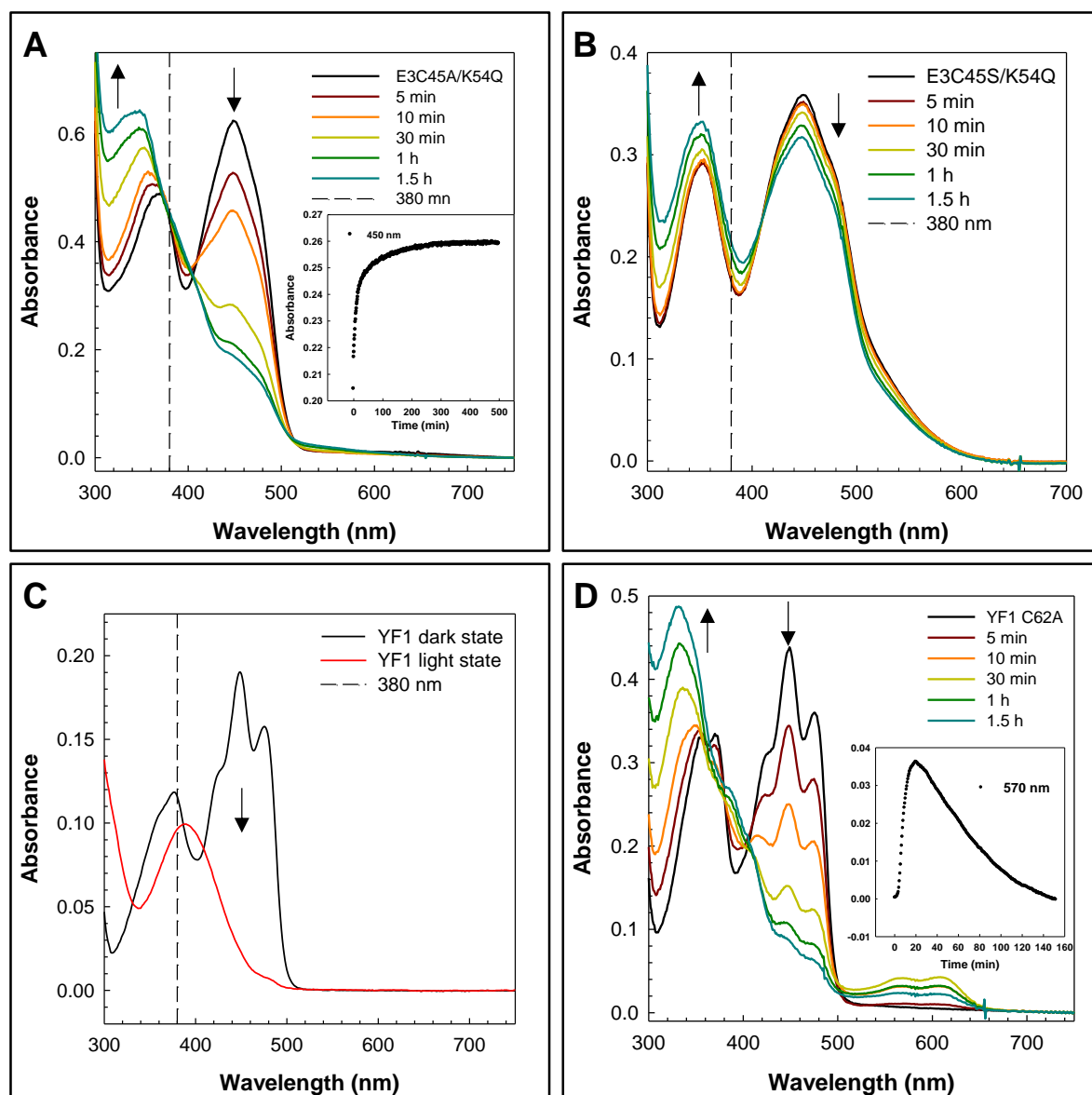


Figure 3.21 Comparison of absorbance changes in variants of pseudoLOVs and LOV domains upon blue light illumination.

UV-Vis spectra of pseudoLOV (A) and thiolateLOV (B) during photobleaching ($50\text{mW}/\text{cm}^2$) with blue light (455 nm). The inset shows the recovery kinetic in the dark. (C) UV-Vis absorbance profiles of YF1 wild-type protein. The black trace represents the dark state spectrum and red trace the lit state spectrum. Data were kindly provided by Prof. Andreas Möglich, HU Berlin. (D) UV-Vis spectra of YF1C62A during photobleaching ($50\text{mW}/\text{cm}^2$). The inset shows formation and decay of the neutral semiquinone radical at 570 nm .

3.4.3 Mass Spectrometric Analysis of the photobleached Flavin Cofactor

To further elucidate the alterations occurring at the flavin site upon light illumination the photobleached cofactor of pseudoLOV (*EcE3C45A/K54Q*) was isolated from the enzyme and subjected to both UPLC-ESI-TOF-MS and UHPLC-ESI-QTOF-MS/MS. MS analysis of FAD (purchased from AppliChem) and of isolated cofactor from unbleached pseudoLOV served as reference measurements. The usage of three different isolation techniques and their subsequent analysis excluded that modifications at the flavin site were due to the respective isolation method (2.2.6.5). All MS spectra belonging to the reference measurements and all spectra for the different isolation techniques for photobleached and unbleached samples are shown in the Appendix (5.9).

UPLC-ESI-TOF-MS analysis of the photobleached flavin cofactor showed the presence of two additional flavin derivatives besides the non-modified FAD (Figure 3.22). The derivative eluting slightly earlier than native FAD has an m/z 782.13 and the corresponding UV-Vis spectrum shows maxima at 367 and 450 nm (Figure 3.22C and D, blue line). The lower m/z ratio of two protons compared to FAD (m/z 784.18) can be explained by a double bond formation whereas a localization of the latter in the isoalloxazine part is unlikely since the UV-Vis spectrum reflects the shape of a non-modified FAD. According to the results obtained this derivative is termed *FAD-2H*. A more detailed investigation to localize the putative double bond is shown later (Figure 3.24).

The retention time of the second derivative is shifted to a later time point with an m/z 241.07 and the UV-Vis spectrum harbors a maximum at 350 nm (Figure 3.22C and D, red line). The latter derivative was identified as lumichrom by comparing the data with the data obtained from a lumichrom standard solution (Figure 5.12 and 5.13). This indicates the formation of lumichrom during photobleaching of pseudoLOV.

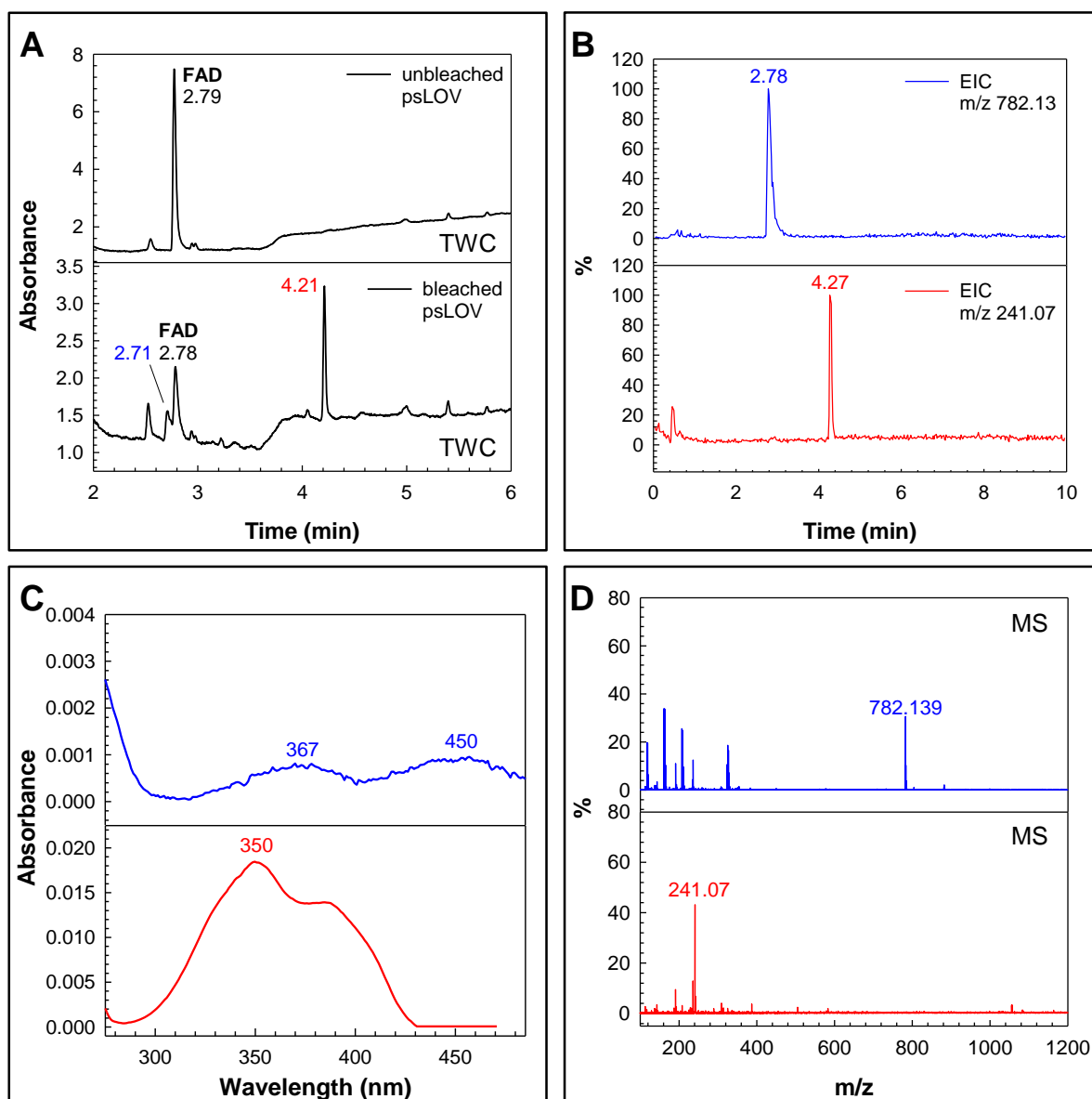


Figure 3.22 UPLC-ESI-TOF-MS analysis of cofactors of bleached and unbleached psLOV.

(A) Total wavelength chromatogram of TCA extracted cofactors from unbleached (top) and photobleached (bottom) pseudoLOV. Corresponding UV-Vis spectra are shown in (C) with the respective color. (B) Extracted ion chromatogram for m/z 782.13 (top) and m/z 241.07 (bottom) and corresponding MS analysis (D) in negative ionization mode. Allocation of FAD is based on the analysis of an FAD standard solution shown in the appendix (Figure 5.8).

Besides the formation of lumichrom and *FAD-2H* a third derivative could be identified during UPLC-ESI-TOF-MS analysis (Figure 3.23). This derivative was not shown in Figure 3.22 since the TCA used for cofactor extraction eluted in the same time scale making a UV-Vis detection impossible. The derivative has an m/z 542.07 and the UV-Vis spectrum shows a single peak with its maximum at 260 nm. This UV-Vis signature is typical for an adenine moiety indicating that this FAD derivative lost its isoalloxazine part. The latter is almost congruent with the obtained mass, however a formation of an additional double bond (as described for *FAD-2H*) is required to achieve the appropriate

observed mass. According to the results obtained this derivative is tentatively assigned as *ribityl-ADP-2H*.

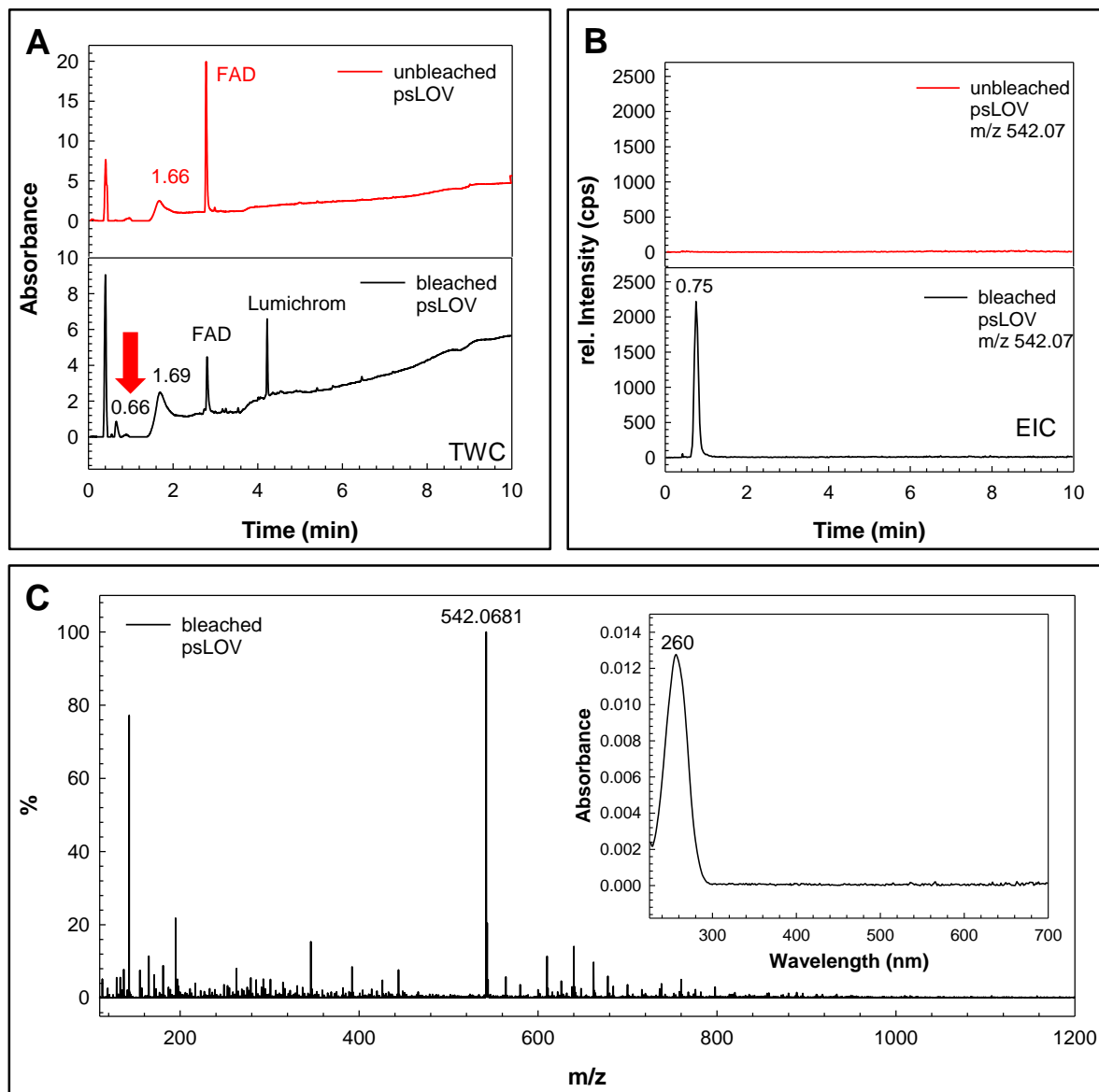


Figure 3.23 UPLC-ESI-TOF-MS analysis of *ribityl-ADP-2H*.

(A) Total wavelength chromatogram of heat extracted cofactors from unbleached (top) and photobleached (bottom) pseudoLOV. (B) Extracted ion chromatograms for m/z 542.07, respectively. (C) MS analysis (negative ionization mode) of B and corresponding UV-Vis spectrum of (inset). Allocation of FAD and lumichrom is based on the analysis of standard solutions shown in the appendix (Figure 5.8 and Figure 5.12).

UPLC-ESI-TOF-MS analysis thus far revealed the presence of three additional FAD derivatives formed upon photobleaching of pseudoLOV: lumichrom, *FAD-2H* and *ribityl-ADP-2H*. On the one hand, lumichrom could clearly be identified on the other hand, the exact position of the double bond in

the two remaining derivatives is unclear. The double bond position was then investigated by subjecting FAD and the *FAD-2H* derivative to UHPLC-ESI-QTOF-MS/MS. The interpreted fragmentation pattern indicates that no double bond is formed in neither the isoalloxazine, nor in the AMP part of the FAD since the respective fragments show the same m/z values (Figure 3.24, black arrows). This indicates that the double bond is positioned in the ribityl part which is consistent with the UV-Vis spectroscopic data obtained by UPLC-ESI-TOF-MS. The UV-Vis signature of *FAD-2H* and of *ribityl-ADP-2H* resemble the one of FAD and an adenine moiety, respectively. Double bond formation in the ribityl part led to an altered MS/MS fragmentation pattern. While two fragments deviate by two protons (m/z 517.05 / 515.04 and m/z 437.08 / 435.07) one further fragment deviates by an additional carbon atom (m/z 180.99 / 192.99). Moreover, the fragment with an m/z 337.09 is exclusive for *ribityl-ADP-2H*.

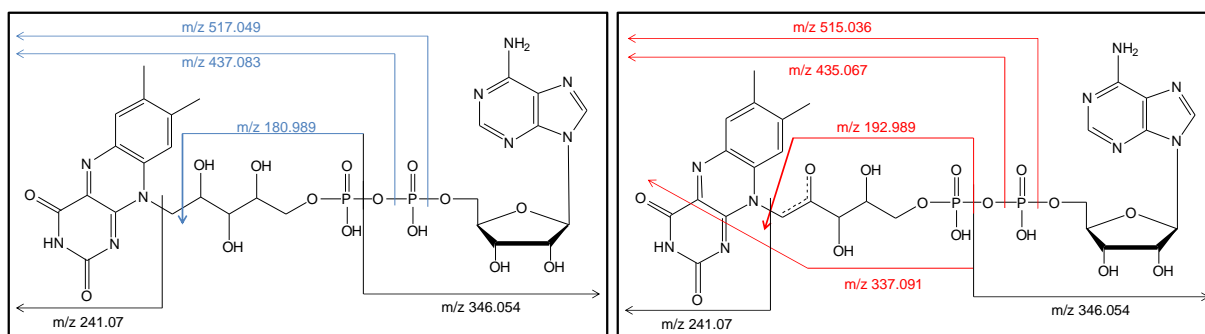


Figure 3.24 The double bond in *FAD-2H* and in *ribityl-ADP-2H* is located the ribityl part. MS/MS fragmentation pattern at 20 eV collision energy for FAD at m/z 784.15 (left) and for *FAD-2H* at m/z 782.13 (right). FAD derivatives were interpreted in comparison to FAD spectra (METLIN ID2302) deposited in the METLIN database. Fragments harboring the same m/z ratios are indicated in black, different ratios are shown in blue and red, respectively. The fragmentation patterns indicate that the modified position is housed in the ribityl part of the FAD derivative. The MS/MS fragmentation pattern is shown in (Figure 5.16).

3.4.3.1 C4a-cysteinyl Adduct Formation in LOV Domains prevents Photodegradation of the Flavin Cofactor

The results obtained so far showed that the generated pseudoLOV minimal systems were not sufficient to promote light-driven cysteinyl-C4a adduct formation. A further spectroscopic and crystallographic investigation of these adducts was therefore not possible. However, the experiments offer a new perception regarding the LOV protein photocycle and photodegradation of enzyme-bound flavin cofactors. The data obtained for YF1 and its active site variant YF1C62A lead to the assumption that

covalent bond formation between the conserved cysteine residue and the FMN cofactor during the photocycle harbors an intrinsic protective function against photodegradation. As described above, high-intensity photobleaching of the wild type LOV domain did not influence the lit state spectrum while the same intensities altered the spectral properties of the *EcE3* wild type and its pseudo LOV derivatives. This spectral change is based on irreversible alterations at the flavin site (3.4.2). Hence, there must be a mechanistic or structural property preventing LOV domains from photodegradation and thus keeping the protein active to perform further rounds of photocycle and concomitant signal transduction. Mutation of the bond forming cysteine residue to alanine (YF1C62A) abolished this resistance leading to spectroscopic changes similar to those obtained for the oxidoreductase (Figure 3.21D). Therefore, bond formation between a cysteine and flavin cofactor seems to be the crucial part of the protective function against photodegradation. C4a-cysteinyl adduct formation leads to loss of aromaticity of the flavin ring system and thereby changes its electronic configuration. This results in a blue shifted spectrum and reduces absorption of light with longer wavelengths (>400 nm). It was demonstrated that longer wavelengths, especially in the range of 415 - 455 nm, drastically damage riboflavin in solution (Sattar, deMan, and Alexander 1977). Since the flavin adduct does not absorb light with this particular wavelength a relation between the latter and resistance against photodegradation is evident. Thus, LOV domains have evolved a structural feature which simultaneously permits both signal transduction on the one hand and protection against photodegradation on the other (Figure 3.25).

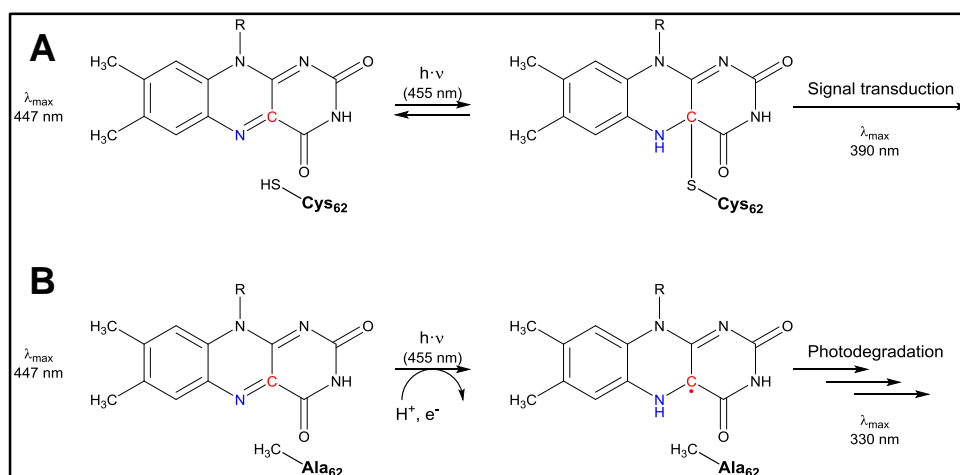


Figure 3.25 Protective mechanism of LOV proteins.

(A) C4a-cysteinyl adduct formation exhibits two functions: Signal transduction and protection against photodegradation. (B) Blue light exposure of the cysteine-lacking variant induces formation of the neutral semiquinone, the potential pre-stage prior to photodegradation.

The formation of the flavin neutral semiquinone radical in YF1C62A was the major difference during photobleaching of the cofactor compared to the pseudoLOV protein. Though, the single peaks are blue-shifted by ~10 nm, the position of the radical band maxima are similar to those observed for glucose oxidase, DNA (6-4) photolyase or an animal-like cryptochrome (aCRY) (Beel et al. 2012; Hitomi et al. 1997; Massey and Palmer 1966). Since there is evidence for a neutral semiquinone intermediate between the excited triplet and the adduct state (Bauer et al. 2011) the accumulation of a neutral radical in the cysteine-missing variant is not unexpected. However, it remains unclear whether formation of the neutral radical lies on pathway, and thus accumulates since adduct formation is impaired, or whether radical formation is a side effect of the photodegradation of the FMN cofactor. According to the rate of the semiquinone formation the latter is more likely since radical formation in aCRY is ~40-fold faster and, even more important, reversible (Beel et al. 2012). To compare the putative influence of the semiquinone radical on the photodegradation a mass spectrometric analysis according to the pseudoLOV protein should be performed (see discussion below).

3.4.3.2 Photodegradation of enzyme-bound FAD leads to Double Bond formation in the ribityl part

Mass spectrometric analysis revealed three major FAD derivatives as photodegradation products upon blue light exposure of the pseudoLOV protein: lumichrom, *FAD-2H* and *ribityl-ADP-2H* (Figure 3.26) whereas the formation of lumichrom was confirmed by reference measurements. Photostability and degradation of riboflavin in aqueous solvents have been extensively studied due to its relevance in food products and pharmaceutical preparations. It is degraded into several photoproducts including the aforementioned lumichrom, but also into formylmethylflavin, lumiflavin, carboxymethylflavin and further derivatives (Sheraz, Kazi, Ahmed, Anwar, et al. 2014). Formation of lumichrom is controversially discussed and both excited singlet and excited triplet states of riboflavin are stated to be precursors in the photodegradation reactions by different mechanisms. On the one hand, lumichrom is formed by the excited triplet state (Ahmad et al. 2004; Huang, Hyun, and Min 2006; Jung et al. 2007) on the other hand, the excited singlet was also claimed as a precursor (Ahmad et al. 2004; Cairns and Metzler 1971; Sheraz, Kazi, Ahmed, Mirza, et al. 2014). However, the distinction between these reactions in the photodegradation process lacks detailed information (Sheraz, Kazi, Ahmed, Anwar, et al. 2014). To get information about the excitations states of the enzyme-bound cofactor nanosecond time-resolved UV-Vis spectroscopy by flash photolysis should be performed (Bauer et al. 2011). This would potentially allow a comparison of the flavin excitations states generated in solution and when bound to an enzyme.

Though information in the nano- and microsecond time regime of the photobleaching event of the pseudoLOV protein are missing alterations of the degradation profile compared to riboflavin in solution are obvious. First, it has been described that the presence of divalent anions, such as

phosphate (HPO_4^{2-}) and sulfate (SO_4^{2-}), exclusively lead to the formation of cyclodehydroriboflavin as photodegradation product (Ahmad et al. 2010; Schuman Jorns, Schöllnhammer, and Hemmerich 1975; Sheraz, Kazi, Ahmed, Mirza, et al. 2014). This product was not identified during MS analysis and thus an influence of the used buffer system (50 mM KPP pH 7.6, 100 mM NaCl) on the degradation process of the enzyme-bound flavin is unlikely. Moreover, among the plethora of riboflavin degradation products thus far described, out of the three derivatives formed lumichrom was the only one which has yet been reported. Hence, an influence of the enzyme surrounding on the photodegradation process is evident. The ultimate structure of the two remaining derivatives (*FAD-2H* and *ribityl-ADP-2H*) could not be determined since information about the absolute position of the light-induced double bond is missing (Figure 3.24). Formation of the latter fragments lead to the assumption that the double bond is delocalized between the C1, C2 and C2=O atoms of the ribityl part (Figure 3.26). This assumption is on the one hand underpinned by the UV-Vis spectroscopic signatures of both fragments indicating no influences of the double bond on the isoalloxazine nor the adenine moiety of FAD (Figure 3.22C and Figure 3.23C) and on the other hand by the altered MS/MS fragmentation pattern. A delocalized double bond between the C1, C2 and C2=O atoms might explain the altered fragmentation pattern around C1 and thus the presence of the one-carbon-elongated fragment with an m/z 192.99. Further, localization of the double bond in the mentioned region could result in a stabilization of *ribityl-ADP-2H*. Assuming an additional bond formation between C2 and C2=O the formation of a pseudo-six-membered ring system could be the consequence. Here the hydrogen atom the C4-OH group could hydrogen bond to C2=O (Figure 3.26). It cannot be ruled out whether *FAD-2H* is a potential precursor of *ribityl-ADP-2H*. Therefore, MS analysis of photobleached samples taken at different time points could provide further insights into the photodegradation process of enzyme-bound flavin.

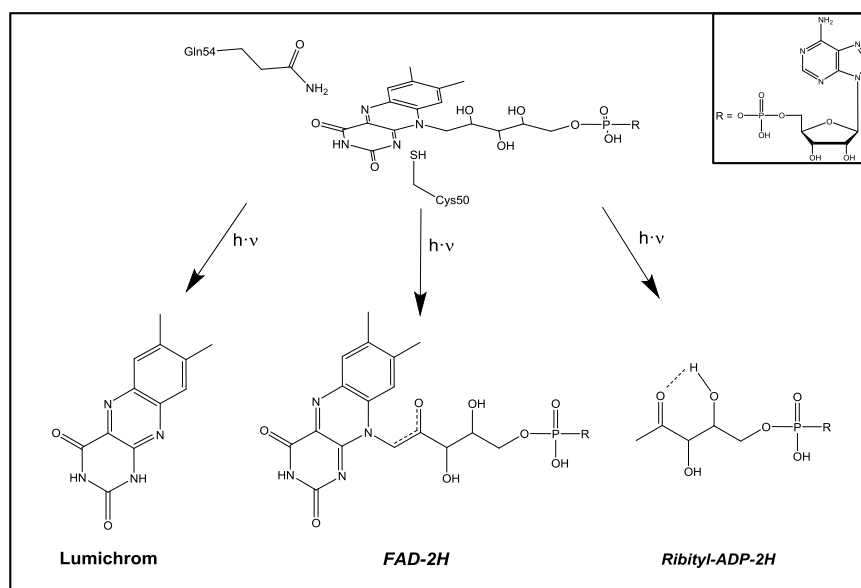


Figure 3.26 Putative FAD derivatives formed upon pseudoLOV photobleaching. The presence of lumichrom was verified by reference measurements with a lumichrom standard solution. The shown structures for *FAD-2H* and *ribityl-ADP-2H* are hypothetical (see discussion). The inset shows the AMP part of the FAD derivatives which is not modified during bleaching.

3.4.4 The H-bonding Network around the Flavin – The next Step on the Way to a light-sensitive Oxidoreductase?

The studies on the re-engineered E3 variants have not yet yielded a light-driven system for production of reduction equivalents yet, but they have provided key insights into the inner workings of both E3 metabolic enzymes and LOV photoreceptors (3.4.3.1 and 3.4.3.2). The used minimal system, in which the redox active cysteine was converted into a monothiol moiety and in which the residue crucial for (de)protonation of FAD-N5 was exchanged (Lys54 → Gln54), was thus too rudimentary to convert the oxidoreductase into a light-sensing protein. Hence, there must be additional factors which are required for light-driven adduct formation. The redox potential of the flavin cofactor in the LOV kinase LOV_k from *C. crescentus* was determined to be -258 mV (Purcell et al. 2010) which is way more positive than the reported -314 mV in *EcE3*_{wt} (Maeda-Yorita et al. 1991). However, redox titrations with the pseudoLOV protein (*EcE3C45A/K54Q*) revealed a redox potential of -268 mV (Table 5.2) which is strikingly close to the reported potential of the cofactor in LOV_k. The elevation is thereby mainly related to the replacement of the N5 interacting lysine by a glutamine rather than the presence of the thiol at the *si* face of the cofactor (3.3.2.1). Though the tendency of the flavin to gain electrons was eased and thus the interaction of the Cys50 thiol moiety with the C4a atom should have been facilitated it is obvious that further features are required to promote adduct formation. It was demonstrated that the extended hydrogen bond network stabilizing the FMN cofactor in LOV domains (Figure 3.27A) can modulate the quantum yield, kinetics, and thermodynamics of the photocycle (Raffelberg et al. 2011). Consequently, a further step to convert *EcE3* into a light-sensing protein should target the surrounding of the chromophore in the oxidoreductase (Figure 3.27B). Putative candidates to alter the microenvironment around the pteridine part of the *EcE3* FAD are His445 and Ala321 which could be exchanged with uncharged, polar amino acids. However, negative side effect altering the FAD's redox potential too much have to be considered. Redox titrations for further variants are hence obligate.

Photobleaching of YF1C62A demonstrated that the LOV protein is capable of stabilizing the neutral flavin semiquinone radical if adduct formation is impaired (Figure 3.25). Taking into account that such species was identified between the triplet and the adduct state in a wild type enzyme (Bauer et al. 2011) it is most likely that these photoreceptors provide a surrounding which relieves neutral semiquinone formation. This is further underpinned by the finding that a replacement of the conserved asparagines interacting with the pteridine part of the FMN with negatively charged aspartates did not affect the dynamics and energetics of adduct formation (Raffelberg et al. 2011). According to the authors the latter would be unlikely if a transiently charged species at the flavin site would occur during photocycle. Furthermore, FTIR techniques have provided evidence that the triplet state of FMN is unprotonated making an ionic mechanism (Alexandre et al. 2009; Pfeifer et al. 2009) even more questionable. Though there are multiple evidences that adduct formation might proceed through an

ionic intermediate (Kennis and Groot 2007; Losi and Gärtner 2011; Zoltowski and Gardner 2011) the results presented here indicate that a radical pair mechanism via a triplet-state $\text{FMNH}^{\bullet}-\text{H}_2\text{CS}^{\bullet}$ biradical yielding the covalent bond between cofactor and cysteine still has to be considered. To demonstrate that neutral semiquinone formation in YF1C62A is not a side effect of the degradation of the cofactor, the method established by BAUR et al. using nanosecond flash photolysis with CCD camera detection should be applied to the active site variant (Bauer et al. 2011). This could proof that formation of the blue flavin radical is also possible in a transient time regime. However, a crucial limitation of the active site mutant is evident: the conserved Cys, the likely candidate for the proton source required for N5 protonation during neutral semiquinone formation (Alexandre et al. 2009; Kennis and Groot 2007; Losi and Gärtner 2011; Pfeifer et al. 2009; Zoltowski and Gardner 2011) is absent. It is hence possible that flash photolysis experiments do not show a transient formation of the neutral semiquinone and that the observation of the latter during the steady-state photobleaching assay (Figure 3.21D) was only possible because radical formation was slowed down due to limited access of a proton from the solvent to FAD-N5.

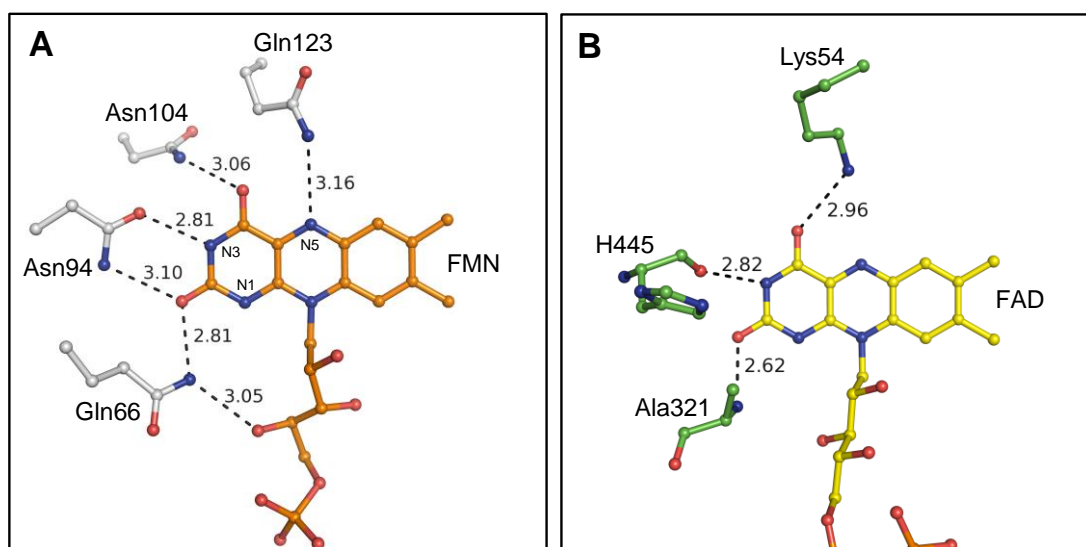


Figure 3.27 Comparison of the H-bonding network around the flavin cofactors in YF1 and *EcE3*. (A) The HB network in LOV proteins consists of interactions between the N5, C4=O, N3H, and C2=O atoms of the isoalloxazine moiety of FMN and a variety of conserved polar, uncharged amino acids (YF1; PDB: 4GCZ). In contrast, the interactions the isoalloxazine moiety in *EcE3* makes are limited to two main chain atoms and the conserved lysine residue (distances in Å).

3.5 Expanding the Active Site – Glu354 is also a Mediator of the Flavin Redox Potential

Mutation of Glu354, a second shell residue in *EcE3* located at the dimer interface, to Lys354 reduced the sensitivity towards NADH inhibition of *EcE3* and thereby affected the fermentation profile of *E. coli* (Kim et al. 2008). However, a more detailed or even a molecular investigation of this alteration was not conducted. In the following, the results obtained by Kim *et al.* will be summarized briefly and further extended with the help of spectroscopic and structural data. This extension shall broaden the understanding in which way the mutation of one single amino acid leads to such global effects.

Kim *et al.* purified *EcE3E354K* from strain SE2378 and determined kinetic steady-state parameters for both the native forward reaction using dihydrolipoic acid and the reverse reaction using NADH as reductant, respectively (Kim et al. 2008). Briefly, *EcE3E354K* only showed 50 % activity in the native forward reaction, however the mutated enzyme was significantly more resistant towards NADH inhibition at saturation NAD^+ concentrations. In the reverse reaction, *EcE3E354K* already reached approximately 75 % of its maximum catalytic activity (~ 75 U) in the absence of added NAD^+ whereas the wild type enzyme required at least a NAD^+/NADH ratio of 2.0 to reach its maximum (~ 70 U).

While the results obtained so far unambiguously demonstrate the physiological importance of the NADH sensitivity of *EcE3* with the inherent potential of unexplored biotechnological applications, a molecular understanding of the altered enzyme properties is missing. To further elucidate the latter *EcE3E354K* was derived from the wild type *E. coli* E3 enzyme by site-directed mutagenesis and subjected to both steady-state kinetics analysis and stopped-flow absorbance spectroscopy. The structural integrity was checked by far-UV CD spectroscopy revealing no significant alterations in the secondary structure compared to the wild type enzyme (5.6C). Further, the UV-Vis absorbance signature is congruent with the wild type spectrum indicating no influences of the mutation to the direct surrounding of the flavin cofactor (5.2 K). *EcE3* follows a non-hyperbolic dependence with respect to lipoamide during the steady-state assay. However, *EcE3E354K* showed clear hyperbolic dependence leading to an ~ 18.5 -fold increase in catalytic proficiency though the maximal specific activity deviated only by ~ 10 % (Figure 3.28A). The comparable catalytic activity of the reverse reaction and the altered behavior with respect to NAD^+ activation (Figure 3.28B) are consistent with the results obtained recently (Kim et al. 2008).

As described in 3.1.2 a 4-fold molar excess of NADH is sufficient to overreduce *EcE3* to the catalytic incompetent four-electron reduced state (EH_4). Assayed under the identical conditions *EcE3E354K* resides in the catalytic active two-electron reduced state (EH_2) (Figure 3.28C). The presence of the charge transfer band at 523 nm and incomplete decrease in absorbance at 455 nm compared to the wild type EH_4 -level are indicative for the charge transfer complex between the thiolate formed by Cys50 and FAD. Thus, overreduction to the dead-end EH_4 status is impaired in *EcE3E354K* under the

conditions tested. It should be noted that the charge transfer complex is formed with comparable rates and amplitudes as in the wild type (*E354K*: $k_{obs} = 135 \pm 2$ versus wt: 143 ± 3 s⁻¹) (Figure 3.28D). In addition, reduction to EH₄ in the wild type enzyme is completed after ~1 s, whereas approximately 90 % of the 523 nm charge transfer signal is still present in *EcE3E354K* in the same time scale.

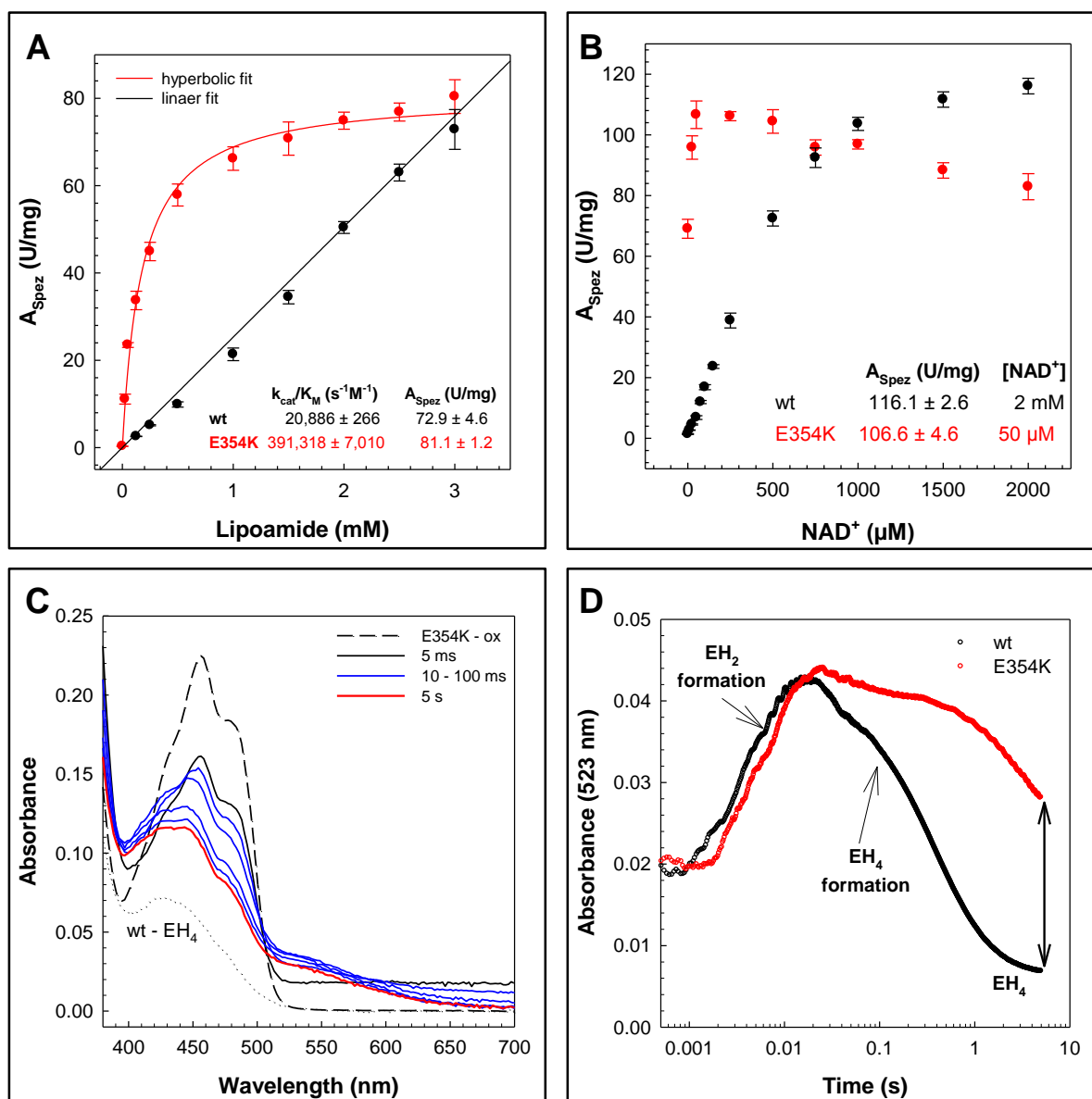


Figure 3.28 Kinetic and spectroscopic comparison between *EcE3E354K* and *EcE3wt*. **A** Comparison of the steady-state activity in dependence of lipoamide (2.2.4.1) and **B** of NAD^+ (2.2.4.2). **C** Stopped-flow absorbance traces after mixing 20 μM *EcE3E354K* with 100 μM NADH at 4 °C. The dotted spectrum reflects the wild type EH₄ spectrum as described in 3.1.2. **D** Comparison of stopped-flow absorbance traces at 523 nm under the conditions as described before.

Considering the results obtained for mutations of Lys54 and Arg386 obtained by stopped-flow absorbance spectroscopy (3.3.2), Glu354 is also a ruler influencing the redox potentials of the different enzyme intermediate species. The altered redox potential in *EcE3E354K* is evident since reduction with a 5-fold molar excess of NADH do not lead to EH_4 formation. The spectroscopic signature obtained rather reflects a spectrum which is similar to the EH_2 status described for pig heart lipoamide dehydrogenase under equal reduction conditions (Massey et al. 1960). The redox potentials of lipoamide dehydrogenases from different organisms have been investigated and the corresponding consequences for the catalytic properties have been drawn. WILKINSON AND WILLIAMS stated the bigger disproportionation of EH_2 to E_{ox} and EH_4 in the *E. coli* lipoamide dehydrogenase to be the major difference compared to the pig heart enzyme (Wilkinson and Williams 1979, 1981). The reason is the larger separation of the $\text{E}_{\text{ox}}/\text{EH}_2$ and EH_2/EH_4 redox potentials determined for the pig heart enzyme (~66 mV) compared to the closer separation (~53 mV) in the *E. coli* enzyme explaining the easier reduction to the 4-electron-reduced inactive enzyme. *EcE3E354K* therefore reflects a pig heart lipoamide dehydrogenase with respect to resistance against overreduction by NADH. To further underpin this assumption the absolute potentials of the $\text{E}_{\text{ox}}/\text{EH}_2$ and EH_2/EH_4 redox pairs in the mutant enzyme should be determined as described earlier (Matthews and Williams 1976).

Though a direct investigation of the absolute potentials is missing, a further elucidation of the molecular basis for the altered catalytic properties of the mutated enzyme based on the secondary structure information of *EcE3* (3.1.3) was used. Glu354 is localized at the dimer interface directly above the interface domain within a loop connecting two anti-parallel β -strands (Figure 3.29). The distance between the carboxylic group of Glu354 and N5 of the flavin cofactor is approximately 15 Å in the wild type enzyme. Thus, a direct interaction in the mutated enzyme is impossible. Further, there is no direct interaction with Lys54, Glu189 and Arg386 residues which were shown to modulate the flavin redox potential and hence susceptibility to overreduction by NADH (3.3.2). In addition, mutations of the latter residues showed remarkable effects in *EcE3* concerning affinity towards NAD^+ (3.3.2). This indicates that the redox potential of the flavin cofactor is not only mediated by residues located in the direct vicinity (Lys54 and Glu189), but also by nearby active site residues (Arg386). A further, aspect which is thought to modulate the cofactor's redox potential is the subunit interaction of the two monomers forming the catalytic functional enzyme. Such ability was attributed to Tyr16 in the *A. vinelandii* E3 which forms a hydrogen bond with a histidine residue of the C-terminus of the adjacent monomer (Benen, Van Berkel, Veeger, et al. 1992). Mutation of the latter residue lead to a significantly raised redox potential, thus altering the catalytic function of the mutated enzyme. However, the corresponding residue in *EcE3* (Tyr19) did not harbor a comparable mediator function (3.3.1.2). Taking into account that mutations at the dimer interface have the potential to act as determinate of the redox potential this role might also be attributed to Lys354 in the mutated *E. coli* enzyme. According to the position of Glu354 at the dimer interface, it is possible that a mutation to a lysine influences the subunit interaction yielding in a lowered redox potential of the FAD and hence a

protection against overreduction by NADH. It still remains puzzling how this modulation proceeds and probably further mutations at the dimer interface are required to further elucidate that striking ability of a putative cross-talk between the two subunits.

In summary, the single mutation of Glu354 to Lys354 in *E. coli* lipamide dehydrogenase not only led to a severe alteration of the regulation of the enzyme activity but thereby concomitantly changed the entire fermentation profile of the bacterium. Thus, the investigation of second shell residues with respect to their physiological role might have an unexplored potential for biotechnological applications.

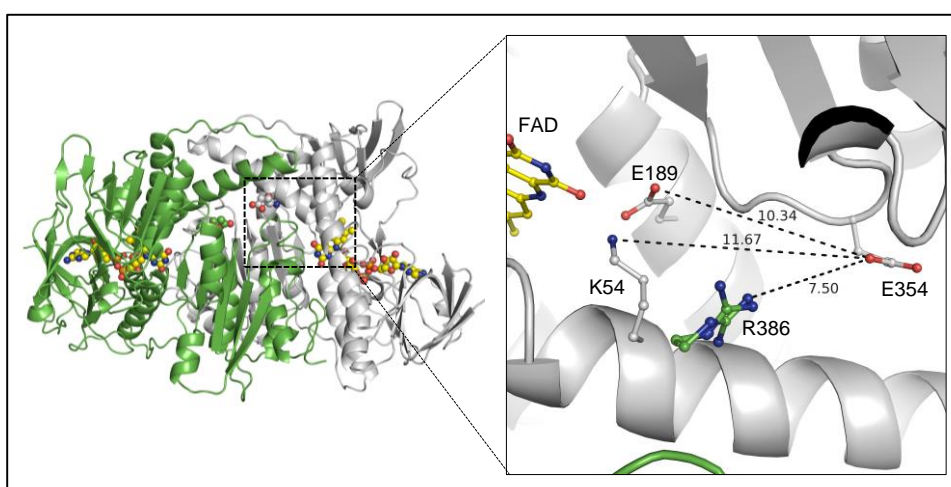


Figure 3.29 Position of Glu354 in *EcE3*.

(left) Cartoon representation of the *EcE3* homodimer. Glu354 and the FAD cofactor are shown in spheres. E354 is localized at the dimer interface, above the interface domain. (right) Distances (\AA) of Glu354 from selected active site residues involved in the oxidative half-reaction of *EcE3*.

4 Summary

The flavoenzyme lipoamide dehydrogenase is an ubiquitously distributed enzyme which is part of several multienzyme complexes involved in cellular carbon metabolism thus contributing to cellular homeostasis. It catalyzes the regeneration of reduced lipoamide cofactors using a disulfide exchange reaction of reduced lipoamide with a redox active cysteine, transfer of two reducing equivalents from this disulfide bridge to the flavin cofactor and hydride transfer from the flavin site to final acceptor NAD^+ (Perham 2000; Reed 1974, 2001). Lipoamide dehydrogenases have been thoroughly studied mechanistically and structurally over the last decades. However, the studies so far lack detailed spectroscopic and structural information about the central FAD-C4a-cysteinyll adduct the enzyme forms during catalysis. Moreover, there are no structural information about the two-electron reduced state (EH_2). This doctoral thesis provides new insights into the nature of those intermediates that are transiently formed along the reaction coordinate in lipoamide dehydrogenase from *E. coli* by means of a structure-function analysis. By combining x-ray crystallography with spectroscopic methods, a more detailed picture of the *EcE3* reaction cycle is now available helping to fill in the aforementioned blank.

Robust expression systems for both *EcE3* and the innermost lipoyl domain (*EcLip3*) of the E2 component of *EcPDHc* were established which allowed a convenient purification of both components to homogeneity. Several reaction intermediates could be identified and allocated in *EcE3* with the help stopped-flow absorbance spectroscopy and a previously established model (Argyrou et al. 2002). However, reduction of the *EcE3* with NADH (reverse direction) and, for the first time, with the reduced form of an isolated lipoyl domain (*EcLip3H₂*; forward direction) did not allow the detection of an absorbance increase which is typical for the covalent flavin adduct, neither in single nor in sequential mixing experiments. These results underpin the transience of the intermediate and that it only accumulates to a very minor extent in solution making an observation difficult which is consistent with previous studies.

Though the spectroscopic detection of a covalent flavin adduct was not possible in the wild type enzyme there is evidence for an NAD^+ -induced FAD-C4a-cysteinyll formation in a monothiol variant, in which the interchange thiol forming the mixed disulfide during catalysis was substituted with an alanine. The necessity for the presence of NAD^+ to trigger adduct formation is presumably based on the following aspect: Binding of the positively charged nucleotide at the *re* face of the flavin increases the electrophilicity of the oxidized flavin and concomitantly permits an active site compression pivotal for adduct formation. However, the spectroscopic signatures clearly demonstrated that the covalent adduct only accumulated to a small amount in the monothiol variant as well.

The structural data obtained during this project suggest that the geometry of the FAD-C4a-cysteinyll adduct is most likely responsible for its transience and thus the reason for its limited accumulation in

solution. Two X-ray structures of *EcE3* were solved, one in which NAD^+ was present during the phase of cryoprotection, and led to models with reasonable quality. Both structures highlight the local flexibility of the disulfide bridge contributing to the redox center and enabled the observation of structural rearrangements required for catalysis. The radiation-induced reduction of the disulfide bridge during data collection lead to partial opening of the latter and was thus used to trigger the formation of the covalent flavin adduct *in crystallo*. The *EcE3* ground state structure allowed the observation of two different redox states of *EcE3* simultaneously: the oxidized (E_{ox}) and the two-electron reduced state (EH_2). In addition, in the E3-NAD^+ structure electron density is observable that is consistent with an FAD-C4a-cysteinylyl adduct, a central long-sought-after intermediate, whose existence has been predicted but has never been proven experimentally in a wild type enzyme. Geometrical analysis revealed that the adduct deviates from tetrahedral geometry harboring an $\text{C}\beta\text{-S}\gamma\text{-C4a}$ angle of $>117^\circ$. It is therefore most likely, that the high transience of the adduct is based on the distorted geometry of the C4a-cysteinylyl adduct. Presumably, this prevents an elongated stabilization of the intermediate as it can be observed for the same kind of adducts in LOV domain photo receptors.

In order to stabilize the FAD-C4a-cysteinylyl adduct with the perspective of a further improved structural analysis, the metabolic *EcE3* should be converted into a light-sensing LOV domain. The generated *EcE3*-pseudoLOV minimal system was not capable of light-induced adduct formation, but provided new insights into the protection mechanism against photo degradation in LOV domains and the formation of new flavin derivatives upon enzyme-bound photo degradation. The data suggest that covalent flavin adduct formation in LOV domains not only serves as structural feature which permits signal transduction, but also provides protection against photodegradation of the cofactor. The isolated flavin derivatives derived from the *EcE3*-pseudoLOV protein unambiguously demonstrate that the enzyme surrounding influenced the photo degradation process. A light-induced double bond formation in an intact FAD molecule has thus far never been described. However, further analytical and photochemical investigations are required to elucidate the mechanism yielding this modification.

The study also demonstrates the susceptibility of the enzyme to alterations of the flavin redox potential. Active site residues could be identified which act as rulers in mediating the potential thereby ensuring a suitable potential which allows optimal catalysis. Even more impressive is the fact, that the redox potential can be influenced by mutations which are not in the direct vicinity of the cofactor. It turned out that especially mutations at the dimer interface drastically alter the redox potential, either raising (R386A) or lowering it (E354K). This not only altered the enzymatic behavior of *EcE3* alone, but moreover led to global effects which altered the entire fermentation profile of the bacterium (Kim et al. 2008). A further investigation of the dimer interface with respect to its ability to modulate the flavin redox potential is therefore mandatory regarding the physiological importance of the enzyme.

5 Appendix

5.1 Amino Acid Sequences

SUMO-*EcLip3*

Number of amino acids: 184 Molecular weight: 20 kDa Theoretical pI: 4.67

10 MSDSEVNQEA	20 KPEVKPEVKP	30 ETHINLKVSD	40 GSSEIFFKIK	50 KTTPLRRLME	60 AFAKRQ GKEM
70 DSLRFlydGI	80 RIQADQTPED	90 LDMEDNDIIE	100 AHREQIGG <u>↓</u> AP	110 AAGVKEVNVP	120 DIGGDEVEVT
130 EVMVKVGD KV	140 AAEQSLITVE	150 GDKASMEVPA	160 PFAGVVKELK	170 VNVGDKVKTG	180 SLIMIFEVEG

AAPA ↓ = SUMO cleavage site

EcLip3

Number of amino acids: 86 Molecular weight: 8777 Da Theoretical pI: 4.39

10 APAAGVKEVN	20 VPDIGGDEVE	30 VTEVMVKVGD	40 KVAAEQSLIT	50 VEGD <u>K</u> ASMEV	60 PAPFAGVVKE
70 LKVNVGDKVK	TGSLIMIFEV	EGAAPA	<u>_</u>		80

_ = lipoyl lysine

EcE3 derived from pGS523

10 MSTEIKTQVV	20 VLGAGPAGYS	30 AAFRCADLGL	40 ETVIVERYNT	50 LGGVCLNVGC	60 IPSKALLHVA
70 KVIEEAKALA	80 EHGIVFGPEK	90 TDIDKIRTWK	100 EKVINQLTGG	110 LAGMAKGRKV	120 KVVNGLGKFT
130 GANTLEVEGE	140 NGKTVINFDN	150 AIIAAGSRPI	160 QLPFIPHEDP	170 RIWDSTDALE	180 LKEVPERLLV
190 MGGGIIGLEM	200 GTVYHALGSQ	210 IDVVEMFDQV	220 IPAADKDIVK	230 VFTKRISKKF	240 NLMLETKVTA
250 VEAKEDGIYV	260 TMEGKKAPAE	270 PQRYDAVLVA	280 IGRVPNGKNL	290 DAGKAGVEVD	300 DRGFIRVDKQ
310 LRTNVPHIFA	320 IGDIVGQPML	330 AHKGVHEGHV	340 AAEVIAGKKH	350 YFDPKVIPSI	360 AYTEPEVAWV

APPENDIX

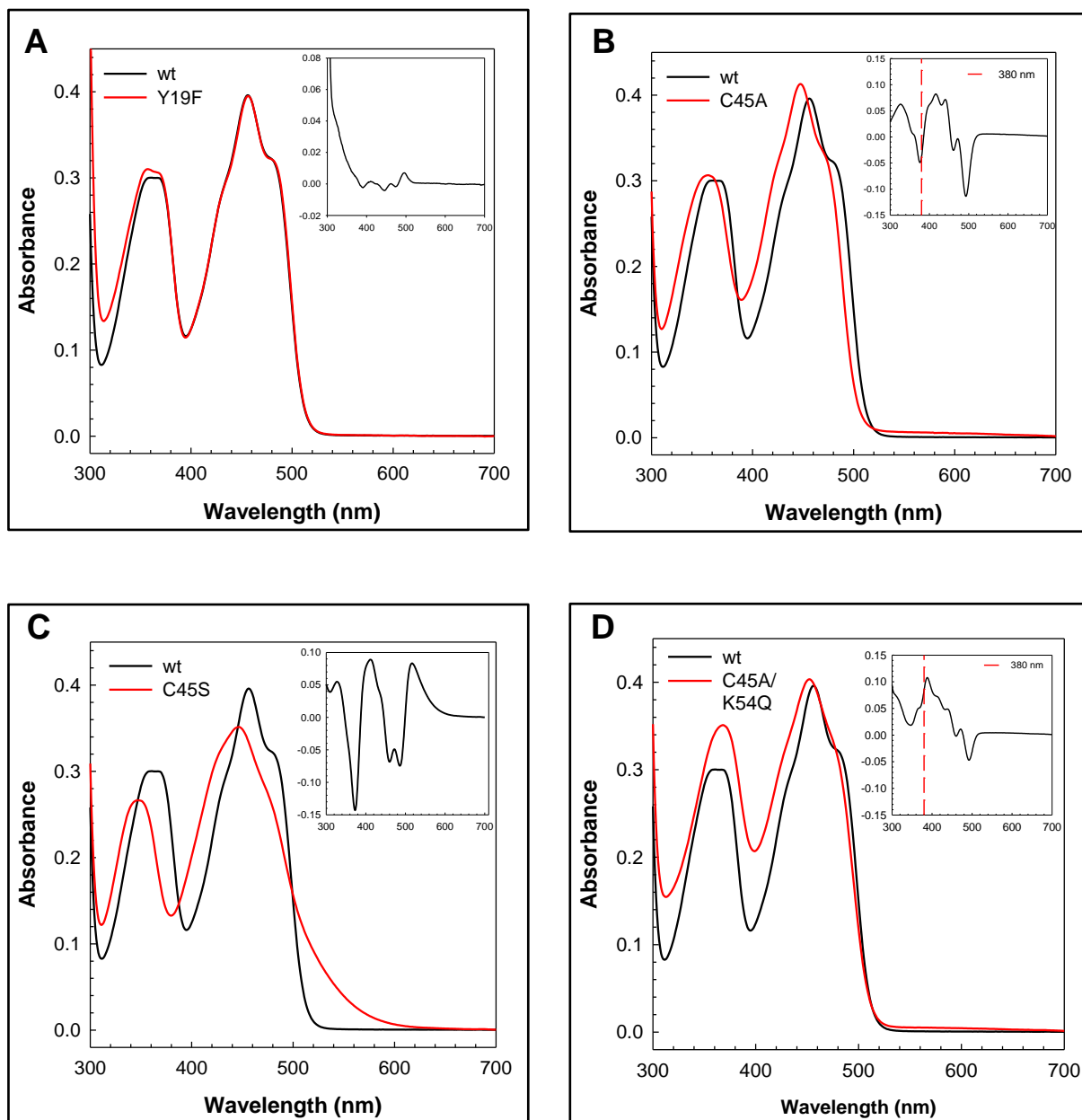
370 GLTEKEAKEK	380 GISYETATFP	390 WAASGRAIAS	400 DCADGMTKLI	410 FDKESHRVIG	420 GAIVGTNGGE
430 LLGEIGLAIE	440 MGCD AEDIAL	450 TIHAHPTLHE	460 SVGLAAEVFE	470 GSITDLPNPK	AKKK

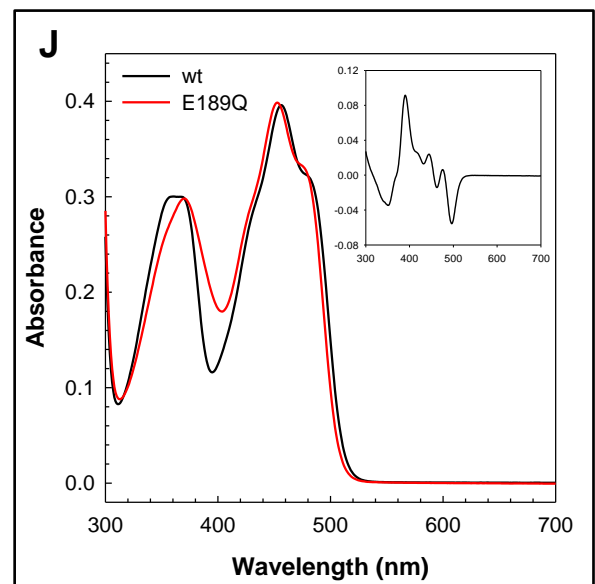
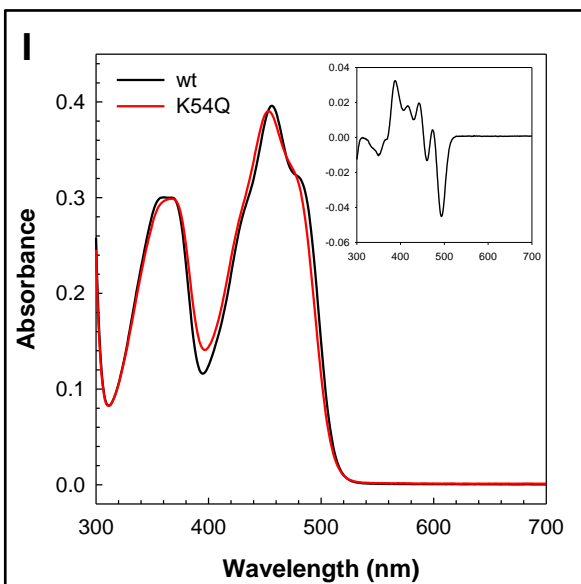
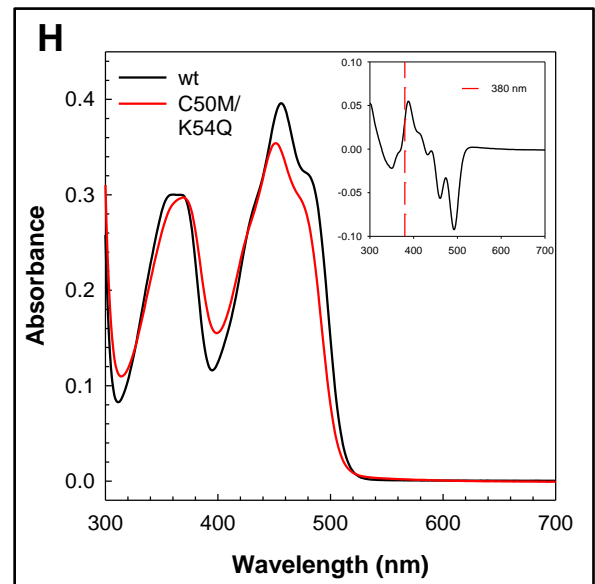
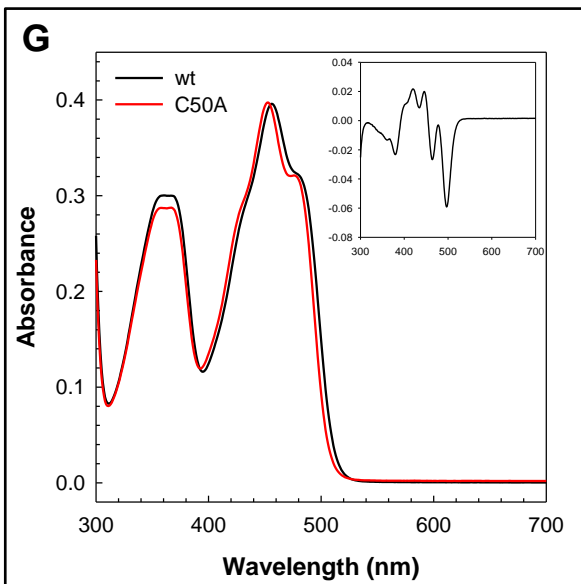
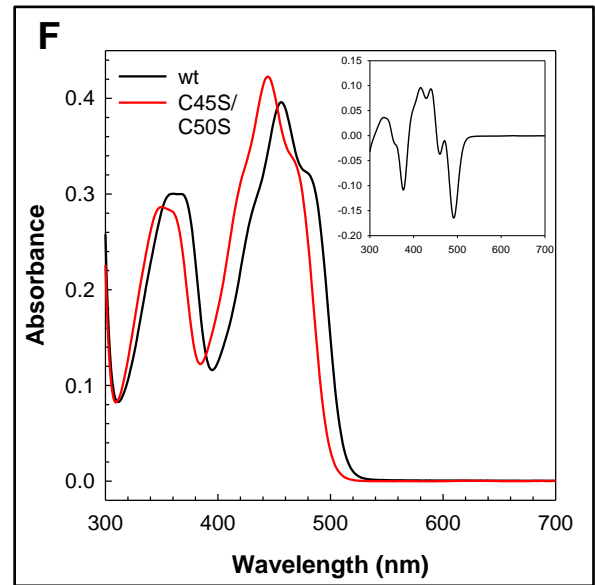
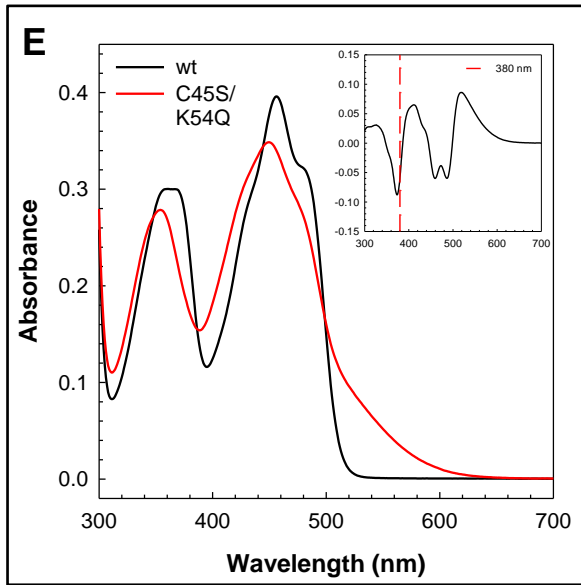
pET28a-EcE3

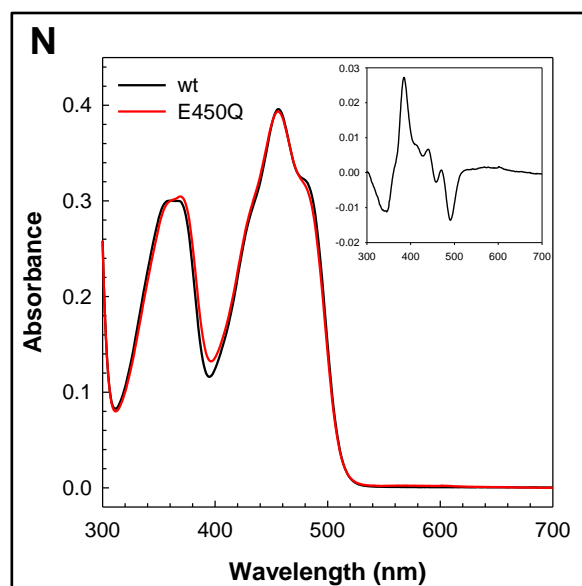
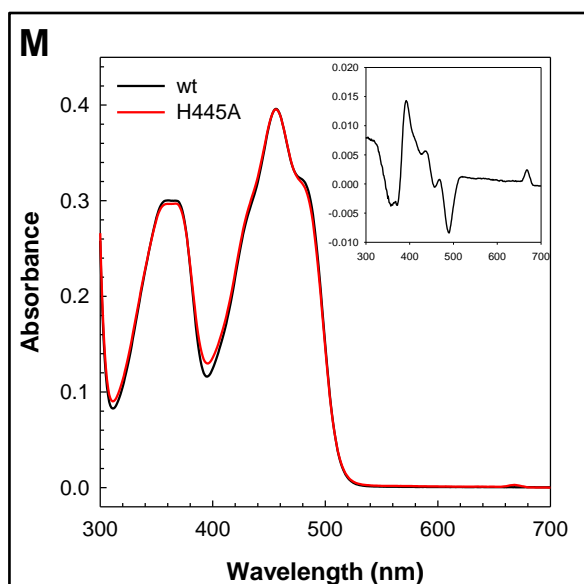
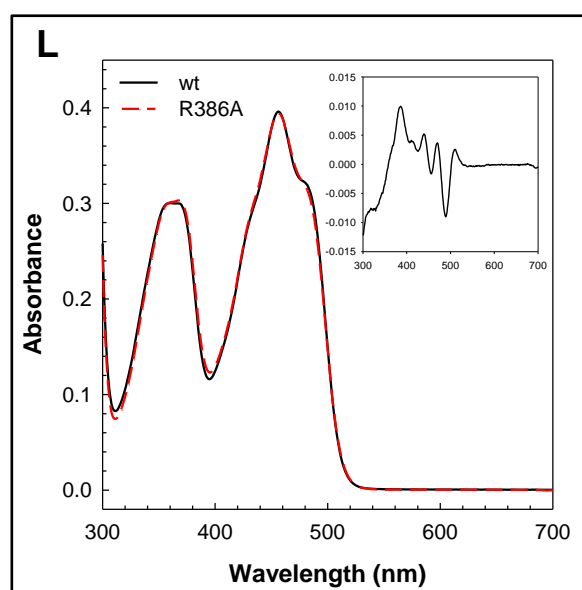
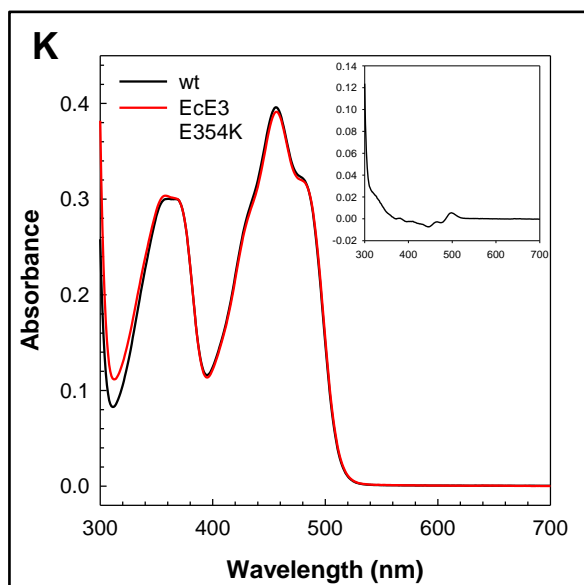
10 MGSSHHHHHH	20 SSGLVPR <u>I</u> GSH	30 MSTEIKTQVV	40 VLGAGPAGYS	50 AAFRCADLGL	60 ETVIVERYNT
70 LGGVCLNVGC	80 IPSKALLHVÄ	90 KVIEEAKALA	100 EHGIVFGEPK	110 TDIDKIRTWK	120 EKVINQLTGG
130 LAGMAKGRKV	140 KVVNGLGKFT	150 GANTLEVEGE	160 NGKTVINFDN	170 AIIAAGSRPI	180 QLPFIPHEDP
190 RIWDSTDALE	200 LKEVPERLLV	210 MGGGIIGLEM	220 GTVYHALGSQ	230 IDVVEMFDQV	240 IPAADKDIVK
250 VFTKRISKKF	260 NLMLETKVTA	270 VEAKEDGIYV	280 TMEGKKAPAE	290 PQRYDAVLVA	300 IGRVPNGKNL
310 DAGKAGVEVD	320 DRGFIRVDKQ	330 LRTNVPHIFA	340 IGDIVGQPML	350 AHKGVHEGHV	360 AAEVIAGKKH
370 YFDPKVIPSI	380 AYTEPEVAWV	390 GLTEKEAKEK	400 GISYETATFP	410 WAASGRAIAS	420 DCADGMTKLI
430 FDKESHRVIG	440 GAIVGTNGGE	450 LLGEIGLAIE	460 MGCD AEDIAL	470 TIHAHPTLHE	480 SVGLAAEVFE
490 GSITDLPNPK	AKKK	<u>I</u> = Thrombin cleavage site			

5.2 UV-VIS Ground-state Spectra

UV-Vis ground-state spectra of *EcE3* and variants thereof were recorded as described in 2.2.5.1. The insets show the differential spectra, calculated by subtraction of the wild type spectrum from the respective variant spectrum. Variants are ordered by the position of their mutation site starting from the N-terminus.

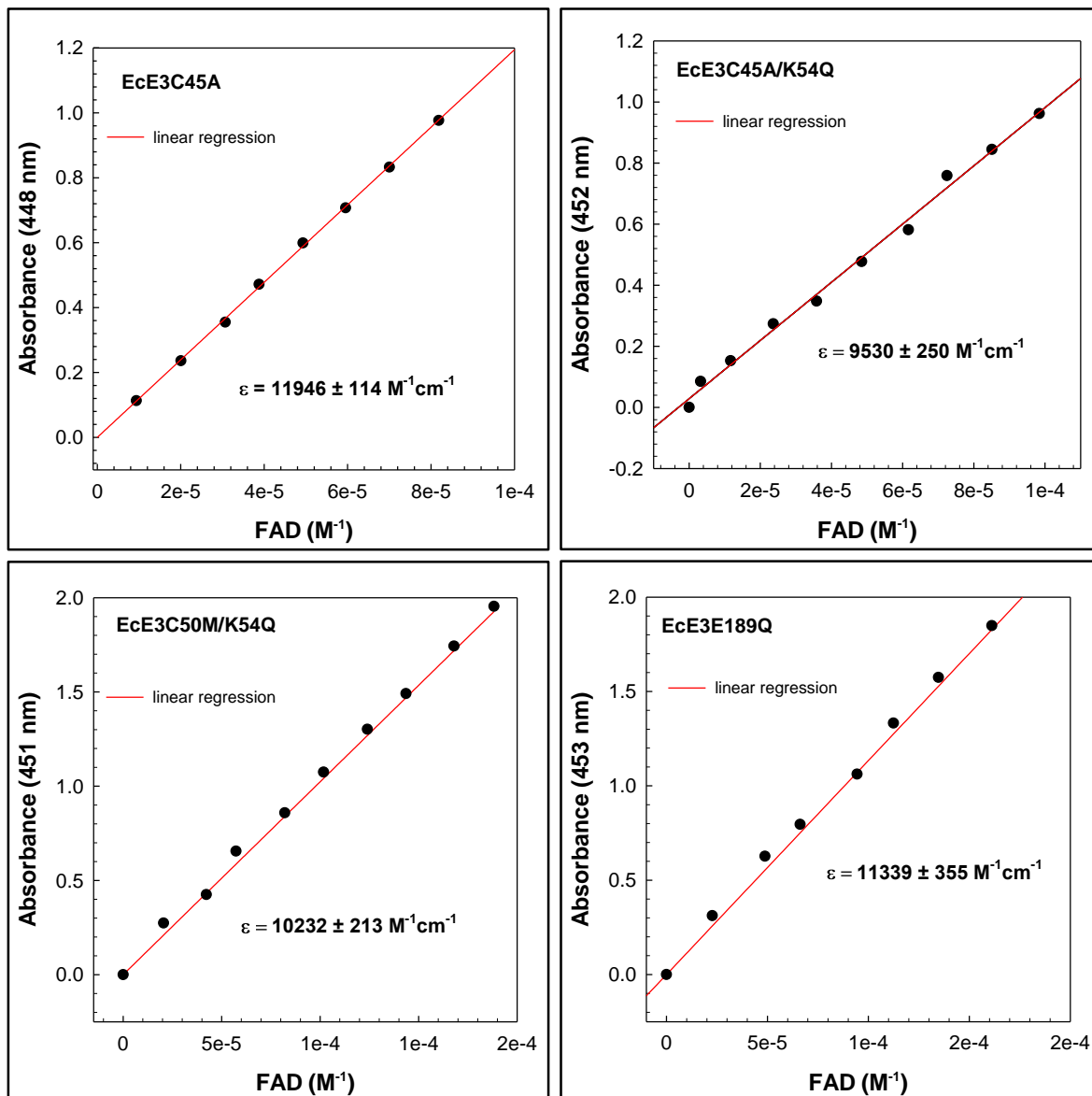






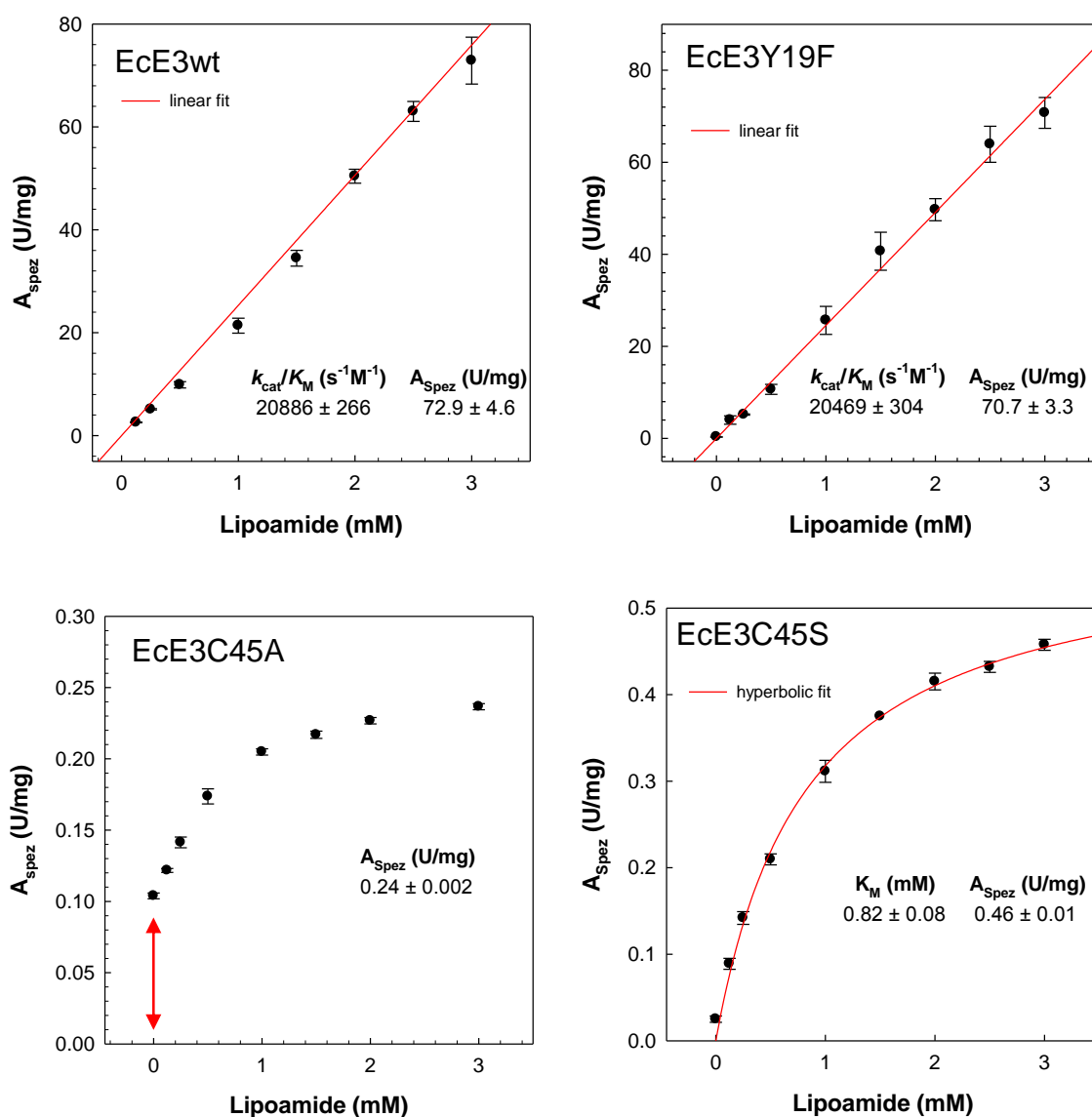
5.3 Molar Extinction Coefficients

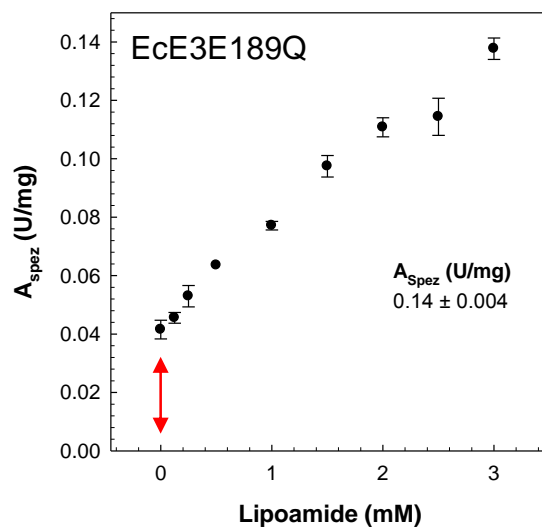
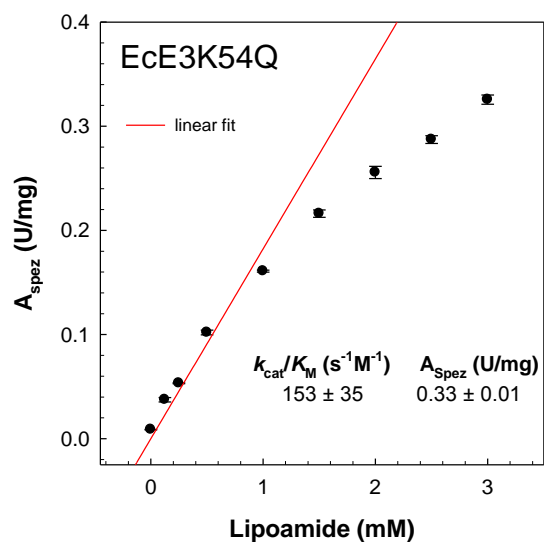
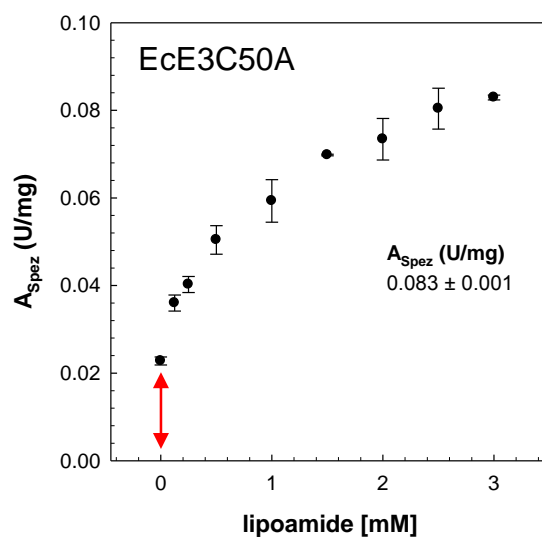
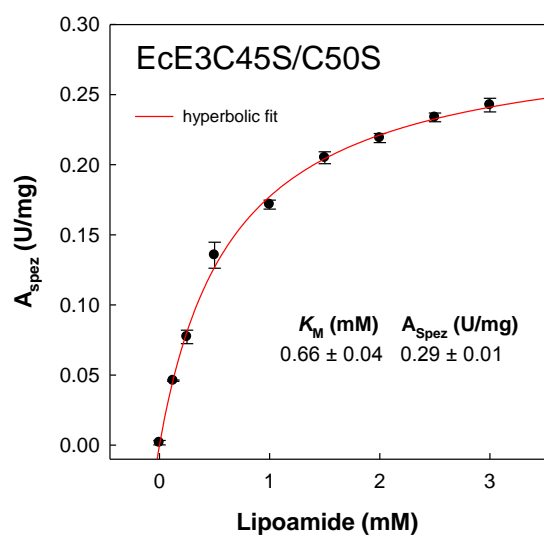
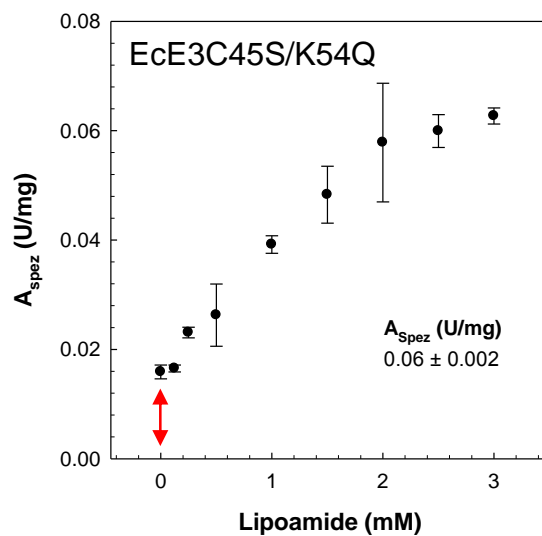
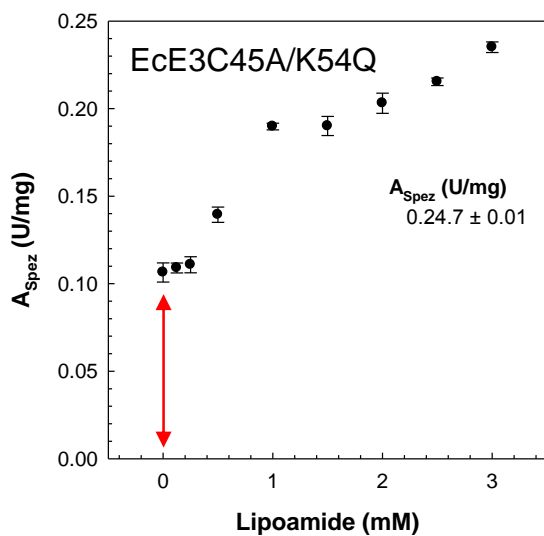
Molar extinction coefficients were determined as described in 2.2.2.8. A linear regression was used for the calculations.

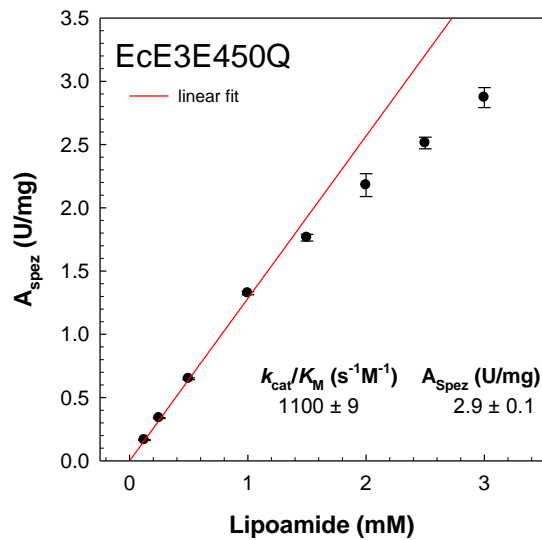
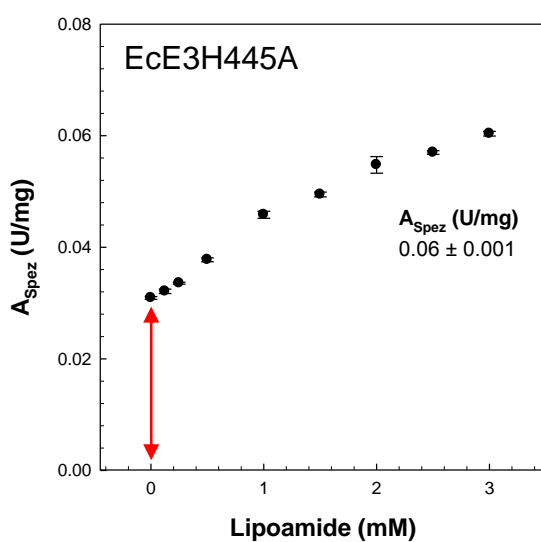
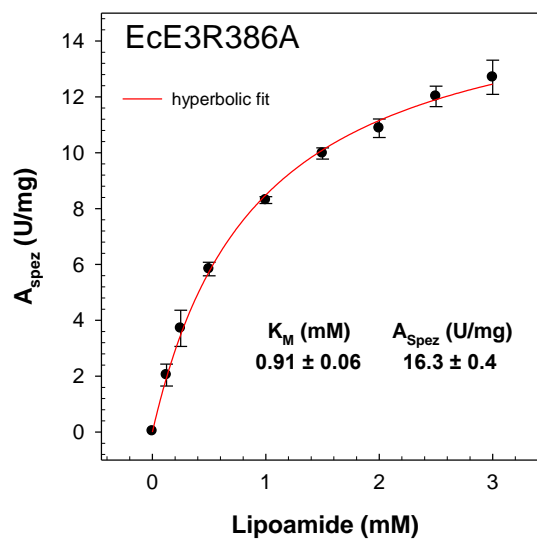
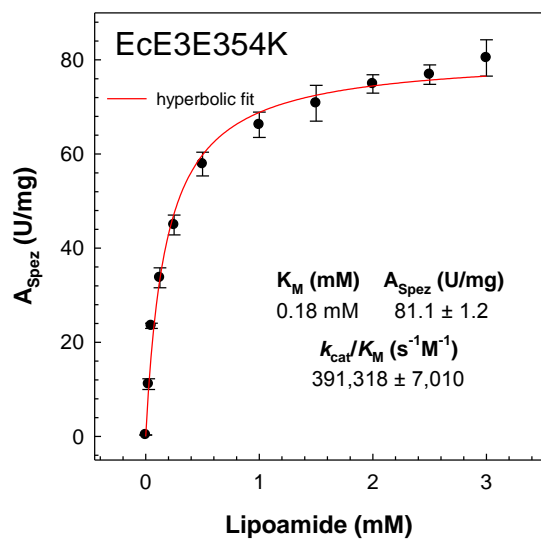


5.4 Steady-state Activity of *EcE3* and Variants thereof

Steady-state activities in dependence of the lipoamide concentration of *EcE3* and variants thereof were determined as described in 2.2.4.1. Data were fitted, if applicable, according to the Michaelis-Menten equation (red lines). Red arrows indicate NADH consumption at 0 mM lipoamide. Variants are ordered by the position of their mutation site starting from the N-terminus. The red arrows at a lipoamide concentration of 0 mM indicate putative diaphorase activity when molecular oxygen serves as electron acceptor.







5.5 Mechanistic Investigation of *EcE3*

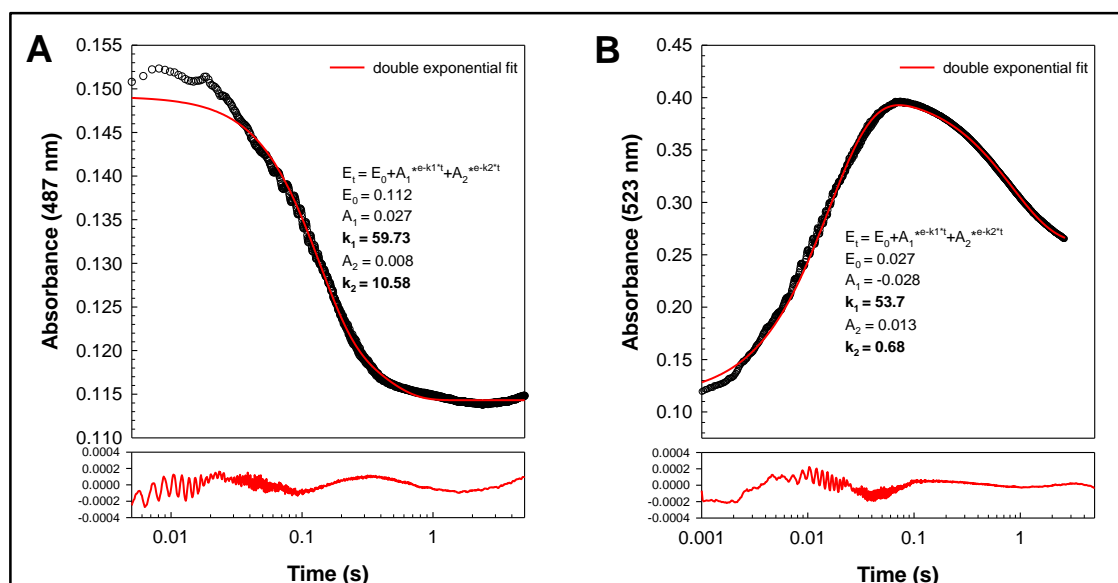


Figure 5.1 Reduction of *EcE3* with NADH under single turnover conditions.

Stopped-flow absorbance traces after mixing 20 μM *EcE3* with 20 μM NADH at 487 nm (**A**) and at 523 nm (**B**) at 4 $^\circ\text{C}$ and at pH 7.6. The points are the experimental data, and the solid lines are the fits to a double exponential equation ($A = A_1 \cdot e^{-k_1 \cdot t} + A_2 \cdot e^{-k_2 \cdot t}$), respectively. Note the logarithmic time-scales.

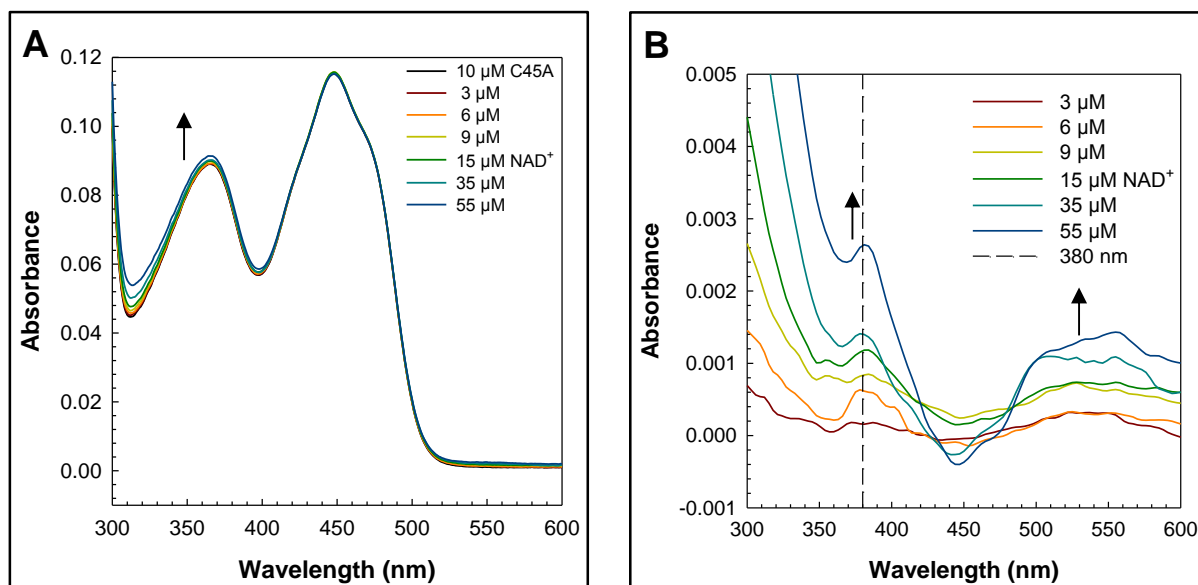


Figure 5.2 NAD⁺ titration of *EcE3EC45A*.

(A) Lower temperature NAD⁺ titration at 10 °C and in 100 mM Tris pH 8.3. Binding of NAD⁺ does not significantly alter the spectrum. (B) Difference spectra of the same titration. NAD⁺ induces a quenching of the flavin signature. Difference spectra were smoothed according to a bisquare weighting technique and a polynomial regression.

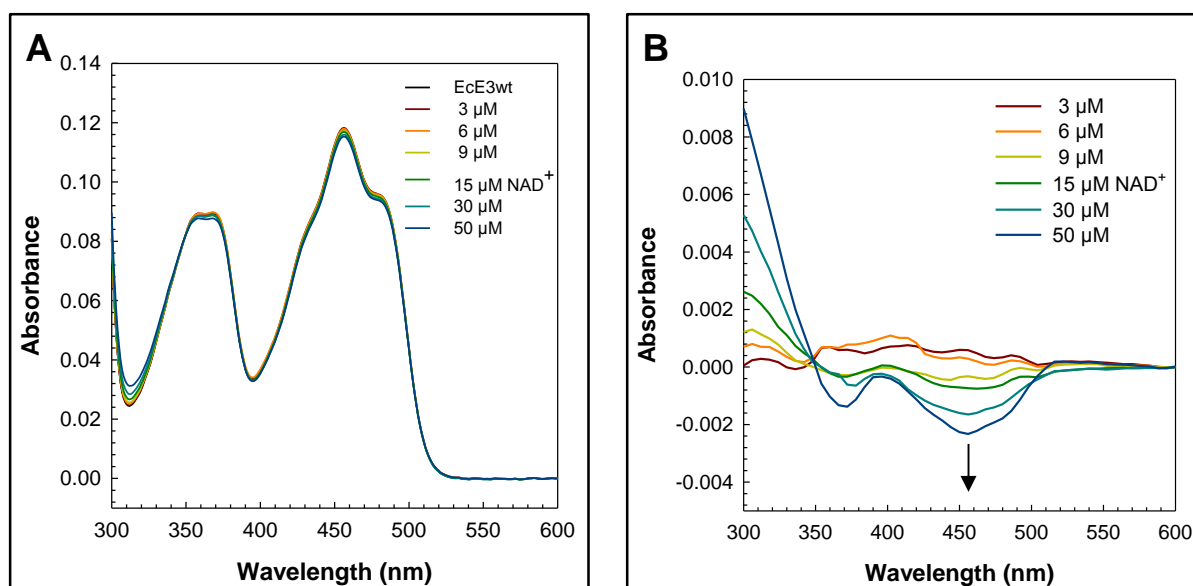


Figure 5.3 NAD⁺ titration of *EcE3wt*.

(A) Lower temperature NAD⁺ titration at 10 °C and in 100 mM MES pH 6.0. Binding of NAD⁺ does not significantly alter the spectrum. (B) Difference spectra of the same titration. NAD⁺ induces a quenching of the flavin signature. Difference spectra were smoothed according to a bisquare weighting technique and a polynomial regression.

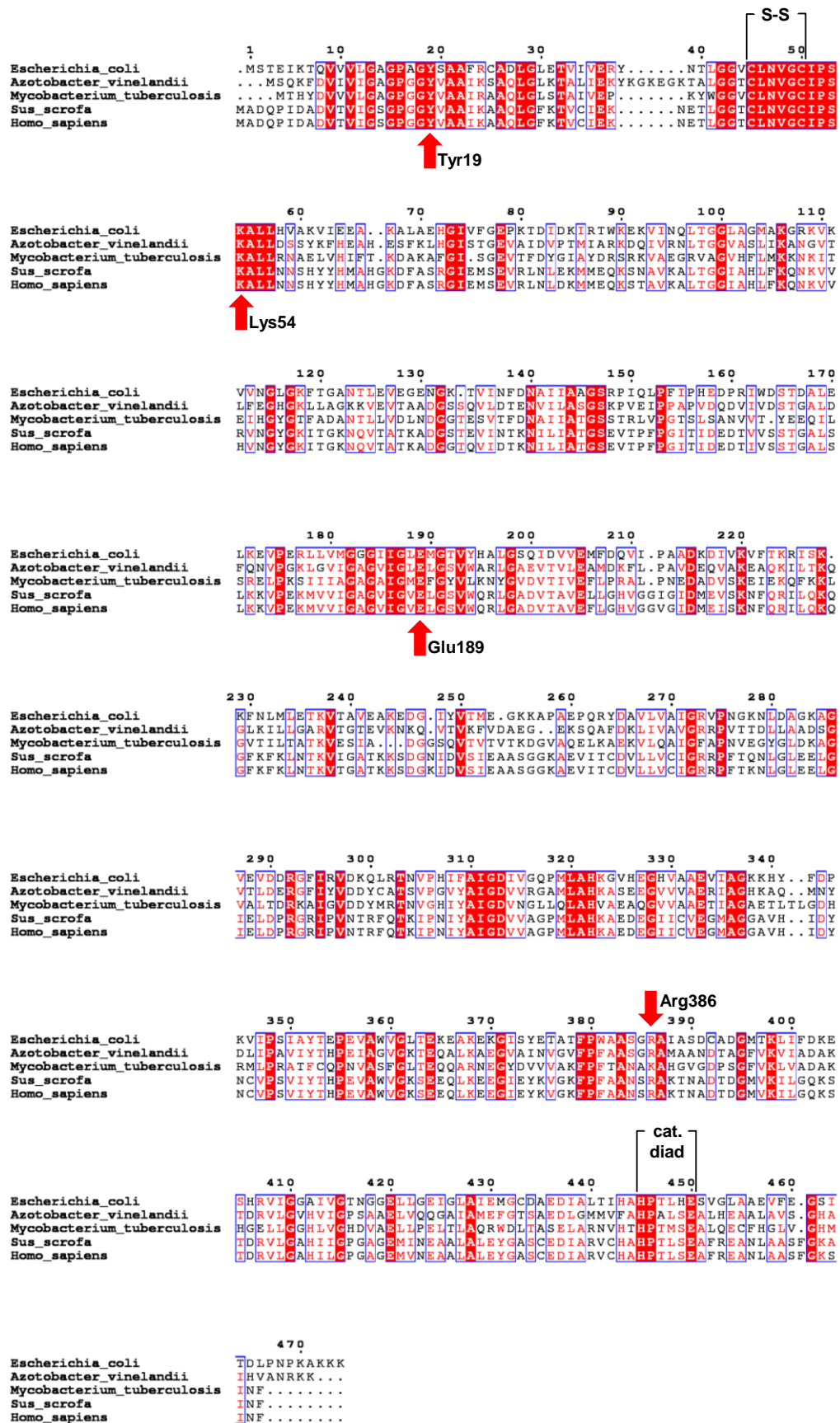


Figure 5.4 Primary amino acid sequences of E3 from different organisms. The residues studied in this thesis are highlighted. Alignment was done with ClustalOmega. The figure was compiled with ESPrpt 3.0.

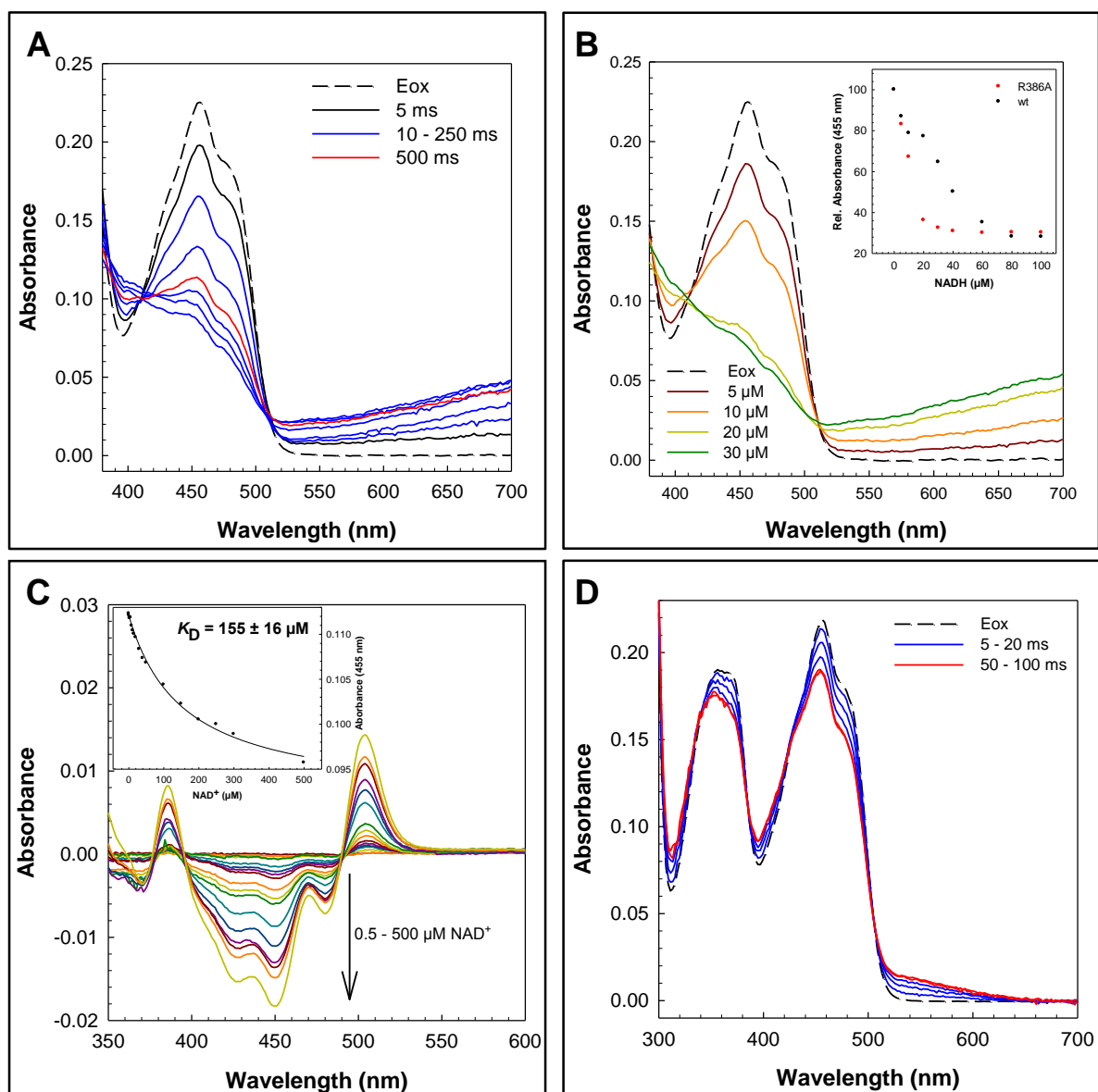


Figure 5.5 Spectral properties of *EcE3R386A*.

(A) Stopped-flow absorbance traces after mixing of 20 μM *EcE3R386A* with 100 μM NADH at 4 $^{\circ}\text{C}$ and pH 7.6. The dashed line represents the oxidized form of the respective enzyme (E_{ox}) derived from a single mixing event with buffer. The solid spectra were recorded using a diode-array detector after mixing. (B) NADH titration of 20 μM *EcE3R386A* at 4 $^{\circ}\text{C}$ and pH 7.6. Flavin reduction is almost complete at an equimolar amount of NADH. The inset shows the relative absorbances at 455 nm plotted against the respective NADH concentration. (C) Lower temperature NAD $^{+}$ titration at 10 $^{\circ}\text{C}$ and pH 7.6. The inset shows a hyperbolic fit for decrease in absorbance at 455 nm giving an apparent binding constant of ~ 155 μM for the nucleotide. (D) Stopped-flow absorbance traces of *EcE3R386A* during reduction with 20 μM *EcLip3H₂* at 4 $^{\circ}\text{C}$ and pH 7.6.

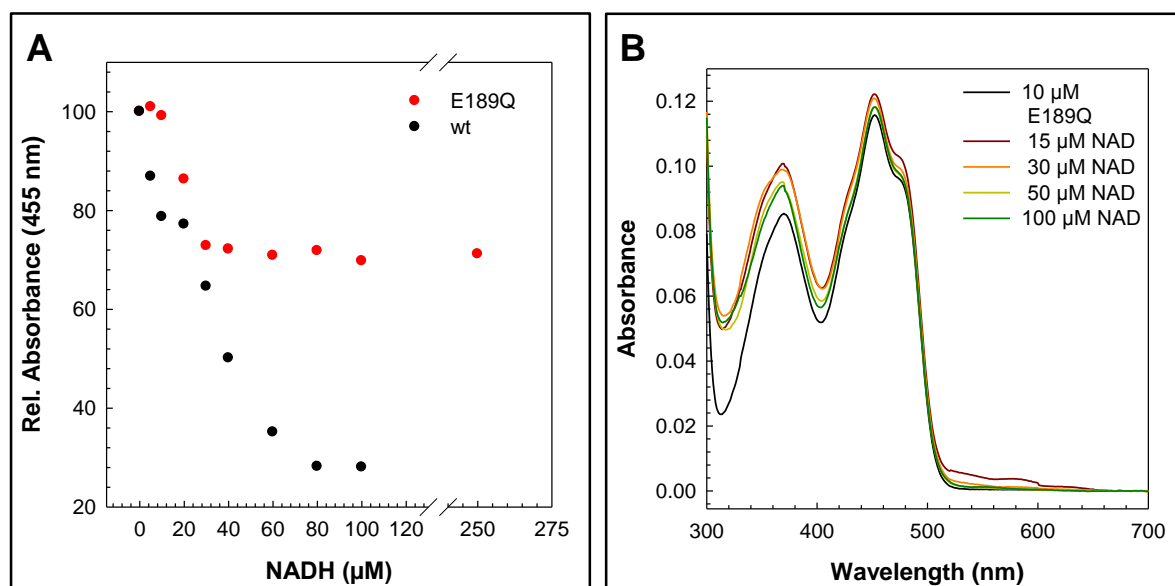
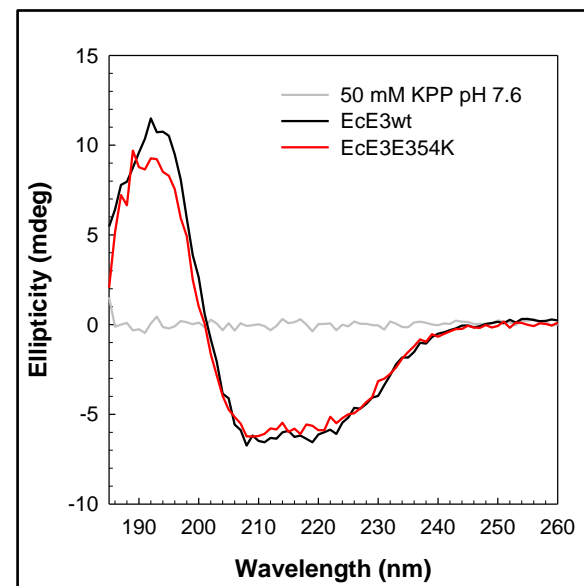
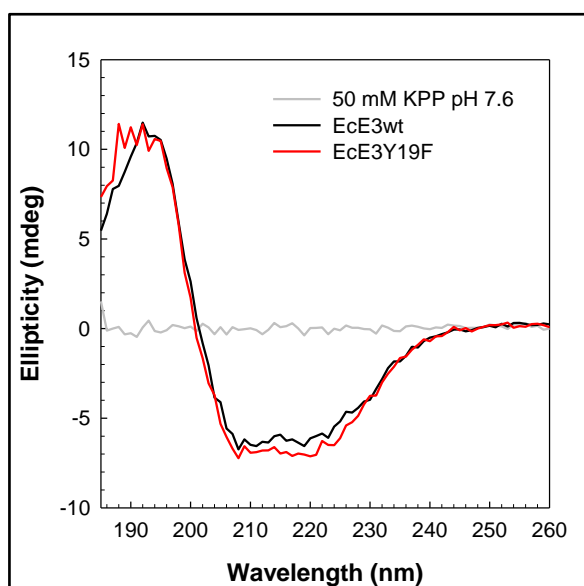
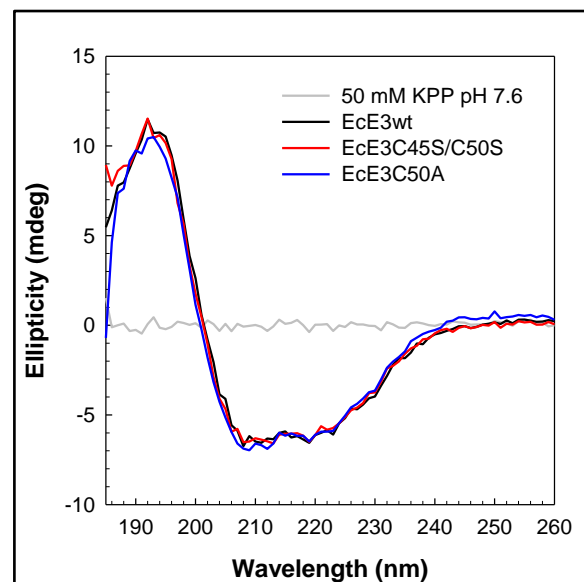
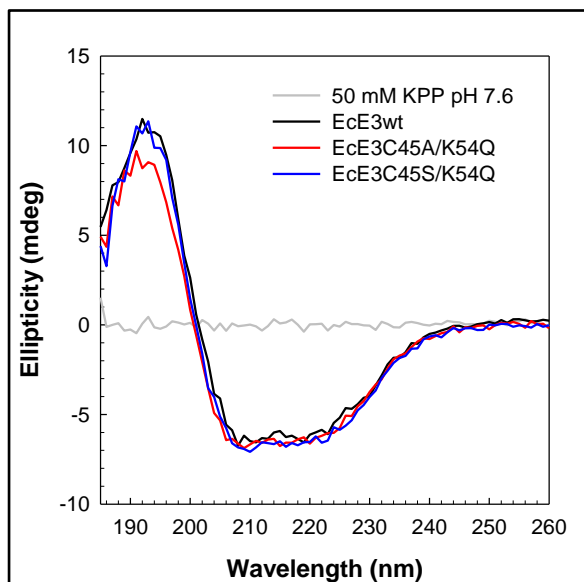


Figure 5.6 Further spectral properties of *EcE3E189Q*.

(A) Relative absorbance at 455 nm derived from a stopped-flow NADH titration of *EcE3E189Q* at 4 °C and pH 7.6. No complete reduction of the flavin can be achieved with a 12.5-fold molar excess of NADH in this variant. (B) Lower temperature NAD⁺ titration (difference spectra) at 10 °C and pH 7.6. Binding of NAD⁺ leads to an increase in absorbance at 360 nm.

5.6 Far-UV CD Spectra

Far-UV CD spectra of *EcE3* and variants thereof were recorded as described in 2.2.5.2.



5.7 Photobleaching of *EcE3*

EcE3 variants were photobleached as described in 2.2.2.10.

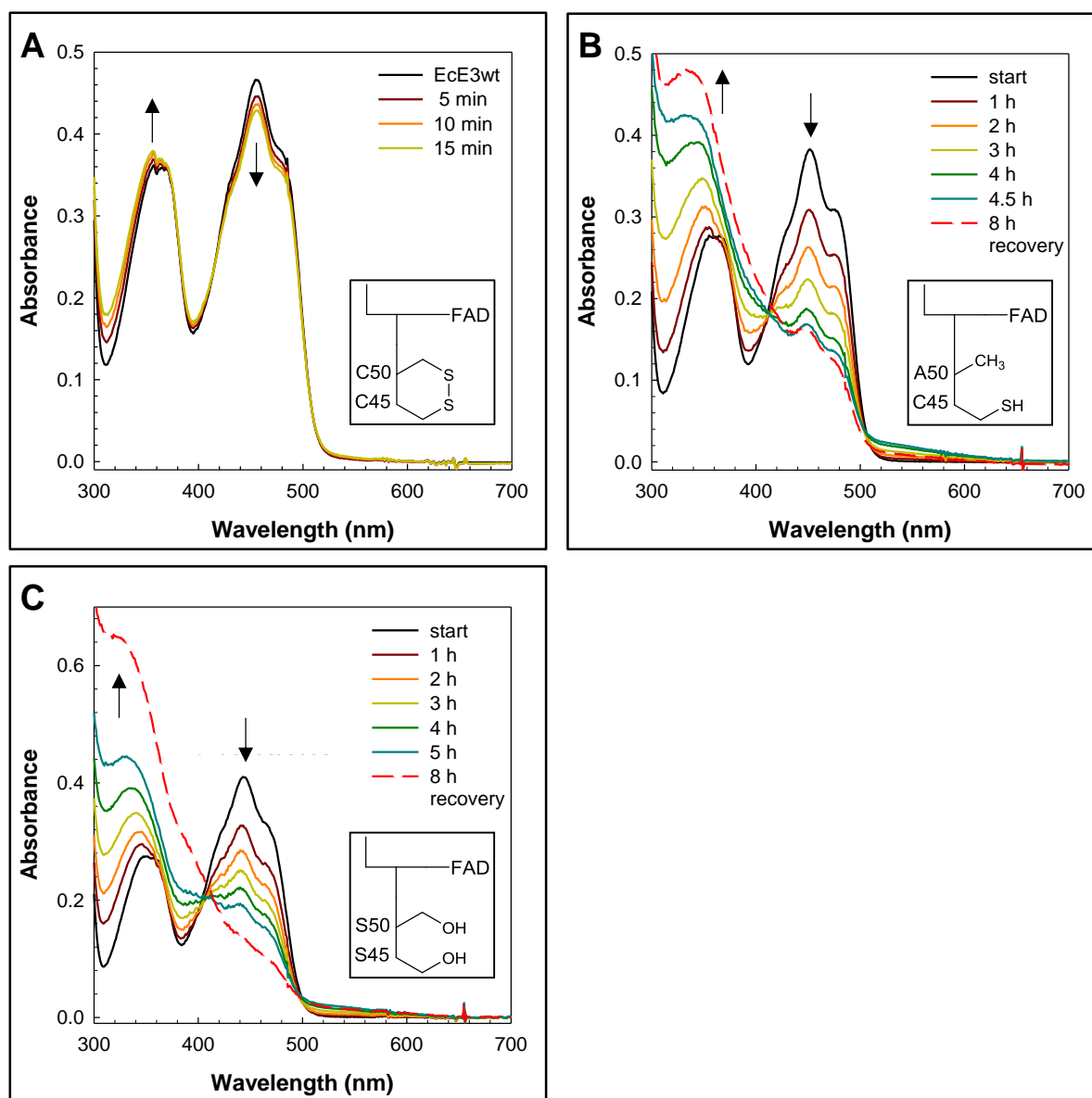
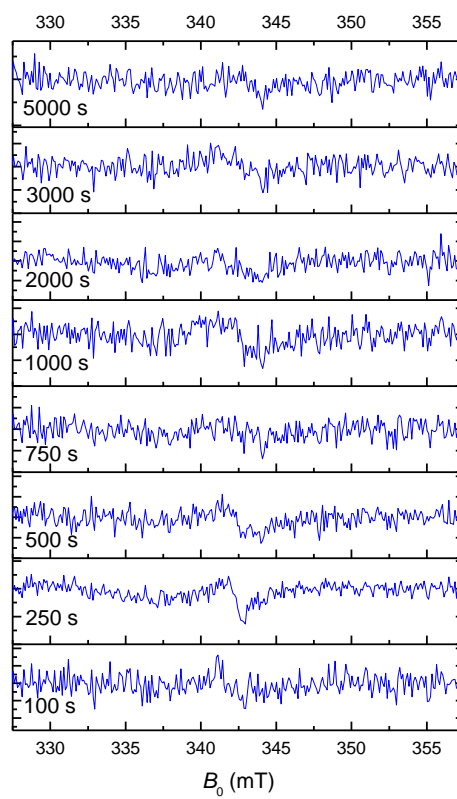


Figure 5.7 Photobleaching of wild type, monothiol or non-thiol variants of *EcE3*. Bleaching of *EcE3*wt (A), *EcE3C50A* (B) and of *EcE3C45S/C50S* (C). The insets show a highly simplified model of the respective active sites used for photobleaching control experiments.

5.8 EPR

EcE3C45A/K54Q (pseudoLOV) was subjected to EPR measurements as described in 2.2.5.4



5.9 Mass Spectrometry - Supplementary

Table 5.1 Expected fragmentation pattern of *EcLip3* after tryptic digestion

Position of cleavage site	Resulting peptide sequence	Peptide length [aa]	Peptide mass [Da]
7	APAAGVK	7	612.727
27	EVNVPDIGGDEVEVTEVMVK	20	2158.406
31	VGDK	4	417.462
45	VAAEQSLITVEGDK	14	1459.616
59	ASMEVPAPFAGVVK	14	1402.672
62	ELK	3	388.464
68	VNVGDK	6	630.699
70	VK	2	245.322
86	TGSLIMIFEVEGAAPA	16	1605.866

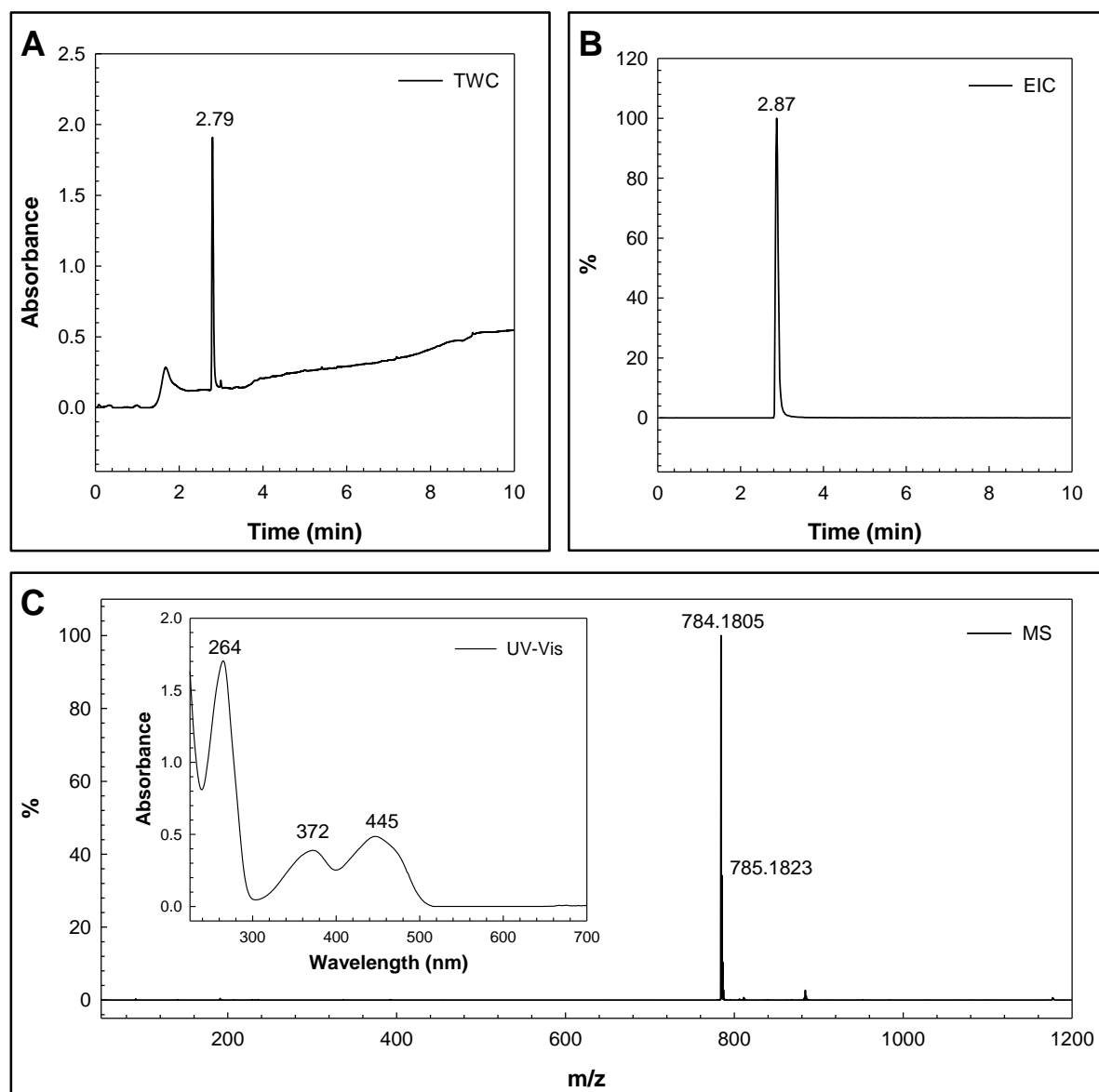


Figure 5.8 UPLC-ESI-TOF-MS analysis of FAD.

Flavin adenine dinucleotide disodium salt hydrate (10 $\mu\text{g}/\text{mL}$ in ddH_2O) was purchased from AppliChem (Darmstadt). **(A)** Total wavelength chromatogram. **(B)** Extracted ion chromatogram for m/z 784.150. **(C)** MS analysis (negative ionization mode) of B and corresponding UV-Vis spectrum of (inset).

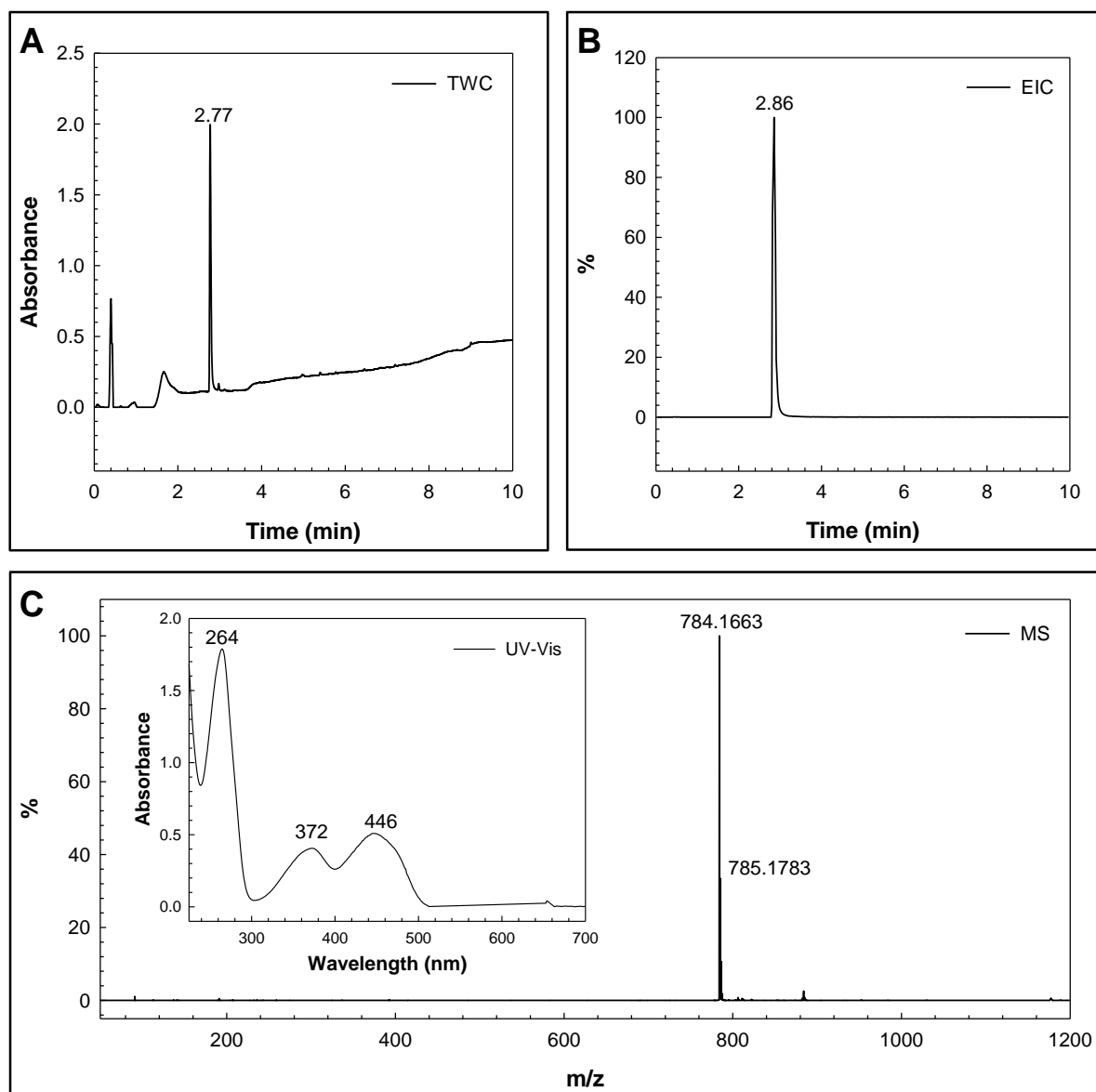


Figure 5.9 UPLC-ESI-TOF-MS analysis of FAD released of *EcE3C45A/K54Q* by heat precipitation. (A) Total wavelength chromatogram. (B) Extracted ion chromatogram for m/z 784.150. (C) MS analysis (negative ionization mode) of B and corresponding UV-Vis spectrum of (inset).

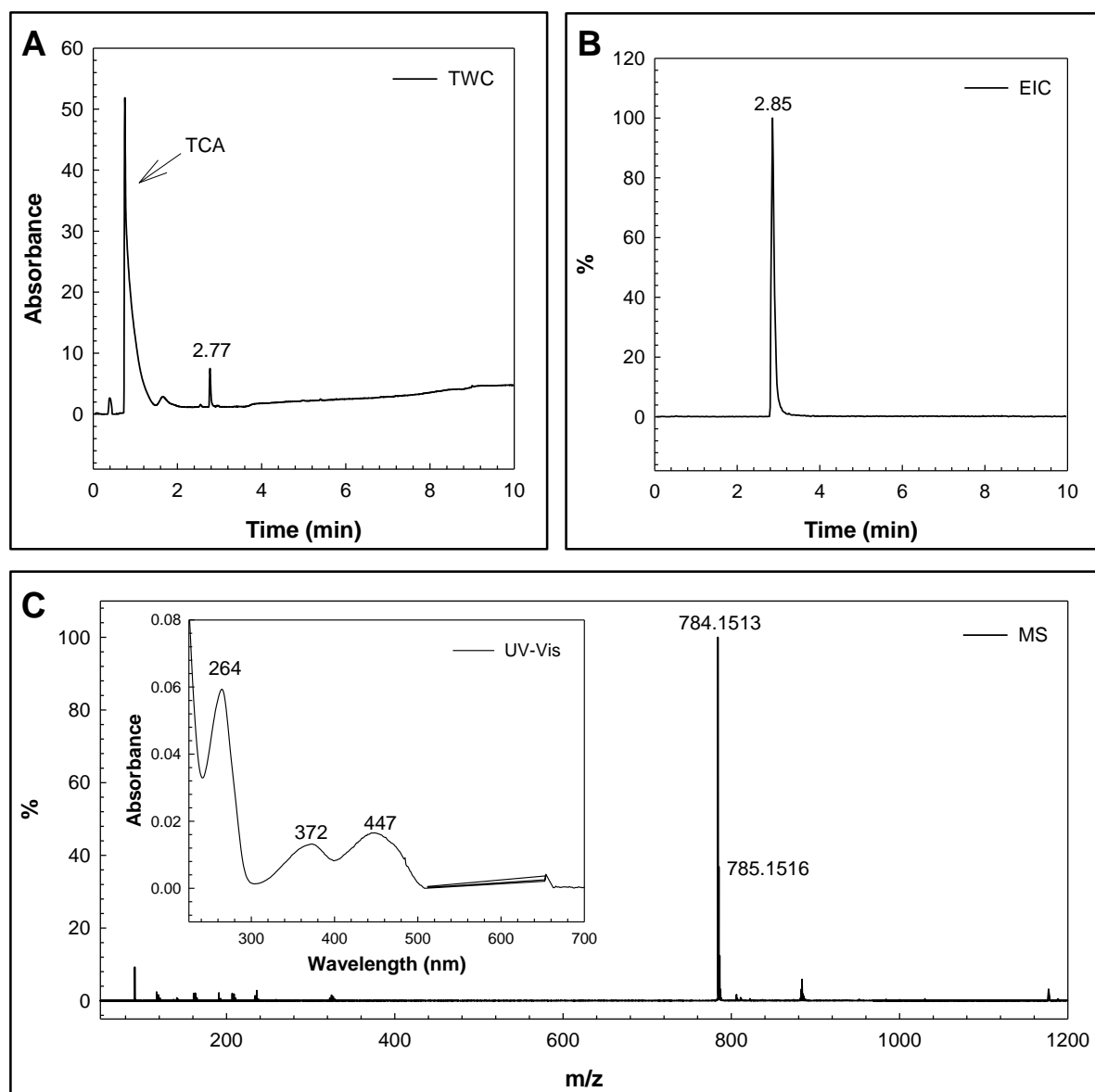


Figure 5.10 UPLC-ESI-TOF-MS analysis of FAD released of *EcE3C45A/K54Q* by TCA precipitation. (A) Total wavelength chromatogram. (B) Extracted ion chromatogram for m/z 784.150. (C) MS analysis (negative ionization mode) of B and corresponding UV-Vis spectrum of (inset).

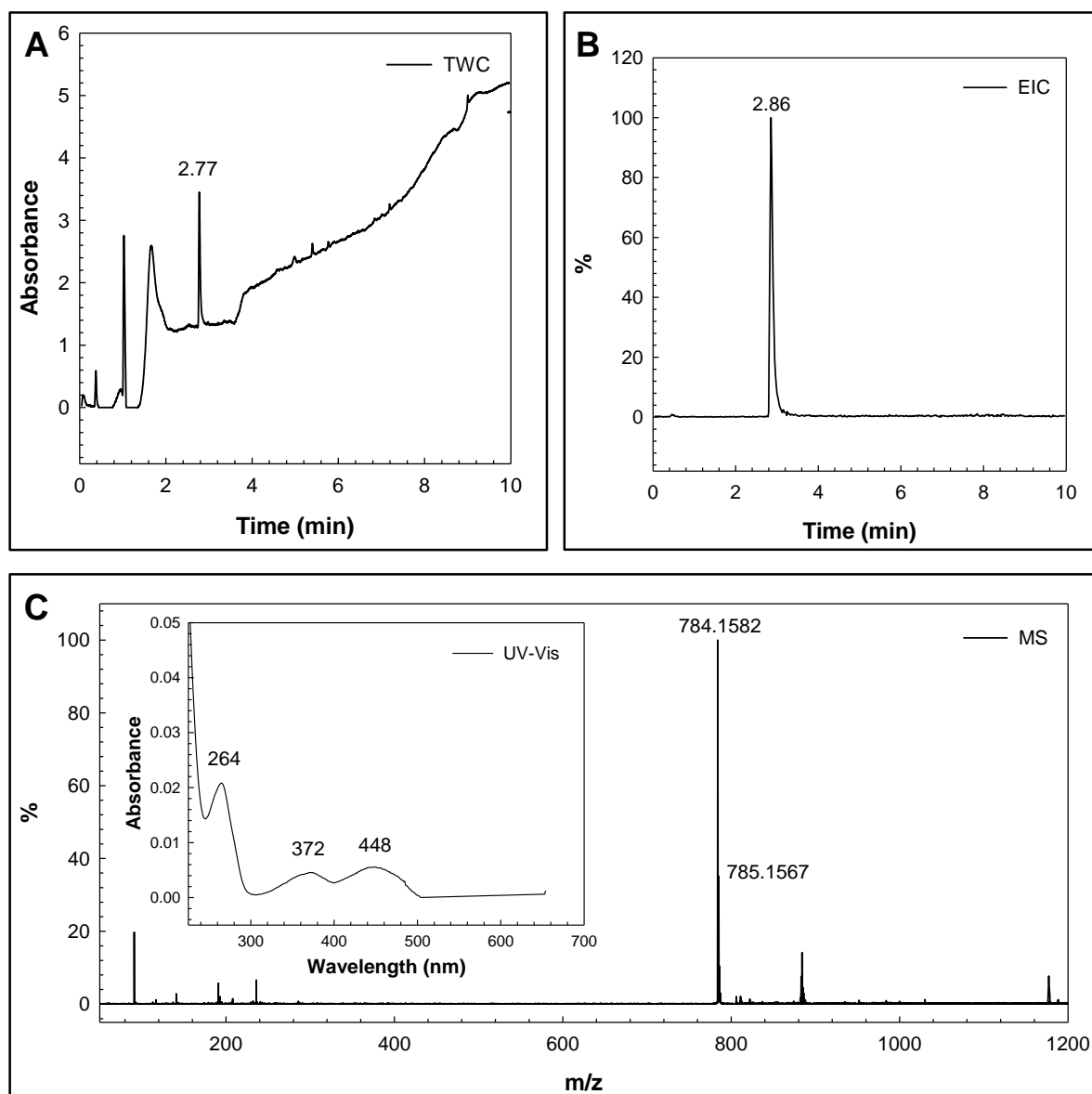


Figure 5.11 UPLC-ESI-TOF-MS analysis of FAD released of *EcE3C45A/K54Q* by acetone precipitation. **(A)** Total wavelength chromatogram. **(B)** Extracted ion chromatogram for m/z 784.150. **(C)** MS analysis (negative ionization mode) of B and corresponding UV-Vis spectrum of (inset).

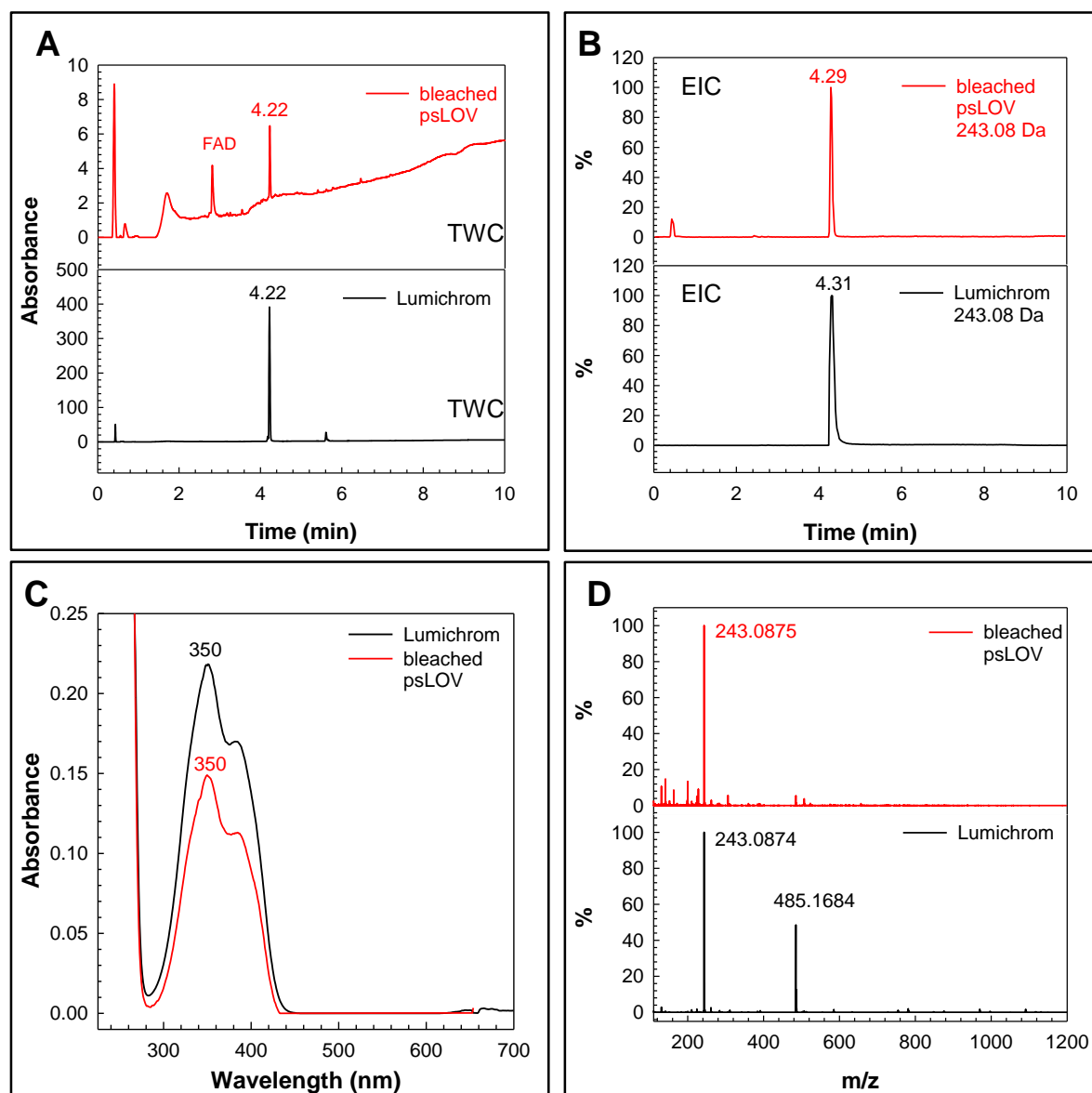


Figure 5.12 UPLC-ESI-TOF-MS comparison of lumichrom.

Released lumichrom from photobleached *EcE3C45A/K54Q* by heat precipitation (red) and lumichrom (100 $\mu\text{g}/\text{mL}$ in MeOH) purchased from Sigma (Deisenhofen) (black).

(A) Total wavelength chromatograms. (B) Extracted ion chromatograms for m/z 243.087. (C) UV-Vis spectra extracted from (A). (D) MS analysis (positive ionization mode) of B.

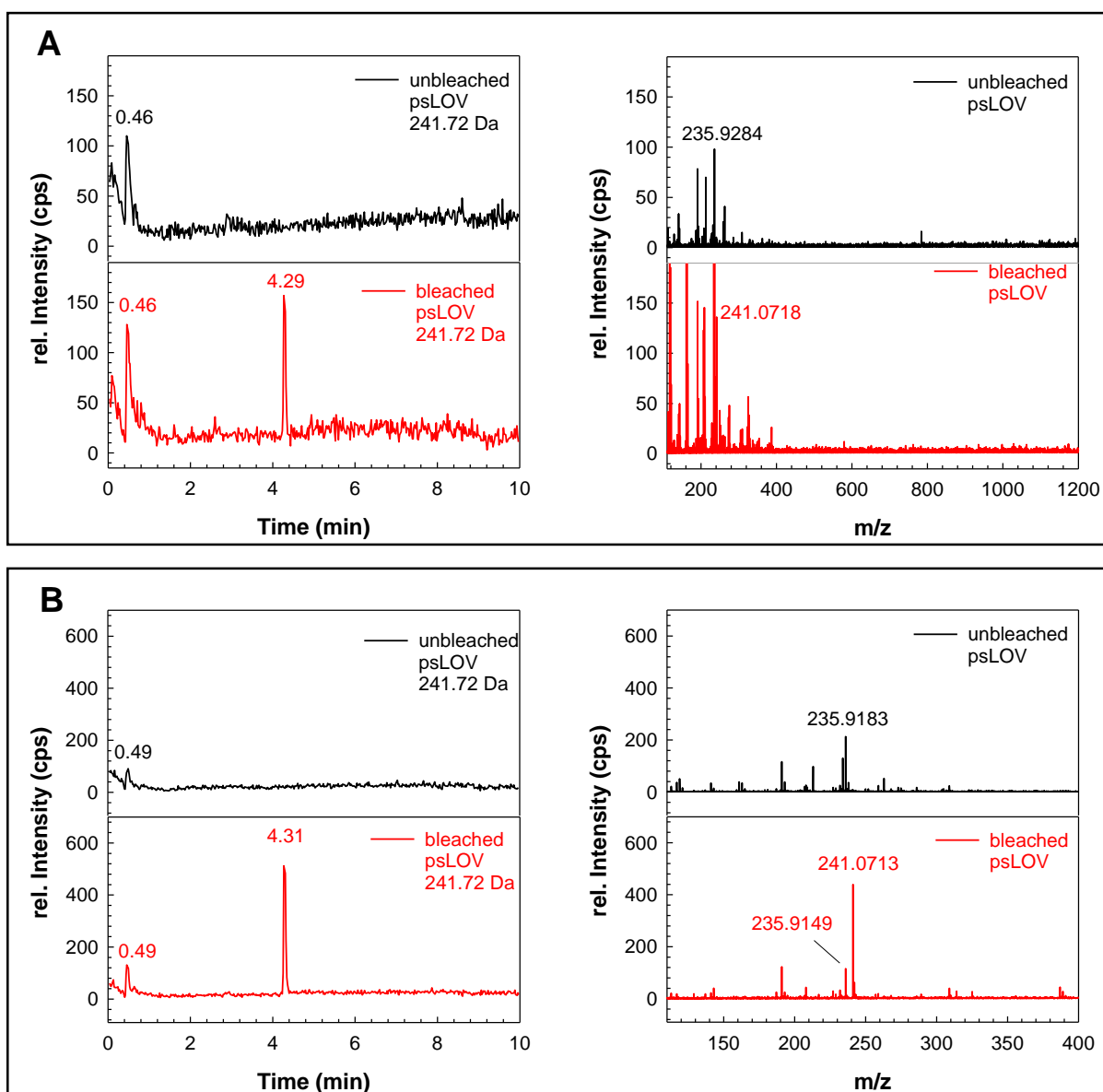


Figure 5.13 Evidence for lumichrom formation in *EcE3C45A/K54Q* by UPLC-ESI-TOF-MS. Comparison of unbleached (black) and photobleached *EcE3C45A/K54Q* (red). (A) Extracted ion chromatograms (left) and corresponding MS analyses in negative ionization mode (right) of heat extracted samples (A) and of TCA extracted samples (B).

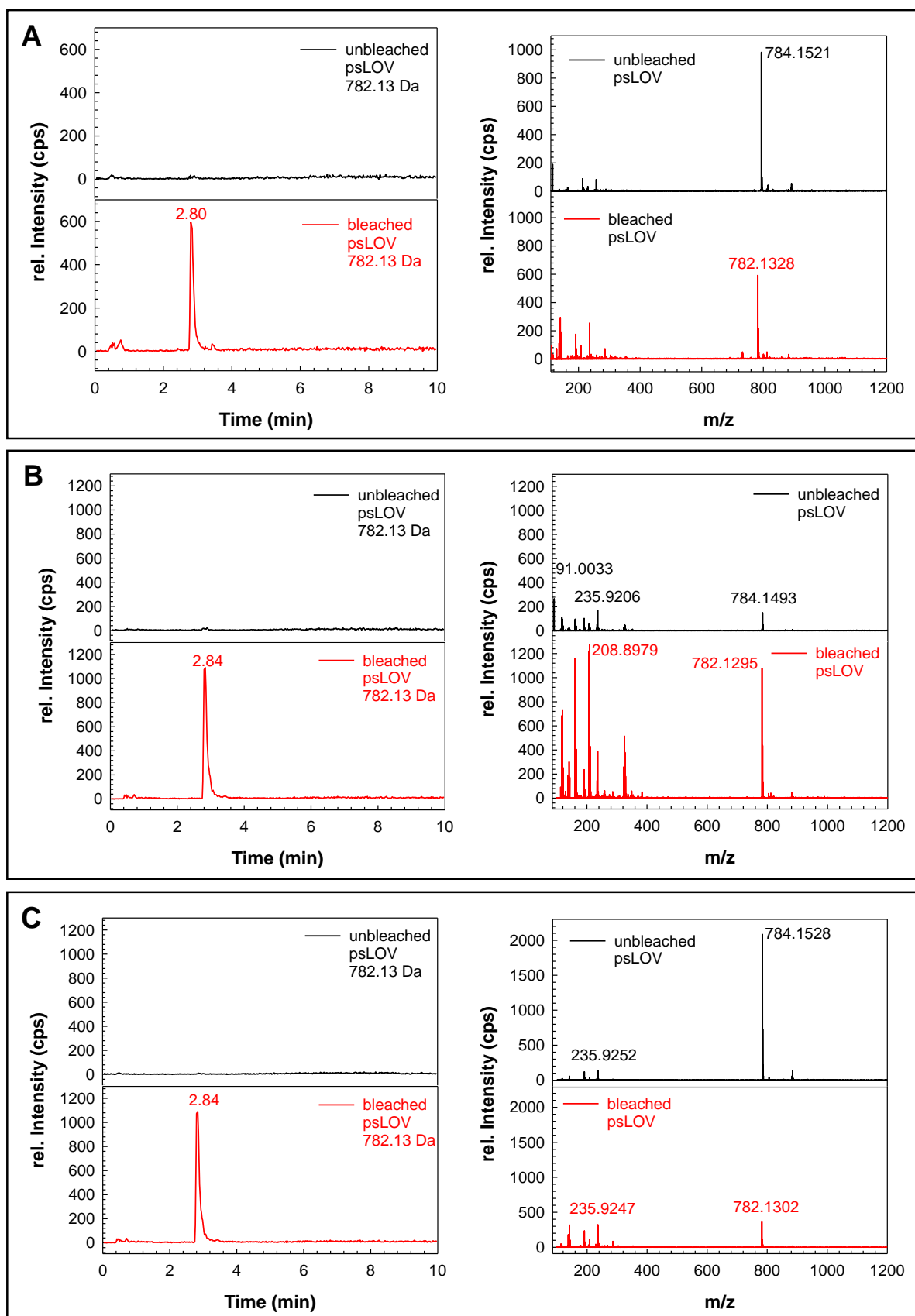


Figure 5.14 Evidence for FAD-2H formation in *EcE3C45A/K54Q* by UPLC-ESI-TOF-MS. Comparison of unbleached (black) and photobleached *EcE3C45A/K54Q* (red). Extracted ion chromatograms (left) and corresponding MS analyses in negative ionization mode (right) of heat extracted samples (A), of TCA extracted samples (B) and of acetone extracted samples (C).

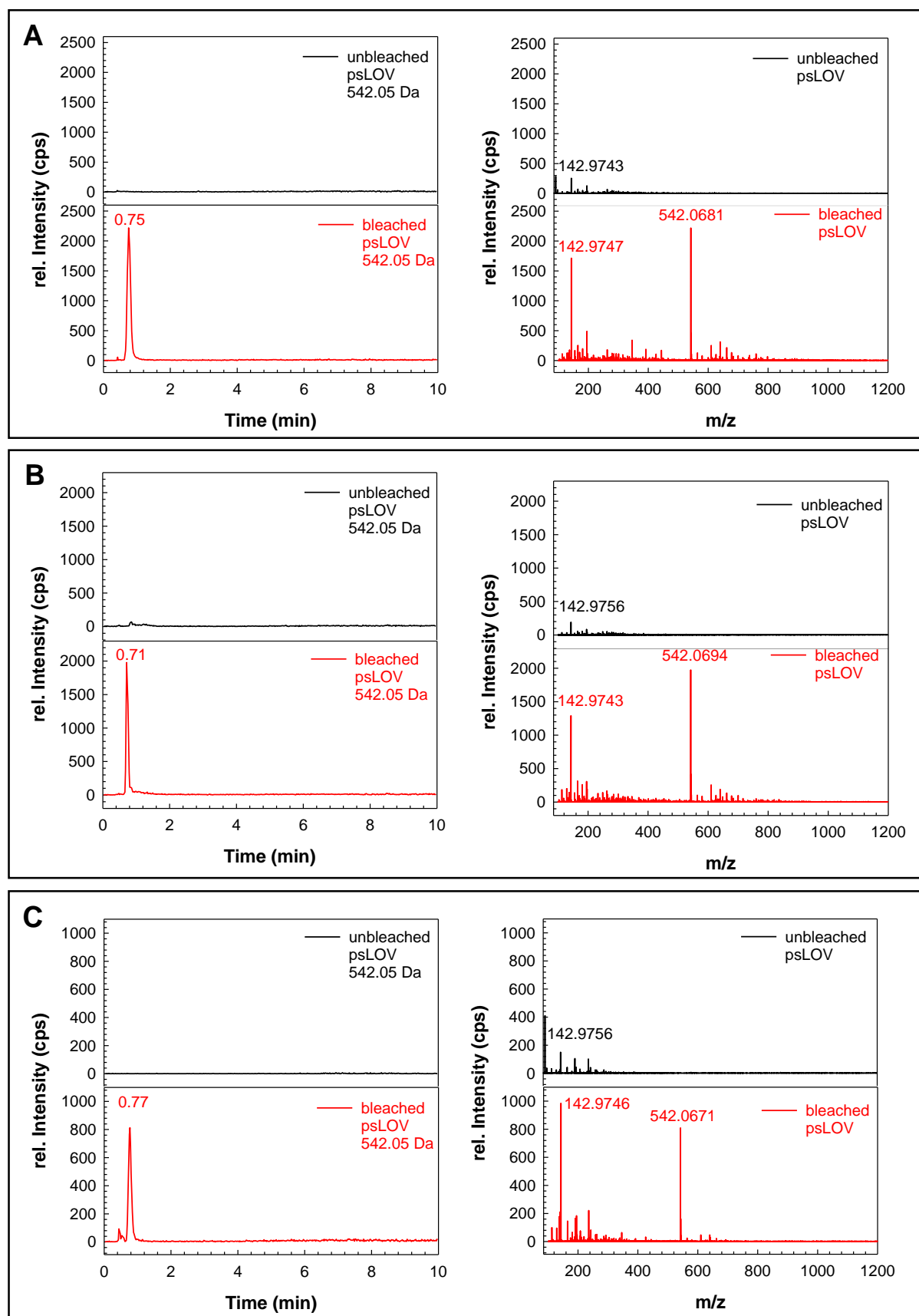


Figure 5.15 Ribityl-ADP-2H formation in *EcE3C45A/K54Q* by UPLC-ESI-TOF-MS. Comparison of unbleached (black) and photobleached *EcE3C45A/K54Q* (red). Extracted ion chromatograms (left) and corresponding MS analyses in negative ionization mode (right) of heat extracted samples (**A**), of TCA extracted samples (**B**) and of acetone extracted samples (**C**).

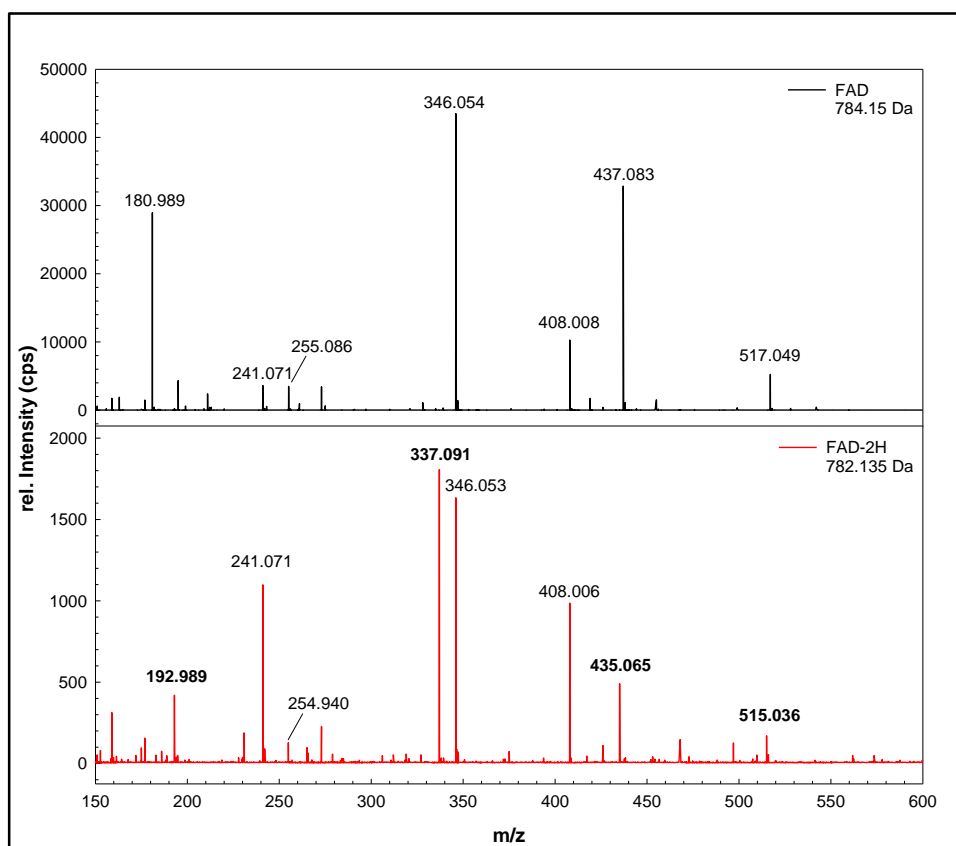


Figure 5.16 UHPLC-ESI-QTOF-MS/MS analysis of FAD and FAD-2H. Extracted from photobleached *EcE3C45A/K54Q*. MS/MS fragmentation pattern at 20 eV collision energy at m/z 784.150 (black) and 782.135 (red), respectively. Deviating values are shown in bold face type.

5.10 Redox Potentials of selected *EcE3* Variants

Determination of the flavin redox potentials was performed as described in 2.2.2.9

Table 5.2 Redox potentials of relevant enzymes

Enzyme	Redox potential (mV)	Reference
<i>EcE3</i> wt	-314	(Maeda-Yorita et al. 1994)
E3C45A/K54Q	-268	This work
E3C50A	-345	This work
E3C45S/C50S	-401	This Work
LovK	-258	(Purcell et al. 2010)

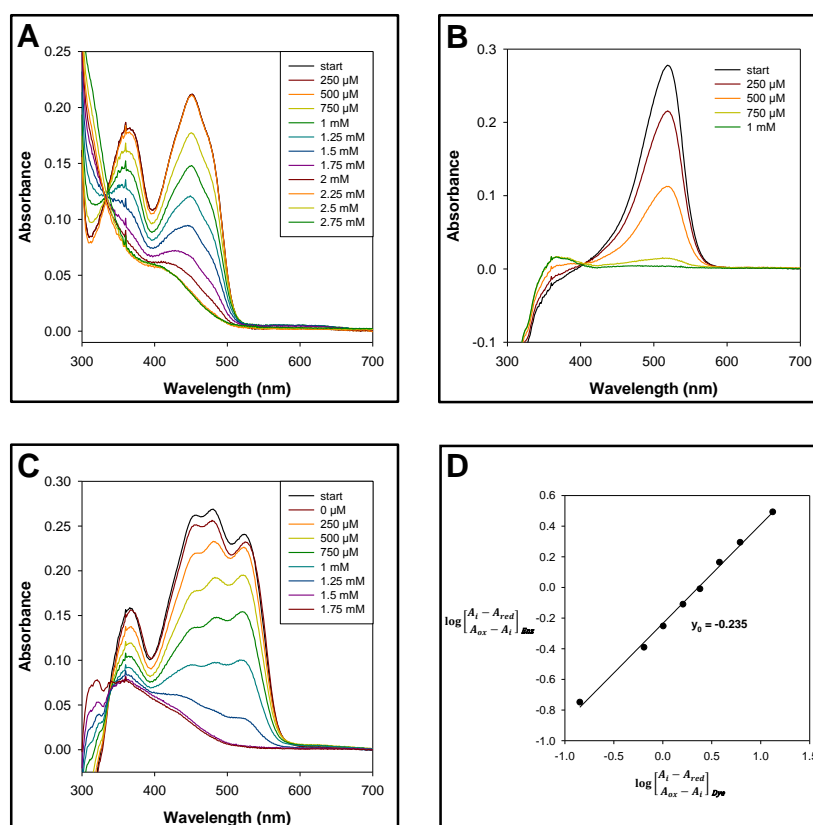


Figure 5.17 Determination of the redox potential of *EcE3C45A/K54Q*. Reduction of the enzyme (A) and of phenosafranin (B) under anaerobic conditions with dithionite. (C) Reduction of enzyme and dye under the same conditions. (D) Nernst analysis of the absorbance changes of the enzyme and dye according to 2.2.2.9.

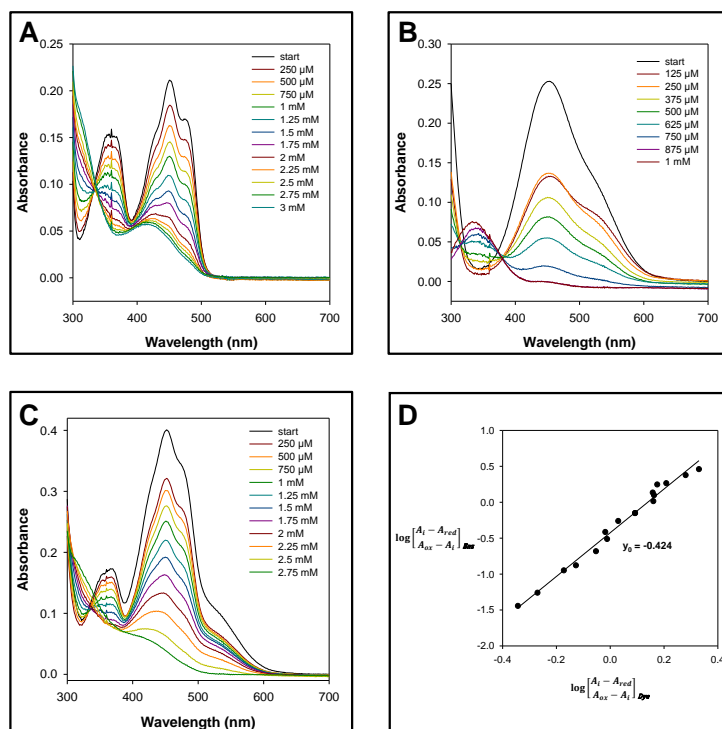


Figure 5.18 Determination of the redox potential of *EcE3C50A*. Reduction of the enzyme (**A**) and of neutral red (**B**) under anaerobic conditions with dithionite. (**C**) Reduction of enzyme and dye under the same conditions. (**D**) Nernst analysis of the absorbance changes of the enzyme and dye according to 2.2.2.9.

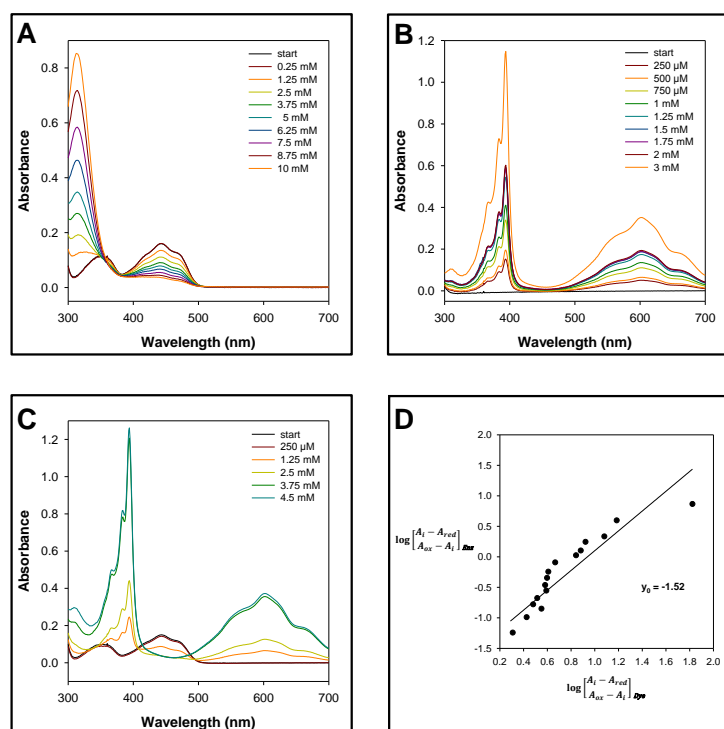


Figure 5.19 Determination of the redox potential of *EcE3C45S/C50S*. Reduction of the enzyme (**A**) and of methyl viologen (**B**) under anaerobic conditions with dithionite. (**C**) Reduction of enzyme and dye under the same conditions. (**D**) Nernst analysis of the absorbance changes of the enzyme and dye according to 2.2.2.9.

5.11 Isothermal Titration Calorimetry

ITC experiments were performed according to 2.2.5.3.

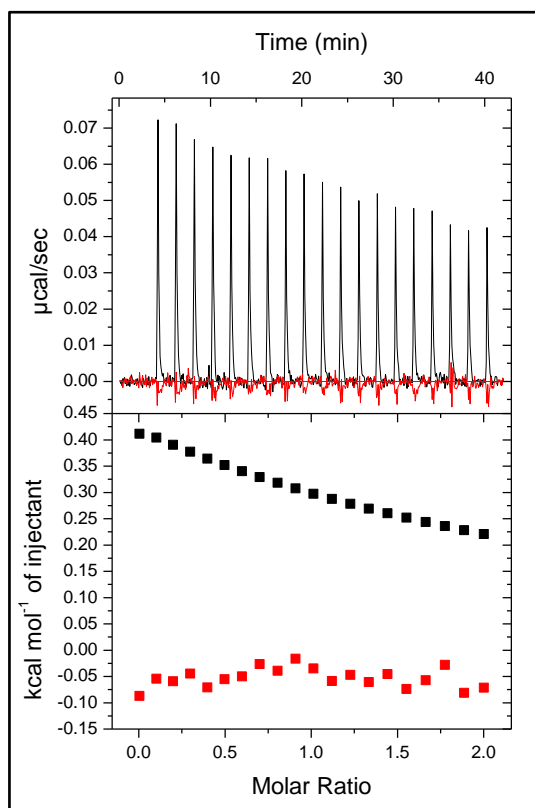


Figure 5.20 Titration of EcLip3 to EcE3.

Both enzymes were desalted into the same buffer (50 mM KPP pH 7.6, 100 mM NaCl). The ITC cell was filled with 100 μM (active sites) EcE3. The injection syringe was filled with 1 mM of EcLip3. Measurements were performed at 20 $^{\circ}\text{C}$ with a stirring speed of 500 min^{-1} . A titration of 1 mM EcLip3 into buffer served as a control to check for heat effects due to dilution (red).

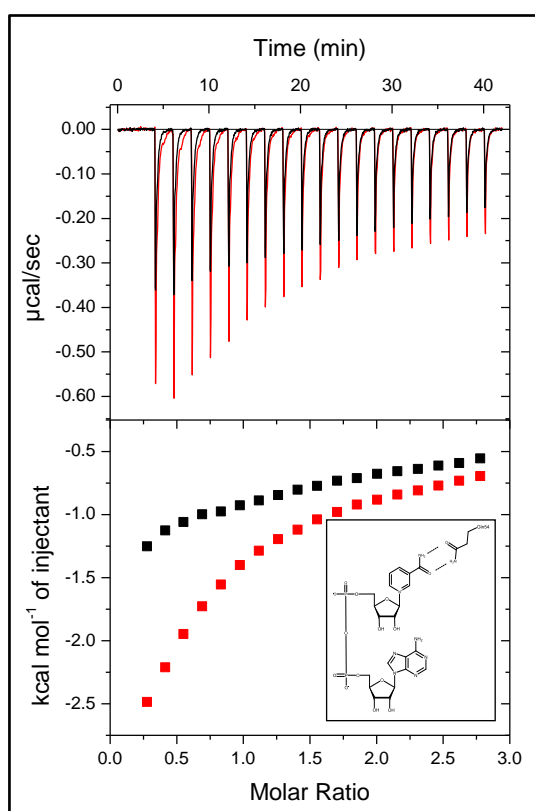


Figure 5.21 ITC titration of EcE3 variants with NAD⁺

Titration of NAD⁺ to EcE3wt (black) and EcE3K54Q (red).

NAD⁺ was dissolved in 50 mM KPP pH 7.6, 100 mM NaCl. The ITC cell was filled with 144 μM (active sites) enzyme, respectively. The injection syringe was filled with 2 mM of NAD⁺ solution. Measurements were performed at 20 $^{\circ}\text{C}$ with a stirring speed of 500 min^{-1} .

The inset shows a putative interaction between Gln54 and the nicotine amide part of NAD⁺.

5.12 Crystallographic Tables

Table 5.3 Crystallographic data and refinement statistics.
The highest resolution shell is shown in parenthesis.

	<i>EcE3</i> ground state	<i>EcE3</i> + NAD ⁺	<i>EcE3C45S</i>
Data collection	BESSYII	PETRAIII	PETRAIII
Wavelength (Å)	0.91841	0.82480	0.92012
Space Group	P2 ₁ 2 ₁ 2 ₁	P2 ₁ 2 ₁ 2 ₁	I422
Cell dimensions			
a (Å)	111.68	112.59	179.90
b (Å)	129.32	129.58	179.90
c (Å)	258.34	257.46	197.17
α (°)	90.0	90.0	90.0
β (°)	90.0	90.0	90.0
γ (°)	90.0	90.0	90.0
Resolution range (Å)	50.00-2.17 (2.27-2.17)	50.00-2.69 (2.81-2.69)	50.00-2.57 (2.67-2.57)
No. of reflections	743377	403884	1338625
No. of unique reflections	198344	103624	51245
Completeness (%)	99.8 (99.9)	98.5 (98.9)	99.7 (98.8)
I/σ(I)	19.3 (2.7)	16.6 (2.6)	34.2 (6.7)
R _{merge} (%)	5.5 (61.8)	6.4 (69.2)	8.9 (62.7)
CC _{1/2}	99.9 (73.3)	99.8 (70.3)	100.0 (96.8)
Redundancy	3.74 (3.78)	3.89 (3.76)	26.04 (25.37)
B-factor from Wilson Plot (Å ²)	44.36	62.28	46.02

	<i>EcE3</i> ground state	<i>EcE3</i> + NAD ⁺	<i>EcE3C45S</i>
Refinement	<i>PHENIX</i>	<i>PHENIX</i>	<i>PHENIX</i>
Resolution Range (Å)	42.51-2.17	47.92-2.69	45.96-2.57
Monomers per AU	6	6	2
Reflections	198214	103540	51228
R _{work} / R _{free} (%)	17.7 / 20.8	17.6 / 22.1	23.3 / 27.4
Number of atoms			
protein	21417	21303	7103
ligands	569	466	192
water	1752	24	78
B-factor protein	38.89	66.29	97.81
B-factor ligands	41.65	66.42	105.32
B-factor water	40.42	54.13	74.32
Deviations from ideals (r.m.s.d)			
Bond distances (Å)	0.006	0.010	0.012
Bond angles (°)	1.083	1.271	1.331
Dihedrals (°)	13.902	15.926	17.072
Ramachandran plot			
favoured regions (%)	96.73	98.12	88.47
allowed regions (%)	3.24	1.88	8.51
outlier regions (%)	0.04	0.00	3.02

5.13 X-ray Figures

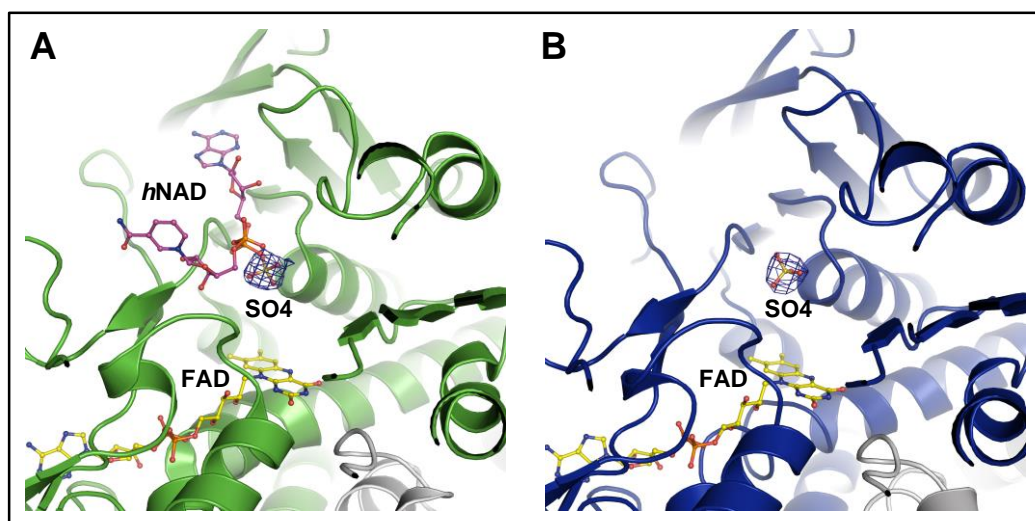


Figure 5.22 The placeholder ability of sulfate ions serving as precipitant. Top views on the *re* face of the flavin showing the nucleotide binding site. **(A)** Cartoon representation of *EcE3* in ground state showing the presence of a sulfate ion at the NAD-binding site. A superposition with the human E3 structure in complex with NAD⁺ (PDB: 1ZMC) confirms the placeholder abilities of the precipitant. For convenience only the nucleotide is presented. **(B)** Repeating motive of the precipitant in the adduct structure. 2mFo-DFc maps are countered at 2 σ (blue mesh), respectively.

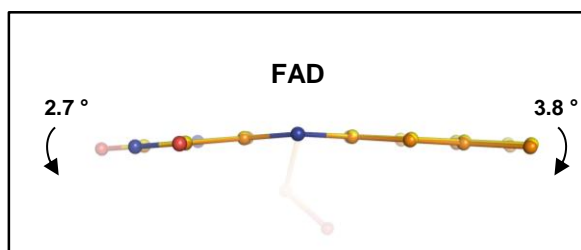


Figure 5.23 Further bending of the flavin cofactor at the two-electron reduced state. Ball and stick representation of the FADs from *EcE3* at ground state (yellow) and in *EcE3C45S* (orange). The dimethylbenzene part is $\sim 1.3^\circ$ further bent compared to the wild type FAD indicating its altered electronic state.

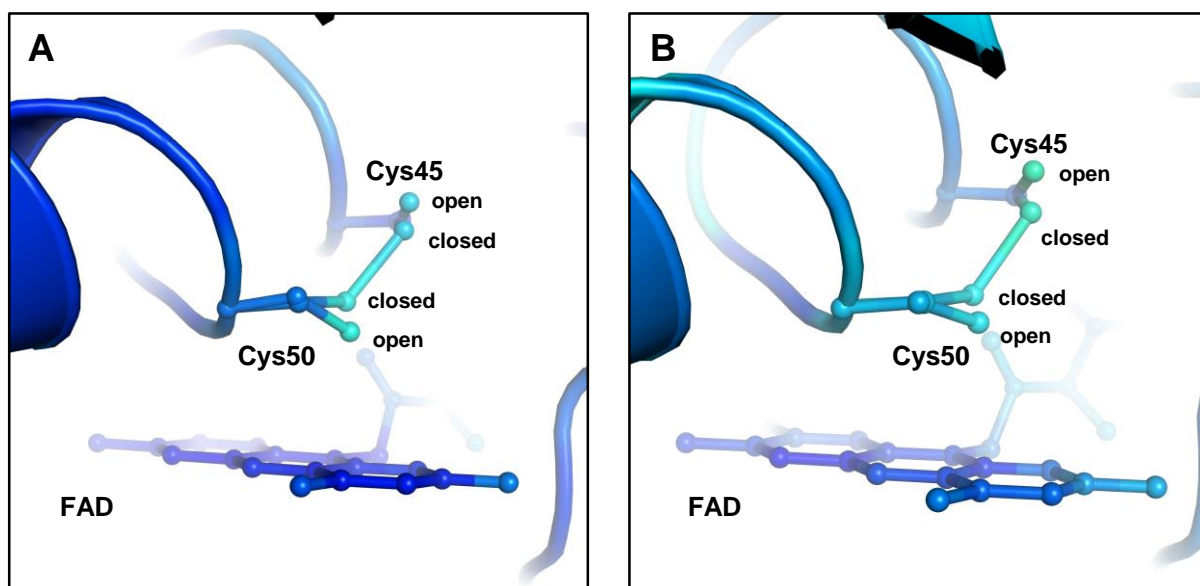


Figure 5.24 B-factor representation of the *EcE3* active site at 2.69 Å.

Atoms of the redox active cysteine and the flavin cofactor are color-coded according to their individual B-factors. Both cysteine residues in molecule A (**A**) and in molecule F (**B**) of the asymmetric unit do not show elevated atomic displacement parameters relative to their enzyme surrounding.

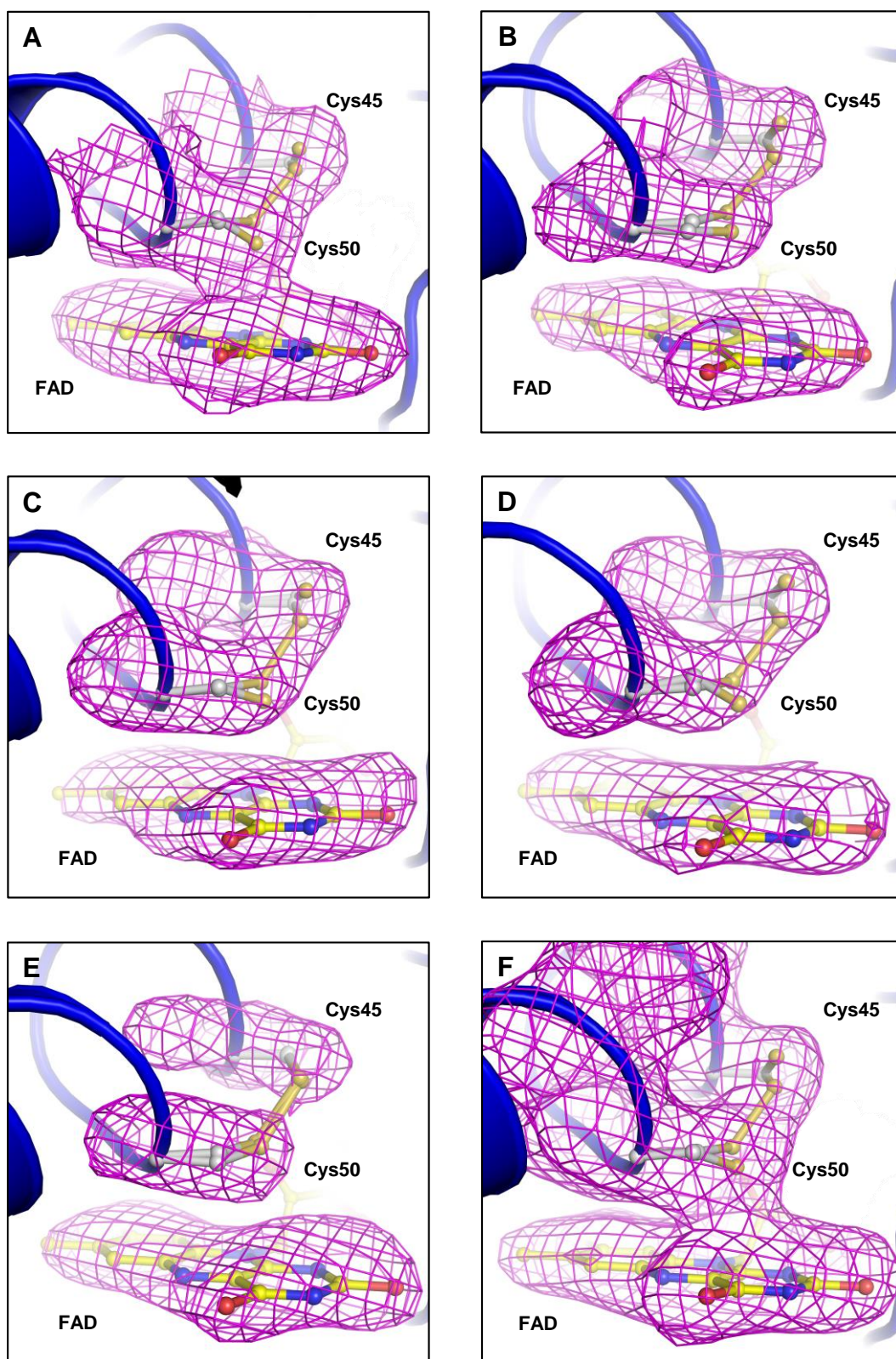


Figure 5.25 Active site of Ece3 at 2.69 Å. Simulated annealing OMIT maps for all molecules in the asymmetric unit (mFo-DFc at 3 σ). Figure numbering reflects the respective molecule label. Cohesive density is present in chain A and chain F, suggesting the formation of a covalent adduct.

6 Bibliography

- Adams, P. D. et al. 2010. "PHENIX: A Comprehensive Python-Based System for Macromolecular Structure Solution." *Acta Crystallographica Section D: Biological Crystallography* 66:213–21.
- Ahmad, I., S. Ahmed, M. A. Sheraz, F. H. M. Vaid, and I. A. Ansari. 2010. "Effect of Divalent Anions on Photodegradation Kinetics and Pathways of Riboflavin in Aqueous Solution." *International Journal of Pharmaceutics* 390(2):174–82.
- Ahmad, I., Q. Fasihullah, A. Noor, A. Ansari, and Q. Nawab Manzar Ali. 2004. "Photolysis of Riboflavin in Aqueous Solution: A Kinetic Study." *International Journal of Pharmaceutics* 280(1-2):199–208.
- Ahmad, R. and D. A. Armstrong. 1984. "Reduction of Lumichrome by the Radical Anions of CO₂ and Lipoamide." *International journal of radiation biology and related studies in physics, chemistry, and medicine* 45:607–14.
- Akiyama, S. K. and G. G. Hammes. 1981. "Elementary Steps in the Reaction Mechanism of Pyruvate Dehydrogenase Multienzyme Complex from *Escherichia coli*: Kinetics of Flavin Reduction." *Biochemistry* 20(May):1491–97.
- Alexandre, M.T.A., J. C. Arents, R. Van Grondelle, K.s J. Hellingwerf, and J. T. M. Kennis. 2007. "A Base-Catalyzed Mechanism for Dark State Recovery in the Avena Sativa Phototropin-1 LOV2 Domain." *Biochemistry* 46:3129–37.
- Alexandre, M.T.A. et al. 2009. "Primary Reactions of the LOV2 Domain of Phototropin Studied with Ultrafast Mid-Infrared Spectroscopy and Quantum Chemistry." *Biophysical Journal* 97(1):227–37.
- Ali, S. T. and J. R. Guest. 1990. "Isolation and Characterization of Lipoylated and Unlipoylated Domains of the E2p Subunit of the Pyruvate Dehydrogenase Complex of *Escherichia coli*." *The Biochemical Journal* 271:139–45.
- Aliverti, A., 2010. "Identifying and Quantitating FAD and FMN in Simple and in Iron-Sulfur-Containing Flavoproteins." Pp. 9–23 in *Flavoprotein Protocols*. Springer Verlag GmbH.
- Argyrou, A. and J. S. Blanchard. 2001. "Mycobacterium Tuberculosis Lipoamide Dehydrogenase Is Encoded by Rv0462 and Not by the lpdA or lpdB Genes." *Biochemistry* 40:11353–63.

- Argyrou, A., J. S. Blanchard, and B. A. Palfey. 2002. "The Lipoamide Dehydrogenase from *Mycobacterium Tuberculosis* Permits the Direct Observation of Flavin Intermediates in Catalysis." *Biochemistry* 41:14580–90.
- Argyrou, A., G. Sun, B. A. Palfey, and J. S. Blanchard. 2003. "Catalysis of Diaphorase Reactions by *Mycobacterium Tuberculosis* Lipoamide Dehydrogenase Occurs at the EH4 Level." *Biochemistry* 42:2218–28.
- Bates, D. L., M. J. Danson, G. Hale, E. A. Hooper, and R. N. Perham. 1977. "Self-Assembly and Catalytic Activity of the Pyruvate Dehydrogenase Multienzyme Complex from *Escherichia Coli*." *Nature* 268:313–16.
- Bauer, C., C. R. Rabl, J. Heberle, and T. Kottke. 2011. "Indication for a Radical Intermediate Preceding the Signaling State in the LOV Domain Photocycle." *Photochemistry and Photobiology* 87(26):548–53.
- Beel, B. et al. 2012. "A Flavin Binding Cryptochrome Photoreceptor Responds to Both Blue and Red Light in *Chlamydomonas Reinhardtii*." *The Plant Cell* 24(July):2992–3008.
- Benen, J. et al. 1991. "Lipoamide Dehydrogenase from *Azotobacter-Vinelandii* - Site-Directed Mutagenesis of the His450-Glu455 Diad - Spectral Properties of Wild Type and Mutated Enzymes." *European Journal of Biochemistry* 202:863–72.
- Benen, J., W. Van Berkel, N. Dieteren, et al. 1992. "Lipoamide Dehydrogenase from *Azotobacter Vinelandii*: Site-Directed Mutagenesis of the His450-Glu455 Diad. Kinetics of Wild-Type and Mutated Enzymes." *European Journal of Biochemistry* 207:487–97.
- Benen, J., W. Van Berkel, C. Veeger, and A. de Kok. 1992. "Lipoamide Dehydrogenase from *Azotobacter Vinelandii* The Role of the C-Terminus in Catalysis and Dimer Stabilization." *European Journal of Biochemistry* 207:499–505.
- Bird, C. L. and A. T. Kuhn. 1981. "Electrochemistry of the Viologens." *Chemical Society Reviews* 10:49.
- Bisswanger, H. 1981. "Substrate Specificity of the Pyruvate Dehydrogenase Complex from *Escherichia Coli*." *The Journal of Biological Chemistry* 256(2):815–22.
- Brautigam, C. A., J. L. Chuang, D. R. Tomchick, M. Machius, and D. T. Chuang. 2005. "Crystal Structure of Human Dihydrolipoamide Dehydrogenase: NAD⁺/NADH Binding and the Structural Basis of Disease-Causing Mutations." *Journal of Molecular Biology* 350:543–52.

- Brünger, A.T. 1992. "Free R Value: Anovel Statistical Quantity for Assessing the Accuracy of Crystal Structures." *Nature* 355:472–75.
- Brunger, A.T. 2007. "Version 1.2 of the Crystallography and NMR System." *Nature protocols* 2:2728–33.
- Cairns, W. L. and D. E. Metzler. 1971. "Photochemical Degradation of Flavins. VI. A New Photoproduct and Its Use in Studying the Photolytic Mechanism." *Journal of the American Chemical Society* 93(5):2772–77.
- Chandrasekhar, K. et al. 2013. "Insight to the Interaction of the Dihydrolipoamide Acetyltransferase (E2) Core with the Peripheral Components in the Escherichia Coli Pyruvate Dehydrogenase Complex via Multifaceted Structural Approaches." *Journal of Biological Chemistry* 288:15402–17.
- Choong, Y. S. and V. Massey. 1980. "Stabilization of Lactate Oxidase Flavin Anion Radical by Complex Formation." *Journal of Biological Chemistry* 255:8672–77.
- Clark, DP. 1989. "The Fermentation Pathways of Escherichia Coli." *FEMS Microbiology Reviews* 63:223–34.
- Conrad, K. S., C. C. Manahan, and B. R. Crane. 2014. "Photochemistry of Flavoprotein Light Sensors." *Nature Chemical Biology* 10(10):801–9.
- Cooper, R. H., P. J. Randle, and R. M. Denton. 1974. "Regulation of Heart Muscle Pyruvate Dehydrogenase Kinase." *The Biochemical Journal* 143:625–41.
- Corpet, F. 2010. "Nucleic Acids Research." *Nucleic Acids Research* 38(22).
- Crosson, S. and K. Moffat. 2001. "Structure of a Flavin-Binding Plant Photoreceptor Domain: Insights into Light-Mediated Signal Transduction." *Proceedings of the National Academy of Sciences of the United States of America* 98(6):2995–3000.
- Crosson, S. and K. Moffat. 2002. "Photoexcited Structure of a Plant Photoreceptor Domain Reveals a Light-Driven Molecular Switch." *The Plant Cell* 14(May):1067–75.
- Davis, I. W. et al. 2007. "MolProbity: All-Atom Contacts and Structure Validation for Proteins and Nucleic Acids." *Nucleic Acids Research* 35(13):375–83.
- DeLano, W. L. 2003. "The PyMOL Molecular Graphics System." <http://www.pymol.org/>.

- Diensthuber, R. P., M. Bommer, T. Gleichmann, and A. Möglich. 2013. "Full-Length Structure of a Sensor Histidine Kinase Pinpoints Coaxial Coiled Coils as Signal Transducers and Modulators." *Structure* 21:1127–36.
- Ehrenberg, A., F. Müller, and P. Hemmerich. 1967. "Basicity, Visible Spectra, and Electron Spin Resonance of Flavosemiquinone Anions." *European journal of biochemistry / FEBS* 2:286–93.
- Ellis, K. J. and J. F. Morrison. 1982. "Buffers of Constant Ionic Strength for Studying pH-Dependent Processes." 87:405–26 in *Methods in Enzymology*.
- Emsley, P., B. Lohkamp, W. G. Scott, and K. Cowtan. 2010. "Features and Development of Coot." *Acta Crystallographica Section D: Biological Crystallography* 66:486–501.
- Fraenkel, DG. 1996. "Escherichia Coli and Salmonella: Cellular and Molecular Biology." Pp. 189–98 in *eds Neidhardt FC, et al.* Washington, DC: ASM Press.
- Ghisla, S., B. Entsch, V. Massey, and M. Husein. 1977. "On the Structure of Flavin-Oxygen Intermediates Involved in Enzymatic Reactions." *European Journal of Biochemistry / FEBS* 76:139–48.
- Ghisla, S. and V. Massey. 1975. "Mechanism of Inactivation of the Flavoenzyme Lactate Oxidase by Oxalate." *Journal of Biological Chemistry* 250:577–84.
- Ghisla, S., V. Massey, J. M. Lhoste, and S. G. Mayhew. 1974. "Fluorescence and Optical Characteristics of Reduced Flavines and Flavoproteins." *Biochemistry* 13(3):589–97.
- Gibson, Q. H., V. Massey, and N. M. Atherton. 1962. "The Nature of Compounds Present in Mixtures of Oxidized and Reduced Flavin Mononucleotides." *The Biochemical Journal* 85(1958):369–83.
- Graef, M. R. De, S. Alexeeva, J. L. Snoep, and M. J. Teixeira De Mattos. 1999. "The Steady-State Internal Redox State (NADH/NAD) Reflects the External Redox State and Is Correlated with Catabolic Adaptation in Escherichia Coli." *Journal of Bacteriology* 181(8):2351–57.
- Green, J. D., E. D. Laue, R. N. Perham, S. T. Ali, and J. R. Guest. 1995. "Three-Dimensional Structure of a Lipoyl Domain from the Dihydrolipoyl Acetyltransferase Component of the Pyruvate Dehydrogenase Multienzyme Complex of Escherichia Coli." *Journal of Molecular Biology* 248:328–43.
- Güttler, B. H.-O. 2008. "Untersuchungen Zum Mechanismus Der Reduktiven Acetylierung Der Acyltransferase Des Humanen Pyruvat-Dehydrogenase-Komplexes." Martin-Luther-Universität Halle-Wittenberg.

- Hald, E., P. Lehmann, and J. Ziegenhorn. 1975. "Molar Absorptivities of β -NADH and / β -NAD at 260 Nm." *Clinical Chemistry* 7:884–87.
- Hansen, HG and U. Henning. 1966. "Regulation of Pyruvate Dehydrogenase Activity in *Escherichia Coli* K12." *Biochim Biophys Acta* 122:355–58.
- Hanukoglu, I. 2015. "Proteopedia: Rossmann Fold: A Beta-Alpha-Beta Fold at Dinucleotide Binding Sites." *Biochem Mol Biol Educ.* 43:206–9.
- Harbury, H., K. LaNoue, P. Loach, and R. Amick. 1959. "Molecular Interaction Of Isoalloxazine Derivatives." *Proceedings of the National Academy of Sciences* 45:1708–17.
- Hasford, Justin J., W. Kemnitzer, and C. J. Rizzo. 1997. "Conformational Effects on Flavin Redox Chemistry." *The Journal of Organic Chemistry* 62(8):5244–45.
- Hitomi, K., S. Kim, N. Harima, M. Ikenaga, and T. Todo. 1997. "Binding and Catalytic Properties of *Xenopus* (6-4) Photolyase." 272(51):32591–98.
- Hopkins, N. and C. H. Williams. 1995a. "Characterization of Lipoamide Dehydrogenase from *Escherichia Coli* Lacking the Redox Active Disulfide: C44S and C49S." *Biochemistry* 34(151):11757–65.
- Hopkins, N. and C. H. Williams. 1995b. "Lipoamide Dehydrogenase from *Escherichia Coli* Lacking the Redox Active Disulfide: C44S and C49S. Redox Properties of the FAD and Interactions with Pyridine Nucleotides." *Biochemistry* 34(151):11766–76.
- Hucho, F., D.D. Randall, T.E. Roche, M.W. Burgett, J.W. Pelley, L.J. Reed. 1972. " α -Keto acid dehydrogenase complexes. XVII. Kinetic and regulatory properties of pyruvate dehydrogenase kinase and pyruvate dehydrogenase phosphatase from bovine kidney and heart." *Archives of Biochemistry and Biophysics* 151:328–340.
- Huang, R., J. K. Hyun, and D. B. Min. 2006. "Photosensitizing Effect of Riboflavin, Lumiflavin, and Lumichrome on the Generation of Volatiles in Soy Milk." *Journal of Agricultural and Food Chemistry* 54:2359–64.
- Inoue, H., H. Nojima, and H. Okayama. 1990. "High Efficiency Transformation of *Escherichia coli* with Plasmids." *Gene* 96:23–28.
- Jung, M. Y., Y. S. Oh, D. K. Kim, H.-J. Kim, and D. B. Min. 2007. "Photoinduced Generation of 2,3-Butanedione from Riboflavin." *Journal of Agricultural and Food Chemistry* 55:170–74.
- Kabsch, W. 2010. "Xds." *Acta Crystallographica Section D: Biological Crystallography* 66:125–32.

- Kato, Masato et al. 2008. "Structural Basis for Inactivation of the Human Pyruvate Dehydrogenase Complex by Phosphorylation: Role of Disordered Phosphorylation Loops." *Structure* 16(12):1849–59.
- Ke, B. 1957. "The Polarographic Behavior of Alpha-Lipoic Acid." *Biochim Biophys Acta* 25:650–51.
- Kennis, J. T. M. and M.-L. Groot. 2007. "Ultrafast Spectroscopy of Biological Photoreceptors." *Current Opinion in Structural Biology* 17:623–30.
- Kim, H. and M. S. Patel. 1992a. "Characterization of Two Site-Specifically Mutated Human Dihydrolipoamide Dehydrogenases (His-452-Gln and Glu-457-Gln)." *Journal of Biological Chemistry* 267:5128–32.
- Kim, L. O. Ingram, and K. T. Shanmugam. 2007. "Construction of an *Escherichia coli* K-12 Mutant for Homoethanogenic Fermentation of Glucose or Xylose without Foreign Genes." *Applied and Environmental Microbiology* 73(6):1766–71.
- Kim, L. O. Ingram, and K. T. Shanmugam. 2008. "Dihydrolipoamide Dehydrogenase Mutation Alters the NADH Sensitivity of Pyruvate Dehydrogenase Complex of *Escherichia coli* K-12." *Journal of Bacteriology* 190(11):3851–58.
- Klinman, J. P. 2009. "An Integrated Model for Enzyme Catalysis Emerges from Studies of Hydrogen Tunneling." *Chemical Physics Letters* 471(4-6):179–93.
- Klinman, J. P. 2010. "Enzyme Dynamics: Control of Active-Site Compression." *Nature Chemistry* 2(11):907–9.
- Korotchkina, L. G. and M. S. Patel. 2001. "Probing the Mechanism of Inactivation of Human Pyruvate Dehydrogenase by Phosphorylation of Three Sites." *Journal of Biological Chemistry* 276(8):5731–38.
- Kottke, T., J. Heberle, D. Hehn, B. Dick, and P. Hegemann. 2003. "Phot-LOV1: Photocycle of a Blue-Light Receptor Domain from the Green Alga *Chlamydomonas reinhardtii*." *Biophysical Journal* 84(February):1192–1201.
- Koziol, J. 1971. "Fluorometric Analyses of Riboflavin and Its Coenzymes." Pp. 253–85 in *Methods in Enzymology*. McCormick, D. B. and Wright, L. D., eds.
- Laemmli, U. K. 1970. "Cleavage of Structural Proteins during the Assembly of the Head of Bacteriophage T4." *Nature* 227:680–85.

- Ledwith, R. et al. 2005. "NmerA, the Metal Binding Domain of Mercuric Ion Reductase, Removes Hg 2+ from Proteins, Delivers It to the Catalytic Core, and Protects Cells under Glutathione-Depleted Conditions." *Biochemistry* 44:11402–16.
- Levitch, E. 1958. "Studies on the Nature Protein-Bound." *The Journal of Biological Chemistry* 232:143–58.
- Lindsay, H. et al. 2000. "FAD Insertion Is Essential for Attaining the Assembly Competence of the Dihydrolipoamide Dehydrogenase (E3) Monomer from *Escherichia coli*." *Journal of Biological Chemistry* 275(47):36665–70.
- Losi, A. and W. Gärtner. 2011. "Old Chromophores, New Photoactivation Paradigms, Trendy Applications: Flavins in Blue Light-Sensing Photoreceptors." *Photochemistry and Photobiology* 87:491–510.
- Losi, A. and W. Gärtner. 2012. "The Evolution of Flavin-Binding Photoreceptors: An Ancient Chromophore Serving Trendy Blue-Light Sensors." *Annual Review of Plant Biology* 63:49–72.
- Losi, A, T. Kottke, and P. Hegemann. 2004. "Recording of Blue Light-Induced Energy and Volume Changes within the Wild-Type and Mutated Phot-LOV1 Domain from *Chlamydomonas reinhardtii*." *Biophysical journal* 86(2):1051–60.
- Losi, A., B. Quest, and W. Gärtner. 2003. "Listening to the Blue: The Time-Resolved Thermodynamics of the Bacterial Blue-Light Receptor YtvA and Its Isolated LOV Domain." *Photochemical & photobiological sciences : Official Journal of the European Photochemistry Association and the European Society for Photobiology* 2:759–66.
- Lüdtke, S. et al. 2013. "Sub-Ångström-Resolution Crystallography Reveals Physical Distortions That Enhance Reactivity of a Covalent Enzymatic Intermediate." *Nature chemistry* 5(September):762–67.
- Lyubimov, A. Y., K. Heard, H. Tang, N. S. Sampson, and A. Vrieland. 2007. "Distortion of Flavin Geometry Is Linked to Ligand Binding in Cholesterol Oxidase." *Protein Science : A Publication of the Protein Society* 16:2647–56.
- Machado, R. S., D. P. Clark, and J. R. Guest. 1992. "Construction and Properties of Pyruvate Dehydrogenase Complexes with up to Nine Lipoyl Domains per Lipoate Acetyltransferase Chain." *FEMS Microbiology Letters* 79:243–48.

- Maeda-Yorita, K., G. C. Russell, J. R. Guest, V. Massey, and C. H. Williams. 1991. "Properties of Lipoamide Dehydrogenase Altered by Site-Directed Mutagenesis at a Key Residue (I184Y) in the Pyridine Nucleotide Binding Domain." *Biochemistry* 30:11788–95.
- Maeda-Yorita, K., G. C. Russell, J. R. Guest, V. Massey, and C. H. Williams. 1994. "Modulation of the Oxidation-Reduction Potential of the Flavin in Lipoamide Dehydrogenase from *Escherichia Coli* by Alteration of a Nearby Charged Residue, K53R." *Biochemistry* 33:6213–20.
- Mande, S. S., S. Sarfaty, M. D. Allen, R. N. Perham, and W. G. Hol. 1996. "Protein-Protein Interactions in the Pyruvate Dehydrogenase Multienzyme Complex: Dihydrolipoamide Dehydrogenase Complexed with the Binding Domain of Dihydrolipoamide Acetyltransferase." *Structure* 4:277–86.
- Mansfield, C. W. 1960. *Oxidation-Reduction Potentials Of Organic Systems*. The Williams & Wilkins Company.
- Massey, V. and Q. H. Gibson. 1964. "Role Of Semiquinones In Flavoproteins Catalysis." *Federation Proceedings* 23:18–29.
- Massey, V., Q. H. Gibson, and C. Veeger. 1960. "Intermediates in the Catalytic Action of Lipoyl Dehydrogenase (Diaphorase)." *The Biochemical Journal* 77(1958):341–51.
- Massey, V. and G. Palmer. 1966. "On the Existence of Spectrally Distinct Classes of Flavoprotein Semiquinones. A New Method for the Quantitative Production of Flavoprotein Semiquinones." *Biochemistry* 5(10):3181–89.
- Mattevi, A., G. Obmolova, K. H. Kalk, A. Teplyakov, and W. G. Hol. 1993. "Crystallographic Analysis of Substrate Binding and Catalysis in Dihydrolipoyl Transacetylase (E2p)." *Biochemistry* 32:3887–3901.
- Mattevi, A., A.J. Schierbeek, and W.G. Hol. 1991. "Refined Crystal Structure of Lipoamide Dehydrogenase from *Azotobacter Vinelandii* at 2.2 Å Resolution. A Comparison with the Structure of Glutathione Reductase." *Journal of Molecular Biology* 220:975–94.
- Matthews, G., P. Ballou, and C.H. Williams. 1979. "Reactions of Pig Heart Lipoamide Dehydrogenase with Pyridine Nucleotides." *The Journal of Biological Chemistry* 254(12):4974–81.
- Matthews, G., and C.H. Williams. 1976. "Measurement of the Oxidation-Reduction Potentials for Two-Electron and Four-Electron Reduction of Lipoamide Dehydrogenase from Pig Heart." *The Journal of Biological Chemistry* 251(13):3956–64.

- McCoy, A. J. 2006. "Solving Structures of Protein Complexes by Molecular Replacement with Phaser." *Acta Crystallographica Section D: Biological Crystallography* 63:32–41.
- McCoy, A. J. et al. 2007. "Phaser Crystallographic Software." *Journal of Applied Crystallography* 40:658–74.
- McDonald, C. A., Y. Y. Liu, and B. A. Palfey. 2013. "Actin Stimulates Reduction of the MICAL-2 Monooxygenase Domain." *Biochemistry* 52:6076–84.
- Miller, S. M. et al. 1990. "Use of a Site-Directed Triple Mutant to Trap Intermediates: Demonstration That the Flavin C(4a)-Thiol Adduct and Reduced Flavin Are Kinetically Competent Intermediates in Mercuric Ion Reductase." *Biochemistry* 29:2831–41.
- Möglich, A., X. Yang, R. A. Ayers, and K. Moffat. 2010. "Structure and Function of Plant Photoreceptors." *Annual Review of Plant Biology* 61:21–47.
- Müller, F., P. Hemmerich, A. Ehrenberg, G. Palmer, and V. Massey. 1970. "The Chemical and Electronic Structure of the Neutral Flavin Radical as Revealed by Electron Spin Resonance Spectroscopy of Chemically and Isotopically Substituted Derivatives." *European Journal of Biochemistry / FEBS* 14:185–96.
- Müller, Y. A., G. Schumacher, R. Rudolph, and G. F. Schulz. 1994. "The Refined Structures of a Stabilized Mutant and of Wild-Type Pyruvate Oxidase from *Lactobacillus plantarum*." *Journal of Molecular Biology* 237:315–35.
- Neumann, P., A. Weidner, A. Pech, M. T. Stubbs, and K. Tittmann. 2008. "Structural Basis for Membrane Binding and Catalytic Activation of the Peripheral Membrane Enzyme Pyruvate Oxidase from *Escherichia coli*." *Proceedings of the National Academy of Sciences of the United States of America* 105(45):17390–95.
- O'Donnell, M. and C. H. Williams. 1984. "Reconstitution of *Escherichia coli* Thioredoxin Reductase with 1-DeazaFAD." *The Journal of Biological Chemistry* 259(4):2243–51.
- Palfey, B. A. and R. Fagan. 2010. "Flavin-Dependent Enzymes." Pp. 38–42 in *Comprehensive Natural Products II*, edited by L. Mader and L. Hung-Wen.
- Patel, M. S. and L. G. Korotchkina. 2001. "Regulation of Mammalian Pyruvate Dehydrogenase Complex by Phosphorylation: Complexity of Multiple Phosphorylation Sites and Kinases." *Experimental & Molecular Medicine* 33(4):191–97.
- Patel, M. S. and T. E. Roche. 1990. "Molecular Biology and Biochemistry of Pyruvate Dehydrogenase Complexes." *The FASEB Journal* 4:3224–33.

- Perczel, A. and G.D. Fasman. 1992. "Quantitative Analysis of Cyclic Beta-Turn Models." *Protein Science : A Publication of the Protein Society* 1:378–95.
- Perham, R. N. 2000. "Swinging Arms And Swinging Domains In Multifunctional Enzymes : Catalytic Machines for Multistep Reactions." *Annu. Rev. Biochem.* 69:961–1004.
- Perham, R. N. and P.A. Reche. 1998. "Swinging Arms in Multifunctional Enzymes and the Specificity of Post-Translational Modification." *Biochem Soc Trans* 26:299–303.
- Pfeifer, A. et al. 2009. "Time-Resolved Fourier Transform Infrared Study on Photoadduct Formation and Secondary Structural Changes within the Phototropin LOV Domain." *Biophysical Journal* 96(4):1462–70.
- Purcell, E. B., C. A. McDonald, B. A. Palfey, and S. Crosson. 2010. "An Analysis of the Solution Structure and Signaling Mechanism of LovK, a Sensor Histidine Kinase Integrating Light and Redox Signals." *Biochemistry* 49:6761–70.
- Raffelberg, S., M. Mansurova, W. Gärtner, and Aba Losi. 2011. "Modulation of the Photocycle of a LOV Domain Photoreceptor by the Hydrogen-Bonding Network." *Journal of the American Chemical Society* 133(5):5346–56.
- Reed, J. K. 1973. "Studies on the Kinetic Mechanism of Lipoamide Dehydrogenase from Rat Liver Mitochondria." *The Journal of Biological Chemistry* 248(11):4834–39.
- Reed, L. J. 2001. "A Trail of Research from Lipoic Acid to Alpha-Keto Acid Dehydrogenase Complexes." *The Journal of Biological Chemistry* 276(42):38329–36.
- Reed, Lester J. 1974. "Multienzyme Complexes." *Accounts of Chemical Research* 7:40–46.
- Reed, Lester J., Masahiko Koike, and P. C. Shah. 1960. "Alpha-Keto Acid Dehydrogenation Complexes - Purification and Properties of Dihydrolipoic Dehydrogenase of *Escherichia coli*." *The Journal of Biological Chemistry* 235(7):1939–43.
- Rizzo, Carmelo J. 2001. "Further Computational Studies on the Conformation of 1,5-Dihydrolumiflavin." *Antioxidants & Redox Signaling* 3(5):737–46.
- Rodríguez-Otero, J., E. Martínez-Núñez, A. Peña-Gallego, and S. A. Vázquez. 2002. "The Role of Aromaticity in the Planarity of Lumiflavin." *Journal of Organic Chemistry* 67(10):6347–52.
- Rosentel, J. K., F. Healy, J.A. Maupin-Furlow, J. Ho Lee, and K. T. Shanmugam. 1995. "Molybdate and Regulation of Mod (molybdate Transport), fdhF, and Hyc (formate Hydrogenlyase) Operons in *Escherichia coli*." *Journal of Bacteriology* 177(17):4857–64.

- Sahlman, L., A.M. Lambeir, and S. Lindskog. 1986. "Rapid-Scan Stopped-Flow Studies of the pH Dependence of the Reaction between Mercuric Reductase and NADPH." *European Journal of Biochemistry / FEBS* 156:479–88.
- Sahlman, L. and C.H. Williams. 1989. "Lipoamide Dehydrogenase from *Escherichia coli* Steady-State Kinetics of the Physiological Reaction." *Journal of Biological Chemistry* 264(14):8039–45.
- Sattar, A., J. M. deMan, and J. C. Alexander. 1977. "Light-Induced Degradation of Vitamins I. Kinetic Studies on Riboflavin Decomposition in Solution." *Canadian Institute of Food Science and Technology Journal* 10(1):61–64.
- Schulz, George E. and Emil F. Pai. 1983. "The Catalytic Mechanism of Glutathione Reductase as Derived from X-Ray Diffraction Analyses of Reaction Intermediates." *The Journal of Biological Chemistry* 258(24):1752–57.
- Schuman Jorns, M., G. Schöllnhammer, and P. Hemmerich. 1975. "Intramolecular Addition of the Riboflavin Side Chain." *FEBS Journal* 57(1):35–48.
- Searls, R., J. Peters, and D. Sanadi. 1961. "Alpha-Ketoglutaric Dehydrogenase - On the Mechanism of Dihydrolipoyl Dehydrogenase Reaction." *The Journal of Biological Chemistry* 236(8):2317–22.
- Seifert, F. et al. 2007. "Phosphorylation of Serine 264 Impedes Active Site Accessibility in the E1 Component of the Human Pyruvate Dehydrogenase Multienzyme Complex." *Biochemistry* 46:6277–87.
- Seifert, F. 2010. "Katalyse und Regulation Der E1-Komponente Des Humanen Pyruvat-Dehydrogenase-Komplexes Auf Molekularer Ebene." Martin-Luther-Universität Halle-Wittenberg.
- Shen, L. C., L. Fall, G. M. Walton, and D. E. Atkinson. 1968. "Interaction between Energy Charge and Metabolite Modulation in the Regulation of Enzymes of Amphibolic Sequences. Phosphofructokinase and Pyruvate Dehydrogenase." *Biochemistry* 7:4041–45.
- Sheraz, M. A., S. H. Kazi, S. Ahmed, T. Mirza, et al. 2014. "Effect of Phosphate Buffer on the Complexation and Photochemical Interaction of Riboflavin and Caffeine in Aqueous Solution: A Kinetic Study." *Journal of Photochemistry and Photobiology B: Biology* 273:17–22.
- Sheraz, M. A., S. H. Kazi, S. Ahmed, Z. Anwar, and I. Ahmad. 2014. "Photo, Thermal and Chemical Degradation of Riboflavin." *Beilstein Journal of Organic Chemistry* 1999–2012.

- Shoyama, Y. et al. 2012. "Structure and Function of Δ 1-Tetrahydrocannabinolic Acid (THCA) Synthase, the Enzyme Controlling the Psychoactivity of *Cannabis sativa*." *Journal of Molecular Biology* 423(1):96–105.
- Smith, M. W. and F. C. Neidhardt. 1983. "2-Oxoacid Dehydrogenase Complexes of *Escherichia coli*: Cellular Amounts and Patterns of Synthesis." *Journal of Bacteriology* 156(1):81–88.
- Snoep, J.L. et al. 1993. "Differences in Sensitivity to NADH of Purified Pyruvate Dehydrogenase Complexes of *Enterococcus faecalis*, *Lactococcus lactis*, *Azotobacter vinelandii* and *Escherichia coli*: Implications for Their Activity in Vivo." *FEMS Microbiology Letters* 114(3):279–83.
- Talfournier, F. et al. 2001a. " α Arg-237 in *Methylophilus methylotrophus* (sp. W₃A₁) Electron-Transferring Flavoprotein Affords ~200-Millivolt Stabilization of the FAD Anionic Semiquinone and a Kinetic Block on Full Reduction to the Dihydroquinone." *Journal of Biological Chemistry* 276:20190–96.
- Thorpe, C. and C. H. Williams. 1976a. "Differential Reactivity of the Two Active Site Cysteine Residues Generated on Reduction of Pig Heart Lipoamide Dehydrogenase." *Journal of Biological Chemistry* 251:3553–57.
- Thorpe, C. and C. H. Williams. 1976b. "Spectral Evidence for a Flavin Adduct in a Monoalkylated Derivative of Pig Heart Lipoamide Dehydrogenase." *Journal of Biological Chemistry* 251:7726–28.
- Thorpe, C. and C. H. Williams. 1981. "Lipoamide Dehydrogenase from Pig Heart. Pyridine Nucleotide Induced Changes in Monoalkylated Two-Electron Reduced Enzyme." *Biochemistry* 20:1507–13.
- Tittmann, K. 2014. "Bioorganic Chemistry Sweet Siblings with Different Faces : The Mechanisms of FBP and F6P Aldolase, Transaldolase, Transketolase and Phosphoketolase Revisited in Light of Recent Structural Data." *Bioorganic Chemistry* 57:263–80.
- Uden, G. and J. Bongaerts. 1997. "Alternative Respiratory Pathways of *Escherichia Coli*: Energetics and Transcriptional Regulation in Response to Electron Acceptors." *Biochimica et Biophysica Acta - Bioenergetics* 1320:217–34.
- Walsh, J. D. and A. F. Miller. 2003. "Flavin Reduction Potential Tuning by Substitution and Bending." *Journal of Molecular Structure: THEOCHEM* 623:185–95.

- Wang, J. et al. 2014. "Structure and Function of the Catalytic Domain of the Dihydrolipoyl Acetyltransferase Component in *Escherichia coli* Pyruvate Dehydrogenase Complex." *Journal of Biological Chemistry* 289:15215–30.
- Wei, W., H. Li, N. Nemeria, and F. Jordan. 2003. "Expression and Purification of the Dihydrolipoamide Acetyltransferase and Dihydrolipoamide Dehydrogenase Subunits of the *Escherichia coli* Pyruvate Dehydrogenase Multienzyme Complex: A Mass Spectrometric Assay for Reductive Acetylation of Dihydrolipoamide." *Protein Expression and Purification* 28:140–50.
- Whitby, L.G. 1953. "A New Method for Preparing Flavin-Adenine Dinucleotide." *The Biochemical Journal* 54(1946):437–42.
- Wilkinson, K. D. and C.H. Williams. 1979. "Evidence for Multiple Electronic Forms of Two-Electron-Reduced Lipoamide Dehydrogenase from *Escherichia coli*." *Journal of Biological Chemistry* 254:852–62.
- Wilkinson, K.D. and C.H. Williams. 1981. "NADH Inhibition and NAD Activation of *Escherichia coli* Lipoamide Dehydrogenase Catalyzing the NADH-Lipoamide Reaction." *Journal of Biological Chemistry* 256(5):2307–14.
- Williams, C. H. 1965. "Studies on Lipoyl Dehydrogenase from *Escherichia coli*." *Journal of Biological Chemistry* 240(12):4793–4800.
- Williams, C.H., G. Zanetti, L. D. Arscott, and J. K. McAllister. 1967. "Lipoamide Dehydrogenase, Glutathione Reductase, Thioredoxin Reductase, and Thioreoxin." *The Journal of Biological Chemistry* 242(22):5226–31.
- Winn, M. D. et al. 2011. "Overview of the CCP4 Suite and Current Developments." *Acta Crystallographica Section D: Biological Crystallography* 67:235–42.
- Zheng, Y. J. and R. L. Ornstein. 1996. "A Theoretical Study of the Structures of Flavin in Different Oxidation and Protonation States." *Journal of the American Chemical Society* 118(16):9402–8.
- Zoltowski, B. D. and K. H. Gardner. 2011. "Tripping the Light Fantastic: Blue-Light Photoreceptors as Examples of Environmentally Modulated Protein-Protein Interactions." *Biochemistry* 50:4–16.
- Zoltowski, B. D., B. Vaccaro, and B. R. Crane. 2009. "Mechanism-Based Tuning of a LOV Domain Photoreceptor." *Nature Chemical Biology* 5(11):827–34.

Curriculum Vitae

Michael Tietzel

Georg-August-University Goettingen
Department of Molecular Enzymology
Justus-von-Liebig Weg 11
37077 Goettingen, Germany

Phone: +49 551 3914000
e-mail: mtietze1@gwdg.de

Date of Birth: March 7th 1986
Place of Birth: Holzminden
Nationality: German

Education

1998-05/2005	Campe Gymnasium Holzminden
10/2005-09/2006	Military service
10/2006-09/2009	BSc Program <i>Biology</i> , Georg-August-Universität Göttingen
09/2009	Bachelor of Science Department of Molecular Structural Biology: „ <i>Biochemische und kristallografische Charakterisierung des TRBP-Dicer-Komplexes</i> “
10/2009-11/2011	MSc/PhD Program <i>Microbiology and Biochemistry</i> , Georg-August-Universität Göttingen
11/2011	Master of Science, Georg-August-Universität Göttingen Department of Molecular Enzymology: „ <i>Biochemical analyses of protein-protein interactions in the E.coli pyruvate dehydrogenase complex</i> “
02/2012-07/2015	GGNB doctoral program <i>Biomolecules: Structure – Function -Dynamics</i> , Georg-August-Universität Göttingen, Department of Molecular Enzymology